ulm university universität
uulm

Universität Ulm | 89069 Ulm | Germany

Equilibrium coverage of electrode surfaces derived from first principles

Dissertation

zur Erlangung des Doktorgrades Dr. rer. nat.
der Fakultät für Naturwissenschaften der Universität Ulm

Vorgelegt von:

Florian Gossenberger

aus Biberach a. d. Riß

Gutachter:
Prof. Dr. Axel Groß
PD. Dr. Joachim Bansmann

Ulm, 2019

Fassung June 7, 2019

Amtierender Dekan: Prof. Dr. Thorsten Bernhardt

1. Gutachter: Prof. Dr. Axel Groß

2. Gutachter: PD. Dr. Joachim Bansmann

Tag der Promotion: 12. November 2019

Contents

1 Introduction

Nowadays efficient catalysts for reactions play a fundamental role in economy. Most of all chemical products involve catalytic processes during their production, for instance cracking in petrochemistry, hydrogenation for margarine production in food chemistry or ammonia synthesis via the Haber-Bosch Cycle. Also important environmental protecting technologies require efficient catalyst materials, like CO oxidation in cars, fuel-cell technology, energy production, energy conversion and energy storage techniques.

For reactions in the chemical industry, even a very small improvement of catalyst usage or an enhancement of the selectivity can have a huge economic impact. For example the Haber-Bosch process is used to produce an immense amount of fertilizer world wide. Therefore more than 100 million tons of N_2 from the air is converted into ammonia each year [32]. An improvement in selectivity of just 0.01% would allow to capture 10.000 tons of nitrogen more for the same cost. That is why these kind of reactions are highly optimized already. However, to improve such reactions, a comprehensive mechanistic understanding is fundamentally important. Moreover it is not just a question of the economic price and profit for the companies, an improved insight into the catalytic processes provides a foundation to develop new environmentally friendly technologies. This is the case in the field of renewable energies. A sophisticated understanding of fundamental atomistic processes is essential.

Modern energy storage and conversion technologies rely often on reactions in an aqueous environment at the solid-liquid interface of the catalyst surface [35]. However this is a rather challenging environment to study a particular reaction. Most of the well-established methods, which are developed at ultra-high vacuum (UHV) conditions, hardly work in aqueous conditions. These include all methods which involve e.g. free electrons like low-energy electron diffraction (LEED), X-ray photoelectron spectroscopy (XPS), or atomic emission spectroscopy (AES). But also microscopic techniques, like scanning tunneling microscopy (STM) or atomic force microscopy (AFM), suffer in the liquid environment, since the probe can-

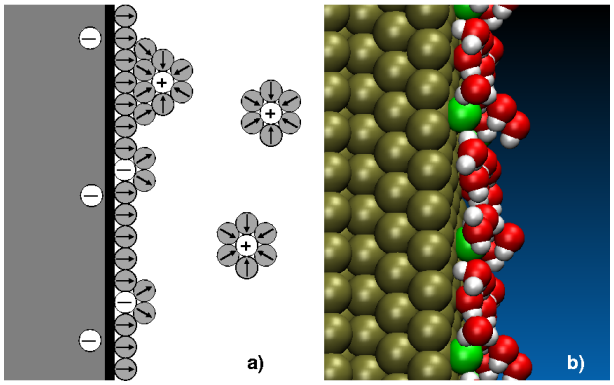

Figure 1.1: Molecules of water interacting with an ion covered electrode surface. a) depicts a schematic drawing, while b) represents a low coverage of the relaxed structure of chlorine on platinum (111).

not just be cooled down to liquid nitrogen temperature which typically improves the resolution significantly. Thus the measurement is done at room temperature, where the atoms or molecules move significantly faster. This difficulty might be even enhanced by the solvent, since the adsorption energy from solution is usually quite smaller than at UHV conditions. Moreover, ions in the double layer changes the electrostatic potential which hampers to get precise microscopic images. However workarounds were developed to improve the quality of atomistic microscopy in solution at the working condition of a catalyst surface, like covering the STM tip with an insulating material.

The efficiency of almost all electrocatalytic reactions depends significantly on the electrode potential of the heterogeneous catalyst. Thus the catalyst material itself becomes basically the electrode. For this transformation the catalyst needs to fulfill several requirements. First, the material needs to be conductive. If the catalyst consists of nanoparticles, attached on a supporting material, conductivity has to be ensured throughout the whole system. If the catalyst is a non-conduction material like oxides, it has to be attached to a conductive surface e.g. as a thin film. Furthermore, it is important to maintain the conductivity and therefore the catalytic activity over numerous cycles. A loss of conductivity connotes dead zones in the catalyst material, therefore this should be avoided in any case.

Another difficulty for studying reactions in aqueous electrolytes is, that the electrode surface is covered with adsorbates on a wide range of electrode potential and various ion concentrations in the electrolyte. The surface coverage depends thereby on the reactivity of the surface, which is governed by two factors. First, the reactivity relies on the band structure of the uncharged electrode material.

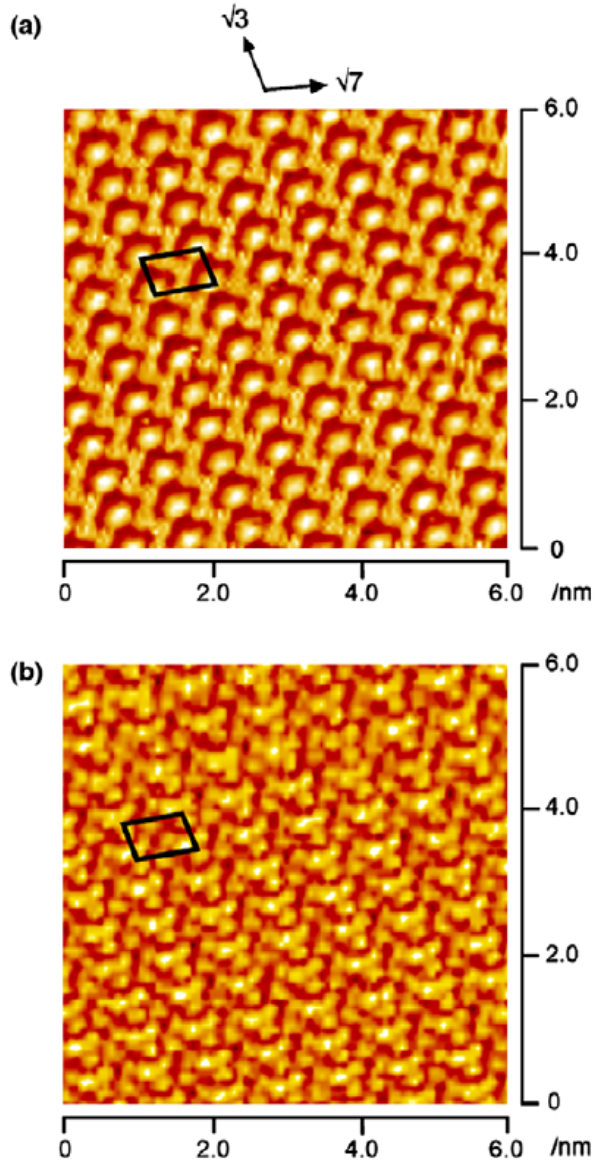

Figure 1.2: High-resolution STM images (6x6 nm^2) of an Au(111) surface in 0.5 M sulfuric acid acquired at 0.9 V. Tunneling current was (a) 3.0 and (b) 1.0 nA. Both STM images show dense coverages of sulfate respectively bisulfate on the surface (Taken from Ref. [176]).

If the electrode has an incompletely filled d-band and an upper d-band edge ϵ_u above the Fermi level,[213], the reactivity of the surface is enhanced and therefore ion adsorption is favored. Additional, the reactivity of the electrode can be vastly modified through the electrode potential. This affects ionic species in the electrolyte, due to their net charge they are stabilized or destabilized at the sur-

face. Besides in an aqueous electrolyte solution at all times a certain amount of ions is present. Even in a sample of pure water, there are at least additional protons and hydroxide ions available. Thus a change in the electrode potential can result in an adsorption or desorption reaction of these ions. Usually the atomistic situation is even more complicated, since electrolytes can contain various other ionic species. These ions are inevitable to ensure the electrolytes conductivity, but also to enhance specific reactions in the system. When the ions adsorb specifically on the surface, they often built a dense packed adlayer. In this way, they can considerably affect all kind of characteristics of the solid-liquid interface at the electrode surface. The ions block particular adsorption sites, change the work function and therefore the electrode potential, modify the wetting behavior of the surface and so on. Therefore it is fundamentally important to study the structure on the ion covered surface first, before looking at any electrochemical reaction.

To summarize, studying an electrochemical reaction at working conditions is a quite challenging task, since the aqueous environment influences the stability of structures by solvating the species in solution, it reduces the number of experimental probes compared to the gas-phase, the variable electrode potential modifies the stability of adsorbate coverages and therefore it changes the structure of the whole double layer, even of the diffusive part further away from the surface. Because of this complexity, it is necessary to simplify the catalyst as much as possible, before studying particular reactions on its surface. An efficient way to do so is to replace the inhomogeneous catalyst material by a well-defined, atomistically fabricated model catalyst. Thereby the complexity of the real system is reduced tremendously. A common example for a model catalyst would be a single crystal of the catalyst material, thus avoiding a nanocrystalline or polycrystalline catalyst with various involved crystallographic faces. Then it is much easier to identify special positions which govern the reactivity like kinks, hollow-sites, islands or adatoms. Model catalysts are nowadays an efficient tool to understand reaction mechanisms in heterogeneous catalysis.

A few decades ago, computer experiments became an additional tool to investigate electrochemical interfaces. With the development of computationally efficient methods and simultaneously faster and more powerful computers it became possible to simulate reactions in a computer experiment. But the simulation of a electrochemical reaction in an aqueous environment at working conditions, inclusive pH, ion concentrations, the double layer region, adsorbates and polarization at the interface, impurities or defects is still very hard to achieve. However, an

approach similar to using model catalysts in experiments is also possible as far as numerical studies are concerned. If the system is sufficiently simplified so that simulations can be performed, it can be used to extract numerous detailed information about the reaction. These simplifications are e.g. to calculate just a particular crystallographic face, replacing the water by a meanfield approach, treating the atoms classically, and omitting pH and other ions. Depending on the particular case, various methods with different assets and drawbacks can be used. Thereby the following classes of approaches are distinguishable:

- In **force-field** molecular mechanics, the atoms are treated classically. Forces within a molecule and among various molecules are handled in a parameterized approach. These parameters involve bonding angles, torsion angles or attractive respectively repulsive forces. However, force-fields typically fail to adequately describe bond breaking and bond making processes. An advanced version of the force-fields methods can handle certain specific reactions, it is the so-called reactive force-field. The advantage of force-fields is generally, that they are numerically very efficient so that large system sizes can be considered.

- The **kinetic Monte Carlo** (kMC) method corresponds to a coarse-grained atomistic simulation technique that considers changes of a system between different states. These involves e.g. the two dimensional movement of adatoms on a surface. Therefore the approach applies a fixed grid of allowed adsorption sites and handles the hopping of adatoms in this grid with clearly defined hopping probabilities, which are used in a statistical manner to determine the processes that are selected. Since probabilities are involved, a kinetic Monte Carlo simulation is not a deterministic method. Sometimes the hopping parameter can be calculated on the fly by electronic structure methods. However, in any case kMC is able to perform numerical studies for relatively large systems and long simulations times.

- In **electronic structure** methods the electrons are treated explicitly using quantum chemical methods. This allows to describe processes such as reactions involving bond-making and bond-breaking and the polarization of molecular bonds. However these methods are numerically very demanding, and it is usually just possible to compute a few hundred atoms at once.

- **Machine learning** came up a few years ago. There the behavior of atoms and molecules is given by a certain parameterized function. The parameters are optimized by a self learning algorithm, performed e.g. by the kernel

ridge regression method (KRR). The function is trained using accurate data from electronic structure methods. After the training process the machine learning approach is able to calculate large systems of atoms with a high accuracy. However the training can be extremely demanding and a change in the composition of atoms in a trained system is difficult.

During this thesis I used density functional theory (DFT), which belongs to the electronic structure methods. Thus it is capable to compute electronic properties like polarization, bonding behavior, work function or adsorption energies accurately. But the price is that the amount of considered atoms is rather limited. Thus I included for instance solvation only, when it was crucial for the determination of the stable adsorption phases.

The results from density functional theory can be embedded in a thermodynamic approach. This enables to link in a grand canonical approach numerically rather fast minimum energy calculations with thermodynamic quantities like pH, electrode potential or temperature. The method I used is called the computational hydrogen electrode (CHE). It is based on the idea to express the electrochemical potential of solvated protons through the corresponding chemical potential of gas-phase H_2 molecules, using the standard hydrogen electrode (SHE). Since the hydrogen gas acts as a reservoir, its chemical potential is constant all over the system. Therefore the chemical potential of hydrogen can be obtained by a gas phase calculation and the expensive thermodynamic average of a solvated protons can be omitted. Furthermore this concept can be applied for anions like halides or sulfate as well. It is even possible to extent the approach to co-adsorbed systems. In this way I used the CHE to compute the adsorption of hydrogen and various anions simultaneously (compare chapter 4.4 and 4.6).

2 Fundamental Basics

Density-functional theory is a remarkable theory that allows one to replace the complicated N-electron wave function $\Psi(x_1, x_2, ...x_N)$ and the associated Schrödinger equation by the much simpler electron density $\rho(r)$ and its associated calculational scheme. Remarkable indeed!

-Robert G. Parr and Weitao Yang [144]

2.1 Hohenberg-Kohn theorem

Quantum mechanical calculations for many-electron systems can be extremely time and computer memory demanding [92]. Although the Schödinger equation looks simple at the first glance, the total many-body wave function is a high-dimensional object, which is complicated to calculate. Thus there are several approaches which tried to reduce the complexity and to improve the efficiency of these calculations. An early attempt was suggested by the two physicists Llewellyn Hilleth Thomas and Enrico Fermi in 1927. The Thomas-Fermi model is a method to calculate the energy of a system using only the electronic density $\rho(r)$. It is possible to calculate an arbitrary amount of electrons, which is represented by only three coordinates. However the Thomas-Fermi model has some disadvantages. For instance it does not consider the exchange energy of electrons [75] and it was at this time unclear if there is a strict relationship between the many body wave function and the electronic density [63].

Pierre Hohenberg and Walter Kohn solved these issues in 1964. They published a paper which comprises two fundamental theorems. First, they described explicitly the connection between the nondegenerate ground state and the electronic density. They showed that the electronic density $\rho(r)$ of an atom or molecule uniquely determine its external potential $v(r)$ [63], and a trivial additive constant.

$$\rho(r) \Leftrightarrow v(r) + const. \tag{2.1}$$

The statement was proven in their paper by $reductio\ ad\ absurdum$ of the variational principle. The second theorem involves that the energy of an arbitrary electronic density is in any case greater or equal to the energy of the ground state E_0.

$$E[\rho(r)] \geq E_0^{exact} \tag{2.2}$$

Thus it is possible to find the exact ground state energy by a variation of the total electronic density in an self consistent approach [75, 150].

2.2 Kohn-Sham equations

A further extension of this approach was published one year later by Walter Kohn and Lu Jeu Sham. They came up with a series of self-consistent equations to calculate the electronic density of a many-electron system. For a system of N electrons, they provide N one-electron equations. Every equation represents thereby a canonical Kohn-Sham orbital.

$$\hat{h}_{KS}\phi_i = \epsilon_i\phi_i \tag{2.3}$$

Here $\hat{h}_{KS}$ is the one-electron Hamiltonian, ϕ_i the one-electron wave function of the electron i and ϵ_i the corresponding eigen energy. In principle the eigen energies of the Kohn-Sham orbitals have no physical meaning, but they are still relevant, since the electronic density arises straightforward out of the one-electron Kohn-Sham orbitals.

$$n(r) = \sum |\phi_i(r)|^2 \tag{2.4}$$

Expanding the one-electron Hamiltonian in eq. 2.3 gives the Kohn-Sham equations.

$$\Big(-\frac{\hbar^2}{2m}\nabla^2 + v_{eff}(r)\Big)\phi_i(r) = \epsilon_i\phi_i(r) \tag{2.5}$$

In this equation m is the electron mass and $v_{eff}(r)$ the effective potential, which depends on the three terms

$$v_{eff}(r) = v_{ext}(r) + v_H(r) + v_{xc}(r)\,. \tag{2.6}$$

The first term of the effective potential $v_{eff}(r)$ is the external potential $v_{ext}(r)$, which comprises the attractive electron-core interaction. The second term is called Hartree potential v_H, which corresponds to the classical electrostatic energy of the electronic charge distribution [63] and the last term $v_{xc}(r)$ is the exchange and correlation potential. This last term is known to exist, but its explicit form is unclear. This will be discussed in the next section.

2.3 Exchange-correlation functional

The exchange and correlation functional E_{xc} represents the contribution of the exchange and correlation potential v_{xc} to the energy of the system.

$$v_{xc}(r) = \frac{\delta E_{xc}(\rho)}{\delta \rho} \tag{2.7}$$

The functional E_{xc} depends thereby on the whole electronic density of the system, since the exchange and correlation energies are non-local properties. However there is no exact solution for E_{xc} available. Most of the approximations which tackle the problem of the exchange and correlation energy are local or semi-local approximations. Despite this crude simplification the results are surprisingly good. However the choice of an appropriate exchange and correlation functional E_{xc} is fundamentally important for every density functional calculation.

2.3.1 Local density approximation LDA

One of the first approaches to describe the exchange and correlation potential is the local density approximation (LDA) which was published in 1965. The LDA is derived from the electron distribution of the homogeneous electron gas. However the LDA functional depends solely on the electronic density at each point in space. Therefore it is called a local functional. Nevertheless Hohenberg and

Kohn showed that this procedure provides a satisfactory description for the exchange and correlation energy, as long as the electronic density of the system is only slowly varying. This is assumed to be the case for simple metals.

$$E_{xc}^{LDA}[\rho] = \int \rho(r)\epsilon_{xc}\big(\rho(r)\big)dr \tag{2.8}$$

Here $\rho(r)$ is the charge density at the point r and ϵ_{xc} is the exchange and correlation energy per electron, derived from the homogeneous electron gas [93]. However for bulk and surface calculations LDA performs surprisingly well. This might be the case because of a cancellation of opposing errors in the exchange and correlation energy [63].

In 1972 Ulf von Barth and Lars Hedin extended the LDA functional to the spin polarized case. Thus, the local spin density approximation (LSDA) is capable to address the electronic structure of magnetic materials [13]. This step was also important for the development of subsequent functionals.

However for molecules or ions the requirement of a slowly varying electronic density is certainly not fulfilled. Thus LDA or LSDA perform poorly in the description of these kind of systems. Also for some surfaces the LDA results are not sufficient, since it overestimates bond length and cohesive energies.

2.3.2 Generalized Gradient Approximation

To improve the results for systems with a more inhomogeneous electronic density, the generalized gradient approximation (GGA) was developed. There the gradient of the local electronic density $\nabla\rho(r)$ is taken into account, therefore these kind of functionals are also called semi-local functionals. The universal form of the GGA functional is

$$E_{xc}^{GGA}(\rho) = \int \rho(r)\epsilon_{xc}^{GGA}(\rho(r), |\nabla\rho(r)|)dr\,. \tag{2.9}$$

One of the first attempts to consider the density gradient is the PW86 functional, which was published by the authors John P. Perdew and Yue Wang in 1986. It expands the gradient of the exchange hole and takes real space cutoffs into account, to guarantee that the hole is negative and represents a deficit of one electron [151]. However the PW86 functional underestimates cohesive energies in

contrast to the overestimation of LDA. Therefore a further improvement of the PW86 functional was published by the same authors in 1991. The so-called PW91 functional contains in addition an analytic expression for the spin scaling factor [206]. Although it incorporates some inhomogeneity effects, the PW91 functional retains many of the best features of the LSDA functional. But it has some more problems, like a long derivation which depends on a long list of details or a complicated and nontransparent analytical function. Besides, this functional is overparametrized and the parameters are not seamlessly joined, what caused some spurious wiggles in the exchange and correlation potential. This lead to the development of the PBE functional, published by John. P. Perdew, Kieron Burke and Matthias Ernzerhof in 1996. In contrast to the PW91 functional the authors focused only on conditions, which are energetically significant and sacrificed less important conditions. Thus the PBE functional has a much simpler derivation and all parameters are fundamental constants. Furthermore, calculations of atomization energies for small molecules yield the same result as PW91 [149]. Because of all of these advantages, PBE became a very popular and widely used functional [34].

For even better results, Bjørg Hammer *et al.* revised the PBE functional and published the RPBE functional in 1998. They constructed RPBE in a way to improve chemisorption energies of small molecules on late transition-metal surfaces, by optimizing the shape of the enhancement function for the local exchange. All the other parameters are similar to the PBE functional. Chemisorption energies calculated using the LDA functional are numerically about 1.5 eV too large. With PBE it was reduced to approximately 0.5 eV and RPBE improves it additional by about a factor of two. However the PBE and the RPBE functional follow the same construction logic, therefore both functionals fulfill the same physical criteria [72].

2.4 Pseudo potentials

In the region close to the nucleus of an atom all of its electrons are present. However, maintaining the orthogonality principle of the corresponding wave functions results in strong oscillations in this region. To model these sharp features in a periodic DFT calculation, a very large set of plane waves is necessary, which causes a high energy cutoff. This is extremely costly to calculate, therefore it limits the size of the studied system extensively. But actually, the exact shape of the wave functions close to the nucleus hardly affect the properties of materials

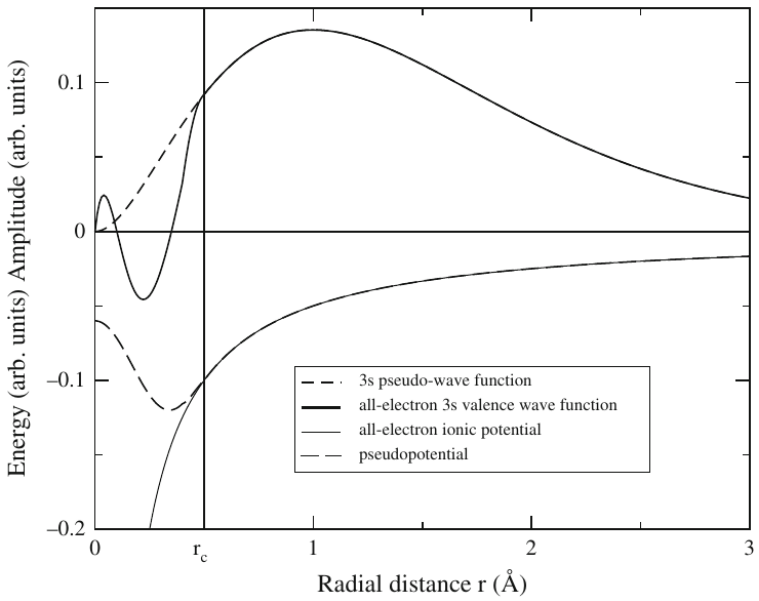

Figure 2.1: The difference between the all-electron wave function (solid line) and the pseudo 3s wave function (dashed line) vanishes for distances lager than the core radius r_c. In the core-near region the pseudo-wave function is much smoother. (Taken from [63].)

or molecules at all. Moreover the wave function of inner shell electrons decays rapidly to zero, thus they do not contribute to the chemical properties.

For this reason it is reasonable to implement pseudo-potentials, which describe the combined system of core and inner shell electrons by an effective potential. Thus the complicated wave functions close to the core were replaced by easily calculable and derivable pseudo-wave functions. This concept speeds up the calculation tremendously, because not only the optimization steps of the wave functions close to the core can be omitted, but also the wave functions of the valence electrons become much smoother in the core-near region (see fig. 2.1). Besides, relativistic effects that are relevant for heavy elements are restricted to the core states and can be incorporated into the pseudo-potential. In contrast the valence electrons are much weaker bound to the core, thus they behave non-relativistic anyway. Therefore the usage of pseudo potentials justifies the neglect of relativistic effects in the Kohn-Sham equations. In this way the usage of pseudo potential even improves the accuracy of a DFT calculation, if heavy elements are involved.

However for situations in which the core electrons play an important role, e.g. for

the calculation of metals under a high pressure, it is suggested to use a pseudo potential with a smaller core radius r_c. In this way the boundary condition of the electrons close to the core is improved.

At the beginning pseudo potentials were not normalized yet, since an explicit normalization leads to a wrong distribution of the core electrons. Therefore D. R. Hamann *et al.* came up with norm-conserving pseudo potentials in 1979 [70]. This concept enabled to develop ab-initio pseudo potentials, which do not depend on fitted parameters of experimental values anymore.

However, the cost of a DFT calculation depends notable on the smoothness of the used pseudo potential. This property is called softness, the harder the pseudo potential, the higher is the required energy cutoff for the plane wave basis set. The plane waves in fact correspond to the Fourier components. More fourier components allow a more accurate computation of the wave function. To improve the accuracy even more, but without increasing the energy cutoff respectively the amount of fourier components, a new class of pseudo potentials was generated. The so-called ultrasoft pseudo potentials or Vanderbilt pseudo potentials enable to use a significantly larger core radius r_c compared to the norm-conserving pseudo potentials. This is possible, because the desired accuracy is managed by an additional auxiliary function [202]. The projected augmented wave (PAW) approach that is nowadays very popular, is very similar to the concept of ultrasoft pseudopotentials.

2.5 Van der Waals interactions

2.5.1 Theory of van der Waals

The van der Waals forces are intermolecular or intramolecular interactions between molecular groups. They are weaker than covalent interactions, but they play an important role in a range of physical phenomena, like adhesion, surface tension, physisorption, wetting, properties of gases or liquids, thin films, strength of solids and more. Usually three different contributions can be distinguished [80]:

- The Keesom interaction between two dipoles,
- Debye interaction between a dipole and a polarizable molecule,
- London dispersion interaction between two neutral, but polarizable molecules.

Although all the van der Waals forces are called $weak$ forces, they can be fairly strong. Dominating van der Waals interactions occur in all states of aggregation, e.g. in gases like naturals gas, in liquids like different alkanes, gasoline or all kind of oils and in solids like graphite or also in candles. In density functional theory the Keesom and the Debye interactions are inherently included. But the London dispersion interaction is a nonlocal interaction, therefore it cannot be captured by local or semilocal functionals like LDA or GGA type functionals. Therefore an additional van der Waals implementation is needed.

2.5.2 D3 implementation by S. Grimme

The D3 correction scheme, developed by Stefan Grimme, adds an additional attractive forcefield-like term to specified atoms in the unit cell. Since all kind of electrostatic interactions are already included in density functional calculations, the D3 correction basically adds the missing London dispersion interaction. The London dispersion is an exclusively attractive force, which is provoked by a spontaneously appearing dipole in a neural molecule, that induces a second, temporary dipole moment in a neutral neighbor molecule. Therefore the London dispersion depends on the polarizability of the involved atoms or molecule groups. Grimme *et al.* constructed a set of C_6 coefficients using highly accurate $ab\ initio$ time-dependent (TD)DFT calculations, which allow to include dispersion interactions in DFT calculations. These coefficients depend on the computed chemical element itself, however in the third revision of their approach they consider additionally a coordination-dependent component, which was not included in the D1 or the D2 approach. The largest fraction of the London dispersion are thereby two-body interactions, whose energy is given in the D3 scheme by

$$E_i \propto \frac{C_6}{r^6}\,. \tag{2.10}$$

The C_6 coefficients decay with r^{-6}, which is the same order than the dispersion but not necessarily the other van der Waals contributions. Higher order contributions from multipole-based perturbation theory were considered up to C_8. However it does not make any sense to include even higher ranked terms, since they become inappropriate at short interatomic distances in a DFT-D calculation. Besides, a regular DFT calculation includes already short range interactions quite satisfactory. Therefore an additional van der Waals term would generate double-counting effects of correlation at intermediate distances. To reduce this error the

D3 correction scheme uses a damping function which diminishes the dispersion contribution for short distances. In this thesis I used in particular the zero damping method, because this is more accurate for the dispersion contribution of liquid water compared with the Becke-Johnson damping [168].

2.5.3 Comparison with other approaches

vdW-DF formalism

In the van der Waals density functional approach, M. Dion *et al.* came up with a density-density interaction formula to consider the nonlocal correlation. Therefore they expand the correlation energy term into two separate fractions. The first part accounts for the short range contribution of the correlation energy, thus it is a nonlocal LDA term. The second part is a full potential approximation which is exact at long distances. Both approximation are seamless linked in a way that prohibits double counting [30].

Tkatchenko-Scheffler method

An alternative van der Waals correction is the Tkatchenko-Scheffler method. This is also a possibility to add London dispersion interaction to DFT. However in this case the C_6 coefficients were calculated on the fly from the electronic density of the unit cell. In this way it is possible to avoid the parametric form of the D3 correction and to consider the exact chemical environment. However this is not necessarily an advantage, since the coefficients in the D3-approach are highly accurately calculated, despite that the electronic environment of the atoms is not entirely known [197].

2.6 Electrode potential in DFT

It is quite valuable to have computed stability informations for various electrode potentials, since the electrode potential is a fundamental parameter in electrochemistry. It governs all electrochemical reactions on the surface of the electrode, since it affects adsorption energies of ions significantly. The electrode potential is

essentially the electrochemical potential of electrons, since it is a constant quantity of the electrons. It is also related to the work function of the electrode, however the work function depends furthermore on the dipole layer on the electrode surface. Thus adatoms which decrease the surface dipole layer or which lower the screening effect of an aqueous environment, increases the electrode potential. This fact raises significant problems for theoretical calculations, since a change in the atomistic structure which happens when atoms or molecules relax into the energy minimum configuration can change the electrode potential of the system. However, a DFT calculation is always a microcanonical approach. This implies, that neither the number of molecules or atoms, nor the amount of electrons can be changed during the calculation. Thus to get information for a specific electrode potential, it is inevitable to compute several different compositions first and to compare afterwards the work functions of the resulting structures.

The most straightforward way to modify the electrode potential in a calculation is possibly to control the initial charge of the system. In fact the trivial change of the amount of electrons in the unit cell will automatically be compensated by a constant and uniform background charge, to keep the unit cell charge neutral. This is mandatory, otherwise the electrostatic energy of the system per unit cell diverges. However this uniform charge in the unit cell can introduce artifacts to the one-electron potential. In particular in the vacuum region, where the charge distribution is entirely given by the background charge, it can lead to a quadratically varying potential. But this erroneously effect is strongly reduced, if in this region polarizable atoms or molecules are present, since they can screen the electric field efficiently [184]. Furthermore the constant background charge bears another problem, since the interaction between the charged slab and the background charge contributes to the total energy of the system. Therefore it has to be subtracted after the calculation [63].

However, in recent years various other attempts were made to run DFT calculations at particular electrode potentials. One alternative is to include an artificial electric field in the DFT calculation by adding a dipole layer into the vacuum region [131]. This is a commonly used method to counterbalance the electric field which is generated through ion adsorption on a non-symmetric slab. However it is not straightforward to relate the applied dipole layer to the corresponding electrode potential. Another method is to implement a counter electrode in the calculation. This can be done either by adding a localized charge distribution with a Gaussian profile perpendicular to the surface into the vacuum region of the unit cell or by integrating a perfect conducting continuum with a non-vanishing surface

charge above a two-dimensional periodic slab. In this ansatz the charge can be related to the electrode potential by comparison with experimentally derived capacities or if several layers of water are present, to the potential profile inside the water bulk region [184]. Furthermore hydrogen atoms can be added to a water bilayer outside the slab. The hydrogens will lead to the formation of hydronium H_3O^+, and the extra electron moves to the electrode. However for fine-tuning of the electrode potential smaller steps would be reasonable, since this approach allows only a change of one electron per unit cell. Especially for smaller unit cells these are quite large steps in the potential. Thus for a proper tuning of the electrode potential, a rather large unit cell is necessary [63].

Another problem comes up, if there is no vacuum level available in the unit cell. In this case it is quite difficult to identify the current electrode potential of the system. This might occur in an solid/liquid interface calculation where the whole unit cell is filled with water. However Taylor *et al.* have provided a possible solution to this problem, for calculations in which a constant background charge is present. They suggested a double-reference method, where the reference value is taken from a second calculation. In this calculation a vacuum level should be present in the middle of the slab. Nevertheless it is important that there are still enough layers of water on the metal surface, that the vacuum level is converged with respect to the number of layers. Since the work function of such a metal-water interface is well defined, this calculation can provide a fix point inside the metal slab where the variation of the one-electron potential does not depend on the vacuum region and its potential. After that, the slab can be filled with water and the selected point serves as a reference point at which the potential is now known [196].

However all these methods provide valuable informations about a change in the electrode potential, but they do actually not control the electrode potential explicitly. They either tackle the problem by charging the metal slab respectively a counter electrode or they implement an electric field into the unit cell. A rearrangement of the solvent molecules in a molecular dynamic simulation or adsorption of ions at the interface can change the specified potential significantly. Due to the limits of DFT, there still exists no workaround to keep the electrode potential constant during a relaxation calculation or a molecular dynamic simulation.

2.7 Computational hydrogen electrode

To model catalytic processes on an electrode, it is crucial to have a correct understanding of the atomistic environment at the solid/liquid interface first, since both anions and cations will cover the surface at specific conditions. However this is not easy to get, since the calculation of adsorption energies under aqueous conditions requires the Gibbs energy of the solvated ions. But this is very challenging to compute, since a thermal average is necessary. Therefore, a sufficiently large unit cell with a proper amount of water molecules to guarantee an adequate solvation is necessary. This needs to be embedded in an ab-initio simulation, long enough that after a thermalization time of about two picoseconds an thermal average can be computed. However, these kinds of calculations are obviously quite expensive and time-consuming. Nevertheless, the computational hydrogen electrode (CHE) developed by Jens Nørskov *et al.* [138, 137] provides an efficient workaround.

2.7.1 Theory of the CHE

The basic idea of the CHE is to assume an equilibrium between hydrogen gas at standard conditions (pH=0, p=1 bar, T=298 K) and solvated protons in the solution, plus the electron at fermi level of the electrode.

$$\frac{1}{2}H_{2(\mathrm{g})} \rightleftharpoons H^{+}_{(\mathrm{aq})} + e^{-}_{fermi} \tag{2.11}$$

Therefore the chemical potentials μ of both hydrogen in the gas phase and solvated protons plus the corresponding electron needs to be equal. Otherwise a reaction, like a diffusion-reaction would take place, until the equilibrium is finally reached.

$$\frac{1}{2}\mu(\mathrm{H}_{2(\mathrm{g})}) = \mu(\mathrm{H}^{+}_{(\mathrm{aq})}) + \mu(e^{-}_{fermi}) \tag{2.12}$$

Here eq. 2.12 links the chemical potential in the gas phase with the computational challenging chemical potential of solvated protons. Since the whole concept is a grand canonical approach, the chemical potential of hydrogen in the gas phase is a constant parameter. Thus the hydrogen gas phase act as a infinite reservoir of hydrogen molecules with a constant chemical potential. This elegant trick en-

ables to get the chemical potential of the solvated protons, just from the chemical potential in the gas phase.

Furthermore the chemical potential μ of the protons depend on the electrode potential U_{SHE}, thus we get the electrochemical potential $\tilde{\mu}$.

$$\tilde{\mu} = \mu + eU_{SHE} \tag{2.13}$$

Here e denotes the elementary charge. In combination with the thermodynamic formulation of the concentration dependence, the electrochemical potential of protons is given by

$$\tilde{\mu}(\mathrm{H}^+_{(\mathrm{aq})}) + \tilde{\mu}(e^-) = \frac{1}{2}\mu(\mathrm{H}_{2(\mathrm{g})}) - eU_{\mathrm{SHE}} - k_{\mathrm{B}}T\ln(10)\mathrm{pH}\,. \tag{2.14}$$

The approach can be extended for other adsorbates as well. In the case of other ions it is important to consider the correct reduction potential of the corresponding equilibrium. This is not necessary for the hydrogen adsorption reaction, since the reduction potential for hydrogen is per definition zero. Thus it is possible to apply the same approach for anionic adsorbates like halides, nitrate or sulfate as-well. It is even possible to consider various co-adsorbed adsorbate mixtures on the electrode surface simultaneously.

Thus, the whole concept of the CHE does not involve any approximations. However inaccuracies arise later when this thermodynamic model is realized by DFT calculations.

2.7.2 Implementation of CHE using DFT

A Pourbaix or phase diagram can be used to get the thermodynamically most stable adsorbate structures at particular chemical conditions. The most stable structure is thereby determined by the lowest Gibbs free energy per surface area A_S. However, the relevant quantity to compare different adsorbate structures is actually the change in the Gibbs free energy of adsorption. Therefore the fundamental equation to investigate the ion covered electrode surface is

$$\Delta\gamma = \frac{1}{A_{\mathrm{S}}}\Big(G_{surf,ads} - G_{surf,0} - \sum_i n_i\mu_i\Big)\,. \tag{2.15}$$

Here $G_{surf,ads}$ is the Gibbs energy of the adsorbate covered surface, $G_{surf,0}$ the

Gibbs energy of the bare surface, μ_i the chemical potential of species i, and n_i the amount of adsorbate molecules or ions in the unit cell.

As explained in the previous section, the chemical potential of the adsorbates can be obtained from the molecules in the gas phase. In periodic density functional theory, this energy is essentially the total energy of a relaxed molecule without any intermolecular interactions. Thereby the unit cell needs to be sufficiently large to prevent intermolecular interaction between molecules in the periodic iterated unit cells. To improve the accuracy of the chemical potential μ, both the zero point energy of the molecule and vibrational entropy can be included. But since both energies are rather small they cancel out to a certain extent. That is why I did not consider them in most of the computations of this thesis.

The Gibbs energy of the adsorbate covered $G_{surf,ads}$ respectively bare electrode surface $G_{surf,0}$ is mainly the total energy of an adsorbate covered or clean metal slab. Here, zero point energy or vibrational entropy improve the accuracy as well. But moreover it is important to investigate if solvation of the adsorbate covered surface affects the adsorption energies. If this is the case, a proper solvation needs to be added to the computation, as explained by Nørskov et.al. [138]. A reasonable way is to include first a layer of explicit solvation, followed by implicit solvation to incorporate the properties of bulk water. The first layer is important to respect hydrogen bond or charge transfer between water and the ions. However if the ions are bulky or the shape of the unit cell inapt, it can be complicated to add a layer of explicit solvation close to the surface. Furthermore it might be possible that the adsorption energy of the adsorbed ions might change with varying electrode potentials. This can occur on nonmetallic surfaces like semiconductors. In this case it is necessary to include multiple adsorption energies at various potentials for each adsorbate structure.

In this ansatz total energies of a density functional theory calculation are embedded in a thermodynamic approach, to determine stability of adsorbate structures at arbitrary electrochemical conditions. Despite the simplicity of this approach, it has proven to be a valuable tool for a variety of systems [156, 165, 73, 170].

3 Calculation Setup

3.1 VASP Code

For all of the calculations in this thesis I used the computer program VASP (Vienna ab-initio Simulation Package) [96]. It was developed by Jürgen Furthmüller and Georg Kresse from the University of Vienna, as a periodic density functional theory code for atomic scale materials modeling. Since VASP requires an periodic supercell approach, it is constructive to compute all quantities in a plane wave basis set. For the interactions between electrons and the ionic cores, VASP supports the projector-augmented-wave method, norm-conserving or ultrasoft pseudopotentials. For my research I used the projector-augmented-wave method.

3.2 Basic INCAR parameters

The INCAR file is the basic input file for VASP. It contains parameters with informations about the calculation to be performed. If a parameter is not stated there, VASP will rather use a default value. The INCAR file specifies the type of calculation that should be performed, which was during this thesis mainly the relaxation of atoms. Furthermore it provides information about how the calculation is performed, which includes accuracy of the calculation, the functional to use, values for implicit solvation or if and how van der Waals interactions should be considered. It provides information for the program about convergence criteria, like stopping parameters for both ionic and electronic steps or a maximum allowed amount of steps. Finally, the INCAR file defines what kind of results the VASP-program should return. This might be a LOCPOT file to extract the work function of the system or a CHGCAR file which includes the charge density distribution of the unit cell. In the following section I will describe some selected parameters of the INCAR file, which are notably important for the VASP calculation.

3.2.1 Cutoff energy

Since plane waves fill the space periodically, they can be used to describe the wave functions in a periodic setup. This is also reflected in the Bloch theorem respectively the Floquet theory. Each plane wave $\psi_i(r)$ is characterized by a wave vector k.

$$\psi_i(r) = \frac{1}{\sqrt{V}} e^{ik_i r} \tag{3.1}$$

Here the plane wave is normalized with respect to the volume element V. To describe an arbitrary electronic structure with a infinite precision, in principle, an infinite expansion of one-electron wave functions in plane waves is required. In the DFT calculation the plane wave basis set $\{\psi_i(r)\}$ is used to handle the electronic structure computationally. However, since the computational capacity is limited only plane waves up to a certain energy can be considered. The energy cutoff determines thereby the upper limit respectively the highest energy for the used plane waves. Essential for the chosen plane wave basis set is the fact that the shortest wave length is small enough to resolve the variation of the electronic wave function. This variation can be significantly reduced close to the nuclei by the use of pseudopotentials. I used for almost all of my calculations the cutoff energy, which is recommended by the applied pseudo potentials.

However if an implicit solvent is used in the calculation, it is crucial to have a rather precise electronic density of the involved molecules. Otherwise features like oscillations in the electronic density at the tail region of the wave function would make it difficult to get the shape of the cavity correct. Thus a high cutoff energy is crucial to get an accurate cavity for the solvent model (compare chapter 3.4.1). Therefore I used in this case a significantly higher cutoff energy of 700 eV.

3.2.2 K-Point mesh

In density functional calculations, one of the core elements is to compute the matrix elements of the Hamiltonian to get kinetic energy and potential energy of the electrons. However the determination of the kinetic energy in principle requires the evaluation of the second derivative of the wave functions. It turns out that the determination of the kinetic energy can be done much more efficiently in momentum or reciprocal space as the momentum operator is diagonal in reciprocal space. This means that taking the first derivative basically corresponds to a multiplication of the momentum. The reciprocal space is hereby the corresponding

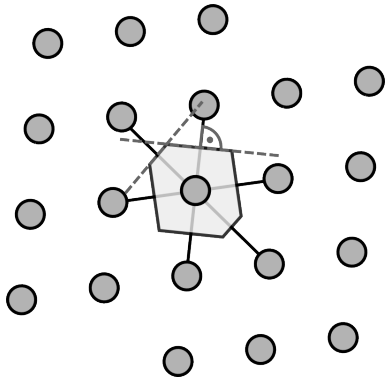

Figure 3.1: The sketch depicts how to construct a wigner seitz cell in two dimensions. The solid lines connect the nearest neighbors of a central atom, cutting them with a perpendicular line (dashed) in the middle gives the wigner seitz cell (gray ares).

dual space to the real space, which reflects mathematically the translation symmetry of the lattice [63]. Plane waves are assigned by the wave vector k, thus they depict a single point in the reciprocal space. Therefore the reciprocal space is also called k-space. The lattice vectors $\boldsymbol{b_1}$, $\boldsymbol{b_2}$, and $\boldsymbol{b_3}$ of the unit cell in the reciprocal space can be derived by

$$\boldsymbol{b_1} = 2\pi\frac{\boldsymbol{a_2}\times\boldsymbol{a_3}}{V}, \quad \boldsymbol{b_2} = 2\pi\frac{\boldsymbol{a_3}\times\boldsymbol{a_1}}{V}, \quad \boldsymbol{b_3} = 2\pi\frac{\boldsymbol{a_1}\times\boldsymbol{a_2}}{V}. \tag{3.2}$$

Here $\boldsymbol{a_1}$, $\boldsymbol{a_2}$, and $\boldsymbol{a_3}$ are the three lattice vectors and V is the volume of the unit cell in real space. The corresponding unit cell in the reciprocal space can be obtained, by the construction of a primitive Wigner-Seitz cell (see Fig. 3.1). This uniquely defined polyhedron is also called the first Brillouin zone. The same construction can also be performed with the next but one neighboring atoms, which results in the second Brillouin zone. However the other Brillouin zones except the first have, for the sake of the DFT calculation, no further meaning.

The shape of the first Brillouin zone enables to identify some high symmetry points. The most trivial point is thereby the Γ-point, located in the origin of the Brillouin zone. In the center of each surrounding line (two-dimensions) respectively plane (three-dimensions) is the X-point, and in the center of each corner (two-dimensions) respectively edge (three-dimensions) is the M-point [31].

To derive energies in reciprocal space requires to integrate over the first Brillouin zone. However, as this integral can not be performed analytically, it has to be

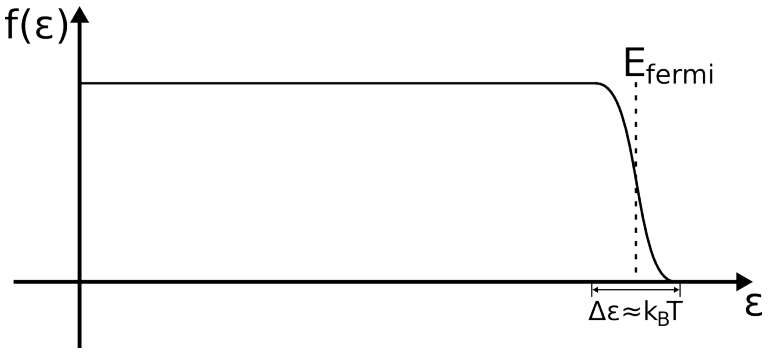

Figure 3.2: The Fermi function describes the occupation of the states in a metal. Close to the Fermi level the occupation is smeared out according to the Fermi-Dirac statistics.

replaced by a summation over the first Brillouin zone. In particular for metallic systems the energy depend strongly on the particular k-points so that a rather large k-point mesh is needed. On the other hand, for a periodic array of isolated systems there should be no dependence of the energy on the particular k-points so that the integral can be replaced by just using one single k-point. This is the case for the calculation of an individual molecule in the periodic approach, more than one k-point would only require longer computation times without any improvement in the accuracy. A special situation occurs for slab calculations, there it is important to get a realistic metallic behavior in x and y direction, but to hinder simultaneously all kind of interaction between the slabs in z direction. Therefore both x and y direction need sufficient k-points but z direction only one. In all my calculations I used a Γ-centered Monkhorst-Pack grid [130] with a various amount of equidistant k-points in slab direction and one k-point in z direction. The Monkhorst-Pack scheme is a widely used, regular grid with similar distances between the k-points.

3.2.3 Electron smearing

The electronic structure of metal is governed by a large amount of states, which is expressed by the density of states (DOS). At finite temperature the occupation around the Fermi level is smeared out. This connotes, that some states below the Fermi level are not occupied with electrons and some states above are. The region of this smearing is in the order of $\Delta\epsilon = k_B T$ (see fig. 3.2) [4], the exact occupation is given by the Fermi function.

In a DFT calculation the situation is rather similar compared to a real metal. There the Kohn-Sham orbitals close to the Fermi energy are partially occupied as well, which results in a similar electronic structure. This electronic smearing in VASP is managed by the ISMEAR parameter. However, the reason to implement the smearing has in this case not a physical, but a computational background. Without smearing it might happen, during the self consistent calculation, that the occupation of the Kohn-Sham orbitals is changed multiple times. This makes the convergence of such a system difficult and expensive. A partial occupation of states close to the Fermi level reduces this effect drastically and speeds up the computation. But conventional smearing with a Fermi-Dirac-like distribution is not the method of choice, since it leads to an error in the integration of the distribution. However the approach by Methfessel and Paxton [123] avoids this error, and it does not come along with the loss of precision of other broadening techniques.

Additional to the type of the smearing (ISMEAR), the extend of the used smearing has to be specified in the INCAR file (SIGMA parameter). In all my slab calculations I used a width of 0.2 eV, which is the recommended default value for metals. The difference between the free energy and the total energy, thus the entropy of the electrons, was always below 1 meV/atom. This is also the recommended value in the VASP manual.

3.3 Used Functionals: PBE and RPBE+D3

The contribution of the quantum mechanically many-body effects exchange and correlation to the total energy rely vastly on the used functional. Functionals, which are based on the generalized gradient approximation (GGA), include thereby the gradient of the local electronic density to calculate these energies. However the contribution of the gradient is only known for two particular cases. First, when the electronic density is vanishing and second for an infinite electronic density. Between these two extremes an interpolation is done, although the exact shape of this function is unknown. Therefore it has to be constructed by following physical principles, or the function is optimized due to experimental measurements for particular benchmark systems. That explains why it is important to chose a suitable functional carefully, depending on the topic of research.

In this thesis I applied two different functionals for my DFT calculations. First the widely used PBE functional, which is a GGA-type functional. This functional is capable to compute accurate energies for surfaces and molecules, as explained

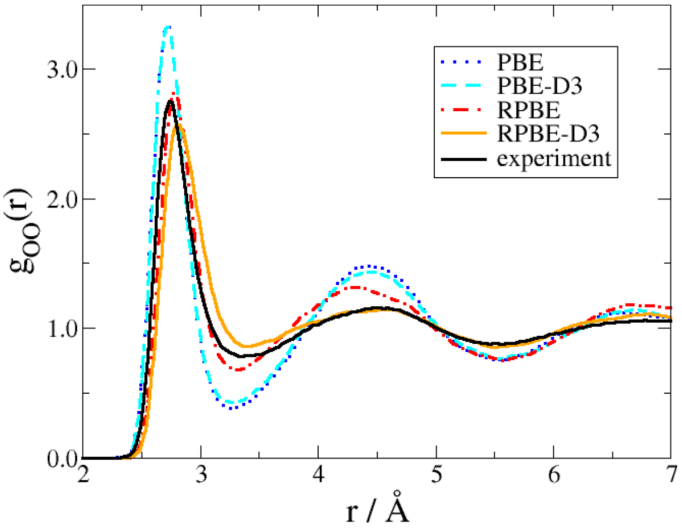

Figure 3.3: The average oxygen distances can be reproduced best with the RPBE+D3 functional. PBE in contrast shows a clear over-structuring, which becomes even worse with PBE+D3. (Taken from Ref. [44].)

in chapter 2.3.2. However a weakness of the PBE functional is its inaccurate description of liquid water. It is well known, that PBE leads to an over structuring of the water network, since the rigidness of hydrogen bonds is overestimated [65, 216, 105]. For my first few publications [57, 158, 58, 59, 107] this point was irrelevant, since the systems were either at UHV conditions or I applied the computational hydrogen electrode approach without any additional explicit solvation. This was possible in the case of halide adsorption on platinum (111), since all of the halides adsorb in dense packed structures on the electrode surface. This results in a passivation of the surface and the bulk water is shifted away from the interface. Therefore the interaction of water with the surface is only weak and the influence of solvation can safely be neglected.

However for the case of (bi)sulfate adsorption on the platinum (111) surface, this assumption is not valid anymore. To get a proper description in this situation, an accurate computation of both liquid bulk water and strongly adsorbed water molecules is inevitable. Therefore the functional of choice was RPBE+D3 [72, 60]. The RPBE functional is optimized for accurate chemisorption energies of small molecules. D3 is an additional van der Waals correction, since London dispersion cannot be captured with local or semi-local functionals. At close distances we used the zero damping method to prevent double-counting of the van der Waals contribution. However zero damping does not meant that the function has

zero damping. It rather means that its damping function decays to zero at short distances. RPBE+D3 reproduces very well the radial distribution function of water (see Fig. 3.3), is succeeds in a benchmark set of 38 water clusters and in a benchmark of 7 crystalline ice clusters [168]. Furthermore it is able to reproduce the correct wetting behavior of water on several metal surfaces [199, 170, 25]. But despite all advantages of the D3 scheme, RPBE+D3 does not describe the screening of the dispersion interaction in bulk metals correctly. Therefore it is required to exclude all metal atoms below the surface from dispersion manually. Then the contribution of dispersion at the solid-liquid interface is captured more correctly.

3.4 Description of liquids

Liquids are computationally the most complicated state of matter. Solids and gases are much easier to tackle. The reason originates in the absence of a long range order of the molecules. Solids have often a certain periodicity, thus they can be characterized by periodic Bloch functions. Molecules of gases on the other hand do hardly interact, therefore it is efficient to calculate them as individual molecules. However both approaches do not work for an accurate description of liquids. A possible way out are reasonable large unit cells or an implicit mean field approach.

Especially for the case of water the situation becomes challenging. One reason is that water molecules have a sizable dipole moment. Therefore they screen the electric field, which is induced by a charged electrode surface. This affects significantly the work function of the electrode and therefore the electrode potential, but even more it can change adsorption energies and geometries as well. Furthermore, not only adsorbed species at the surface are influenced by water, also dissolved ions or molecules become hydrated and their charges gets screened by the water molecules. That is why this effect is fundamentally important for adsorption or desorption processes, since it stabilizes charged objects and enables ionic or polar compounds to be solvable in water easily. Furthermore the water molecules form hydrogen bonds. These strong intermolecular forces raise the complexity of liquid water even more. Thus fast proton transfer becomes possible via the Grotthuss mechanism, and below the freezing point of water, the hydrogen bonded network becomes extensively structured, which can clearly be observed in snow flakes.

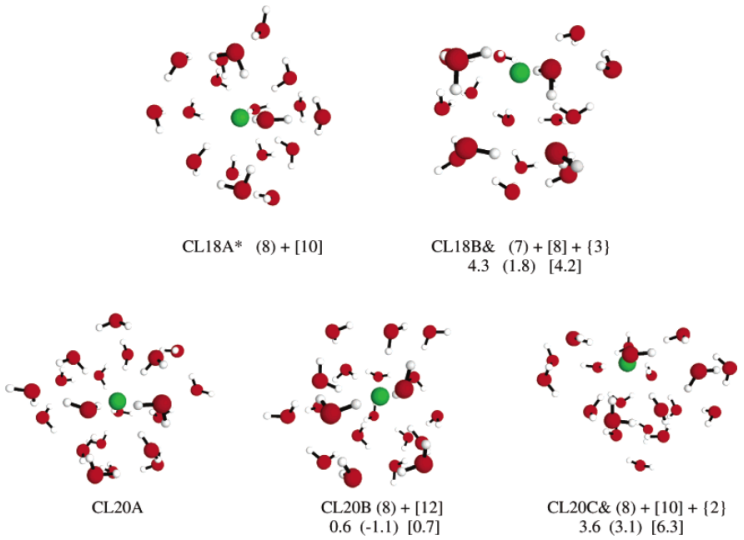

Figure 3.4: Stable structures of chloride, solvated by up to 20 water molecules. The most stable situation is CL18B&, where the solvation shell contains 18 molecules. The & symbol stand for the most stable configurations. (Taken from ref. [87])

3.4.1 Solvation of ions

Solvation of molecules or ions in water is a fundamental process in electrochemistry. It describes the interaction between polar molecules or ions with the solvent. Thereby the solvated species gains a significantly amount of solvation energy, when the water molecules screen its charges. This is in particular important for solvation processes. If the solvation energy of a dissolved molecule is larger than its lattice energy in the bulk crystal, dissolution of the ions or molecules will occur. Thus a larger solvation energy stabilize the dissolved ions better and results in a faster dissolution. However, the amount of water molecules which are necessary to build up a full solvation shell can be rather large. For example, Daniel D. Kemp and Mark S. Gordon recommend to use 18 molecules of water for the complete solvation of a chloride ion [87], however the structure of this large solvation shell is quite diffuse (see fig. 3.4.).

The reverse process of the dissolution is the precipitation of the excess of an solute, or also the adsorption of ions on a surface. These reactions occur when the change of the Gibbs free energy of adsorption reaction $\Delta\gamma$ is negative, therefore it depends amongst others on both the solvation of the ions and the solvation of the solid bulk structure. The change of the Gibbs free energy of the adsorption

of a particular species is given by $\Delta\gamma = \frac{1}{A_{surf}}\left(G_{surf,ads} - G_{surf,0} - n\mu_{ads}\right)$. Here A_{surf} is the surface area of the unit cell, $G_{surf,ads}$ the Gibbs free energy of the adsorbate covered surface, $G_{surf,0}$ the Gibbs free energy of the clean surface, n the amount of adsorbates per unit cell and μ_{ads} the chemical potential of a single adsorbed ion/molecule in the reservoir. For an adsorption process at UHV conditions, entropy effects are typically neglected so that Gibbs free energies are replaced by total energies. However, if more precision is required, both entropy and zero point energy can be considered.

However, to make a more comprehensive analysis at aqueous conditions, the situation becomes significantly more difficult. Because not only the effect of solvation to the system, but also temperature, concentration of the adsorbate species and the pH of the solution play an important role. Therefore total energy calculations like DFT needs to be embedded into a thermodynamic model, or simulations at finite temperature have to be prepared. In this thesis I applied the computational hydrogen electrode (compare chapter 2.7.2).

3.4.2 Explicit/implicit solvent models

To cover the influence of solvation in a DFT calculation, two distinct approaches are possible. Either an explicit solvation by a sufficient amount of additional water molecules or an implicit solvation where the solvent is described by a continuous dielectric medium [37].

A simple method of explicit solvation is to cover the surface with a ice-like, usually one or two layer thick structure of water molecules in a relaxed minimum energy configuration. Such a hexagonal, honeycomb-shaped layer is called bilayer, since it contains both flat adsorbed molecules and upright standing molecules of water. If one of the hydrogen atoms of the upright standing molecules is pointing towards the surface, the layer is a H-down bilayer. If the hydrogen atom points away from the surface it is a H-up bilayer. This method is simple and straightforward, but it provides valuable insights how solvation affects the surface. However it requires that the bilayer structure fits reasonably into the underlaying unit cell. Therefore the surface needs to be rather flat. On stepped surfaces or when low coverages of large ions are attached to the surface, the bilayer concept is not necessarily reliable anymore. Furthermore the bilayer approach is actually not a very realistic model for liquid water on weakly binding, non-wetting electrode/electrolyte interfaces. On the platinum (111) surface, the first water bilayer is at room temperature

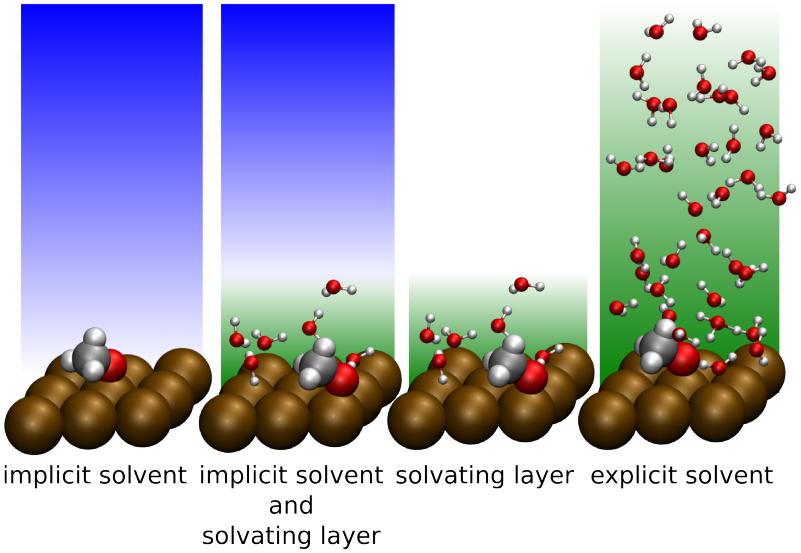

Figure 3.5: Four possible solvation schemes. The left image involve an implicit solvation model, right image represents explicit solvation. In the middle are two examples for either a combination of implicit and explicit solvation and a relaxed water bilayer model. The solvation energy is given for the first three examples by a static minimum energy configuration, whereas the solvation energy of the explicit solvation example is given by thermodynamic sampling.

actually not a crystalline structure at all. Moreover S. Nie *et al.* found out in 2010, that even at a very low temperature, the water molecules do not crystallize in the popular honeycomb structure on platinum (111). Instead they observed much more complicated $\sqrt{37}$ or $\sqrt{39}$ structures, involving pentagons and heptagons in the first adlayer [132].

To overcome all these issues of simple ice-like solvation models, and to get a more comprehensive solvation of the surface, a thermal averaging over many configuration in a large unit cell is necessary. But this is a rather costly procedure [184, 170]. Nevertheless, with increasing computer power this trivial solution became possible in recent years. However, a sufficiently thick water environment needs to be modeled explicitly in an ab-initio molecular dynamic simulation (AIMD) over a timespan of several picoseconds. This approach is expensive, but it provides precise values of various parameter like work function, adsorption energies, solvation energies and more. However a satisfactory functional which is able to describe accurately both water-water and water-metal interaction, is of

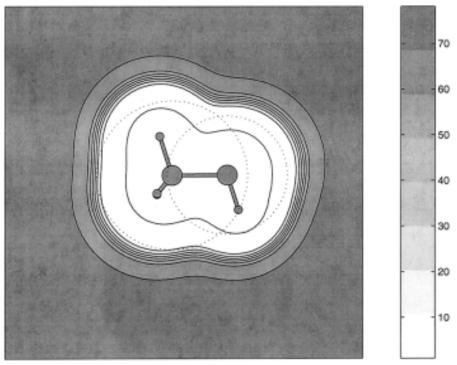

Figure 3.6: Cavity of the implicit solvation scheme around a molecule. The contour plot is a function, which depends on the electronic density of the molecule. The dashed circles denote the spheres composing the cavity. (Taken from Ref. [37].)

fundamental importance. But despite the fast compute clusters which are available nowadays, it is still not reasonable to use this expensive solvation scheme, if a lot of different systems are involved. There a faster alternative should be taken.

In such a case an implicit solvation model can help. Since this is a mean field solvation approach, often no additional water molecules are necessary. The implicit model surrounds all atoms by a region with the uniform dielectric constant of the selected solvent. Therefore an AIMD simulation it not necessary anymore, which reduces the computational cost to a energy minimum calculation. Besides the implicit solvation scheme does not significantly affect the effort of the DFT calculation directly, since it is implemented just as another term in the functional itself. Therefore it does not complicate the self consistent cycles considerable. The effective potential of the DFT calculation (compare eq. 2.6) can be rewritten as

$$v_{eff}(r) = v_{ext}(r) + v_H(r) + v_{xc}(r) + v_{sol}(r)\,. \tag{3.3}$$

However to get accurate results, the implicit solvation scheme needs to attach a cavity around the molecules. Thereby it is important, that the shape of this cavity is computed precisely and therefore an accurate wave function is essential. That is why in all my calculations where implicit solvation was involved, I used a cutoff energy of 700 eV as this guarantees an accurate wave function and cavity. However the implicit model cannot handle all contributions of water completely. If the system involves e.g. strongly adsorbed water molecules or particular hydrogen

bonds, an additional explicit solvation part underneath the implicit solvated region of bulk water is required. However, since these are tightly bond molecules, an energy minimum calculation is still adequate.

4 Results and Discussion

4.1 Change of the work function of platinum electrodes induced by halide adsorption

The following section was published in Beilstein Journal of Nanotechnology 2013, 5, 152-161: F. Gossenberger, T. Roman, K. Forster-Tonigold and A. Groß “Change of the work function of platinum electrodes induced by halide adsorption” [57]. Florian Gossenberger prepared the DFT calculations of halides on platinum in this chapter, whereas Katrin Forster-Tonigold did the DFT calculation of fluorine adsorbed on calcium. The analysis was done by Florian Gossenberger, inspired by a paper about chlorine and iodine adsorption on Cu(111), by Roman et al [159]. Furthermore, Florian wrote the main part of the paper, except the section about fluorine on calcium, which was written by Katrin. Please note that the format of the journal article was modified in order to fit the style and layout of the thesis. Hence a consecutive numbering of figures and references for the whole thesis was applied as well.

4.1.1 Abstract

The properties of a halogen-covered platinum(111) surface have been studied by using density functional theory (DFT), because halides are often present at

electrochemical electrode/electrolyte interfaces. We focused in particular on the halogen-induced work function change as a function of the coverage of fluorine, chlorine, bromine and iodine. For electronegative adsorbates, an adsorption-induced increase of the work function is usually expected, yet we find a decrease of the work function for Cl, Br and I, which is most prominent at a coverage of approximately 0.25 ML. This coverage-dependent behavior can be explained by assuming a combination of charge transfer and polarization effects on the adsorbate layer. The results are contrasted to the adsorption of fluorine on calcium, a system in which a decrease in the work function is also observed despite a large charge transfer to the halogen adatom.

4.1.2 Introduction

In electrochemistry, processes at the interface between an electron conductor, the electrode, and an ion conductor, the electrolyte, are studied [94]. In order to be charge neutral, the electrolyte contains equal amounts of anions and cations. In aqueous electrolytes, protons acting as cations are always present [155] whereas halides are often chosen as anions. The contact of a particular solvent with an electrode surface can lead to a rather complex situation at the electrode surface [185, 161]. The characteristics of the solvent significantly affects processes such as adsorption and desorption. Because of the strong interaction of halogen atoms with metal electrodes, the metal electrodes typically become halogen-covered through specific adsorption. These adsorbed anions are not only part of the electrochemical double layer, in general they also change the work function of the electrode, which is directly related to the electrode potential [200]. Furthermore, they also affect the chemical properties of the electrodes [64].

In spite of the importance of the specific adsorption of anions in electrochemistry, atomistic details of the role of anions in surface electrochemistry are still poorly understood [201]. Here, surface science studies focusing on the change of the properties of metal surfaces upon halide adsorption can help to elucidate the role of anionic specific adsorption at electrode/electrolyte interfaces, in particular with respect to the adsorption-induced change of the work function. It is known that the work function is strongly influenced by the adsorption of ions, which can lead to both an increase and a decrease of the work function [125, 159, 128, 127, 102, 146, 12, 10, 9, 11]. In a previous study, we have addressed the adsorption of iodine and chlorine on Cu(111) [159] by using periodic density functional theory (DFT) calculations. Whereas chlorine causes the

expected increase of the work function upon adsorption of an electronegative adsorbate, iodine leads to a surprising decrease of the work function for coverages up to approximately 0.4 ML. By analyzing the underlying electronic structure, we were able to show that this behavior can be explained through a combination of charge transfer and polarization effects of the adsorbate layer.

We have now extended this previous study by considering the adsorption of fluorine, chlorine, bromine and iodine on Pt(111) in order to check whether the findings for halogen adsorption on Cu(111) are also valid for the technologically important electrode material platinum. It has already been observed experimentally [33, 15, 84] as well as theoretically [11, 127, 146] that the adsorption of chlorine, bromine and iodine on Pt(111) leads to an unexpected decrease of the work function. Based on calculations for several adsorbates on tungsten surfaces, Leung, Kao and Su pointed out that it is possible to relate the electronegativity scale to the direction of the charge transfer but not necessarily to the induced work function change. It has also been shown that the formation of halogen oxides at the surface of a metal oxide leads to a decrease in the work function [73]. The problem of the unexpected decrease of the work function was also tackled by Michaelides et al. [125] for a system of nitrogen adsorbed on a tungsten (100) surface. They showed that the decrease of the work function depends strongly on the length of the chemisorption bond. If the adatom is located close to the surface, it is in the region of the overspill electron density of the metal. This leads to an area of electron depletion far from the surface, and in combination with an electron buildup in the area around the adsorbed ion, to a decrease of the work function.

In this paper we present a detailed study of the halogen-induced change of the work function on Pt(111) as a function of the halogen coverage, which has still been missing. We will show that the observed decrease of the work function upon the adsorption of chlorine, bromine and iodine on Pt(111) at low coverages can be explained by the strong polarization of the adsorbed halogen atoms, as in the case of I/Cu(111) [159]. We contrast these results with findings obtained for fluorine adsorption on calcium, for which an adsorption-induced decrease of the work function is also observed. However, due to the particular geometric conditions in this system, the spillout mechanism [99, 125] is operative.

4.1.3 Methods

For the following calculations, the periodic density functional theory (DFT) program Vienna Ab initio Simulation Package (VASP) was used. The exchange and correlation energy was calculated by using the generalized gradient approximation (GGA) with the PBE functional, developed by Perdew, Burke and Ernzerhof [149]. This functional is widely used, as it has been shown to give reliable results in terms of atomization energy, chemisorption energies [143, 72], work function changes [111], and good estimates of bulk properties of metals [1]. Hybrid functionals are not necessarily improvements to PBE; for example they do not yield a satisfactory description of the characteristics of transition metals [1].

To describe the ionic cores of the atoms, we used the projector augmented wave potentials (PAW) constructed by Kresse and Joubert [97]. The electronic wave functions were expanded in a plane wave basis set up to an energy cutoff of 400 eV. For the calculations, a periodic slab with a thickness of 7 atomic layers and 4×4 lateral periodicity was chosen. All calculations were done by using a symmetric setup of the slab, i.e., the halogen atoms were adsorbed on both sides of the slab, the middle three layers of the slab were kept fixed and the outermost two layers of both sides of the slab together with the adatoms were relaxed. Thus no dipole correction was necessary in order to derive the work function of the surface terminations. The unit cell was computed with a gamma-centered $4\times4\times1$ k-point mesh.

The optimized lattice constant for platinum was found to be $a = 3.98$ Å, which is only 1.48% larger than the standard experimental value [89]. For low coverages the halogens iodine, bromine and chlorine adsorb most stably at the fcc threefold hollowsite position on a platinum (111) surface. Since the hcp threefold-hollow position is also quite stable, the halogens were ordered in symmetric patterns on the surface with the highest possible nearest neighbor distance to other adsorbed atoms in hcp and fcc positions. The threefold-hollow adsorption positions are considered as the most probable adsorption sites for halogens on metals [128, 77, 12, 159]. In this manner, six different coverages – 1/16 ML, 2/16 ML, 3/16 ML, 4/16 ML, 6/16 ML and 8/16 ML – were created, which are illustrated in Figure 4.1. The structures of iodine, bromine and chlorine were relaxed completely.

Interestingly enough, fluorine atoms adsorb more stably at the on-top position of platinum. At this position, the average distance to the topmost surface layer is larger than on the threefold-hollow sites. Since we are interested in getting trends among the halogen atoms in order to understand and predict adsorption

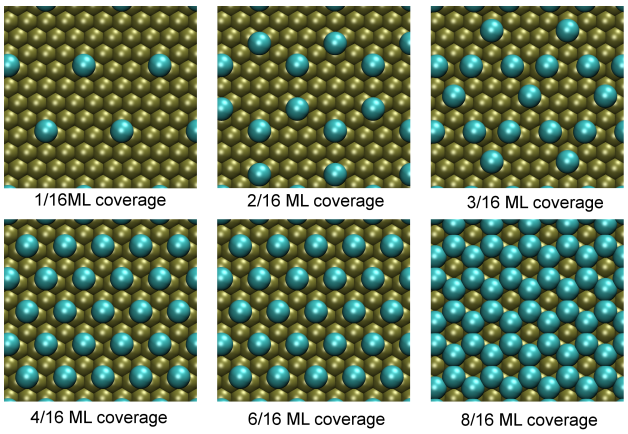

Figure 4.1: The figures show the relaxed structures of different coverages of chlorine on a Pt(111) surface.

processes, we kept the fluorine in the threefold-hollow site positions, but allowed for vertical relaxation, which made a better comparison with the results for the chlorine, bromine and iodine adsorption structures possible.

4.1.4 Results and Discussion

Of central importance for this particular work is the determination of the change of the work function as a function of the halogen coverage. In periodic slab calculations, the work function is given by the difference between the Fermi energy and the value of the one-electron potential in vacuum. Vacuum is reached when the potential does not change anymore with increasing distance from the surface.

Figure 4.2 shows the work function of halogen-covered Pt(111) as a function of the halogen coverage. For clean Pt(111), the calculations yield a value of 5.71 eV. Various experimental measurements in the last decades do not agree well with each other. They are in the range of 5.6 eV to 6.1 eV [27, 42, 136, 134, 135, 84, 172, 29]. The presence of fluorine on Pt(111) always increases the work function, which is qualitatively consistent with what one expects from a dipole involving a negative charge on the adsorbate. The adsorption of chlorine, bromine or iodine on a platinum (111) surface reduces the work function at low coverages. While the trend reverses at 0.25 ML, $\Delta\Phi$ becomes positive not until the coverage reaches half a monolayer. The experimental trends [33, 15, 84] as well as theoretical values by Migani et al. [128] agree with the calculated results.

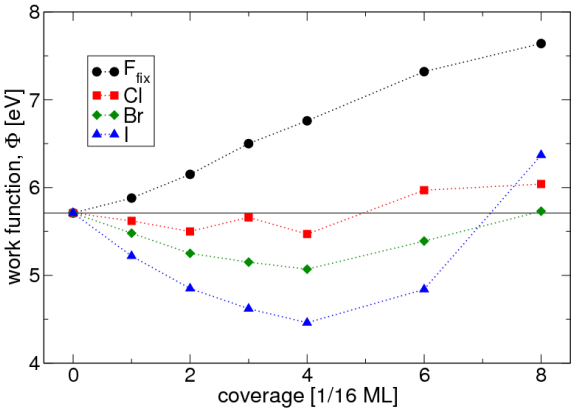

Figure 4.2: Calculated change of the work function vs coverage for the adsorption of fluorine, chlorine, bromine and iodine on Pt(111). The high value for the 0.5 ML calculation of iodine is due to a double layer structure of the adsorbates, caused by the larger size of iodine atoms.

Aside from the sign of the work function change, the dependence of $\Delta\Phi$ on the halogen coverage is another aspect that needs to be clarified. In a simple model, one may completely neglect the interaction between the adsorbates. In this case, a linear trend $\Delta\Phi(\theta) \propto -\theta\Delta\mu$ would be expected, where θ is the surface coverage and $\Delta\mu$ is the change in the surface dipole moment brought about by the adsorption of a halogen atom. Obviously, this model is applicable only at low coverages in Figure 4.2. In a more advanced model, the electrostatic interaction between adjacent dipoles is taken into account by assuming that the mutual repulsion of the dipoles leads to a decrease in the polarity of the halogen-metal bond. The term $\Delta\mu$ thus becomes dependent on the halogen coverage, which causes a saturation of $\Delta\Phi$ at high coverages. However, this does not explain the observed non-monotonic behavior of the work function change and so a more comprehensive explanation is needed.

In general, an adsorbate layer that involves charge transfer in the adsorption reaction can produce an observable change in the work function of the metal surface since electrons, in leaving the metal surface, will have to pass through the resulting interface dipole layer. Depending on the orientation of the dipole, this can either make removing electrons easier or harder. More precisely, the connection between work function change and surface dipole moment change is given by

$$\Delta\Phi = -\frac{e}{\epsilon_0}(\mu_z - \mu_{z,0}) = -\frac{e}{\epsilon_0}\Delta\mu, \tag{4.1}$$

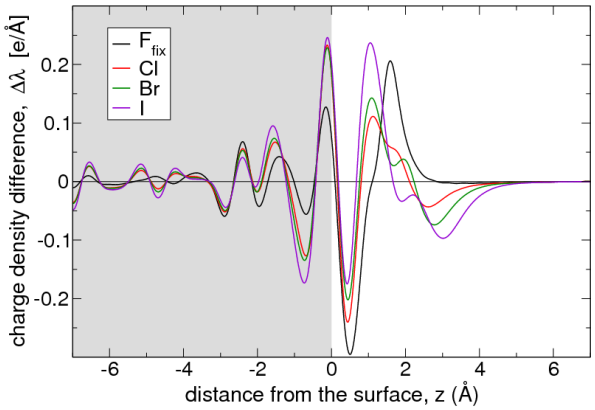

Figure 4.3: Charge density difference $\Delta\lambda(z)$ for the adsorption of fluorine, chlorine, bromine, and iodine on Pt(111) at the fcc hollow position for a coverage of 1/16 ML. The subsurface region corresponds to the gray-shaded area at $z < 0$.

where $\mu_{z,0}$ is the surface-normal dipole moment per unit area of the clean surface, μ_z is the surface-normal dipole moment per unit area for the adsorbate-covered surface. A positive value of μ has traditionally been assigned to a dipole pointing away from the bulk, which leads to a decrease of the work function ($\Delta\Phi < 0$). Conversely, a negative μ points into the bulk and increases the work function ($\Delta\Phi > 0$).

The surface dipole moment changes when the electron density close to the surface becomes redistributed upon bond formation. The most straight-forward description of this redistribution is through the electron density difference that is given by the difference of the electron density of the interacting system with the total electron density of the non-interacting metal slab and halogen layer at the same atomic positions, $\rho_{\text{diff}} = \rho_{\text{Hal+Pt}} - (\rho_{\text{Hal}} + \rho_{\text{Pt}})$. The electron density difference profile $\Delta\lambda(z)$ along the z direction corresponds to the lateral sum of the electron density difference in the x and y directions,

$$\Delta\lambda = \frac{1}{N} \iint_{\text{cell}} \rho_{\text{diff}} \, dx \, dy, \tag{4.2}$$

where N is the number of halogen atoms adsorbed on one side of the slab per unit cell. The $\Delta\lambda$ profiles for a coverage of 1/16 ML of the four halogens are shown in Figure 4.3. The shape of the diagrams for higher coverages look similar. The profiles illustrate how the electron density is reorganized along the z direction

when the adatoms adsorb. The gray area on the left hand side denotes the metal slab. The topmost metal atoms are centered at z = 0 Å. The electron density difference profile shows a significant electron depletion far from the surface for the case of chlorine, bromine and iodine, followed by an electron buildup close to the surface, and oscillations in the metal. In the case of fluorine, there is just an electron buildup around the fluorine atom, followed by oscillations into the bulk. This electron buildup around the fluorine atom indicates an ionic state. Fluorine is partially constrained to remain at the threefold-hollow sites, where the average distance from the center of the adsorbates to the topmost surface layer is smaller than for fluorine adsorbed at the on-top position. Calculations for F atoms at the most stable adsorption site may give slightly different results in charge transfer and dipole moments.

In the next step, the resulting surface dipole moment change $\Delta\mu_N$ can be determined by analyzing $\Delta\lambda$, as in [159] for the adsorption of iodine and chlorine on Cu(111). The N indicates that this is the total surface dipole moment of N atoms adsorbed in the unit cell. The dipole moment change due to the adsorption process can be calculated by integration of $\Delta\lambda_N(z) = N\Delta\lambda(z)$ along the z direction, perpendicular to the surface,

$$\Delta\mu_N = -\int_{\text{bulk}}^{\text{vac}} z\Delta\lambda_N(z)\, dz \tag{4.3}$$

where the negative sign is introduced because positive regions of $\Delta\lambda_N$ (i.e., electron buildup) are in fact negatively charged. The integration runs from the central layer of the platinum slab to the middle of the vacuum. Figure 4.4 shows the good correlation between the calculated work function and the dipole moment derived from the charge distribution, which verifies the assumptions that underlie Equation 4.3.

Since $\Delta\lambda$ of the fluorine-covered platinum slab shows for all coverage values the structure of an electron buildup far from the surface, followed by an electron depletion close to the surface, the dipole moment on each face of the slab becomes more negative as a function of the coverage, which is consistent with a work function increase. For the other three halogens, the electron density difference profile looks more complicated. There is an electron depletion far from the surface, followed by an electron buildup. This structure is sufficiently strong to invert the dipole moment, so that $\Delta\mu_N$ changes sign as a function of the coverage.

It has been suggested that adsorbates that are located rather close to a sur-

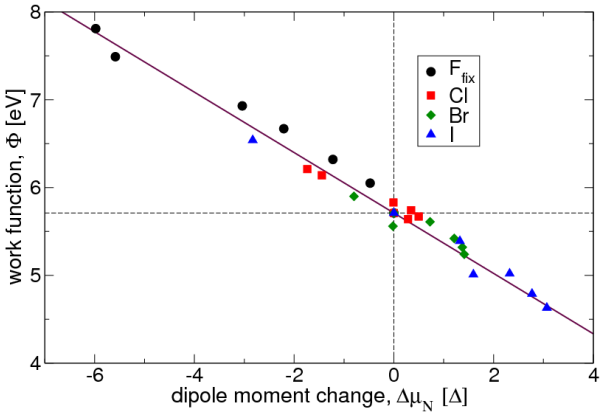

Figure 4.4: Calculated work function versus dipole moment. The solid line corresponds to the expectation according to Equation 4.1.

face can decrease the electron spillout at the surface. This can cause unexpected changes of the work function, such as the decrease of the work function observed for N on the W(100) surface [125] or the small dipole moment for O on Al(111) [99]. However, the area of electron depletion for chlorine, bromine and iodine is approximately 2.5-4.0 Å away from the center of the topmost platinum atoms, far beyond the region of a sizable electron spillout for the uncovered surface. This electron density shift rather corresponds to a redistribution of the electron density in the adatom layer, which can be associated with a covalent character of the chemisorption bond. This rearrangement is particularly strong for the adsorption of iodine, and slightly weaker for bromine and chlorine. The character of the chemisorption bond between iodine and platinum was discussed in the past [11, 128] and conflicting results in terms of the charge of the adatom were presented.

In this study, we find that the charge buildup between the iodine and the Pt surface indicates the presence of a covalent bond. Similar conclusions have been found, for example for the adsorption of I on Cu [159] or Cl on Au [12]. Furthermore, in a chronocoulometric study [49] it was found that the adsorbed species is basically a neutral chlorine atom which agrees nicely with our findings. Fluorine, on the other hand, tends to adsorb to the Pt(111) surface mainly in the ionic form.

Coverage trends

Our calculations confirm the experimental observations [33, 15, 84] of a work function minimum as a function of the halogen coverage. Several mechanisms have been proposed to explain its occurrence. For cationic adsorbates, the subsequent increase of Φ beyond the work function minimum was attributed to a reduction of the ionicity of the cationic adsorbate [20]. This explanation, however, does not apply to the halogen adsorption considered here as we still find no indication of cationic adsorption.

The work function minimum has also been explained through differences in site occupancies that occur as halogen coverage increases. Subsurface penetration followed by surface adsorption was one of the possibilities considered in explaining the work function minimum for chlorine on platinum [33]. This was based on the assumption that subsurface penetration and surface adsorption lead to opposite dipole moments at the surface. In contrast, for iodine on platinum, an adsorption site effect was suggested under the assumption that threefold-site adsorption decreases the work function, while adding iodine to top sites increases it [84]. As the coverage increases, more top sites get occupied by iodine, which leads to the increase in Φ beyond the minimum. Still, the change of the surface work function remained negative over the entire coverage range that was considered.

A more recent computational study has shown that the adsorption of isolated iodine atoms at the hollow or top sites both lead to $\Delta\Phi < 0$, although the decrease in the work function is larger for the adsorption of iodine at the hollow site [11]. Another explanation for the minimum of the work function was proposed, namely changes in the polarization of the metal substrate. The authors found that the polarization in the platinum substrate that is induced by the presence of the iodine anion adsorbate is reduced with increasing coverage, hence explaining the nonmonotonic behavior in $\Delta\Phi$.

While changing site occupancy with increasing coverage can and will lead to observable changes in the work function, in this study we focus on changes of the work function that are caused by effects that are primarily electronic in nature, i.e., that are not due to changes in the adsorption or absorption site. Hence a deeper analysis of charge transfer, internal redistribution of charge in the metal substrate, and redistribution of charge on the halogen adatoms is needed. To analyze the surface dipole moments in detail, we use the total surface dipole moment per unit cell normalized to the number of adatoms to define the dipole

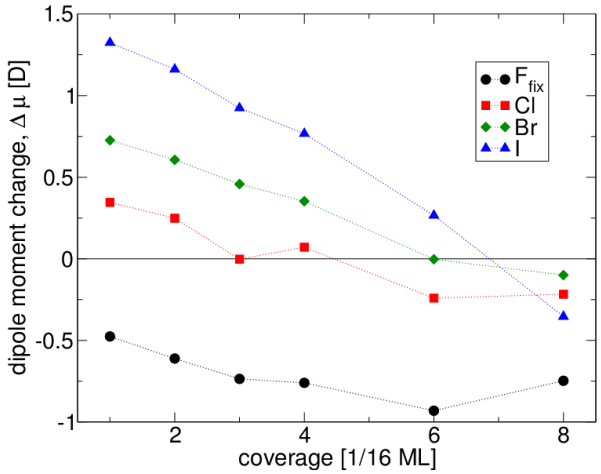

Figure 4.5: Calculated normalized dipole moment as a function of the coverage of fluorine, chlorine, bromine and iodine on Pt(111).

moment change created per adsorbed atom,

$$\Delta\mu = \frac{\Delta\mu_N}{N}. \tag{4.4}$$

The normalized dipole moments are shown in Figure 4.5. The plots are nowhere flat, suggesting the presence of considerable neighboring adatom interactions even at the lowest coverages. There is also a clear tendency for the dipole moment induced by the adsorption of a single halogen atom to be reduced as the concentration of adatoms increases at the Pt surface. Note that the 0.5 ML coverage of iodine is so closely packed that the repulsion of the electron shells induces a two-layer structure of the adsorbate layer. Every second iodine atom becomes a part of a second adsorbate layer, which is positioned about 1.7 Å farther from the surface than the first layer of iodine atoms.

Looking at the charge transfer as a function of the coverage is useful to understand the negative slopes of $\Delta\mu$ for the adsorption of halogens. Quantifying charge transfer between atoms however always involves a more or less ambivalent choice as far as associating the electron density to a particular atom is concerned. We have therefore considered two limits: a maximum-charge-transfer picture, and a zero-charge-transfer picture of halogen adsorption on platinum.

The maximum charge transfer is obtained by assuming that the complete electron buildup between an adatom and the surface is always counted to the adsorbate. In practice, this is done by determining the plane $z = z_q$ between the metal and

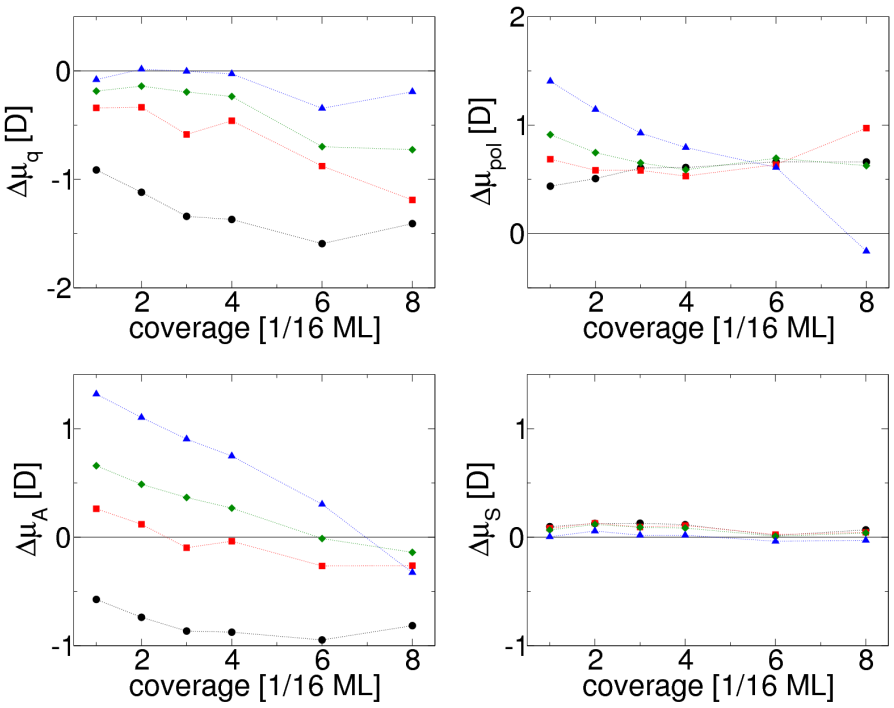

Figure 4.6: Contributions to the total dipole moment change $\Delta\mu$ coverage according to Equation 4.6 and Equation 4.7 as a function of halogen coverage. The term $\Delta\mu_q$ describes the purely charge transfer induced dipole moment and $\Delta\mu_{\text{pol}}$ the polarization induced dipole moment; $\Delta\mu_A$ shows the effect of the adsorbate layer on the total dipole moment and $\Delta\mu_S$ indicates substrate effects. The color code denoting the different halogen atoms is the same as used in the previous figures.

the adatom that maximizes the area under $\Delta\lambda(z)$ at the halogen side. The charge transfer from the metal surface to the adatoms gives rise to a change of the dipole moment, $\Delta\mu_q$. By using a simple model that assumes charge transfer from the topmost Pt layer to the halogen adlayer, the contribution of the electron transfer to the surface dipole moment can be quantified,

$$\Delta\mu_q = -\bar{z}_X \int_{z_q}^{\text{vac}} \Delta\lambda(z)\, dz, \tag{4.5}$$

where $\bar{z}_X$ is the average distance of the halogen adatoms from the metal surface. We combine all other parts contributing to the total dipole moment in the term $\Delta\mu_{\text{pol}}$, because it involves polarization effects in the metal and in the adlayer. The combination of both contributions leads to the total dipole moment change,

$$\Delta\mu = \Delta\mu_q + \Delta\mu_{\text{pol}}. \tag{4.6}$$

These contributions are plotted in Figure 4.6a and Figure 4.6b, respectively. The effect of the charge transfer $\Delta\mu_q$ to the surface dipole is nearly zero for iodine. For fluorine, however, charge transfer plays a significant role, which can be expected since it is more electronegative than the other halogens, as also reported by Migani et al. [128]. Moreover, the negative dipole moment change for the adsorption of fluorine decreases even more with increasing coverage, which is due to the fact that the adsorption distance and charge transfer to the F adatoms increase with increasing coverage.

The results also suggest that higher surface concentrations of adatoms decrease the dipole moment change per adatom through mutual depolarization. This effect is most pronounced for iodine, as well as for a low-coverage adsorption of bromine and chlorine, but not for fluorine because of the low polarizability of small atoms. Besides the repulsion of the dipoles, the electron shells of adsorbed atoms at a higher coverage start to repel.

Another interesting question concerns the importance of the electron density oscillations in the subsurface, as shown in Figure 4.3. It might be speculated that these oscillations could be responsible for the significant polarization part, $\Delta\mu_{\text{pol}}$ of the total dipole moment $\Delta\mu$. To answer this question, we have divided $\Delta\lambda$ into two parts, one representing the dipole moment change due to polarization in the adsorbate layer and the other part representing the dipole moment change due

to polarization in the substrate,

$$\Delta\mu = \Delta\mu_A + \Delta\mu_S. \tag{4.7}$$

This zero-charge transfer picture for breaking down polarization is especially effective for iodine adsorption on platinum. Such a distinction between pure substrate and adsorbate contributions is again an arbitrary choice. In order to obtain trends, the integration was started from the point z_0, at which the unit cell is divided exactly into the charge neutral part of the adlayer and the charge neutral part of the platinum slab, defined by the condition

$$\int_{z_0}^{\text{vac}} \Delta\lambda(z)\, dz = 0 \tag{4.8}$$

For this choice, the analogous integral on the metal side is also zero due to the overall charge neutrality of the supercell. It is then possible to estimate the surface dipole moment μ_S and the adsorbate dipole moment μ_A by using

$$\Delta\mu_S = \int_{\text{bulk}}^{z_0} z\Delta\lambda(z)\, dz \tag{4.9}$$

and

$$\Delta\mu_A = \int_{z_0}^{\text{vac}} z\Delta\lambda(z)\, dz. \tag{4.10}$$

We briefly summarize the difference in the integration limits z_q and z_0 of Equation 4.5 and Equation 4.9, respectively: These equations have the purpose of dividing the unit cell into two parts, but it is not clear where exactly the adatom ends and where the platinum begins or vice versa. The two integration limits mark special points in the graph of $\Delta\lambda$. The limit z_q divides the unit cell at the point of maximum charge at the adatom, in contrast to z_0 which divides at the point of zero charge at the adatom.

The adsorbate and the substrate dipole moments, which are plotted in Figure 4.6c and 4.6d, respectively, indicate that the contribution of the change of the metal substrate dipole moment $\Delta\mu_S$ to the total change of the dipole moment $\Delta\mu$ is minor compared with the impact of adsorbate polarization $\Delta\mu_A$, which affects the total dipole moment change quite dramatically. This also means that our analysis does not support the view [11] that substrate polarization plays an important role in explaining the halogen-induced work function decrease.

Additionally, it is noticeable that the decrease in the total change of the dipole

moment in the case of iodine and chlorine at around 0.25 ML is much more significant on platinum compared with the total change of the dipole moment of copper [159]. The work function of the copper surface is about 1 eV smaller, thus the charge transfer is larger from copper than from the platinum surface to the halogen adatom. It is for this reason that the adsorption of chlorine on copper does not exhibit a work function minimum with increasing adsorption coverage [159, 148], similar to the work function plot of F on Pt in the current study.

Fluorine on calcium

We have shown that the strong polarizability of large atoms such as iodine leads to a considerable buildup of charge in the adatom-surface bonding regions, which is consistent with covalent bonding, and an accompanying electron depletion region far from the surface which creates a net dipole on the adatom that in turn promotes a decrease in the work function. Here we show that the adsorption of fluorine can also decrease the work function of a metal surface, namely calcium, but through a different mechanism. Calcium is considered to be an attractive electrode material in electrochemical energy storage because of its low electronegativity, earth abundance, and low cost [88]. Fluorine adsorbs stably at a threefold hollow site on calcium, which is a metal with fcc structure and a calculated lattice constant that is 39% larger than that of platinum. At its equilibrium adsorption position, fluorine is only 0.73 Å from the topmost layer of Ca atoms. In contrast, iodine adsorbs 2.07 Å from the platinum surface.

In Figure 4.7, we compare two systems, in which halogen adsorption decreases the work function of the metal substrate. The left panel shows the adsorption of iodine on Pt(111) at a coverage of 1/9 ML. The right panel shows fluorine adsorption on Ca(111) at a coverage of 1/4 ML. This yields similar absolute values for the coverage per area for the two systems given the stark difference between the lattice constants of Pt and Ca. At these adsorption coverages, iodine reduces the platinum work function by 0.79 eV, while fluorine reduces the calcium work function by 0.20 eV.

Figure 4.7 shows that halogen adsorption can create a surface dipole that reduces the work function in two very distinct mechanisms, namely adatom polarization and spillout depletion. Iodine on platinum is characterized by a negligible charge transfer, covalent bonding, and polarization on the adatom. There is no evidence for a dominantly ionic bond for I/Pt(111) reported in [11]. Fluorine adsorption on calcium on the other hand is characterized by a large charge transfer

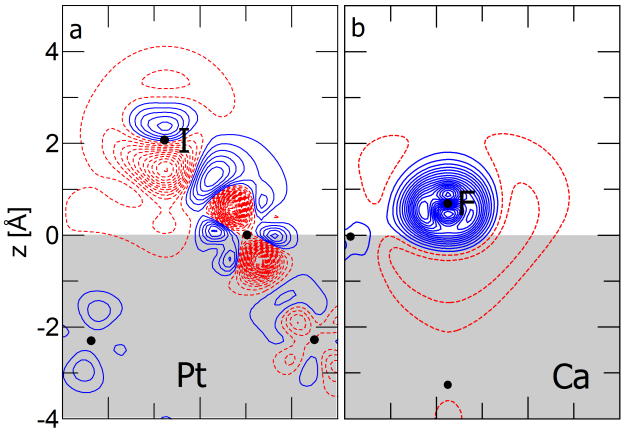

Figure 4.7: Cross sections of electron density difference $\rho_{\text{diff}}(\mathbf{r})$ at the surface. Solid-blue (dashed-red) contours denote regions of electron buildup (depletion). The interval between contours of constant electron density is 0.01 electrons/Å^3. The region of the metal slab is shaded gray as a visual aid.

to the adatom with negligible polarization, creating a system, which is comprised of a negative ion enveloped by electron depletion. Since fluorine is adsorbed very close to the surface, it is embedded within the electron spillout region of calcium. The depletion of electron density in the spillout region not only reduces the effect of the strongly negative fluorine on the net dipole, but even overcompensates it, resulting in a decrease of the work function.

4.1.5 Conclusion

The change of the work function induced by halogen adsorption on Pt(111) as a function of the coverage was studied by electronic structure calculations. In general, because of their electronegativity, the adsorption of halogens is associated with a charge transfer from the metal substrate to the adsorbate layer. In the case of fluorine adsorption, this leads to the expected increase in the work function. However, for chlorine, bromine and iodine adsorption on Pt(111), the charge transfer effect is overcompensated by a significant polarization of the adsorbate, causing a work function decrease. The decreasing change of the dipole moment per adatom with an increasing adsorption coverage leads to a maximum in the total surface dipole moment and a minimum in the work function at a coverage of approximately 0.25 ML. The mutual depolarization within the adsorbate layer contributes to the eventual work function increase.

The anomalous work function change on platinum is large because of the high work function of clean platinum, which favors only a small electron transfer to the halogen adatoms compared with other metals. Therefore, polarization effects that reverse the dipole moment attributed to charge transfer are more pronounced than on metals with smaller work functions such as copper.

Furthermore, we showed that fluorine adsorption can also lead to an anomalous work function decrease, but through a different mechanism. On calcium, fluorine is adsorbed close to the surface because of the large spacing between the calcium atoms. This causes a depletion of the electron density in the spillout region, which results in a decrease of the work function.

4.1.6 Acknowledgements

This research has been supported by the German Science Foundation (DFG) through the research unit FOR 1376 (DFG contract GR 1503/21-1). Computer time has been provided by the BW-Grid of the federal state of Baden-Württemberg and by a computer cluster financed through the stimulus programme “Electrochemistry for Electromobility” of the German Ministry of Education and Science (BMBF).

4.2 Halide adsorption on close-packed metal electrodes

Reprinted with permission from Physical Chemistry Chemical Physics.

The section extends chapter 1, which is about halogen adsorption on platinum (111). Here we investigated the adsorption of halides on ten common fcc metals (Ca, Sr, Ni, Pd, Pt, Cu, Ag, Au, Al, and Pb). The paper was published in Physical Chemistry Chemical Physics 2014, 16, 13630–13634: T. Roman, F. Gossenberger K. Forster-Tonigold and A. Groß "Halide adsorption on close-packed metal electrodes" [158]. Katrin Forster-Tonigold prepared the DFT calculations on Calcium and Strontium. Florian Gossenberger did all remaining DFT calculations and contributed to the analysis, which was done in collaboration with Tanglaw Roman. The paper and figures were realized by Tanglaw Roman. Please note that the format of the journal article was modified in order to fit the style and layout of the thesis. Hence a consecutive numbering of figures and references for the whole thesis was applied as well.

4.2.1 Abstract

Two mechanisms have been cited as the reason for unexpected work function decrease upon adsorption of electronegative adatoms: electron spillout depletion [Michaelides *et al., Phys. Rev. Lett.*, 2003, **90**, 246103] and polarization of the adatom [Roman *et al., Phys. Rev. Lett.*, 2013, **110**, 156804]. We attempt to bridge the two pictures in this work. Work function changes due to the adsorption of halides on (111) surfaces of fcc metals (Ca, Sr, Ni, Pd, Pt, Cu, Ag, Au, Al and Pb) were studied using periodic density functional theory. The two mechanisms were found to be clearly independent of each other because of the opposite factors that lead to the work function decrease, and are therefore easy to distinguish. A more general picture of interpreting bond ionicity based on observed work function changes is discussed.

4.2.2 Introduction

Electrochemical processes typically occur at the interface between an electron conductor, the electrode, and an ion conductor, the electrolyte [94]. Therefore the structure of the electrode/electrolyte interface is of strong interest in electrochemistry. At this interface, an electric double layer is formed, consisting of an electronic charge on the electrode and a corresponding ionic counter charge in the electrolyte. Of particular importance is the adsorption of anions on metal electrodes [116, 201]. Often they adsorb specifically, i.e., they form chemical bonds with the metal surface. These adsorbed anions not only affect the chemical properties of electrodes [64], but in general they also change the work function of the electrode, which is directly related to the electrode potential [200].

As part of a systematic effort to model electrode/electrolyte interfaces using first-principles [184, 185, 108, 161], we have recently addressed the work function change induced by the adsorption of halides on Cu(111) [159] and on Pt(111) and Ca(111) [57]. Cu and Pt are metals well-studied in electrochemistry [23, 119], whereas calcium is considered to be an attractive electrode material in electrochemical energy storage because of its low electronegativity, earth abundance, and low cost [88]. The equilibrium coverage of halides as a function of the electrode potential using a simple thermodynamical model was also investigated [58, 148].

An adsorbed halogen layer is expected to produce an observable increase in the work function Φ of the metal surface since electrons, on leaving the metal surface, will have to pass through the resulting interface dipole layer comprised of a positively-charged metal substrate and a negatively-charged halogen layer. However, it has already been observed experimentally [33, 15, 84] as well as theoretically [11, 127, 146] that the adsorption of chlorine, bromine and iodine on metal surfaces can lead to an unexpected decrease of the work function.

In our previous work [159, 57], we have identified two different mechanisms that can explain the unexpected negative work function change if a halogen is adsorbed on a metal substrate: polarization of the adatom [159], and reduction in the surface spillout electron density [125, 57]. In the former mechanism, the strong polarizability of large atoms like iodine leads to a considerable charge accumulation in the adatom–surface bonding regions, consistent with covalent bonding, and an accompanying charge depletion region far from the surface. This creates a dipole on the adatom that in turn promotes a decrease in the work function. Fluorine adsorption on calcium, on the other hand, is characterized by a large

charge transfer to the adatom with negligible polarization, creating a system comprised of a negative ion enveloped by an electron density depletion region. Since fluorine is adsorbed very close (ca. 0.7 Å) to the surface, it is embedded within the electron spillout region of calcium. The depletion of electron density in the spillout region not only reduces the effect of the negatively-charged fluorine on the overall dipole, but overcompensates it, resulting in a work function decrease.

A complete picture of the factors leading to a decrease in the work function is however still missing. It is for instance not clear as to which particular circumstances would make one specific mechanism dominant, or perhaps in which situations would these two independent mechanisms contribute on an equal footing to the decrease in the work function. In the present study we have therefore extended our previous work by systematically studying the adsorption properties of halogens at (111) surfaces of several fcc metals (Ca, Sr, Ni, Pd, Pt, Cu, Ag, Au, Al, and Pb). We will show that halogen atoms can lower the work function on most of the considered metals, and we will discuss the mechanisms leading to this still unexpected work function decrease.

4.2.3 Computational details

Periodic DFT calculations that employ the exchange-correlation functional of Perdew, Burke, and Ernzerhof (PBE) [149] were done using the Vienna ab initio simulation package (VASP) [96]. Electron-core interactions were accounted for by the projector augmented wave method [18, 97]. The electronic one-particle wavefunctions were expanded in a plane-wave basis set up to an energy cutoff of 500 eV. The metal substrates were represented by slabs of seven atomic layers, of which the inner three layers were kept fixed in the bulk position during geometry optimizations while the rest of the system was allowed to relax. Halogen atoms were placed symmetrically on both sides of the slab.

For these systems, it is possible to quantify work function changes brought about by adatoms through two methods: straightforwardly from the local potential of electrons, and from the dipole moment (multiplied by a factor $-e/\epsilon_0$) based on changes in electronic density.

We have already shown and discussed in detail that these two methods lead to in principle identical findings [57]. In this study we use only the former, in which the work function is obtained from the difference between the Fermi energy and

Table 4.1: Computed lattice constants a, work function Φ of the clean (111) surface, and halogen relative and absolute coverages (Θ_{rel} and Θ_{abs}, respectively) on (111) surfaces of fcc metals used in this study

	a (Å)	Φ (eV)	Θ_{rel} (ML)	Θ_{abs} (1/Å^2)
Ni	3.524	5.03	1/9	2.067×10^{-2}
Cu	3.636	4.77	1/9	1.941×10^{-2}
Pd	3.964	5.23	1/9	1.633×10^{-2}
Pt	3.978	5.71	1/9	1.622×10^{-2}
Al	4.051	4.04	1/9	1.564×10^{-2}
Ag	4.164	4.35	1/9	1.480×10^{-2}
Au	4.174	5.07	1/9	1.473×10^{-2}
Pb	5.040	3.69	1/4	2.273×10^{-2}
Ca	5.531	2.96	1/4	1.887×10^{-2}
Sr	6.030	2.59	1/4	1.588×10^{-2}

the average local potential of electrons in the vacuum, where the potential does not change anymore with increasing distance from the surface.

The coverage has a strong impact on the work function change [159, 57]. Since the various fcc metals studied span a broad range of lattice constants, the absolute coverage (adatoms per unit area) and not the relative coverage per surface atom has to be similar in order to allow a fair comparison among the different substrates. The coverages used within this study are shown in Table 4.1. For the integration over the first Brillouin zone we used a mesh of $5 \times 5 \times 1$ special k-points [130] with a Methfessel-Paxton smearing [123] of 0.1 eV.

4.2.4 Results and discussion

The differences in the energies between fcc and hcp hollow site-adsorption of halogens on fcc metals are shown in Fig. 4.8. Aluminum is not included here because of its unique preference for top-site adsorption. The top position is also the most stable in the case of F/Pt(111). Halogens mostly favor fcc hollow site adsorption on the transition metals, whereas adsorption on the hcp hollow site is more favored on the alkaline earth metals. The copper group of coinage metals (Cu, Ag, and Au) shows the least absolute difference between fcc and hcp adsorption, which implies that the occupancies of hcp and fcc sites are similarly probable. The energetic difference between the adsorption energies on the two threefold-hollow sites decreases with increasing adatom size, i.e. fluorine discriminates between the hcp and fcc sites more strongly than iodine. Also, the fig-

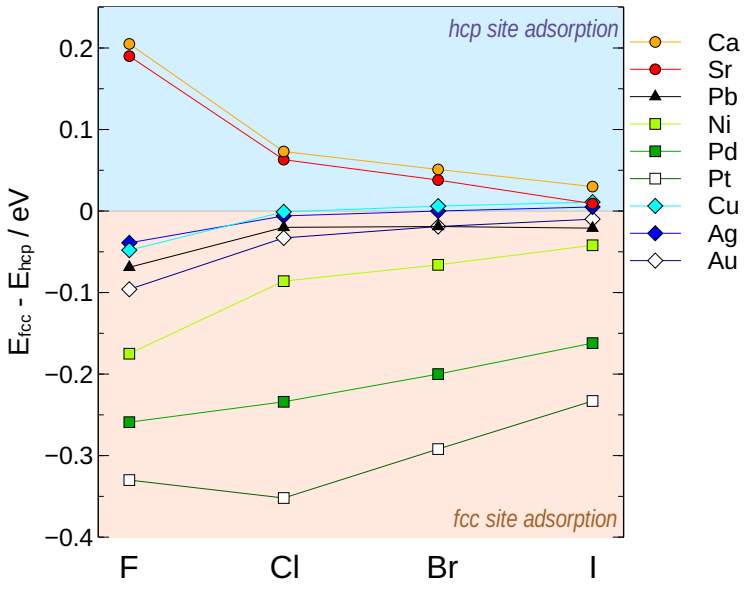

Figure 4.8: Relative stability of fcc-site adsorption compared with hcp-site adsorption.

ure shows that fcc metals with higher work functions generally have more stable fcc-site adsorption of halogens. There is no simple explanation for these trends.

Adsorption energies of halogen atoms with respect to the free halogen molecule are shown in Fig. 4.9. Most metals interact strongly with F and more weakly with Cl, Br and the least with I. However, Pd, Pt and Au do not follow this trend, which can be rationalized as a transition from predominantly ionic bonding to predominantly covalent bonding. Surfaces with low work functions such as Ca and Sr easily transfer electronic charge to electronegative adsorbates such as halogen atoms, resulting in a more ionic bonding situation. Hence the more electronegative (i.e., smaller) halogen atoms exhibit the strongest bonding. On the other hand, surfaces such as Pt, Pd and Au which have large work functions exhibit a smaller charge transfer to electronegative adsorbates so that the bonding becomes mostly covalent in nature, as we have already shown [159, 57]. And here the more polarizable (i.e., larger) halogen atoms then bind most strongly.

In Fig. 4.10 the work function changes due to the adsorption of halogen atoms on different fcc metal surfaces is shown as a function of the adsorption distance d_{ads} of the halogen atom to the surface. From the knowledge that halogens mostly prefer fcc-site adsorption, we have used the fcc adsorption site for all metals in order to calculate comparable work function changes. We note that adsorption

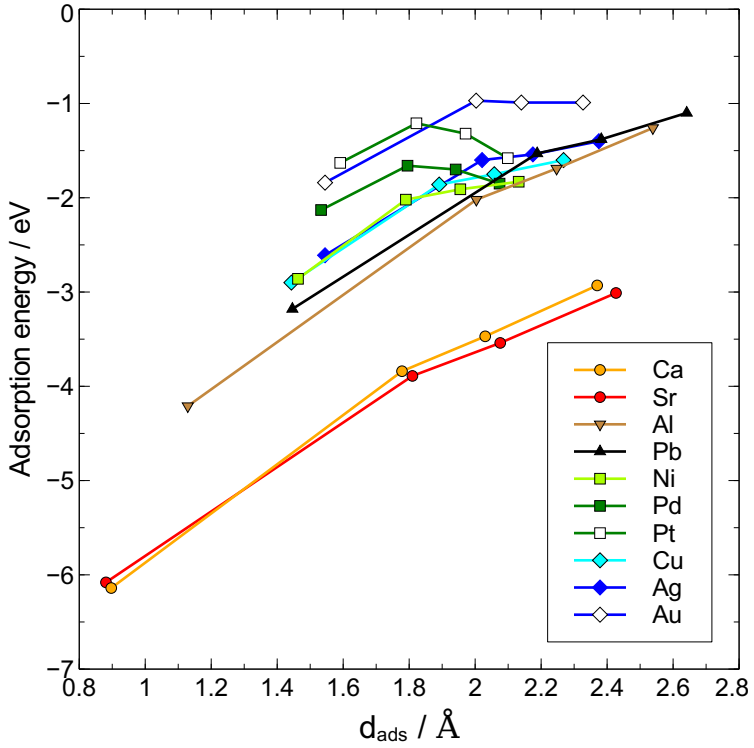

Figure 4.9: Adsorption energies of halogens on the (111) surface of different fcc metals as a function of the adsorption distance of the halogen to the surface. The four data points shown for each substrate correspond to the adsorption of F (smallest adsorption distances), Cl, Br and I (with increasing adsorption distance, respectively).

on a substrate with a larger lattice constant does not necessarily mean that the adatom will adsorb more closely to the surface. This is visible for iodine adsorption on Ca, Sr and Pb, in contrast to Pt, Pd and Ni. Strong covalent bonding on the nickel group of elements leads to this trend.

We find rather short adsorption distances for a fluorine atom adsorbing on Ca(111), Sr(111) and Al(111). The work function change in these systems is negative due to a reduction of the electron spillout of the metal. On the other hand, the larger adsorption distances of Cl, Br and I lead to the expected increase of the work function, in accordance with the jellium model. They adsorb at distances that are larger than a certain critical distance that determines whether a negative work function change due to a reduction of the electron spillout occurs. The critical distance is the distance at which the work function change is zero in Fig. 4.11. The metal atoms were fixed at the structure of the clean surface in these calcu-

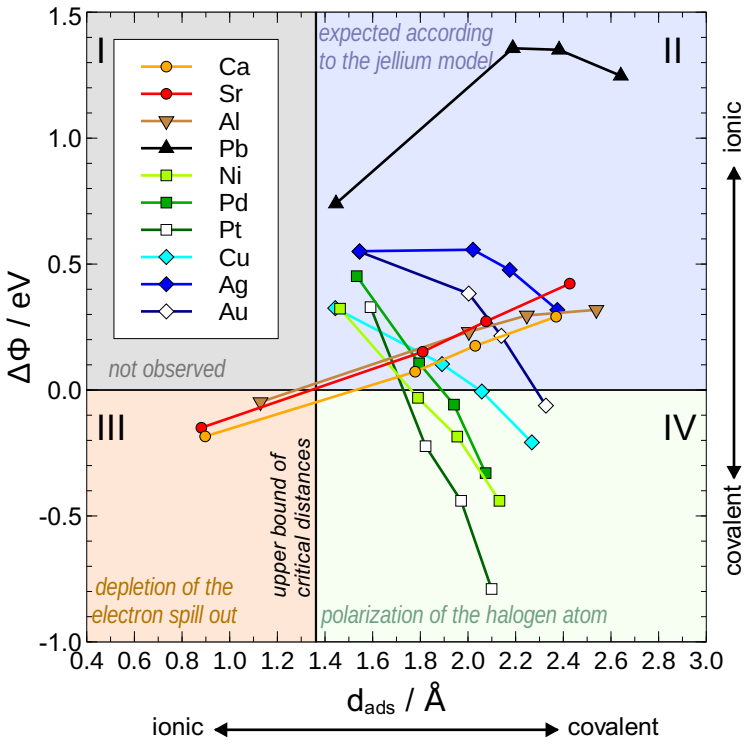

Figure 4.10: Work function changes due to the adsorption of halogens on the (111) surface of different fcc metals as a function of the adsorption distance. The four data points shown for each substrate correspond to the adsorption of F (smallest adsorption distances), Cl, Br and I (with increasing adsorption distance, respectively).

lations. This figure excludes the work function change curve on nickel because of challenges in correctly describing the spin-polarized electronic structure of the adsorption energy minimum.

Depending on the nature of the metallic substrate, a weaker or stronger polarization of the halogen atom occurs. On surfaces with low work functions (i.e., alkaline earth metals), the work function change increases with increasing adatom size because a larger halogen-metal separation increases the magnitude of the dipole moment associated with the negative charge on the halogen and positive charge on the surface. On the other hand, for surfaces with large work functions (i.e., transition metals), the work function decreases with increasing adatom size because larger atoms have lower electronegativities and are more polarizable. Now while the work function change increases monotonously for halogens adsorbed on Ca(111), and decreases monotonously on Pt(111), there is a kink in

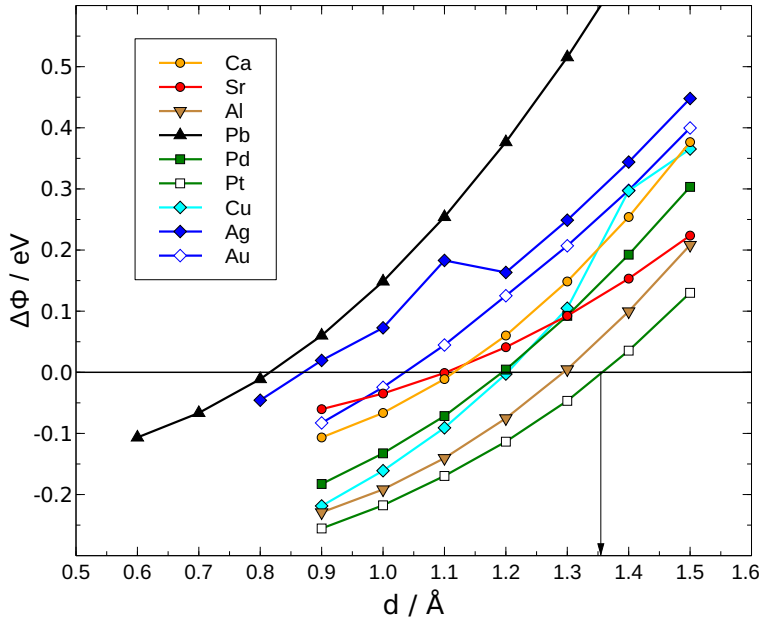

Figure 4.11: Determination of the critical distance: it is defined as the distance of a fluorine atom to the surface at which the work function of the metal surface does not change due to the presence of the adatoms. The upper bound of critical distances is indicated by the arrow.

the plot of work function change for halogens adsorbed on Pb(111): while the adsorption of Cl leads to a larger work function change than the adsorption of F, the adsorption of I induces a lower work function change than Cl. Such a trend can be interpreted as the result of the two opposing mechanisms acting on an equal footing.

Based on an analysis of how the electron distribution rearranges because of the adsorption, a correlation between the observed change in the work function, the adsorption distance, and the bonding mechanism is summarized in Fig. 4.10. Systems that fall under quadrants II and III of Fig. 4.10 show dominantly ionic bonding, while all dominantly covalent systems lie in quadrant IV.

The adsorption of iodine decreases the work function of clean Pt by 0.79 eV, while chlorine increases the work function of Pb(111) by 1.36 eV. This contrast emphasizes how starkly different the effects of halogen adsorption are on the work function of metals. The adsorption of iodine on platinum yields the largest decrease in the work function because Pt has the largest work function among the fcc metals considered, and I has the lowest electronegativity. Ionic bonding is hence weak. Calcium on the other hand has the lowest work function, and

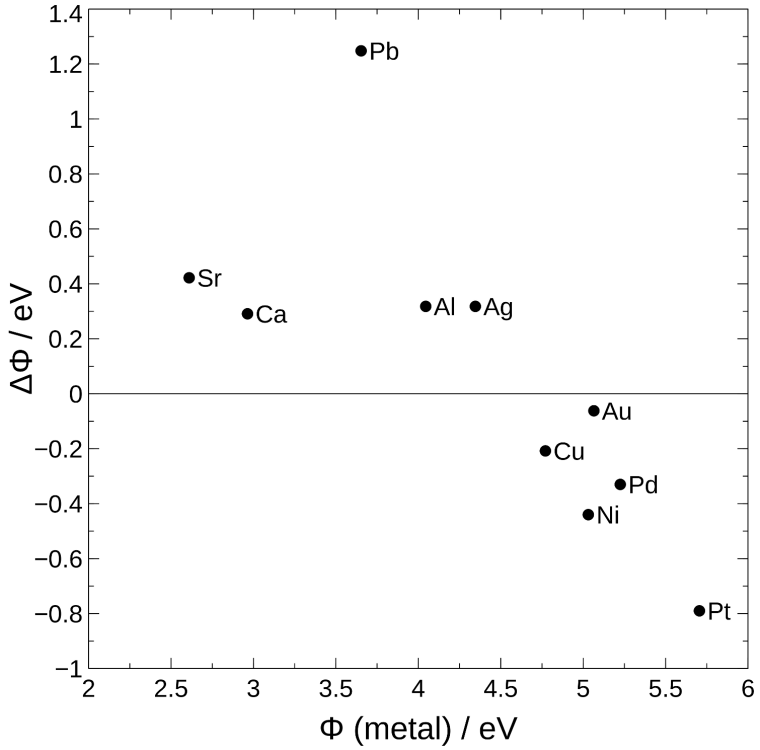

Figure 4.12: The polarization mechanism: the work function change due to the adsorption of I on different metal substrates is plotted against the work function of the respective metal.

F has the highest electronegativity among the halogens, and so one can expect that the adsorption of fluorine on calcium should give the strongest work function increase. This is however not seen due to the fact that F adsorbs within the metal's electron spillout region. The work function of Pb is lower compared with the transition metals, and Cl has a high electronegativity. Thus one can expect the Cl-Pb bond to have a strong ionic character. The Cl-Pb bond is much longer compared to the F-Ca bond, and so the adatom is outside the spillout region of Pb. This therefore leads to a large work function increase.

Furthermore, a more strongly charged atom that is adsorbed/absorbed into a metal induces a stronger screening charge surrounding it. It is then no surprise that fluorine, the most electronegative element, adsorbs on calcium with an accompanying electron density depletion region envelope [57]. Together with their small sizes, this explains why the electronegative second row elements have been observed to create anomalous surface dipole moments [99, 125] upon adsorption onto metals.

Finally, Fig. 4.12 shows the dependence of the work function changes on the electronic properties of the various metal surfaces: the work function changes due to the adsorption of I on different fcc metal surfaces are plotted versus the work function of the bare metals. The trend is obvious. The higher the work function of the bare metal, the lower the work function change. For transition metals, the adsorption of I leads to a decrease of the work function. The exception is Ag, due the high charge transfer to iodine, given the low work function of silver. A similar dependence has been reported by Migani *et al.* [127]: they looked at the halogen charge transfer as a function of the work function of the metal. They observed that the higher the work function, the less the charge transfer. This also means that the higher the work function, the less ionic and the more covalent is the bond. Additionally, it can be said that the more covalent the metal-halogen bond, the stronger the polarization of the halogen atom. Finally, a stronger polarization leads to a more negative work function change.

4.2.5 Conclusions

We have discussed the role of the substrate in promoting a decrease in the work function upon halogen adsorption, governed by two mechanisms: electron spill-out depletion associated with ionic interaction, and polarization on the adatom associated with covalent bonding. These two mechanisms are clearly independent of each other because of the opposite factors that lead to the work function decrease. With the exception of adsorption on Pb and Ag, we have shown that halogen adsorption can decrease the work function on (111) faces of fcc metals.

The two mechanisms are well-distinguishable. A work function decrease due to electron spillout depletion is favored for (1) small adatoms, which adsorb more closely to the metal surface, are more strongly charged, and are less polarizable, and (2) substrates with small work functions, which promote a more ionic and less covalent character to the adsorption interaction. Consequently, a decrease in the work function due to adatom polarization is seen more for large adatoms and substrates with large work functions. The fact that iodine adsorption does not decrease the work function of calcium, as well as fluorine on platinum, suggest that both conditions have to be met. The stark difference between the two mechanisms suggest that a system in which both of them operate together to decrease the work function of the metal may not exist.

4.2.6 Acknowledgments

This research has been supported by the German Science Foundation (DFG) through the research unit FOR 1376 (DFG contract GR 1503/21-1). Generous supply of computer time at the Leibniz Rechenzentrum is gratefully acknowledged.

4.3 Equilibrium coverage of halides on metal electrodes

The majority of halide adsorption processes do not occur under UHV condition but in electrochemical environment. Hence the following section combines DFT calculation with thermodynamics using the model of the computational hydrogen electrode, firstly implemented by Nørskov et al. [138]. The article was published in Surface Science 2015, 631, 17-22: F. Gossenberger, T. Roman and A. Groß "Equilibrium coverage of halides on metal electrodes" [58]. All the DFT calculations concerning platinum were performed by Florian Gossenberger, the calculations on the copper surface were done by Tanglaw Roman. Axel Groß wrote the article. The format of the journal article was modified in order to fit the style and layout of the thesis. A consecutive numbering of figures and references for the whole thesis was applied as well.

4.3.1 Abstract

The adsorption of halides on Cu(111) and Pt(111) has been studied using periodic density functional theory calculations. The equilibrium coverage of the halides as a function of the electrode potential was determined using a thermodynamic approach in which the electrochemical environment is not explicitly taken into account. For all considered systems, halide coverages between 1/3 and 3/8 should be stable over a wide potential range. Although some quantitative discrepancies with experiment are obtained, the qualitative trends derived from the calculations are consistent with experimental observations. The reasons for the remaining discrepancies with the experiment are discussed.

4.3.2 Introduction

The adsorption of anions on metal electrodes is of particular interest in electrochemistry [116, 201]. At the electrochemical interface between the electrode and the electrolyte an electric double layer is formed consisting of an electronic

charge on the electrode and a corresponding ionic counter charge in the electrolyte [180, 67]. Anions such as halides often adsorb specifically, i.e., they form chemical bonds with the metal surface. These adsorbed anions not only affect the chemical properties of electrodes [64] by either directly participating in reactions at the surface or by modifying the electronic properties of the electrodes or by simply blocking adsorption and reaction sites [116], but in general they also change the work function of the electrode, which is directly related to the electrode potential [200].

As part of a systematic effort to model electrode/electrolyte interfaces from first-principles [184, 185, 108, 161], we have recently addressed the work function change induced by the adsorption of halides on Cu(111) [159] and on Pt(111) and Ca(111) [57]. In particular, we focused on the anomalous work function change observed at low coverages for some halide/metal systems [33, 15, 84, 11, 127, 147] which could be explained either by a polarization of the adatom [159] or a reduction in the surface overspill electron density [126, 57].

Here we extend our previous studies in order to determine the equilibrium coverage of halides on Cu(111) and Pt(111). Although recently there is a growing number of first-principles studies addressing structures and processes at electrochemical metal/liquid interfaces [41, 196, 188, 207, 142, 86, 14, 17, 155], there have been only few computational attempts to focus on the role of anions on metal electrodes [127, 175, 28], and it is certainly fair to say that a systematic approach to study anion adsorption on metal electrodes from first-principles in an electrochemical setup is still missing. In an electrochemical situation, the anion coverage on the electrodes is a function of the electrode potential. Although the concentration of anions in the electrolyte is typically relatively low, their concentration on the electrode can be rather high because of their strong interaction with metal electrodes [147, 127, 11, 161]. However, the exact coverage is often not known.

The realistic modeling of electrochemical metal/liquid interfaces is hampered by three facts: i) In electrochemistry, structures and properties of the electrode-electrolyte interfaces are governed by the electrode potential, which adds considerable complexity to the theoretical treatment since charged surfaces have to be considered [184]. ii) The theoretical treatment of processes at solid-liquid interfaces includes a proper description of the liquid which requires to determine free energies instead of just total energies. This means that computationally expensive statistical averages have to be performed [184, 161]. iii) Electronic structure methods based on density functional theory (DFT) combine numerical efficiency

with a satisfactory accuracy. However, there are severe shortcomings of the DFT description of liquids, in particular water, using current functionals [25, 199, 24].

These problems can be avoided if the electrochemical environment is not explicitly but only implicitly taken into account. In a very elegant approach [138, 137] that is now termed “Computational hydrogen electrode” and that is similar to the ab initio thermodynamics approach used in heterogeneous catalysis [156], the electrochemical environment is just considered as a reservoir the adsorbates come from, but the explicit influence of the electrochemical environment on the adsorption properties is not taken into account. This is of course a severe approximation, but it is computationally very attractive, and it allows to establish trends in electrochemistry and electrocatalysis [117].

Here we also use this approach to determine the equilibrium coverage of halides on Cu(111) and Pt(111) in the spirit of the work by Hansen *et al.* [73]. We will show that the trends in the electrochemical halide coverage observed experimentally can be well reproduced using this approach. Still, discrepancies remain whose possible reasons will be discussed.

4.3.3 Computational details

Periodic DFT calculations that employ the exchange-correlation functional of Perdew, Burke, and Ernzerhof (PBE) [149] were done using the Vienna ab initio program package (VASP) [96]. Electron-core interactions were accounted for by the projector augmented wave method [18, 97]. The electronic one-particle wave functions were expanded in a plane-wave basis set up to an energy cutoff of 500 eV.

The metal substrates were represented by slabs of seven atomic layers, of which the inner three layers were kept fixed in the bulk position during geometry optimizations while the rest of the system was allowed to relax. Halogen atoms were placed symmetrically at both sides of the slab. Most of the calculations were performed in a 4×4 surface unit cell for halide coverages between 1/16 and 1/2. The corresponding energy minimum structures for chlorine on Cu(111) are illustrated in Fig. 4.13 . For the integration over the first Brillouin zone we used a mesh of at least $4 \times 4 \times 1$ special k-points [130] with a Methfessel-Paxton smearing [123] of 0.1 eV. In addition, $\sqrt{3} \times \sqrt{3}$ unit cells were used to study different halide coverage of 1/3. Experimentally, halide adsorbate structures with other geometries than those considered in our computational study have been found (see the discussion below). Still, we are mainly interested in qualitative trends and the

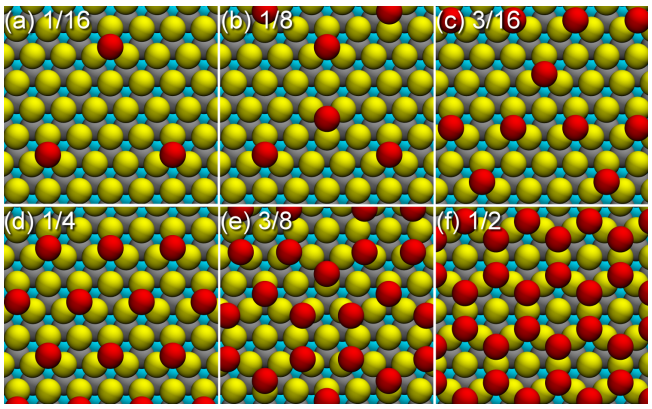

Figure 4.13: Relaxed structures of chlorine atoms in a 4×4 geometry on Cu(111) for coverages between 1/16 and 1/2.

characteristic differences between the studied systems. Hence we made no effort to address further geometries.

4.3.4 Results and discussion

Theoretical background

The calculated adsorption energies per halogen atom referred to the corresponding free halogen molecule for the considered systems are shown in Fig. 4.14. The results are in satisfactory agreement with previous computational studies using similar setups (see, e.g., [148]). As a general trend, it can be seen that the adsorption on Cu(111) is stronger than that on Pt(111) although for iodine adsorption the effect is rather small. The trend among the halides is not identical: on Cu(111) chlorine adsorption is stronger than iodine adsorption, while on Pt(111) it is the other way around.

In order to understand these trends, we determined the adsorption energies of the halogen atoms at a coverage of 1/9 on (111) surfaces of Ag, Cu, Ni, Au, Pd, and Pt, where we have ordered the substrates according to increasing work function (see Tab. 4.2). In fact, we find a gradual change in the trend in the adsorption energies of Cl, Br, and I. Whereas on Ag and Cu, Cl exhibits the strongest adsorption on Pd and Pt it is I. Thus there is a strong correlation between the work function and the trend in the adsorption energies among the halogen atoms, except for fluorine which exhibits the strongest adsorption of the halogen atoms on

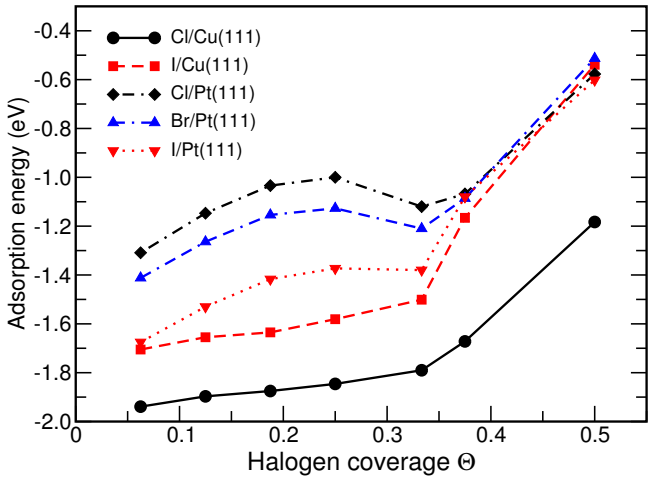

Figure 4.14: Adsorption energies of halogen atoms on Cu(111) and Pt(111) with respect to the free halogen molecule as a function of the coverage.

all surfaces.

The trend in the adsorption energies, except for fluorine, can then be rationalized as a transition from predominantly ionic bonding to predominantly covalent bonding. Surfaces with low work function such as Ag and Cu easily transfer electronic charge to electronegative adsorbates such as halogen atoms resulting in a more ionic bonding situation. And then the more electronegative (i.e., smaller) halogen atoms exhibit the strongest bonding.

On the other hand, the surfaces with large work function such as Pd and Pt exhibit a smaller charge transfer to electronegative adsorbates so that the bonding becomes mostly covalent in nature, as we already showed [159, 57]. And here the more polarizable (i.e., larger) halogen atoms then bind most strongly.

In general, binding to the metal substrates becomes weaker at higher coverage,

Table 4.2: Adsorption energies in eV of halogen atoms with respect to the free halogen molecule on (111) metal surfaces at a coverage of 1/9. The metal surfaces are ordered according to increasing work function.

E_{ads} (eV)	Ag	Cu	Ni	Au	Pd	Pt
F	-2.61	-2.90	-2.86	-1.84	-2.13	-1.63
Cl	-1.60	-1.86	-2.02	-0.97	-1.66	-1.21
Br	-1.54	-1.75	-1.91	-0.99	-1.70	-1.32
I	-1.40	-1.60	-1.83	-0.99	-1.85	-1.58

indicating a repulsive interaction between the adsorbed halogen atoms which becomes particularly evident for coverages $\Theta \geq 1/3$. It is also obvious that the halogen coverage 1/3 corresponding to a $\sqrt{3} \times \sqrt{3}$ structure is rather stable, especially for chlorine and bromine on Pt(111). Note that the $\sqrt{3} \times \sqrt{3}$ structure corresponds to the two-dimensional close-packed structure, but at the same time it is the structure with the largest mutual distances among the adsorbates for a given density. This might explain its stability for adsorbates that repel each other such as halides.

From the adsorption energies shown in Fig. 4.14 it is, however, not directly clear what the thermodynamically stable structures under specific conditions are. In order to address this issue, we will first briefly recall the theoretical background for the determination of an adsorbate coverage in thermal equilibrium. It is important to note that in equilibrium, every species is characterized by its chemical potential which is constant throughout the whole system. At gas/solid interfaces – as they occur in heterogeneous catalysis – the Gibbs free energy of adsorption $\Delta\gamma$ for N_{ads} adsorbates bound to a surface area A_s at a given temperature T and pressure p can be expressed [156] as

$$\begin{aligned} \Delta\gamma(T,p) &= \gamma(T,p,N_{\mathrm{ads}}) - \gamma_{\mathrm{clean}}(T,p,0) && (4.11)\\ &= \frac{1}{A_s}\Delta G^{ads}(T,p) && (4.12)\\ &= \frac{N_{\mathrm{ads}}}{A_s}\left(E_{\mathrm{ads}} - \mu_{\mathrm{ads}}(T,p)\right) \ . && (4.13) \end{aligned}$$

Here, $\Delta G^{ads}(T,p)$ is the difference in free energy and $\mu_{\mathrm{ads}}(T,p)$ is the chemical potential of the adsorbate. In the last Eq. (4.13) above, E_{ads} is the total adsorption energy per particle, and any change in entropy and zero-point energies upon adsorption is neglected, as often done in theoretical studies addressing systems in heterogeneous catalysis and surface science [156].

In the adsorption at electrochemical interfaces, the reference state corresponds to species in solution in the presence of an electrode potential U. This means that the chemical potential μ has to be replaced by the electrochemical potential

$$\tilde{\mu} = \mu + neU \ , \qquad (4.14)$$

where n is the charge of the particle. Still the problem remains that the electrochemical potential includes all solvation effects of the species. The determination of solvation energies requires computationally demanding thermal integration

schemes [100]. These efforts can be avoided using the concept of the computational hydrogen electrode. It is based on the fact that at standard conditions (pH$= 0$, $p = 1\,$bar, $T = 298\,$K) $U = 0$ is defined as the electrode potential at which there is an equilibrium between a proton and an electron in aqueous solution $\mathrm{H^+(aq)} + e^-$ and hydrogen in the gas phase, $\frac{1}{2}\mathrm{H_2(g)}$. Furthermore, it is well known how the electrochemical potential of the proton and the electron change if the proton concentration and the electrode potential are varied [182], namely according to

$$\tilde{\mu}(\mathrm{H^+(aq)}) + \tilde{\mu}(e^-) = \frac{1}{2}\mu(\mathrm{H_2(g)}) - eU_{\mathrm{SHE}} - k_{\mathrm{B}}T\ln(10)\mathrm{pH}\,, \tag{4.15}$$

where U_{SHE} is the electrode potential with respect to the standard hydrogen electrode (SHE). The success of the computational hydrogen electrode is based on the fact that it allows to derive adsorption energies with respect to solvated species without the need to determine any solvation energies.

This concept does not only work for hydrogen, it works also for any redox couple $\frac{1}{2}$ A$_2 + e^- \rightleftarrows$ A$^-$, as applied by Hansen *et al.* to describe the electrochemical chlorine evolution at rutile oxide (110) surfaces [73]. Here we follow the same approach (note that there are typos in Ref. [73] in the corresponding equations), i.e., we derive the electrochemical potential for a halide A, where A stands for Cl, Br or I, as

$$\tilde{\mu}(\mathrm{A^-(aq)}) - \tilde{\mu}(e^-) = \frac{1}{2}\mu(\mathrm{A_2(g)}) + e(U_{\mathrm{SHE}} - U^0) + k_{\mathrm{B}}T\ln a_{\mathrm{A^-}}\,, \tag{4.16}$$

where U^0 is the reduction potential of the corresponding halide and $a_{\mathrm{A^-}}$ its activity. The reduction potentials for the halides considered in this study are collected in Table 4.3.

The change of zero-point energies upon adsorption of the halogen atoms can safely be neglected [62] mainly because of their relatively large mass. For example, in the adsorption of chlorine on rutile oxide (110) surfaces they have been

Table 4.3: Reduction potentials of the halides considered in this work.

Redox couple	Reduction potential U^0 (V)
$\frac{1}{2}$ Cl$_2 + e^- \rightleftarrows$ Cl$^-$	1.36
$\frac{1}{2}$ Br$_2 + e^- \rightleftarrows$ Br$^-$	1.09
$\frac{1}{2}$ I$_2 + e^- \rightleftarrows$ I$^-$	0.54

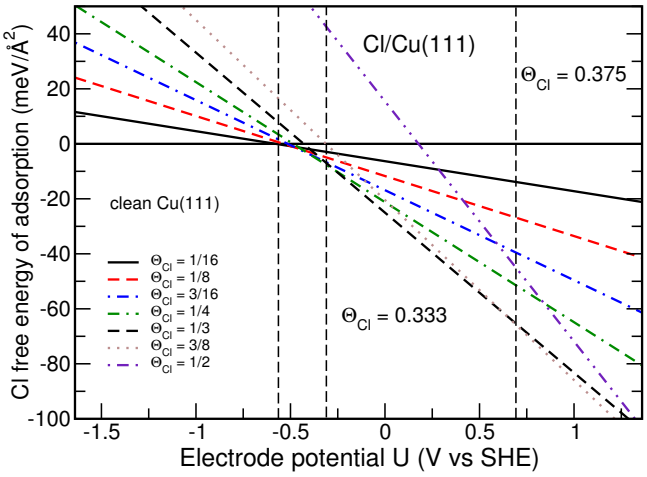

Figure 4.15: Calculated electrochemical equilibrium coverage of chlorine on Cu(111) at standard condition as a function of the electrode potential vs. SHE.

estimated to be in the order of 0.02 eV [73]. Furthermore, we also neglect the entropy change upon adsorption. In the following, we will also assume standard conditions, i.e., we assume that the activity of the halides a_{A^-} is unity. Thus we arrive at the following expression for the free energy of adsorption as a function of the electrode potential,

$$\Delta\gamma(U_{\mathrm{SHE}}) = \frac{N_{\mathrm{ads}}}{A_s}\left(E_{\mathrm{ads}} - e(U_{\mathrm{SHE}} - U^0)\right) \ . \tag{4.17}$$

For other concentrations of the halides in the electrolyte, the electrode potential needs to be shifted by $k_{\mathrm{B}}T \ln a_{\mathrm{A}^-}$ which corresponds, e.g., to about 60 meV if the activity is changed by one order of magnitude at room temperature.

It should be emphasized that within our approach, the adsorption energy E_{ads} appearing in Eq. 4.17 is calculated without taking the electrochemical environment into account. Furthermore, the varying excess charge at the metal electrodes as a function of the electrode potential is also not considered. These are certainly severe approximations. Comparing our results with experimental findings is a first step to assess the validity of this approach.

Halides on Cu(111)

The first system we discuss is the adsorption of chlorine on Cu(111) which is a rather well-studied system in electrochemistry [116, 98, 78, 23, 66], among others motivated by the fact that chloride adlayers on copper electrodes are of major importance in corrosion and electroplating. Although there was some debate about the equilibrium structure of chloride on Cu(111), more recent studies indicate that a simple $\sqrt{3}\times\sqrt{3}$ structure with a coverage of 1/3 should result in an electrochemical environment [98, 23]. In addition, a compressed chloride adlayer has been suggested [78, 66]. It should be noted that on Cu(100) even nominal coverages of 1/2 have been observed [116, 175].

Our prediction concerning the equilibrium structure of chlorine on Cu(111) as a function of the electrode potential at standard conditions is shown in Fig. 4.15. Note that these diagrams can be read as a kind of phase diagram. The structure with the lowest free energy of adsorption is supposed to be the thermodynamically stable structure. In Fig. 4.15 and the following figures we show the free energy curves in a potential range of about 3 eV. This is larger than the stability range of some of the considered systems. Still we have chosen such a broad range in order to make the diagrams clearly arranged.

We find that at potentials below -0.6 V, the clean Cu(111) electrode is stable. Between -0.6 V and -0.3 V, structures with increasing coverage become stable before at -0.3 V a large potential window opens in which the $\sqrt{3} \times \sqrt{3}$ structure is assumed to be realized in thermodynamical equilibrium. The onset of the formation of the chloride adlayer at about -0.3 V is consistent with the peaks assigned to the adsorption and desorption of Cl in cyclic voltammograms [98, 78, 23].

Hence our calculations confirm the prominent role the $\sqrt{3} \times \sqrt{3}$ structure plays for the adsorption of chlorine on Cu(111) under electrochemical conditions. The compressed chlorine adlayers which have been found on Cu(111) [78, 66] cannot be addressed by our periodic setup as they have been identified to be an incommensurate adlayer with a rotated hexagonal structure [66]. Still, the fact that we find a chlorine adlayer structure corresponding to a coverage of $\Theta_{\mathrm{Cl}} = 3/8$ which is almost as stable as the $\Theta_{\mathrm{Cl}} = 1/3$ structure indicates that compressed chlorine adlayer structures with coverages slightly above 1/3 should indeed be possible.

Next, we address the equilibrium structures of iodine on Cu(111). Experimentally, basically only the $\sqrt{3} \times \sqrt{3}$ structure was observed [78]. Although initially no compression of the iodine adlayer as a function of the electrode potential

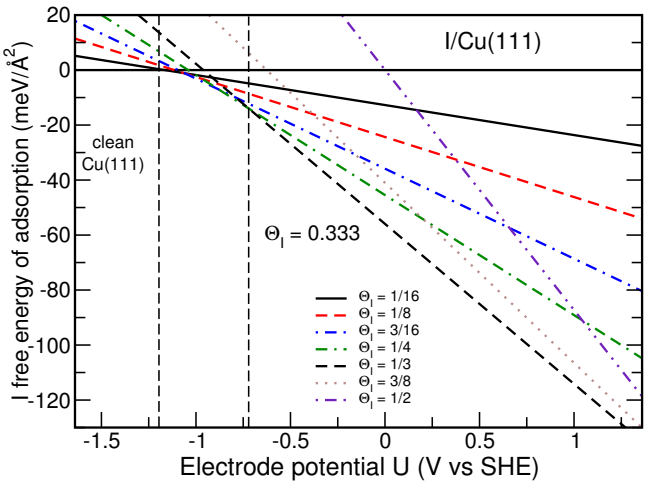

Figure 4.16: Calculated electrochemical equilibrium coverage of iodine on Cu(111) at standard condition as a function of the electrode potential vs. SHE.

was observed [78], later studies found uniaxially incommensurate iodide adlayers caused by a unidirectional compression of the $\sqrt{3} \times \sqrt{3}$-I at vacuum at higher iodine coverages [2] or in an electrochemical environment at more positive potentials close to the onset of the copper dissolution reaction [139].

The calculated free energy of adsorption of iodine on Cu(111) as a function of the electrode potential is plotted in Fig. 4.16. Iodine adsorption on Cu(111) occurs at lower potentials than chlorine adsorption which is in qualitative agreement with the experiment [23, 139] although iodine adsorption on Cu(111) is weaker than chlorine adsorption, as Fig. 4.14 demonstrates. This lower onset potential is caused by the fact that the reduction potential of iodine is much lower than the one of chlorine (see Table 4.3).

We find a potential region between -1.2 V and -0.7 V in which a series of structures with increasing coverage becomes stable. At potentials above -0.7 V, only the $(\sqrt{3} \times \sqrt{3})$ structure is found. Again, the uniaxially incommensurate compressed iodide adlayer could not be addressed by the periodic calculations since the corresponding superstructures are too large. For I/Cu(111), the $\Theta = 3/8$ is more unfavorable compared to the $\Theta = 1/3$ than in the case of Cl/Cu(111). This is consistent with the fact that Inukai *et al.* did not find any compression of the iodine adlayer in the potential window between -0.5 V and -0.7 V vs. SCE [78].

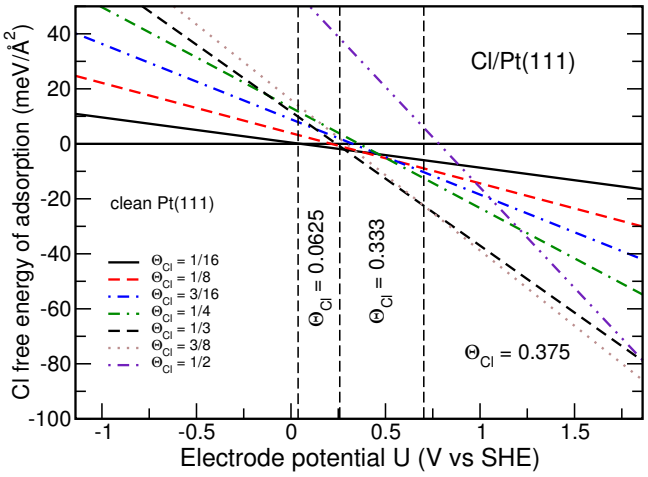

Figure 4.17: Calculated electrochemical equilibrium coverage of chlorine on Pt(111) at standard condition as a function of the electrode potential vs. SHE.

Halides on Pt(111)

Turning to the Pt(111) electrode, we start with the system Cl/Pt(111). Using *in situ* surface X-ray scattering, Lucas *et al.* were not able to detect any ordered chlorine adlayer over the entire potential range where chloride is present on the Pt(111) electrode [114]. They estimated the chloride coverage to be between 0.4 and 0.6. To the best of our knowledge, there is no study revealing an atomistic structure of chlorine on Pt(111) in an electrochemical environment. In a chronocoulometric study [49], the structure of Cl/Pt(111) was not addressed, however, it was found that the adsorbed species is basically a neutral chlorine atom which agrees nicely with our computational findings [57].

We find (see Fig. 4.17) that at standard conditions a chlorine adlayer on Pt(111) should start to form at potentials close to 0 V. This is a significantly higher onset-potential than on Cu(111) because of the weaker binding of chlorine to Pt(111) (see Fig. 4.14). Up to about 0.25 V, a chlorine layer with a coverage of 1/16 should be stable, followed by the $\sqrt{3} \times \sqrt{3}$ structure. This $\Theta = 1/3$ structure, however, is only stable up to 0.7 V where $\Theta = 3/8$ becomes more favorable. Furthermore, the layers corresponding to $\Theta = 1/3$ and $\Theta = 3/8$ are rather close in energy. This might yield an explanation why no specific ordered structure could be identified in the experiment [114].

For bromine on Pt(111), *in situ* STM experiments yielded asymmetric and hexag-

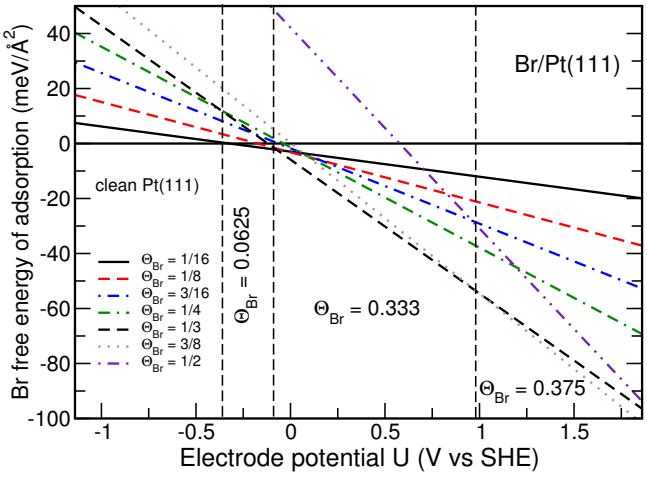

Figure 4.18: Calculated electrochemical equilibrium coverage of bromine on Pt(111) at standard condition as a function of the electrode potential vs. SHE.

onal (3×3) structures at a coverage of $\Theta = 4/9$ [195]. Using X-ray scattering experiments, Lucas *et al.* [114] observed a series of high-order commensurate structures as a function of electrode potential which are poorly ordered unless the size of the unit cell is small. These unit cells corresponded to (3×3) and (7×7) structures with coverages of $\Theta = 4/9$ and $\Theta = 25/49$, respectively. Based on rotating disk experiments, Gasteiger *et al.* [55] found that in 0.1 M $HClO_4$ with 10^{-4} M Br^- bromide adsorption starts at about 0.1 V and reaches a coverage of about $\Theta = 0.42$ at 0.75 V.

As shown in Fig. 4.18, according to our calculations bromine starts to adsorb on Pt(111) at standard conditions at about -0.35 V with a $\Theta = 1/16$ structure. This onset occurs at lower potentials than chlorine adsorption on Pt(111) because both bromine bonding to Pt(111) is stronger than the chlorine bonding, and the reduction potential of bromine is lower than the one of chlorine. In a wide potential range from -0.1 V and 1.0 V, the $(\sqrt{3} \times \sqrt{3})$ structure with $\Theta = 1/3$ is stable, followed above 1.0 V by the $\Theta = 3/8$ structure. Similar to Cl/Pt(111), the layers corresponding to $\Theta = 1/3$ and $\Theta = 3/8$ are rather close in energy.

In our calculations, we did not consider (3×3) and (7×7) structures, hence we cannot compare our results directly with experiment [114]. Still, our results are consistent with the fact that over a wide range of potentials, bromine coverages of $\Theta \geq 0.4$ have been found. Note that the $k_B T \ln a_{Br^-}$ term in Eq. 4.16 leads to

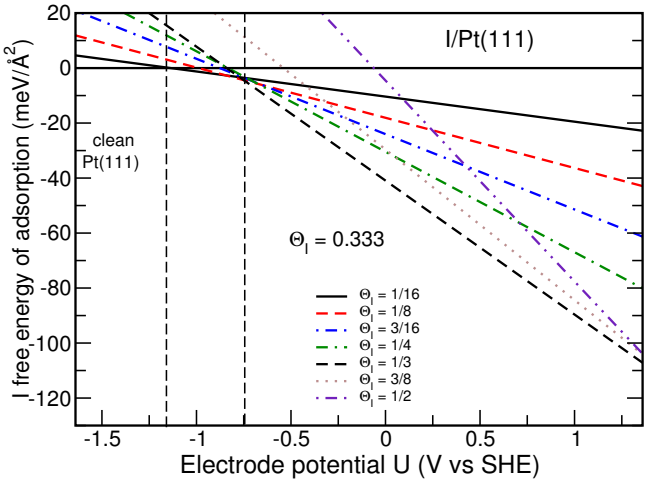

Figure 4.19: Calculated electrochemical equilibrium coverage of iodine on Pt(111) at standard condition as a function of the electrode potential vs. SHE.

a shift of the free energy curves by about 60 mV to higher potentials if the activity is decreased by one order of magnitude. Furthermore, increasing the pH-value of the electrolyte by one leads to the same shift. Considering such a shift, the observed potential range for bromide adsorption on Pt(111) [55] is compatible with our calculated order of stability.

In ultrahigh vacuum (UHV), iodine dosing of a Pt(111) leads to two ordered structures, $(\sqrt{3} \times \sqrt{3})$ with a coverage of $\Theta = 1/3$ and $(\sqrt{7} \times \sqrt{7})R19.1°$ with $\Theta = 3/7$ [38].

In temperature-programmed desorption (TPD) experiments, Jo and White [84] observed a shift of the desorption peaks to lower temperatures with increasing coverage with is consistent with the lower iodine binding energies for higher coverages shown in Fig. 4.14. In addition, they found a non-monotonic decrease of the I/Pt(111) work function as a function of the iodine coverage which is well reproduced by our calculations [57]. Early *in situ* STM experiments confirmed the existence of the $(\sqrt{3}\times\sqrt{3})$ structure also in an electrochemical environment [214]. Later X-ray scattering [114] and *in situ* STM experiments [79] found the coexistence of a hexagonal (3×3) structure with $\Theta = 4/9$ and the $(\sqrt{7} \times \sqrt{7})R19.1°$ structure under potential control.

Again, we have considered neither the (3×3) nor the $(\sqrt{7}\times\sqrt{7})R19.1°$ structure. As Fig. 4.19 shows, our calculations yield that iodine adsorption starts at -1.2 V,

and above -0.75 V only the $(\sqrt{3} \times \sqrt{3})$ is stable. As our calculations are done at the solid-vacuum interface, it is no surprise that the UHV structure of I/Pt(111) has been reproduced.

The onset potential of iodine adsorption on Pt(111) is very close to the one on Cu(111) because of the similar adsorption energies (see Fig. 4.14). As discussed above, whereas iodine adsorption on Pt(111) is stronger than chlorine adsorption on Pt(111), it is the other way around on Cu(111), which means that there is no general trend of the adsorption energies among the halides for metal electrodes.

Discussion

In the previous sections, we have compared experimental findings with respect to the stability of halide structures on Cu(111) and Pt(111) at electrochemical conditions with the predictions of a very simple thermodynamical model that does not explicitly take into account the electrochemical environment. The calculated stability range of the halide structures together with their corresponding coverage are in qualitative or even in semi-quantitative agreement with experiment. However, some characteristic quantitative differences between experiment and the simple thermodynamic model remain. This is partially due to the fact that we did not consider all structures observed in the experiment. Still, there are three main reasons that could be responsible for the discrepancies.

First of all, the change of the adsorption energy for varying surface excess charge or varying electric fields has not been taken into account. According to a DFT study, electric field effects should only play a minor role in the oxidation reaction on Pt(111) [85], however, it is not clear whether these findings can be transferred to halide adsorption.

Second, the aqueous environment was not explicitly considered. Now water is relatively weakly interacting with metal electrodes [184, 124, 56] so that chemisorption energies are only weakly influenced by the presence of water [167, 166]. Therefore we do not expect that water layers change the adsorption energies of the halides significantly. However, reorientation of the water molecules due to the presence of the halides might still affect the work function of the electrodes and thus the corresponding electrode potential.

Third, the presence of additional adsorbates is not taken into account. This is particularly important for Pt(111) where at low potentials hydrogen adsorption [183, 118] and at higher potentials OH adsorption take place. There might be

some competition for the adsorption sites. Furthermore, co-adsorbates influence the adsorption energy either through direct adsorbate-adsorbate interactions or indirectly through modifying the electronic properties of the substrate [71, 112]. Both effects might affect the stability of the halide adsorption phases.

Last but not least, it should be mentioned that errors might of course also be introduced through the approximate nature of the exchange-correlation functional used in the DFT calculations. A quantitative assessment of the reliability of the functional, however, can only be achieved once the electrochemical interface is realistically modeled. Such a realistic modeling of the structure of electrochemical interfaces is not only interesting in its own right, it is also crucial for a reliable description of electrocatalytic processes as they occur, e.g., in fuel cells. Therefore we are in the process of studying the importance of all the effects discussed above in our ongoing work.

4.3.5 Conclusions

Using a very simple thermodynamical model corresponding to the computational hydrogen electrode [138, 137], we have estimated the stability of halide structures on Cu(111) and Pt(111). According to our calculations, for all considered systems halide coverages between 1/3 and 3/8 should be stable in a wide potential range. Although in this model the electrochemical environment at the interface is not explicitly taken into account, the theoretical results are consistent with experimental observations. Thus this model offers a computationally convenient way to estimate anion coverages at electrochemical interfaces under potential control. Still further work is needed in order to assess the importance of the effects neglected in the simple thermodynamical model.

4.3.6 Acknowledgments

This research has been supported by the German Science Foundation (DFG) through the research unit FOR 1376 (DFG contract GR 1503/21-1) and by the Baden-Württemberg Foundation within the Network of Excellence *Functional Nanostructures*. Computer time has been provided by the BW-Grid of the federal state of Baden-Württemberg and by a computer cluster financed through the stimulus program “Electrochemistry for Electromobility” of the German Ministry of Educa-

tion and Science (BMBF). Useful discussions with Jan Rossmeisl and Wolfgang Schmickler are gratefully acknowledged.

4.4 Hydrogen and halide co-adsorption on Pt(111) in an electrochemical environment: a computational perspective

Reprinted with permission from Elsevier.

An electrode surface under sufficiently negative electrode potentials is covered by a significant amount of cations e.g., protons. They might compete with anionic adsorbate structures or even build co-adsorped coverages. Therefore both hydrogen and halide co-adsorption is the topic of the following article. It was published in Electrochimica Acta 2016, 216, 152-159: F. Gossenberger, T. Roman and A. Groß "Hydrogen and halide co-adsorption on Pt(111) in an electrochemical environment: a computational perspective" [59]. Florian Gossenberger accomplished all DFT calculations, did the analysis, and wrote the paper.

4.4.1 Abstract

The adsorbate structures on electrode surfaces in an electrochemical environment are controlled by thermodynamic parameters such as temperature, concentration, pH and electrode potential. Knowledge of these structures is important as specifically-adsorbed ions on an electrode impact catalytic reactions that take place at the electrode-electrolyte interface. From a theoretical point of view, the equilibrium structures of adsorbates can be conveniently estimated using the concept of the computational hydrogen electrode. Here we extend this concept to determine equilibrium co-adsorption structures of halides with hydrogen on Pt(111) as a function of the corresponding electrochemical potentials. We find that hydrogen-halide co-adsorption is of a competitive character, which means that mainly dense-packed structures of either halides or hydrogens are stable on the surface, in good agreement with experiment.

4.4.2 Introduction

The adsorption of anions on metal electrodes is of particular interest in electrochemistry which is concerned with structures and processes at the interface between an ion and an electron conductor [182]. An electric double layer is formed

at the electrochemical interface between the electrode and the electrolyte consisting of an electronic charge on the electrode and a corresponding ionic counter charge in the electrolyte. Anions such as halides often adsorb specifically [116], i.e., they form chemical bonds with the metal surface. These adsorbed anions change the work function of the electrode [159, 158], which is directly related to the electrode potential [200]. In addition, they affect the chemical properties of electrodes by either directly participating in reactions at the surface or by modifying the electronic properties of the electrodes or by simply blocking adsorption and reaction sites [190, 208, 71, 3, 201, 64], or through cooperative effects, as in the underpotential deposition of metals [186].

In a previous paper we tackled the adsorption of halides on Pt(111) and Cu(111) [58] as a function of the electrode potential using the concept of the computational hydrogen electrode [138]. A similar work was also performed by McCrum *et al.* on halide adsorption at different Cu surfaces [122]. There is a rich literature on halide adsorption experiments on Pt(111) performed in ultra-high vacuum (UHV), air, or in electrochemical environments [116, 33, 191, 203, 179, 189, 204, 114, 171, 15, 195, 177, 141, 38, 36, 113, 214, 193, 178, 26, 79, 192]. Our previous study confirmed the experimentally-observed high coverage [116] of halides on metal electrodes [58]. Note that it is not distinguishable whether a single adatom, which in general has a partial charge on the surface, was an ion or a neutral atom before adsorption. We therefore treat adsorbed halogen atoms and adsorbed halides as semantically identical; adsorbed hydrogen and adsorbed protons are likewise synonymous. However, any aqueous electrolyte also contains a certain concentration of protons, depending on the pH value. Especially platinum electrodes are covered by hydrogen at low electrode potentials [183, 118] because of the favorable hydrogen adsorption energy on Pt [185]. Here we extend the concept of the computational hydrogen electrode to describe the co-adsorption of halides and protons from first principles, similar to what has been done in heterogeneous oxidation catalysis using the related concept of ab initio thermodynamics [157]. This is in particular interesting as there might be some attractive electrostatic interaction between cations such as protons and anions such as halides adsorbed on a metal electrode.

Yet, to the best of our knowledge, the co-adsorption of halides and hydrogen on platinum has not yet been systematically studied from a theoretical perspective. The particular mechanisms underlying adsorbate-adsorbate interactions are still the subject of considerable debate [121]. Here we will derive phase diagrams of the stable co-adsorption structure of hydrogen with chlorine, bromine and iodine.

Furthermore, for given concentrations of the ions, we will determine the surface coverage of hydrogen and halides as a function of the electrode potential and compare the results with those of corresponding experiments.

4.4.3 Theoretical Background and Computational Details

The aim of this paper is to link total energies of density functional calculations of a co-adsorbate system to thermodynamic values such as pH or electrode potential in order to derive phase diagrams of adsorbate structures. As a concrete system, a Pt(111) electrode covered by hydrogen and halides will be addressed, based on the concept of the computational hydrogen electrode [138].

Stable adsorption on surfaces is associated with a gain in Gibbs free energy of adsorption which is typically given per adsorbing atom or molecule. However, in this paper we will normalize the Gibbs energy to surface area A_{S} as this is the relevant entity to address the stability of surface phases. The most stable adsorbate structure in thermal equilibrium is therefore the structure with the lowest Gibbs free energy of adsorption $\Delta\gamma$,

$$\Delta\gamma = \frac{1}{A_{\mathrm{S}}}\left(G_{surf,ads} - G_{surf,0} - \sum_i n_i\mu_i\right). \tag{4.18}$$

In this equation $G_{\mathrm{surf,ads}}$ and $G_{\mathrm{surf,0}}$ are the Gibbs free energies of the adsorbate-covered and the clean surface, n_i is the number of adsorbed atoms of the type i per surface area A_{S}, and μ is the corresponding chemical potential of the ions in solution.

In the gas phase, the Gibbs free energy G and the chemical potential μ depend on temperature and partial pressure of the molecules. The latter corresponds to the thermodynamic activity in solution. As far as solids are concerned, the temperature and pressure-dependent change in the Gibbs energy is rather small compared with the change in the Gibbs energy of liquids or gases. Therefore it is feasible to neglect this dependence and to consider it only for the ions in solution $\mu_i(T, p_i)$.

Furthermore, the chemical potential of charged particles is influenced significantly by the presence of the electrode potential. This is reflected in the so-called electrochemical potential $\tilde{\mu} = \mu + zeU$, where z is an integer number for the charge of the particle, e the elementary electric charge and U the electrode potential.

Note that we use the convention that the elementary electric charge is a negative number, in some publications a positive probe charge and an opposite sign are used. The adsorption energies of oxygen, hydrogen and hydroxyl on metal electrodes depend only very weakly on an applied electric field [138, 165], which has been attributed to the small dipole moment associated with the adsorbed species [138]. Furthermore, it has been demonstrated that the energetics of the barriers in the formic acid degradation on Pt(111) is hardly influenced by varying an electric field [205]. This is obviously a consequence of the good screening properties of metals which is one of the reasons why the computational hydrogen electrode approach has been so successful in describing adsorption trends on metal electrodes as a function of the electrode potential.

Furthermore, a potential dependence of adsorption energies can also occur when the charge of an adsorbing ion is not fully transfered to the electrode but a fractional charge remains in the diffuse double layer, as discussed by Schmickler and Guidelli [181]. The exact amount of charge transfered to the electrode quantified through the so-called electrosorption valence cannot be measured, it can only be estimated, for example from the dipole moments associated with the adsorbed species [181]. Thus it could be shown that the electrosorption coefficients of halides adsorbed on Ag [43] and Au [110] are non-integer which is normally interpreted as an indication that double layer effects are important in adsorption.

However, the adsorption of Cl, Br and I on Pt(111) is associated with a strong polarization of the adsorbed atoms causing an anomalous work function change: it leads to a decrease of the work function instead of an increase as would be expected from the adsorption of negatively charged species [57, 159, 158]. In addition, a charge analysis yields a rather small net charge on the adsorbed halogen atoms [57]. This indicates that Pt acts differently compared to Ag and Au as far as the electrosorption valence in halide adsorption is concerned. This can be understood considering the fact that the d-band of Pt is not completely filled, in contrast to Ag and Au, resulting in a stronger interaction.

Jinnouchi et al. considered the influence of solvation and electric field effects by the electric double layer by combining explicit water layers and a implicit water model within a static solvation approximation [83]. They found that effects caused by the presence of the electric double layer on hydrogen adsorption energies are very small.

Hence we neglect the dependence of $G_{\mathrm{surf,ads}}$ and $G_{\mathrm{surf},0}$ on temperature, partial

pressure or activity, and electrode potential, so that Eq. 4.18 can be written as

$$\Delta\gamma = \frac{1}{A_{\mathrm{S}}}\Big(E_{\mathrm{surf,ads}} - E_{\mathrm{surf},0} - \sum_i n_i\tilde{\mu}_i(T,p,U)\Big). \tag{4.19}$$

The Gibbs energy G of both the adsorbate-covered and the clean surface can be evaluated using density functional theory (DFT) calculations. To be more precise, we can derive the internal energy U_{int} from the total energy E_{tot} in DFT. Furthermore, as the terms TS as well as pV are often quite small [156], we can approximate $G \approx U_{\mathrm{int}}$.

To calculate the last term that corresponds to the electrochemical potential of the ions in solution, we use the concept of the computational hydrogen electrode [138]. It is based on the observation that under standard conditions (pH= 0, T= 298 K, p= 1 bar), defining the standard hydrogen electrode (SHE) there is an equilibrium between hydrogen molecules in the gas phase and solvated protons. Therefore the Gibbs free energy of the molecules in the gas phase $\mu_{\mathrm{H_2}}$ is equal to the Gibbs free energy of the protons in aqueous solution plus the energy of an electron at the Fermi level in the metal $\tilde{\mu}_{\mathrm{H^+}} + \tilde{\mu}_{\mathrm{e^-}}$. Thus for this condition we do not need to compute the solvation energy of a proton in an aqueous solution but instead use the energy of the H_2 molecule in the gas phase as a reference which is much easier to derive from first principles. Note that within this approach it is the correct mode to consider the adsorption of a neutral hydrogen atom. This is equivalent to the assumption that upon adsorption the proton from solution recombines with the electron that has already be transfered to the Fermi energy.

Furthermore, it is also known how the electrochemical potential depends on concentration and electrode potential. For these other thermodynamic conditions we just have to correct the SHE expression by an additional term $-eU_{\mathrm{SHE}}$ for the electrode potential and by $-k_BT\ln(10)\mathrm{pH}$ for the proton concentration.

$$\tilde{\mu}_{\mathrm{H^+}} + \tilde{\mu}_{\mathrm{e^-}} = \frac{1}{2}\mu_{\mathrm{H_2}} - eU_{\mathrm{SHE}} - k_BT\ln(10)\mathrm{pH}\ . \tag{4.20}$$

Therefore it is possible to derive, starting from SHE conditions, the electrochemical potential at different electrode potentials and/or different concentrations. Hansen et al. pointed out that the same approach can be used for any redox couple $\frac{1}{2}A_2 + e^- \rightleftharpoons A^-$ [73]. In this way, this approach can be used to calculate the

electrochemical potentials of any halides such as Cl^-, Br^-, and I^- by

$$\tilde{\mu}_{\mathrm{A^-}} - \tilde{\mu}_{\mathrm{e^-}} = \frac{1}{2}\mu_{\mathrm{A_2}} + e(U_{\mathrm{SHE}} - U^0) + k_B T \ln(a_{\mathrm{A^-}}), \tag{4.21}$$

where U^0 is the reduction potential of the corresponding halide which are listed in Table 4.4, and a is the thermodynamic activity of the anion A^-. Since the reduction potential of hydrogen defines 0 V on the SHE scale, it does not appear in Eq. 4.20.

In the following, we will normalize the electrochemical potentials with respect to the total energy of the corresponding gas phase species. The electrochemical potentials $\Delta\tilde{\mu}$ of the proton H^+ and the anions A^- are then given by

$$\begin{aligned} \Delta\tilde{\mu}_{\mathrm{H^+}}(T,p,U) &= \tilde{\mu}_{H^+}(T,p,U) + \tilde{\mu}_{\mathrm{e^-}} - \frac{1}{2}E_{\mathrm{H_2}} \\ &= -eU_{\mathrm{SHE}} - k_B T \ln(10)\mathrm{pH} \end{aligned} \tag{4.22}$$

and

$$\begin{aligned} \Delta\tilde{\mu}_{\mathrm{A^-}}(T,p,U) &= \tilde{\mu}_{A^-}(T,p,U) - \tilde{\mu}_{\mathrm{e^-}} - \frac{1}{2}E_{\mathrm{A_2}} \\ &= e(U_{\mathrm{SHE}} - U^0) + k_B T \ln(a_{\mathrm{A^-}}) \end{aligned} \tag{4.23}$$

which means that the internal total energies $\frac{1}{2}E_{\mathrm{H_2}}$ and $\frac{1}{2}E_{\mathrm{A_2}}$, respectively, at standard conditions (that we will later derive from DFT calculations) have been taken out of the electrochemical potentials. When we then apply Eq. 4.19 to a co-adsorbed system of protons and halides, the Gibbs free energy of adsorption depends on the change of the chemical potentials of the protons $\Delta\tilde{\mu}_{H^+}(T,p,U)$ and the anions $\Delta\tilde{\mu}_{A^-}(T,p,U)$. Therefore the different co-adsorbed structures are planes in a three-dimensional diagram, where the x- and y-axes are the terms $\Delta\tilde{\mu}_{\mathrm{H^+}}(T,p,U)$ and $\Delta\tilde{\mu}_{\mathrm{A^-}}(T,p,U)$ and the z-axis corresponds to the Gibbs free

Redox couple	Reduction potential U^0 (V)
$\frac{1}{2}\mathrm{Cl_2} + e^- \rightleftharpoons \mathrm{Cl^-}$	1.36
$\frac{1}{2}\mathrm{Br_2} + e^- \rightleftharpoons \mathrm{Br^-}$	1.09
$\frac{1}{2}\mathrm{I_2} + e^- \rightleftharpoons \mathrm{I^-}$	0.54

Table 4.4: Reduction potential of the halides considered in this work.

energy of adsorption $\Delta\gamma$,

$$\Delta\gamma(T,p,U) = \frac{1}{A_{\mathrm{S}}}\Big(E_{\mathrm{ads}}^{\mathrm{tot}} - \sum_i n_i \Delta\tilde{\mu}_i(T,p,U)\Big) \; . \tag{4.24}$$

The adsorption energy E_{ads}^{tot} of n_{H} hydrogen atoms and n_{A} halide atoms per unit cell (with A=Cl, Br, or I) is evaluated according to

$$E_{\mathrm{ads}}^{\mathrm{tot}} = E_{\mathrm{ads/slab}} - E_{\mathrm{slab}} - \frac{n_{\mathrm{H}}}{2}E_{\mathrm{H_2}} - \frac{n_{\mathrm{A}}}{2}E_{\mathrm{A_2}} \tag{4.25}$$

where $E_{\mathrm{ads/slab}}$, E_{slab}, $E_{\mathrm{H_2}}$ and $E_{\mathrm{A_2}}$ are the total energies of the adsorbate-covered metal slab, the isolated metal slab, the H_2 molecule and the A_2 halogen molecule, respectively. Note that in the following we will neglect any dependence of $E_{\mathrm{ads}}^{\mathrm{tot}}$ on the thermodynamic conditions.

At given thermodynamic conditions, the stable adsorbate structure is given by the plane with the lowest Gibbs free energy of adsorption. It should be emphasized, that each area of stable equilibrium structures is derived from one DFT structure optimization. This makes the model computationally very attractive. However, the dependence of the adsorption energies on the presence of the electrolyte and of varying electrode potentials is entirely neglected. In principle, these dependencies can be included in the formalism of the computational hydrogen electrode. They are not taken into account here for the following reasons. First, adsorption energies of specifically adsorbed species such as hydrogen or CO are hardly modified by the presence of water, as shown by DFT calculations [167]. Furthermore, using an implicit water model is was also shown by first-principles calculations that H, O, and OH adsorption energies on Pt(111) are only modified by less than 0.1 eV due to the presence of water [170]. We also considered the interaction of an explicit water layer with a halide adsorbate layer at higher coverage above 0.3. We found that water molecules do not penetrate the halide layer but rather form a flat and dense water network above the adsorbed halide atoms indicative of a weak interaction. Second, on metals there is also little influence of any varying electric field on the adsorption energy [138], as already mentioned above.

Note also that the adsorption of hydroxide ions on the Pt(111) surface, which are always present in water, is not considered here as it is suppressed through the presence of halides because their adsorption energy of 1.2 to 1.7 eV is larger than the OH-adsorption energy [120].

Halide	Structure	Θ (ML)	Refs.
Cl	(3×3)	0.44	[33, 191, 203, 179, 189, 204]
Cl	c(4×2)	0.50	[189]
Br	(3×3)	0.44	[114, 171, 15, 195, 177]
Br	$(3 \times 3\sqrt{3}/2)$	0.44	[141]
Br	$(\sqrt{7} \times \sqrt{7}R19.1^\circ)$	0.57	[114]
I	$\sqrt{3} \times \sqrt{3}$	0.33	[38, 36, 113, 214]
I	(3×3)	0.44	[114, 113, 193, 178, 26, 79]
I	$(\sqrt{7} \times \sqrt{7}R19.1^\circ)$	0.43	[114, 38, 36, 113, 214, 192, 193, 178, 26, 79]

Table 4.5: Experimentally found surface structures of halides and co-adsorbed hydrogen on Pt(111).

All DFT calculations in this paper were performed in a periodic supercell approach, using the density functional program VASP [96]. The exchange and correlation energy was taken into account by the functional of Perdew, Burke and Ernzerhof (PBE) [149]. For the electron-core interaction the projector augmented wave method was used [18, 97]. The electronic one-particle wave functions were expanded in a plane-wave basis set up to an energy cutoff of 500 eV.

The metal surface was represented by a slab of five atomic layers, the lower two layers were kept fixed at their bulk positions during the calculations and the upper three layers were completely relaxed. To model a variety of different surface structures and coverages, (3×3), c(4×2) and $(\sqrt{7}\times\sqrt{7}R19.1^\circ)$ surface unit cells were considered containing between 9 and 12 metal atoms per layer. The integration over the first Brillouin zone was done using a gamma-centered k-point mesh with $7 \times 7 \times 1$ special k-points and a Methfessel-Paxton smearing of 0.1 eV [123].

4.4.4 Results and Discussion

Experimental data

Before discussing the results of our calculations, we first review the available experimental data on halide adsorption on Pt(111). Table 4.5 summarizes the results of some experimental studies of halide adsorption, which have been performed in UHV, air, or in electrochemical environments. Structures have been studied through both UHV and electrochemical in-situ techniques. Coverage/-packing densities of adsorbed halides were deduced from Auger spectroscopic data in the vast majority of these studies. While several ordered structures of

halides were found, a degree of uncertainty is always present in the assignment of adsorption sites.

As far as co-adsorbed systems are concerned, there are several studies that used HCl to introduce chlorine onto Pt(111) in UHV environments. High-resolution electron energy loss spectroscopy experiments [204] gave no hint of a Cl-H stretch for all HCl exposures used, indicating that HCl, upon adsorption, undergoes dissociation. Several studies [204, 51] have suggested that the adsorption of HCl molecules does not simply lead to a Cl-covered platinum (111) surface, but to a metal surface that is covered by both adsorbed atomic H and Cl. Low exposures (up to 0.25 L) of HCl undergo complete dissociation on Pt(111) at 90 K to form a disordered mixture of adsorbed H and adsorbed Cl. The simple kinetics and lack of an ordered LEED pattern in this regime suggests high mobility of the adatoms and/or adsorption into a well-mixed, disordered phase containing both adsorbed H and adsorbed Cl [204].

Wagner et al. [204] also found that exposures of 0.5 to 2 L HCl produce an ordered (3×3) phase in UHV. The fact that the same LEED pattern is seen for dosed HCl as for dosed Cl_2 shows that the Pt-Cl interaction is sufficiently strong to establish the Cl adsorption structure. It has been suggested [204] that the co-adsorbed H is simply located in the areas unoccupied by Cl. The structure of the H atoms within the field of Cl atoms is unknown. One can question whether such structures even exist since H adatoms on pristine metal surfaces could be very mobile [7], but we also note that the presence of other adsorbed species can raise surface diffusion barriers [162], stabilizing co-adsorption. Hydrogen is believed to be co-adsorbed because the H_2 desorption following HCl dosing, though small, significantly exceeds the desorption area of background-derived hydrogen [204]. Adsorbed hydrogen leaves the surface through competing processes producing both H_2 and HCl. In contrast, in the study of Fukushima et al. [45] no hydrogen desorption was observed which led to the suggestion that atomic hydrogen and chloride exists in equal amounts on the (3×3) structures.

Chemisorbed iodide ions have been found to cause an overall decrease in the amount of adsorbed hydrogen on polycrystalline Pt surfaces [8]. There is practically no hydrogen adsorption on the surface covered by a monolayer of adsorbed iodide ions. This is consistent with the fact that on Pt(111), iodine forms a protective layer which prevents readsorption of contaminants while the clean sample cools to room temperature. Therefore it is possible to investigate iodine-covered Pt surfaces using STM in air [178, 26]. On the other hand, a monolayer of hydrogen was claimed to be adsorbed even when the surface is covered by the maxi-

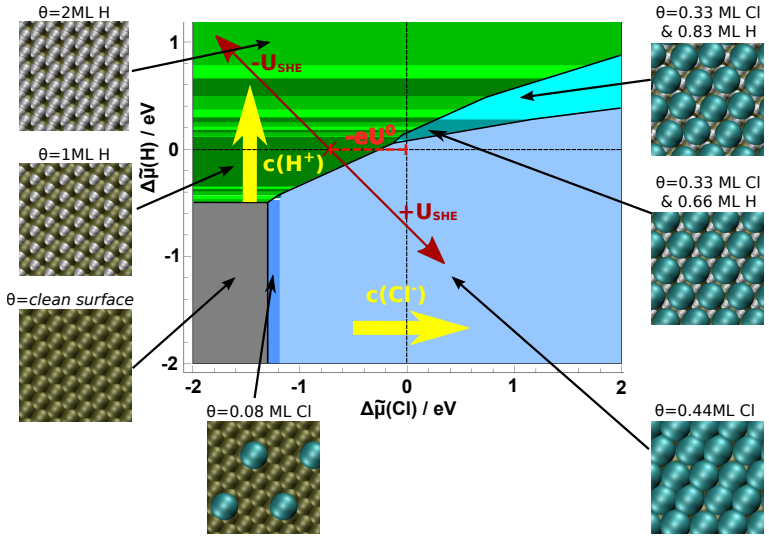

Figure 4.20: Stable phases of co-adsorbed chlorine and hydrogen on Pt(111) as a function of the electrochemical potential of hydrogen and chlorine. The green areas correspond to hydrogen-containing adsorbate structures, the blue areas to chlorine-containing structures and the cyan areas to mixed structures of both hydrogen and chlorine. The yellow arrows illustrate the effect of increasing the concentration of the species individually. The red double-arrow represents the effect of varying the electrode potential for fixed concentrations.

mum amount of chloride and bromide anions [8]. From the observed increase in the second peak in the I-V curves, which corresponds to more weakly-bound H, it has been concluded that adsorbed chloride and bromide on polycrystalline Pt affect the energy distribution of adsorbed hydrogen (decreasing the bond energy, rather than the total amount adsorbed), while the total amount of the adsorbed H does not change [8]. This is supported by the finding that different reaction rates on Pt(100) were obtained with and without hydrogen transfer, attributed to interdiffusion of adsorbed hydrogen atoms in mixed chloride domains [91].

In electrochemical environments, it has been reported earlier [104] that the co-adsorption of chloride and hydrogen atoms has a synergistic character: the presence of hydrogen adatoms enhances chloride adsorption. This conclusion was however later shown to be a result of a surface that contained step defects [49, 51]. In these particular studies it was demonstrated that at positive potentials, where Cl and H adsorption overlap, the adsorption has a competitive character.

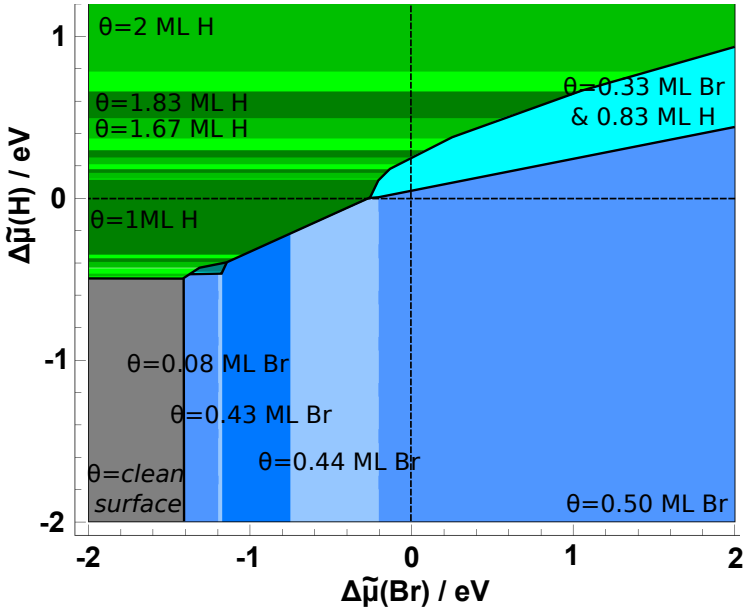

Figure 4.21: Stable phases of co-adsorbed bromine and hydrogen on Pt(111) as a function of the electrochemical potentials of hydrogen and bromine.

There is also evidence that the adatoms are not necessarily ionic at electrode-electrolyte interfaces, as the surface dipole is close to zero [51]. This is confirmed by DFT calculations which show that chlorine adsorption has an covalent character and that even a pure chlorine coverage does not cause an significant change in the surface dipole moment [57, 158].

Calculated phase diagrams for halide-hydrogen co-adsorption

In order to evaluate the phase diagram of stable halide-hydrogen co-adsorption phases, we first calculated the adsorption energies of 113 different structures within (3×3), c(4×2) and $(\sqrt{7} \times \sqrt{7}R19.1°)$ geometries. The corresponding adsorption energies E_{ads} (Eq. 4.25) that are listed in the supplementary material were then used in Eq. 4.24 to construct the planes giving the Gibbs free energy of adsorption $\Delta\gamma$ as a function of the electrochemical potentials $\Delta\tilde{\mu}_{\mathrm{A}^-}$ and $\Delta\tilde{\mu}_{\mathrm{H}^+}$.

In Fig. 4.20, the stable phases of co-adsorbed chlorine and hydrogen on Pt(111) as a function of the electrochemical potential of hydrogen and chlorine are plotted. The electrochemical potential depends on the concentration of the species and the electrode potential. The yellow arrows illustrate how the electrochemical

potential varies when the concentrations of the chlorine anions and the protons are varied separately, the red arrows indicate the effect of varying the electrode potential for fixed concentrations. The structures of some of the stable phases are illustrated in the pictures surrounding the phase diagram.

It is interesting to note that only a very small portion of the phase diagram corresponds to a true co-adsorption structure of hydrogen and chlorine. The phase diagram is dominated by areas that correspond either to pure hydrogen-adsorption or pure chlorine-adsorption phases or to the clean surface. As mentioned above, one would naively expect that there is some electrostatic attraction between adsorbed cations (protons) and anions (chloride). However, the simple picture of anionic adsorption of halides on metal surfaces is obviously not correct. Experimentally, it is well-known that the adsorption of halogen atoms on metal surfaces leads to a reduction of the metal work function at low coverages [33, 15]. In principle, one would expect an increase in the work function upon the adsorption of negatively charged species. We have recently shown in a periodic DFT study that these anomalous work function changes upon halogen adsorption can be explained by the significant polarization of the adsorbed halogen atoms [159] which is particularly strong for iodine, but also present for bromine and chlorine [57, 158]. There is still a rather small net negative charge on the adsorbed halides, but the atomic polarization leads to a dipole moment at the surface that is opposite to what is expected for the adsorption of negatively charged species. Hydrogen adsorption on Pt(111) also leads to a small decrease in the work function [39], which means that there is a dipole-dipole repulsion between adsorbed hydrogen and halides. Furthermore, there might also be an indirect effect through the modification of the electronic and thus chemical properties of the Pt(111) electrode upon the adsorption of the species that leads to an effective repulsion [208, 71]. According to the calculated phase diagram, mixed structures may only exist for unusually high concentrations of both anions and protons.

We have furthermore also evaluated the phase diagram of stable phases of hydrogen co-adsorbed with bromine (see Fig. 4.21) and iodine (Fig. 4.22). In principle, the phase diagrams of the three halides on Pt(111) look rather similar, indicating that the interactions of the adsorbed halides are comparable. For instance, our calculations yielded that the stabilities of the c(4×2) and the (3×3) halides structures are rather similar.

Still, there are characteristic differences. In the chloride adsorption regime, Pt(111) is covered with the dense (3×3) structure over a broad range of electrochemical potentials, whereas iodine shows five different stable patterns. Iodine is the

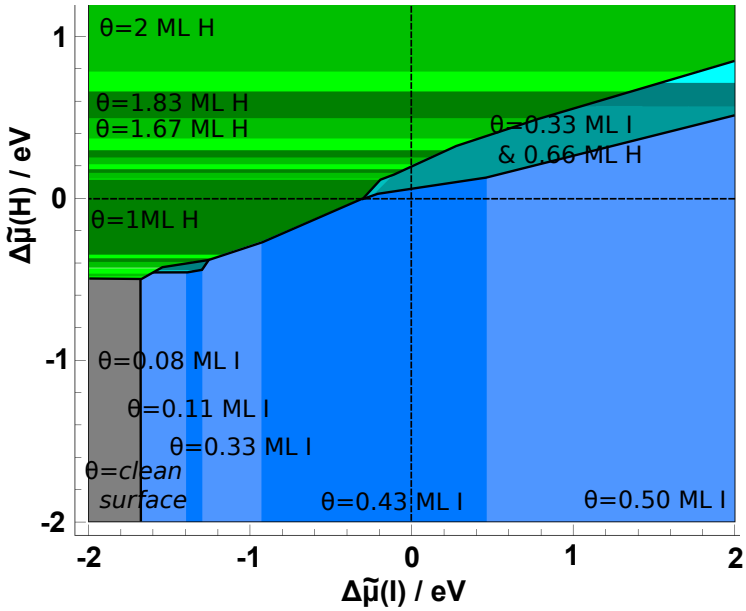

Figure 4.22: Stable phases of co-adsorbed iodine and hydrogen on Pt(111) as a function of the electrochemical potentials of hydrogen and iodine.

only halide that exhibits a stable $\sqrt{3} \times \sqrt{3}$ adsorption structure at a coverage of 1/3 ML as has also been observed in experiments [38, 36, 113, 214]. This $\sqrt{3} \times \sqrt{3}$ adsorption phase is particularly stable for iodine [58] compared to the higher coverage phases which might be caused by the fact that at higher coverages the significantly larger size of iodine compared to bromine and chlorine leads to a relatively larger repulsive interaction. Furthermore, iodine is the only halide for which the $(\sqrt{7} \times \sqrt{7}R19.1°)$ structure is stable at a coverage of 3/7 ML at larger electrochemical potentials, again in agreement with the experiment [114, 38, 36, 113, 214, 192, 193, 178, 26, 79].

We now focus on the regime in which hydrogen adsorption is stable. It is well known that under electrochemical conditions and low potentials, Pt(111) is covered by hydrogen [183, 118]. There is still some controversy between experiment and theory regarding the exact hydrogen equilibrium coverage. Whereas experiments indicate that a full monolayer of adsorbed hydrogen on Pt(111) is only complete at -0.1 V and Pt(111) becomes only partially hydrogen-covered at higher potentials [194, 118], DFT calculations rather yield a hydrogen coverage of 1 ML at positive potentials [188, 185, 170]. This is in fact also the case for our calculations here (for $\Delta\tilde{\mu}_{\mathrm{H^+}} = 0\ eV$). Still, there is a qualitative agreement that there is a significant hydrogen coverage. Furthermore, note that a recent DFT

study [5] using a charged electrode with the counter charge in a polarized electrolyte [81] closely supports the recent experimental findings [194] with respect to the hydrogen coverage as a function of potential.

In the electrochemical literature, this strongly-adsorbed hydrogen is typically referred to as underpotential deposited (upd) hydrogen [182]. The presence of this hydrogen upd layer also has a significant influence on the water structure on Pt(111) at low potential as it weakens the metal-water interaction [161].

There is another, weakly-adsorbed hydrogen species that has been observed which is called overpotential deposited (opd) hydrogen [182]. The role of this opd hydrogen in the hydrogen electrocatalysis has just been intensively discussed from a theoretical point of view [174]. In particular, on transition metal surfaces, this weakly-bound species might play an important role in the hydrogen evolution reaction which is for example a crucial step in the electrolysis of water [103]. Our calculations confirm that at more positive chemical potentials of hydrogen much higher coverages become stable, reflected the presence of opd hydrogen on Pt(111).

Note that the precise structure of ordered hydrogen phases on Pt(111) at different coverages is hard to identify by experimental techniques. This is due to two reasons: as hydrogen is a very weak scatterer, it cannot be easily detected by LEED, X-ray scattering, or STM. Furthermore, hydrogen can be very mobile – the hydrogen adatom's diffusion barrier on Pt(111) is in the order of only 0.06 eV, and can even be effectively lower when delocalized nuclear quantum states of the hydrogen atom are considered [7, 160].

Adsorbate structures as a function of electrode potential

In electrochemical experiments, results are usually not reported as a function of electrochemical potentials, but rather as a function of the electrode potential for a given pH value and ion concentration. This information is all included in the phase diagrams Figs. 4.20-4.22. However, the explicit dependence of the stability of the considered adsorption phases on the electrode potential is not directly visible as the electrochemical potential scale has to be converted into an electrode potential scale. In fact, a variation of the electrode potential with all other parameters kept unchanged corresponds to a diagonal cut through the two-dimensional phase diagrams, as illustrated in Fig. 4.20. The exact position of this diagonal depends on the concentrations.

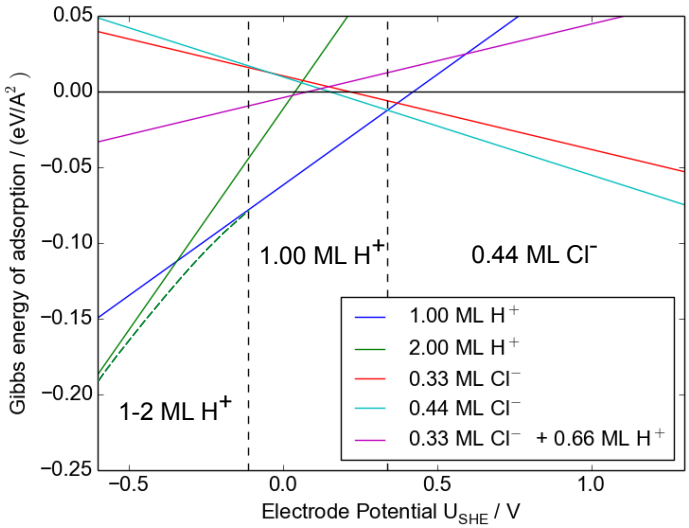

Figure 4.23: Calculated electrochemical equilibrium coverage of chlorine and hydrogen, co-adsorbed on a Pt(111) surface under standard conditions. At low electrode potentials, a variety of different stable hydrogen coverages between one and two ML exists (compare Figs. 4.20-4.22). To keep the figure comprehensive and clear, the Gibbs energy of these coverages are represented by a green, dashed line and exemplified by the 1 and 2 ML structures.

In a previous paper, we addressed equilibrium adsorbate structures of halides on Cu(111) and Pt(111) as a function of the electrode potential, but without taking the effect of co-adsorbed hydrogen into account [58]. Here we present the stable structures of chlorine, bromine and iodine as a function of the electrode potential in Figs. 4.23-4.25, but this time with taking into account the presence of protons in the electrolyte. Furthermore, we have considered more possible structures than done in Ref. [58].

The diagrams in Figs. 4.23-4.25 still correspond to a given combination of pH value and anion activity. For all three figures, we have assumed "standard conditions", i.e., we have assumed $\mathrm{pH} = 0$ and $\mathrm{a_{A^-}} = 1$. This means that the cuts correspond to diagonals with slope -1 through the points $(\Delta\tilde{\mu}_{\mathrm{A^-}}, \Delta\tilde{\mu}_{\mathrm{H^+}}) = (-eU^0, 0)$ in the two-dimensional phase diagrams where U^0 is the corresponding reduction potential of the halides listed in Tab. 4.4. For these conditions, the free

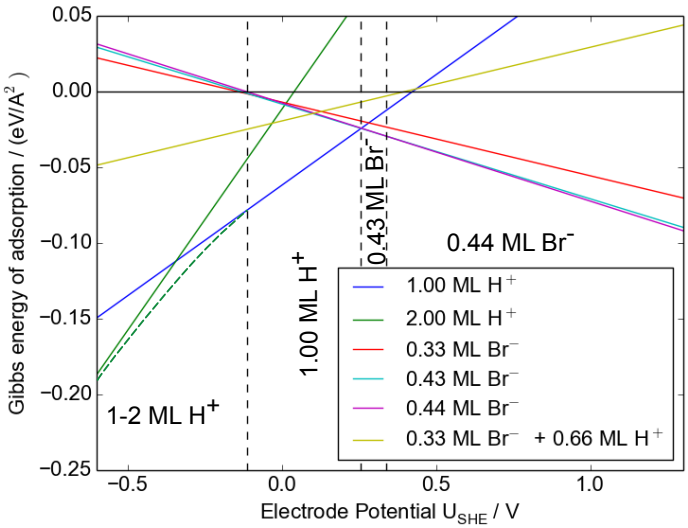

Figure 4.24: Calculated electrochemical equilibrium coverage of bromine and hydrogen, co-adsorbed on a Pt(111) surface under standard conditions. The hydrogen coverage phases at low electrode potentials are represented in the same way as in Fig. 4.23.

energy of adsorption can be expressed as

$$\Delta\gamma(U_{\mathrm{SHE}}) = \frac{1}{A_{\mathrm{S}}}\Big(E^{\mathrm{tot}}_{\mathrm{ads}} - n_{\mathrm{A}}e(U_{\mathrm{SHE}} - U^0) + n_{\mathrm{H}}eU_{\mathrm{SHE}}\Big). \tag{4.26}$$

For the pure halide and the pure hydrogen adsorption phases this equation simplifies to [58]

$$\Delta\gamma_{\mathrm{A^-}}(U_{\mathrm{SHE}}) = \frac{n_{\mathrm{A}}}{A_{\mathrm{S}}}\Big(E^{\mathrm{A^-}}_{\mathrm{ads}} - e(U_{\mathrm{SHE}} - U^0)\Big)\,, \tag{4.27}$$

$$\Delta\gamma_{\mathrm{H^+}}(U_{\mathrm{SHE}}) = \frac{n_{H}}{A_{\mathrm{S}}}\Big(E^{\mathrm{H^+}}_{\mathrm{ads}} + eU_{\mathrm{SHE}}\Big)\,, \tag{4.28}$$

where E^i_{ads} is the adsorption energy per adatom, E^{tot}_{ads}/n_i. For other concentrations in the electrolyte, the reference point in the phase diagram needs to be shifted by $k_{\mathrm{B}}T\ln a_{\mathrm{A^-}}$ and/or by $k_{\mathrm{B}}T\ln(10)\mathrm{pH}$ which at room temperature, e.g., corresponds to about 59 meV if the activity is changed by one order of magnitude or if the pH is changed by one, respectively.

Again, the one-dimensional cuts through the phase diagrams for chlorine, bromine and iodine co-adsorption with hydrogen plotted in Figs. 4.23-4.25 look rather sim-

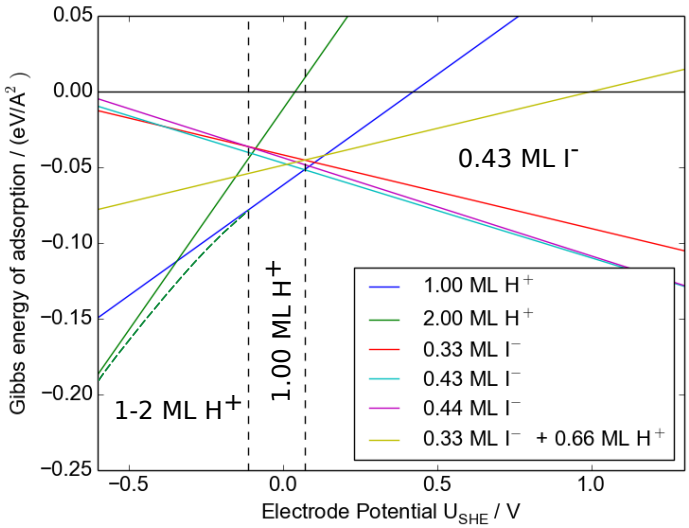

Figure 4.25: Calculated electrochemical equilibrium coverage of iodine and hydrogen, co-adsorbed on a Pt(111) surface under standard conditions. The hydrogen coverage phases at low electrode potentials are represented in the same way as in Fig. 4.23.

ilar which is not too surprising considering the fact that the phase diagrams are rather similar. For all considered systems, no ordered co-adsorption phase becomes stable as a function of electrode potential. The calculated dependence of the free energy of adsorption of the purely hydrogen-covered phases on the electrode potential agrees well with recent results obtained in DFT calculations with the aqueous electrolyte represented in a implicit solvent model [170]. There is a region at intermediate potentials in which both hydrogen adsorption and halide adsorption alone are thermodynamically stable, however, the adsorption has a competitive character, i.e., at lower potentials hydrogen adsorption is more stable, at higher potentials halide adsorption becomes more stable.

In the case of chloride and hydrogen adsorption on Pt(111) (see Fig. 4.23), chloride adsorption becomes thermodynamically stable at a potential of about 0.35 V. Experimentally, measurements of the chloride and the hydrogen Gibbs excesses [49, 51] showed that in a narrow potential range $0.2 < U < 0.3$ V (SHE) hydrogen and chloride can adsorb simultaneously on Pt(111). Still, the analysis of the electrosorption valencies implies that the adsorption of hydrogen and chloride has a competitive character [49, 51].

Note that the driving force for the adsorption of ions from solution is the gain in

free energy per area upon adsorption. Hence an electrode surface might remain uncovered even when ions are present in solution as it rather corresponds to an open system in contact with a reservoir. This means that in contrast to, e.g., solid solutions the concentration of ions on the surface is no parameter that can be modified continuously. Consequently, two distinct adsorbate phases can in principle only exist simultaneously on the surface if they are associated with exactly the same free energy of adsorption per area, which is realized at the potentials in Figs. 4.23-4.25 where the curve of the most favorable hydrogen adsorption phase crosses the curve of the most favorable halide adsorption phase. These considerations imply that thermodynamically, the competitive co-adsorption of two distinct adsorption phases over a range of potentials should not be possible if the dependence of their free energies of adsorption on the electrode potential is different. However, the experimental results concerning the co-adsorption of hydrogen and chloride were derived from cyclic voltammetry so that kinetic effects influence the results. Hence we believe that the experimental findings of hydrogen and chloride co-adsorption in a competitive manner over a narrow potential range are not at variance with our conclusions based on the surface phase diagrams.

As far as bromine (Fig. 4.24) and iodine adsorption (Fig. 4.25) on Pt(111) is concerned, these systems should also not exhibit any synergistic character according to the phase diagrams, but rather be competitive with respect to hydrogen co-adsorption. And indeed, for bromine adsorption, these results are consistent with the experimental observation that the substitution of hydrogen by bromine at Pt(111) [141, 50] and Pt(100) [54, 48] takes place in a very narrow potential range. Also for iodine adsorption on Pt(111), there is experimental evidence for the competitive character of the co-adsorption with hydrogen [113, 140]. Note that according to our calculations the onset of halide adsorption for bromine and iodine is shifted to lower electrode potentials compared to chlorine. This is caused by their stronger binding to Pt(111) [58], but also by their lower reduction potentials, as an analysis of Eq. 4.27 indicates.

Note that we extended the electrode potential range in Figs. 4.23-4.25 to negative values below -0.5 V. In principle, at negative potentials hydrogen evolution would take place which is, however, kinetically hindered. For that reason, it is also experimentally possible to scan to negative electrode potentials. Our calculations show that at potentials below -0.1 V hydrogen coverages larger than unity should become stable. This reflects the experimentally well-established observation of the occurrence of opd hydrogen. Finally, we like to emphasize that the phase diagrams shown in Figs. 4.20, 4.21 and 4.22 can be directly transformed

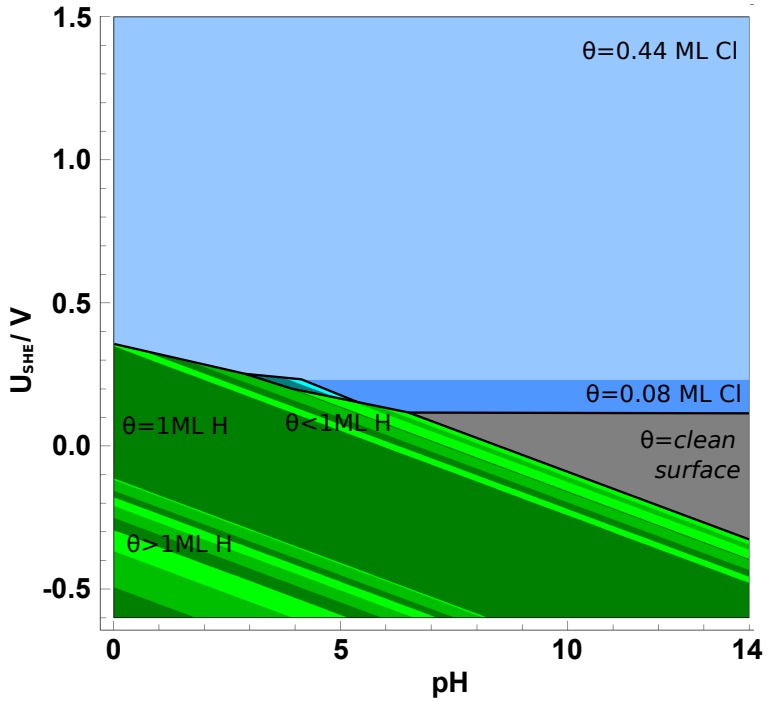

Figure 4.26: Calculated Pourbaix diagram, i.e., a map of the stable phases of co-adsorbed chlorine and hydrogen on Pt(111) as a function of pH and electrode potential for a fixed chlorine concentration corresponding to an activity of 0.1.

into Pourbaix diagrams, i.e., into maps of the stable phases as a function of pH and electrode potential. Taking the coadsorption of chlorine and hydrogen as an example, the phases along the red double arrow in Fig. 4.20 correspond to a cut through the Pourbaix diagram for pH=0 and a given Cl concentration that corresponds to an activity of one, i.e. this cut corresponds to the y-axis of a Pourbaix diagram. The whole Pourbaix diagram at room temperature can then be constructed by shifting the arrow by -59 meV along the y-axis of Fig. 4.20 for a change of the pH value by one and recording the phases along the arrow. Deriving the Pourbaix diagram from the phase diagram Fig. 4.20 thus corresponds to transforming a parallelogram into a rectangle.

As an example, we plot in Fig. 4.26 the Pourbaix diagram of co-adsorbed chlorine and hydrogen on Pt(111) for a fixed chlorine concentration with an activity of 0.1 which for an ideal solution would correspond to a chloride concentration of 0.1 M. The Pourbaix diagram contains regions of pure hydrogen adsorbate phases in greenish colors, pure chlorine phases in bluish colors and a region where the

clean Pt(111) surface is stable in grey. There is also a very small region at about pH ≈ 4 and $U \approx 0.2$ V where mixed hydrogen/chloride phases on Pt(111) are stable that are almost not visible in Fig. 4.20. The boundaries of the pure hydrogen phases exhibit a slope of -59 meV per change of the pH value of 1 which reflects the fact that hydrogen is involved in the formation of these phases. In contrast, the horizontal boundaries between the pure chlorine phases and the clean surface are indicative of the fact that hydrogen is not involved in the formation of these phases so that their absolute stability is independent of the pH value.

4.4.5 Conclusions

The co-adsorption of hydrogen with the halides chlorine, bromine and iodine on Pt(111) surface has been studied by density functional theory calculations. Using a thermodynamic model based on the concept of the computational hydrogen electrode, the stable adsorbate phases as a function of the electrochemical potentials of hydrogen and halides have been derived. Because of the repulsive interaction between adsorbed hydrogen and halogen atoms, their adsorption is mainly competitive, which means that either purely hydrogen-covered phases or purely halogen-covered phases are stable.

By performing cuts through the two-dimensional phase diagram we have determined the stable adsorbate structures on Pt(111) as a function of the electrode potential. In the presence of chloride anions, according to our calculations there is small potential window in which hydrogen and chloride could in principle both adsorb individually on Pt(111). Still, their adsorption occurs in a competitive way which means that there is an electrode potential at which adsorbed hydrogen is replaced by chlorine upon increasing the electrode potential. As adsorbate phases correspond to an open system in contact with a reservoir, in thermal equilibrium no phase-separated co-existence of two immiscible adsorbate structures can occur except when their free energy of adsorption per area is exactly the same. Nevertheless, due to kinetic hindering there might still be a potential range over which the simultaneous adsorption of two separate phases might be observed. These findings are in good agreement with corresponding experiments.

For bromine and iodine adsorption, the phase diagrams for the co-adsorption with hydrogen look very similar, only the replacement of hydrogen by these halides occurs at lower electrode potentials, caused by their stronger binding to Pt(111) and their lower reduction potentials. In general, our study confirms that the concept of

the computational hydrogen electrode is rather useful for determining the structure of metal electrode/electrolyte interfaces.

4.4.6 Acknowledgments

Useful discussion with Karsten Reuter, Technical University of Munich, Jacek Lipkowski, University of Guelph, and Sung Sakong, Universiy of Ulm, are gratefully acknowledged. This research has been supported by the German Science Foundation (DFG) through the research unit FOR 1376 (DFG contract GR 1503/21-2) and by the Baden-Württemberg Foundation within the Network of Competence "Functional Nanostructures" through project CT-04 ORR-Scale of the CleanTech program. The numerical work was performed on the computational resource bwUniCluster funded by the Ministry of Science, Research and Arts and the Universities of the State of Baden-Württemberg, Germany, within the framework program bwHPC5.

4.4.7 Supplementary Material

Adsorption energies

The following tables report the adsorption energies of all the structures considered in this study. All coverage values are in monolayer and E_{ads} is the total adsorption energy per square Ångström. The adsorption energy has been determined according to

$$E_{ads} = \frac{1}{A_s}\big(E_{surf,A} - E_{surf,0} - \sum_A \frac{n_A}{2} E_{A_2}\big), \tag{4.29}$$

where $E_{surf,A}$ is the energy of the covered unit cell, $E_{surf,0}$ is the energy of the clean unit cell and A denotes H, Cl, Br, and I.

structure	H coverage	Cl coverage	Br coverage	I coverage	E_{ads} [meV/Å]
2r3	0	0	0	0	
2r3	0	0	0	0.08	-20.3615
2r3	0	0	0	0.33	-68.1115
2r3	0	0	0.08	0	-17.1903
2r3	0	0	0.33	0	-60.0644
2r3	0	0.08	0	0	-15.8780
2r3	0	0.33	0	0	-55.8375
2r3	0.83	0	0	0	-53.0693
2r3	0.83	0	0	0.08	-62.8470
2r3	0.83	0	0	0.33	-59.3859
2r3	0.83	0	0.08	0	-62.0309
2r3	0.83	0	0.33	0	-74.3311
2r3	0.83	0.08	0	0	-61.7651
2r3	0.83	0.33	0	0	-63.5659
2r3	0.92	0	0	0	-57.5818
2r3	0.92	0	0	0.08	-65.5466
2r3	0.92	0	0.08	0	-64.6535
2r3	0.92	0.08	0	0	-64.1802
2r3	1	0	0	0	-61.8281
2r3	1.08	0	0	0	-60.4512
2r3	1.08	0	0	0	-57.9064
2r3	1.17	0	0	0	-59.0036
2r3	1.17	0	0	0	-55.3351
2r3	0.08	0	0	0	-6.0969
2r3	0.08	0	0	0.08	-25.9627
2r3	0.08	0	0.08	0	-22.9134
2r3	0.08	0.08	0	0	-21.6494
2r3	0.17	0	0	0	-11.9761
2r3	0.17	0	0	0.08	-30.2687
2r3	0.17	0	0	0.08	-31.3971
2r3	0.17	0	0.08	0	-27.4777
2r3	0.17	0	0.08	0	-28.4581
2r3	0.17	0.08	0	0	-26.3382
2r3	0.17	0.08	0	0	-27.2437
2r3	0.25	0	0	0	-17.6429
2r3	0.25	0	0	0.08	-32.9268
2r3	0.25	0	0	0.08	-34.2404
2r3	0.25	0	0.08	0	-30.5706
2r3	0.25	0	0.08	0	-31.7391
2r3	0.25	0.08	0	0	-29.6107

structure	H coverage	Cl coverage	Br coverage	I coverage	E_{ads} [meV/Å]
2r3	0.25	0.08	0	0	-30.7097
2r3	0.33	0	0	0	-22.4981
2r3	0.33	0	0	0.08	-37.8347
2r3	0.33	0	0	0.33	-72.0556
2r3	0.33	0	0.08	0	-35.6272
2r3	0.33	0	0.33	0	-67.0287
2r3	0.33	0.08	0	0	-34.6861
2r3	0.33	0.33	0	0	-63.9674
2r3	0.42	0	0	0	-28.0817
2r3	0.42	0	0	0.08	-42.6216
2r3	0.42	0	0	0.33	-73.1659
2r3	0.42	0	0.08	0	-40.5505
2r3	0.42	0	0.33	0	-69.3459
2r3	0.42	0.08	0	0	-39.6946
2r3	0.42	0.33	0	0	-67.0073
2r3	0.5	0	0	0	-33.4575
2r3	0.5	0	0	0.08	-47.4860
2r3	0.5	0	0	0.33	-74.1208
2r3	0.5	0	0.08	0	-45.5029
2r3	0.5	0	0.33	0	-71.3870
2r3	0.5	0.08	0	0	-44.6678
2r3	0.5	0.33	0	0	-70.1729
2r3	0.58	0	0	0	-38.6816
2r3	0.58	0	0	0.08	-52.1286
2r3	0.58	0	0	0.33	-74.7444
2r3	0.58	0	0.08	0	-50.1815
2r3	0.58	0	0.33	0	-72.5722
2r3	0.58	0.08	0	0	-49.3961
2r3	0.58	0.33	0	0	-71.3685
2r3	0.67	0	0	0	-43.2038
2r3	0.67	0	0	0.08	-56.3082
2r3	0.67	0	0	0.33	-74.9849
2r3	0.67	0	0.08	0	-54.5078
2r3	0.67	0	0.33	0	-72.5016
2r3	0.67	0.08	0	0	-53.7184
2r3	0.67	0.33	0	0	-70.3110
2r3	0.75	0	0	0	-48.2749
2r3	0.75	0	0	0.08	-59.7021
2r3	0.75	0	0	0.33	-68.0623
2r3	0.75	0	0.08	0	-58.3203

structure	H coverage	Cl coverage	Br coverage	I coverage	E_{ads} [meV/Å]
2r3	0.75	0	0.33	0	-65.4447
2r3	0.75	0.08	0	0	-57.4700
2r3	0.75	0.33	0	0	-63.6795
3x3	0	0	0	0	
3x3	0	0	0	0.11	-26.0275
3x3	0	0	0	0.44	-78.7526
3x3	0	0	0.11	0	-22.0504
3x3	0	0	0.44	0	-78.2862
3x3	0	0.11	0	0	-20.3818
3x3	0	0.44	0	0	-78.6087
3x3	0.11	0	0	0	53.9559
3x3	0.11	0	0	0.11	-33.0503
3x3	0.11	0	0.11	0	-29.2703
3x3	0.11	0.11	0	0	-27.6725
3x3	0.22	0	0	0	-15.1752
3x3	0.22	0	0	0.11	-39.3318
3x3	0.22	0	0.11	0	-35.5366
3x3	0.22	0.11	0	0	-33.8812
r7	0	0	0	0	
r7	0	0	0	0.43	-81.0501
r7	0	0	0.43	0	-76.5413
r7	0	0.43	0	0	-74.1512
r7	0.14	0	0	0	69.3926
r7	0.29	0	0	0	-15.7505
2r3	1.25	0	0	0	
2r3	1.33	0	0	0	-54.9253
2r3	1.42	0	0	0	-52.3750
2r3	1.5	0	0	0	-49.3180
2r3	1.58	0	0	0	-45.7183
2r3	1.67	0	0	0	-41.2444
2r3	1.83	0	0	0	-29.2230
2r3	1.92	0	0	0	-21.2088
2r3	2	0	0	0	-11.6715
c4x2	0	0	0	0	
c4x2	0	0	0	0.5	-76.2117
c4x2	0	0	0.5	0	-79.9492
c4x2	0	0.5	0	0	-48.2331

4.5 Ionic adsorbate structures on metal electrodes calculated from first principles

The following section focuses on both nitrate adsorption on lead and bromide adsorption on platinum. In the case of lead, surface reconstruction plays an extensive role. The paper was published in Industrial & Engineering Chemistry Research 2016, 55 (42), 11107-11113: X. Lin, F. Gossenberger, and A. Groß "Ionic Adsorbate Structures on Metal Electrodes Calculated from First-Principles" [107]. Florian Gossenberger performed all the calculation and did the analysis concerning bromide adsorption on platinum, whereas Xiaohang Lin prepared all calculations and analysis of nitrate adsorption on lead. Xiaohang Lin wrote the paper.

4.5.1 Abstract

The equilibrium coverage of metal electrodes in contact with an electrolyte has been addressed by periodic quantum-chemical calculations based on density functional theory. The electrolyte has been treated in a grand-canonical approach using the concept of the computational hydrogen electrode. After briefly reviewing the theory and illustrating it using the coadsorption of bromide and hydrogen as an example, the interaction of nitrate with a Pb(111) electrode is addressed. A spontaneous reconstruction of the uppermost Pb layer is observed leading to the formation of a salt-like layer.

4.5.2 Introduction

Electrochemistry is concerned with structures and processes at the interface between an electron conductor, the electrode, and an ion conductor, the electrolyte [182]. The electrolyte is often in the liquid phase, in particular in electrocatalysis, containing ions to make it conductive. Typically, these ions, especially anions, are subject to an attractive interaction with electrodes leading to a concentration of the ions on or near the electrodes that is much higher than their equilibrium concentration in the bulk electrolyte [201]. These ions are part of the

electrical double layer, but their interaction with the electrode can also modify the electronic and chemical and even structural properties of the electrodes significantly [198, 208, 71, 3, 201]. Because of this significant effect that the presence of ions in the electrolyte can have on electrode properties, it is important to understand and predict the thermodynamically stable structure of adsorbed ions as a function of environmental parameters such as ion concentration in the electrolyte and electrode potential.

The theoretical description of the interfaces of electrodes with liquid electrolytes represents a considerable conceptual and numerical challenge as both the liquid phase of the electrolyte and the presence of electrified surfaces need to be taken into account [184, 185, 168] which requires to perform computationally costly statistical averages and consider charged electrodes. Note that at electrochemical interfaces the reference for the adsorption energy has to be determined with respect to the corresponding species in solution. However, in a very elegant grand-canonical approach that is now coined computational hydrogen electrode (CHE) [138, 137] the evaluation of solvation energies can be avoided. The CHE corresponds to the combination of atomistic calculations with a grand-canonical approach to describe the reference energy of the adsorbates [129, 156]. It is particularly useful for electrochemical systems as it is based on the observation that at specific thermodynamic conditions species in solution are in equilibrium with corresponding gas-phase species which are much easier to describe theoretically [138, 137, 163, 164]. In addition, the dependence of the reference energy on electrochemical parameters such as the electrode potential, pH, and ion concentration is known. Furthermore, at metal electrodes adsorption energies are often only weakly dependent on the presence of the electrochemical environment [138, 137, 167, 165, 205, 83]. This concept has been rather successfully used to address electrocatalytic reactions on metal and oxide electrodes [138, 137, 117, 69, 133, 169]. We have recently used this concept to derive the equilibrium coverage of halides on metal electrodes [58], furthermore we extended this approach to address the coadsorption of halides and hydrogen on Pt(111) [59]. We could successfully reproduce and explain the experimental observation [140, 49, 50] of the competitive adsorption of halides and hydrogen as a function of electrode potential.

In this paper, we will first briefly review the concept to derive the equilibrium coverage of ions on electrode surfaces from first-principles electronic structure calculations based on density functional theory (DFT) and illustrate the findings. We will then extend this approach to address the interaction of nitrate with Pb(111).

This system was chosen because it corresponds to the electrochemical setup recently used in a single-atom transistor controlled by the electrode potential [211, 210, 209, 212] as a model for a microscopic quantum device [76]. There we will demonstrate that the presence of anions in the electrolyte can lead to a severe restructuring of metal electrodes, for example leading to the formation of a salt layer.

4.5.3 Computational details

The DFT calculations presented in this paper were done using the periodic electronic structure code VASP [96], employing the Perdew, Burke and Ernzerhof (PBE) functional to account for the exchange and correlation effects [149]. For the electron-core interaction the projector augmented wave method was used [18, 97]. The electronic one-particle wave functions were expanded in a plane-wave basis set up to an energy cutoff of 500 eV. Different surface unit cell sizes were employed in these studies. In each case it had been made sure that the special k-points sets used to replace the integration over the first Brillouin zone are chosen large enough to yield converged results.

Stable adsorbate phases are characterized by the minimum in the free energy of adsorption per surface area A_{S} [58]:

$$\Delta\gamma = \frac{1}{A_{\mathrm{S}}}\big(G_{surf,ads} - G_{surf,0} - \sum_i n_i\mu_i\big)\ . \tag{4.30}$$

Here $G_{\mathrm{surf,ads}}$ and $G_{\mathrm{surf},0}$ are the Gibbs free energies of the adsorbate-covered and of the clean surface, n_i is the number of adsorbed atoms of the type i per surface area A_{S}, and μ is the chemical potential of the adsorbates in their corresponding reservoir. In electrochemical systems, the chemical potential has to be replaced by the electrochemical potential $\tilde{\mu}_i = \mu_i + z_i eU$, where z_i is the charge state of the particle, e the elementary electric charge and U the electrode potential. As mentioned above, in electrochemical situations the electrochemical potential is given with respect to the solvated particle whose energy is hard to calculate as it involves a thermodynamic integration scheme. However, one can take advantage of the fact that there are specific thermodynamic conditions in which the solvated particle is in equilibrium with a corresponding particle in the gas phase. For example, the proton in solution is in equilibrium with the hydrogen

molecule in the gas phase at standard conditions,

$$\mathrm{H}^+ + e^- \rightleftharpoons \frac{1}{2}\mathrm{H}_2 \; . \tag{4.31}$$

In fact, this equilibrium defines the standard hydrogen electrode (SHE). This means that one can use the H_2 molecule in the gas phase as a reference which is much easier to evaluate than the proton in solution. Furthermore, it is known how the electrochemical potential of the proton in solution depends on electrode potential U and pH:

$$\tilde{\mu}_{\mathrm{H}^+} + \tilde{\mu}_{\mathrm{e}^-} = \frac{1}{2}\mu_{\mathrm{H}_2} - eU_{\mathrm{SHE}} - k_B T \ln(10)\mathrm{pH} \; . \tag{4.32}$$

This concept is not restricted to hydrogen, but can be used for any redox couple [73]. For example, for halides such as Cl^-, Br^-, and I^-, the corresponding relation for the electrochemical potential reads

$$\tilde{\mu}_{\mathrm{A}^-} - \tilde{\mu}_{\mathrm{e}^-} = \frac{1}{2}\mu_{\mathrm{A}_2} + e(U_{\mathrm{SHE}} - U^0) + k_B T \ln(a_{\mathrm{A}^-}), \tag{4.33}$$

where U^0 is the reduction potential of the corresponding halide, and a is the thermodynamic activity of the anion A^-.

This is the essence of the concept of the computational hydrogen electrode. It still remains the problem that in eq. 4.30, the free energies of adsorbate-covered electrode and the uncovered electrode need to be determined. It is common practice in applications of the computational hydrogen electrode to neglect entropic contributions and the influence of the electrochemical environment, namely the presence of the electrolyte and the variation of the electrode potential, in the determination of $G_{\mathrm{surf,ads}}$ and $G_{\mathrm{surf},0}$. As far as metal electrodes are concerned, this approximation seems to be justified [138, 137, 167, 165, 205, 83] because of the strong chemical interaction with electrodes and the good screening properties of metals. This allows the use of DFT total energies instead of free energies so that eq. 4.30 can be replaced by

$$\Delta\gamma = \frac{1}{A_{\mathrm{S}}}\Big(E_{\mathrm{surf,ads}} - E_{\mathrm{surf},0} - \sum_i n_i \tilde{\mu}_i(T, p, U)\Big). \tag{4.34}$$

Finally we reformulate this expression by referring the electrochemical potentials of the solvated species to the corresponding stable gas-phase species and the electrochemical potential of the electrons [59] that corresponds to the Fermi en-

ergy of the metal electrode, similar to what is done in *ab initio* thermodynamics [156] arriving at

$$\Delta\gamma(T,p,U) = \frac{1}{A_{\mathrm{S}}}\Big(E_{\mathrm{ads}}^{\mathrm{tot}} - \sum_i n_i \Delta\tilde{\mu}_i(T,p,U)\Big) \; . \tag{4.35}$$

where the adsorption energies $E_{\mathrm{ads}}^{\mathrm{tot}}$ are taken with respect to the gas-phase species. Note that in this particular formulation the dependence of the free energy of adsorption on entropic contributions entirely enters through the corresponding dependence of the electrochemical potentials of the species in the reservoir on temperature, pressure, and electrode potential.

4.5.4 Results and Discussion

We will illustrate the approach to determine the thermodynamically stable adsorbate structure at electrochemical electrode/electrolyte interfaces using the coadsorption of hydrogen and bromine on Pt(111) as an example. Experimentally, it has been observed that the substitution of adsorbed hydrogen by bromine on Pt(111) as a function of electrode potential occurs in a very narrow potential range [141, 50], indicative of competitive adsorption. Cyclovoltammograms further show [171, 16] that on the negative going scan the bromine desorption peaks appear at potentials negative to the hydrogen adsorption peaks on the clean surface, demonstrating that hydrogen is replaced by bromine. This is at first glance surprising because one would expect that there is an attractive electrostatic interaction between an adsorbed cation (proton) and an adsorbed anion (bromide).

As a first step, several adsorbate structures of hydrogen and bromine alone and both adsorbates together within (3×3), c(4×2) and $(\sqrt{7} \times \sqrt{7}R19.1^\circ)$ surface unit cells were determined and the adsorption energy evaluated. The (3×3) and $(\sqrt{7} \times \sqrt{7}R19.1^\circ)$ structure were observed in experiments[141, 114, 116] whereas the c(4×2) structure was seen for a chlorine adlayer on Pt(111) [189]. In these calculations, no electrolyte was present. However, we have recently shown [61] that for halide coverages above 1/3 closed water layers form above the halide adsorbate layer; that is, the water molecules do not penetrate into the halide adsorbate structure.

Note that according to eq. 4.35, as a function of the electrochemical potentials of the proton and of bromide, each adsorbate structure is represented by a plane in a three-dimensional space spanned by $\Delta\tilde{\mu}_{\mathrm{H^+}}$, $\Delta\tilde{\mu}_{\mathrm{A^-}}$ and the Gibbs free energy

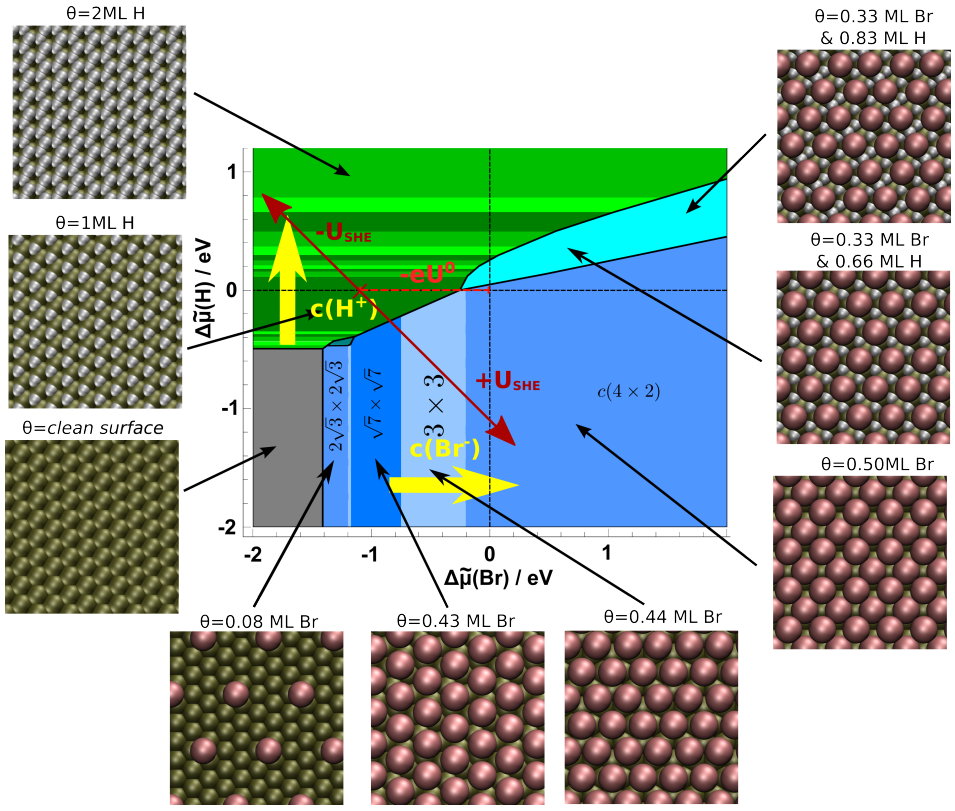

Figure 4.27: Stable phases of coadsorbed bromine and hydrogen on Pt(111) as a function of the electrochemical potentials of hydrogen and bromine. Bluish areas denote pure bromine coverages, greenish colors show pure hydrogen coverages, and the turquois area denotes a coadsorbed structure of both H and Br. Only the most stable structures are illustrated in the subfigures. Especially in the case of hydrogen adsorption there are regions where the stable coverage is a varying dynamic in between the subfigures. The red double arrow denoted by $-eU^0$ indicates a variation of the electrode potential with all other parameters kept fixed at standard conditions, whereas the yellow arrows illustrate the influence of the ion concentration.

of adsorption $\Delta\gamma$, and for a given set of electrochemical potentials the structure with the lowest $\Delta\gamma$ corresponds to the thermodynamically stable phase.

The resulting phase diagram is plotted in Figure 4.27 together with an illustration of the structure of the stable phases. Most of the phase space is characterized by either a purely hydrogen-covered (greenish colors) or a purely bromine-covered (bluish colors) region. Typically there is an indirect repulsive interaction between adsorbates through adsorption-induced modifications of the metal substrate [71]. However, one could imagine that this might be compensated by an attractive dipole-dipole interaction between adsorbed anions and cations. However, there is apparently no attractive interaction between adsorbed hydrogen and bromide. This result can be understood considering the fact that the adsorption of bromine on Pt(111) leads to an anomalous work function decrease [15] caused by the strong polarization upon adsorption [57, 158, 159]. As a consequence, a dipole-dipole repulsion between adsorbed bromine and hydrogen results.

However, in electrochemistry, the electrochemical potential of solvated species is typically not specified, but rather the concentration and the electrode potential. The variation of the electrode potential at standard conditions is illustrated by the red arrows in Figure 4.27.

Hence it is rather helpful to transform the phase diagram into a Pourbaix diagram, that is, into a map of the stable phases as a function of pH and electrode potential. The Pourbaix diagram derived from the phase diagram plotted in Figure 4.27 is shown in Figure 4.28. For a given pH value, the stable surface structures as a function of the electrode potential can be immediately read off, information that is directly relevant for the interpretation of cyclic voltammograms. The diagram demonstrates that indeed upon increasing the electrode potential purely hydrogen-covered phases are replaced by purely bromine-covered phases. Because of the presence of bromine, the upper potential edge of the stable hydrogen phases is shifted to lower potentials, confirming the competitive nature of hydrogen and bromine inferred from the experiment [50, 141, 171, 16].Only at higher pH values there is a small pocket in which hydrogen and bromine coadsorption structures are stable, but only over a rather narrow potential range, thus confirming experimental findings. [141, 50]

The stable bromine phases correspond either to a $(\sqrt{7} \times \sqrt{7}R19.1^\circ)$ structure with a coverage of $\Theta = 3/7$ or a 3×3 structure with $\Theta = 4/9$. Both structures have been observed in the experiment [141, 114, 116]. The calculated results for the coadsorption of hydrogen with chlorine and iodine are also all consistent with

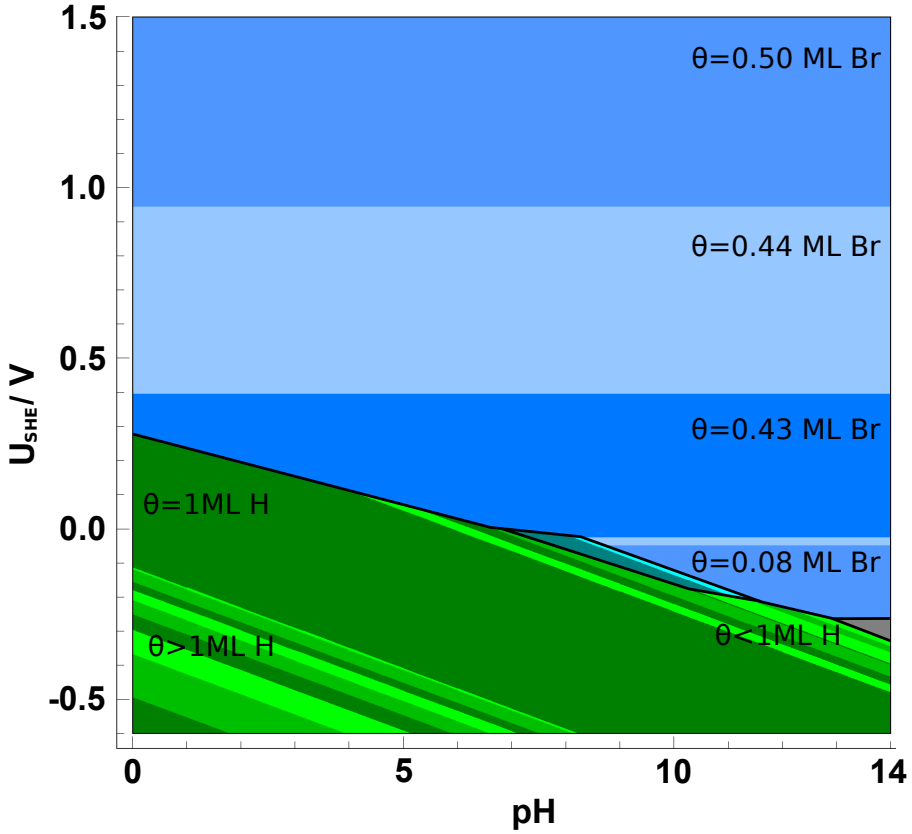

Figure 4.28: Calculated Pourbaix diagram, that is, a map of the stable phases of coadsorbed bromine and hydrogen on Pt(111) as a function of pH and electrode potential for a fixed bromine concentration corresponding to an activity of $a = 0.1$. The color code is the same as in Figure 4.27 where also the geometric structures of the corresponding phases are given. Greenish colors denote a pure hydrogen phase, bluish colors denote a pure bromine phase. In between the hydrogen and bromine phases, there is a thin region, where a coadsorbate structure with both species is stable. The gray area corresponds to a region where the clean, uncovered electrode is stable.

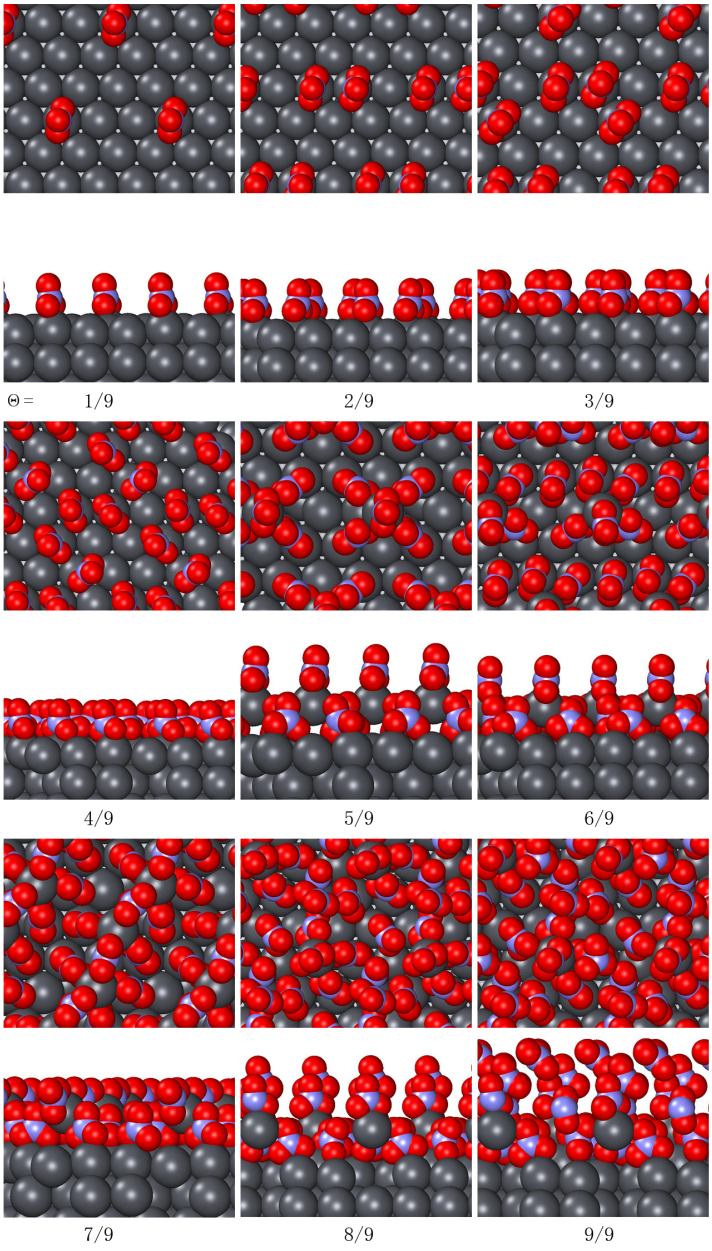

Figure 4.29: Illustration of the structures of nitrate adsorbed on Pb(111). Pb atoms are colored in dark gray, oxygen is red, and nitrogen is blue.

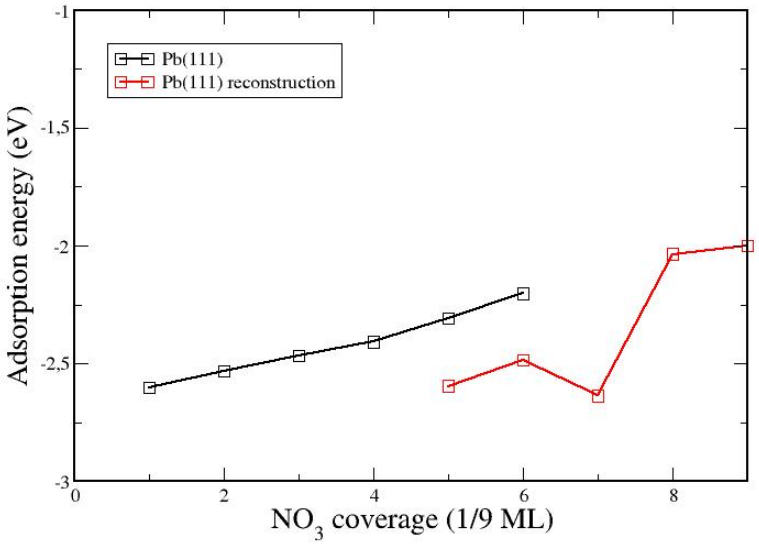

Figure 4.30: Adsorption energy of NO_3 on Pb(111) per molecule as a function of the coverage. Black circles denote adsorption on the unreconstructed electrode, red boxes correspond to adsorption involving a reconstruction of the Pb(111) electrode.

experimental observations [58] indicating the reliability of the approach outlined here based on the computational hydrogen electrode.

This same approach has also been used to evaluate the interaction of nitrate with Pb(111). Pb electrodes have recently been of interest as they are one of the materials used to realize a single-atom transistor in an electrochemical environment [211, 210, 209, 212] which opens attractive perspectives to prepare microscopic quantum devices [76]. It is based on the fact that atomic-scale quantum point contacts can be reversibly switched as a function of the electrode potential. Still, the details of the operation of the single-atom transistor are not understood. Therefore, in a series of first-principles-based studies we have tried to elucidate possible mechanisms to form atomic contacts at Pb electrodes [106] and to determine the water structure at flat and stepped Pb electrodes [61, 109]. We have now extended this project in order to assess the influence of nitrate (NO_3^-) on the structure of Pb electrodes as a nitrate-based electrolyte has been used in the experiments realizing the single-atom transistor [209].

Again, the first step is to search for minimum energy adsorbate structures for var-

ious coverages. To the best of our knowledge, there is no experimental study identifying the structure of nitrate on Pb(111). Therefore, we have chosen a 3×3 surface unit cell that should be sufficiently large to allow the formation of different structures. Still it should be admitted that thus we might miss some stable structures. However, without prior knowledge of the periodicity of adsorbate structures a search for all possible arrangements is computationally extremely demanding.

The considered structures within the 3×3 surface unit cell are illustrated in Figure 4.29, the corresponding adsorption energies are shown in Figure 4.30. At low coverages, the molecules arrange on the unreconstructed Pb(111) surface, the adsorption energies become less negative with increasing coverage indicative of a repulsive interaction between the adsorbed nitrate molecules. Interestingly enough, at coverages starting from $\Theta = 5/9$, Pb(111) spontaneously reconstructs upon exposure to nitrate. A lead atom is extracted from the Pb electrode and forms a Pb-NO_3 complex. This is associated with a significant energy gain. The ease to form such a complex involving the extraction of a Pb atom from the surface is obviously a consequence of the relatively low cohesive energy of lead of 2.03 eV/atom [90]. Note that in these calculations the presence of the electrolyte was ignored. However, water is relatively weakly interacting with lead. For example, the adsorption energy of water monomers on Pb(111) is only -0.07 eV [109]. Hence we do not expect that the chemically driven reconstruction of Pb(111) will be strongly modified by the presence of water.

The stable adsorption phases as a function of the electrode potential are plotted in Figure 4.31. To derive this phase diagram based on the concept of the computational hydrogen electrode, the following redox couple has been used to define a reference for nitrate,

$$2\mathrm{H}^+(\mathrm{aq}) + \mathrm{NO}_3^-(\mathrm{aq}) + e^- \rightleftharpoons \mathrm{NO}_2(\mathrm{g}) + \mathrm{H}_2\mathrm{O}(\mathrm{aq})\,. \tag{4.36}$$

Furthermore, a nitrate activity of $a_{\mathrm{NO}_3^-} = 1$ has been assumed. Up to an electrode potential of about -0.4 V vs SHE, the clean Pb(111) electrode is thermodynamically favored. For higher electrode potentials, the reconstructed Pb(111) electrode at a nitrate coverage of $\Theta = 7/9$ becomes stable over a wide potential window corresponding to the conditions typical for electrochemical experiments in aqueous electrolytes. Inspecting Figure 4.29 reveals that for this coverage a complete lead nitrate layer evolves. At lower coverages, this layer is not completed, at higher coverages a new layer starts to grow.

To understand the origin of the stability of the reconstructured Pb(111) electrodes

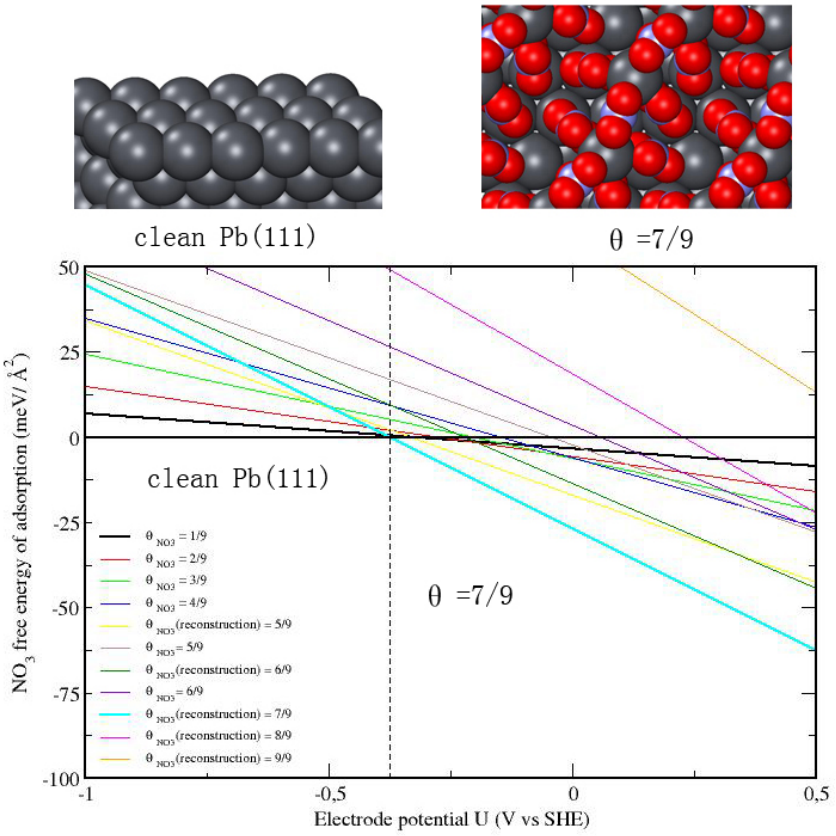

Figure 4.31: Phase diagram of the stable nitrate structures as a function of electrode potential.

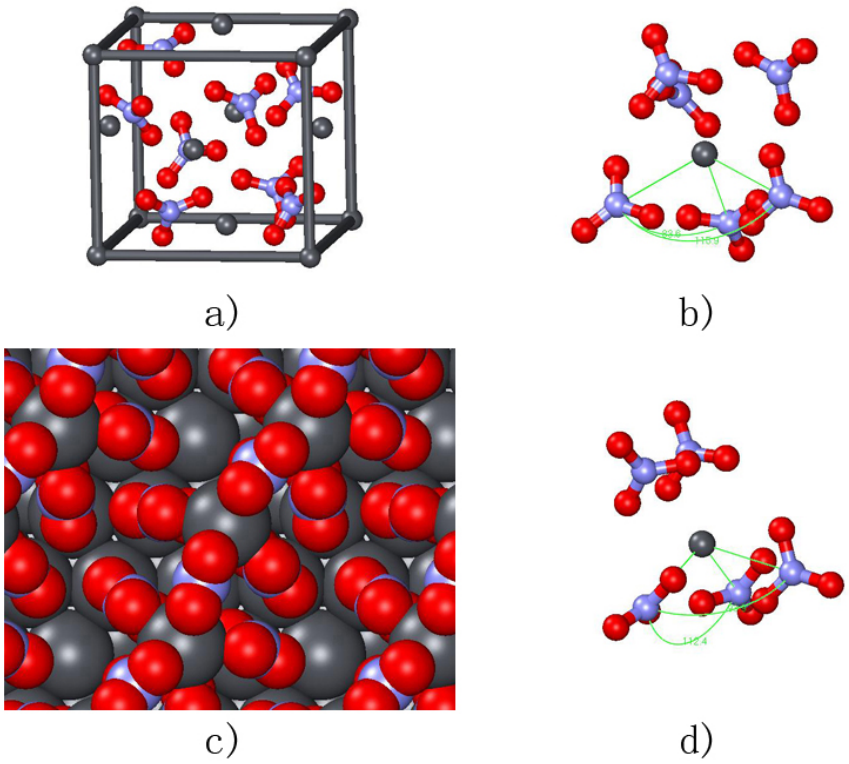

Figure 4.32: Comparison of the $Pb(NO_3)_2$ bulk structure and the structure of the lead nitrate complex formed spontaneously on Pb(111) at a nitrate coverage of $\Theta = 7/9$. (a) Bulk unit cell of $Pb(NO_3)_2$, (b) arrangement of nitrate around a Pb atom in the bulk, (c) top view of reconstructed Pb(111) surface, (d) arrangement of nitrate around a Pb atom in the surface complex.

at a nitrate coverage of $\Theta = 7/9$ involving the formation of a Pb-NO_3 complex even further, we compare in Figure 4.32 the structure of bulk lead nitrate with the corresponding complex on the Pb(111) surface. Panels a and c show the bulk unit cell of $Pb(NO_3)_2$ and the top view of reconstructed Pb(111) surface, respectively. The local nitrate arrangements around the lead atom in the bulk and in the surface complex are compared in panels b and d. Due to the lattice mismatch between bulk lead nitrate and Pb(111), no perfect agreement should be expected. Still the local arrangements are rather similar. We illustrate this by particularly considering the N-Pb-N angles with regard to the NO_3 groups nearest to the Pb atom. In the bulk, these angles have values of 83.6° and 116.9°, as indicated in Figure 6b. In the case of the reconstructed Pb(111) surface, these particular angles

are only slightly modified to values of 93.9° and 112.4°, respectively, and the local coordination is also hardly changed, as Figure 6d shows. This indicates that the nitrate-induced surface reconstruction of Pb(111) can be viewed as the formation of a surface lead nitrate layer or as the initial step of lead nitrate salt formation [145],despite lead nitrate readily dissolving in water [40].

Our results show that the exposure of a metal electrode to an aqueous electrolyte can lead to a substantial surface restructuring. This is of course not the case for any anion-containing electrolyte. However, once such a surface reconstruction occurs, it significantly modifies the structural, electronic, and chemical properties of the electrode and should not be neglected.

The results presented in this study show that first-principles calculations using the concept of the computational hydrogen electrode are a powerful tool to determine equilibrium structures of metal electrode/aqueous electrolyte interfaces. In the determination of the adsorption energies entering the formalism, the explicit influence of the electrolyte and of varying electrode potentials has been neglected. This approximation is justified by the good screening properties of metals. However, there is certainly a need to assess the validity of this approximation by including the electrochemical environment explicitly. First steps along this route have already been taken [165, 205, 83, 19, 169]. For the results presented in this work, explicitly considering the electrochemical environment in the calculations will change the results quantitatively to a certain extent, but it is not expected that any qualitative trends will become modified.

4.5.5 Conclusions

The structure of metal electrode/aqueous electrolyte interfaces has been studied by first-principles calculations treating the electrochemical environment in a grand-canonical approach based on the concept of the computational hydrogen electrode. Phase diagrams of the thermodynamically stable adsorbate structures as a function of electrochemical potentials have been derived which allows, for example, a derivation of the Pourbaix diagrams which can be directly compared to experimental results. Regarding the coadsorption of hydrogen and bromine on Pt(111), the results were able to reproduce the experimentally observed competitive nature of the coadsorption. The presence of a nitrate-containing electrolyte over a lead electrode leads to a significant reconstruction of the lead electrode presenting the first steps of lead nitrate salt formation.

4.5.6 Acknowledgments

This research has been supported by the German Research Foundation (DFG) through Contract GR 1503/21-2 within the DFG research unit FOR 1376 and by the Baden-Württemberg Foundation within the Network of Competence “Functional Nanostructures”. Computer time has been provided by the bwHPC initiative and the bwHPC-C5 project funded by the Baden-Württemberg government (MWK) and the German Research Foundation (DFG). This contribution was identified by Session Chair Oleg Borodin (U.S. Army Research Laboratory, Adelphi, MD 20783, USA) as the Best Presentation in the session “Electrochemistry at Solid/liquid Interfaces” of the 2016 ACS Spring National Meeting in San Diego, CA.

4.6 Ab-initio study of sulfate, bisulfate and hydrogen co-adsorption on Pt(111) and Au(111) in an electrochemical environment

Sulfate is a very common anion in electrochemistry since it does hardly interfere with most electrochemical reactions going on at the solid/liquid interface of the electrode. However, it is well known, that sulfate ions build up dense coverages at positive electrode potentials. These structures are essential to understand first, before studying reactions under these conditions. The following paper illuminates the stability of various structures containing sulfate, bisulfate, and hydrogen. Thereby we compare structures on the Pt(111) and Au(111) surface. All calculations on platinum were performed by Florian Gossenberger, all calculation about gold were done by Fernanda Juarez. The Introduction and the part about computational details of the paper wrote Florian, the section about basic equations Fernanda. The extensive analysis was done in close collaboration together. However, the article is not published yet. It is still in preparation.

4.6.1 Abstract

Sulfate, bisulfate and hydrogen co-adsorption was investigated on a Pt(111) and Au(111) surface. Solvent effects were taken into account by both an implicit solvent model, and explicit solvation as well. The importance of both aspects of solvation is discussed in detail. Finally, we provide phase diagrams and pourbaix diagrams for platinum and gold.

4.6.2 Introduction

All electro-catalytic reactions take place on the solid-liquid interface of the electrode surface. This region is therefore crucial for every electrochemical system. On this account, the interaction of widely used electrolytes on catalytic surfaces was studied intensively in the last decades. One of the most prominent systems is sulfate adsorption on platinum, but despite various investigations, the surface structure of the ad-layer is still controversial. The origin of this problem lies in the equilibrium between sulfate and bisulfate since both anions can hardly be distinguished by most electrochemical technics. Quantumchemical calculations, on

the other hand, depend significantly on proper solvation of the system. But this is challenging since the (bi)sulfate ions are rather large, they do not build close-packed layers, and they are extensively influenced by hydrogen bonds to both specifically adsorbed water molecules and the aqueous environment.

However, the cyclic voltammogram of (bi)sulfate on Pt(111) hints four dominant regions, separated by significant structural changes. For low electrode potentials, platinum is covered with a certain amount of protons. The stability window depends thereby on the pH of the solvent. A lower pH shifts the onset potential of the hydrogen adsorption regime to higher potentials, but it is always below 0.4 V [74, 53, 22].

Between the hydrogen desorption and about 0.5 V, the adsorption of (bi)sulfate takes place. This region is governed by the adsorption of mobile species since STM experiments do not show a particular adsorbate pattern on the surface. Density functional studies by Santana *et al.* have shown that bisulfate ions adsorb in this regime with two oxygen atoms down, stabilized by hydrogen bonds to the surrounding water molecules [173].

At the region of 0.5 V-0.6 V a sharp feature appears in the cyclic voltammogram, sometimes called the “spike”. At this potential, a serious rearrangement in the adsorbate structure happens. A highly ordered $\sqrt{3} \times \sqrt{7}$ structure appears immediately in STM experiments [46, 47], the surface coverage is thereby 0.2 ML [46, 74, 173] and the adsorption geometry of the (bi)sulfate ions changes to a three-point adsorption [154]. Theoretical works showed that the row-like $\sqrt{3} \times \sqrt{7}$ structure is stabilized by explicit molecules of water, which are adsorbed in-between the sulfate rows. [28, 173]. However, the precise position of the spike is shifted slightly to more negative potentials if the sulfate concentration [74] or the pH is increased. However, if the pH value is larger than 4, the spike is not observable in the cyclic voltammogram anymore. Garcia-Araez *et al.* have shown in an extensive analysis, that in the pH-range of 0.8-4.5 rather sulfate than bisulfate is present on the surface [53]. DFT calculations support for electrode potential values larger than 0.48 V sulfate as the favored species as well [82]. Thus the origin of the spike is assumed to be the result of deprotonation of the preadsorbed bisulfate ions. However, the situation is still an open discussion, since linear sweep voltammetry simulations and DFT calculations by Yeh *et al.* showed the spike is actually the result of a rapid coverage change rather than deprotonation [215].

This row-like structure is stable until about 0.7 V is reached, than the STM images becomes noisy and disappears [46]. At this point a phase transition happens, the

surface gets oxidized by additional sulfate adsorbates if the pH is below 2. At a higher pH value, the surface gets oxidized by competitive OH^- adsorption [47, 22]. However, if the spike feature is not present, the phase transition at 0.7 V is also not observable. Thus both structure changes are closely related [52].

For the case of (bi)sulfate adsorption on the Au(111), the situation is comparable. There also a "spike" appears, but at a potential of 0.8 V. At the spike involves a serious restructuring of the adlayer, which happens in a similar way. An unordered structure of preadsorbed (bi)sulfate becomes ordered and the long ranged periodic $\sqrt{3} \times \sqrt{7}$ structure appears on the gold surface [176]. IR studies have shown, that in this structure the (bi)sulfate ions are again adsorbed with three oxygens down to the surface [6].

Here in this study, we used the computational hydrogen electrode to calculate phase-diagrams and pourbaix diagrams of sulfate adsorption on Pt(111) and Au(111). We will explain the importance of proper solvation in theoretical models, and we will show detailed how both explicit and implicit solvation impact the adsorbates.

4.6.3 Theoretical Background and Computational Details

All the calculations were performed using the periodic density functional theory (DFT) program *Vienna ab initio simulation package* (VASP) [96]. The exchange and correlation energy was taken into account by generalized gradient approximation (GGA) applying the RPBE functional. To include van-der-Waals interactions, we used the D3 correction by Grimme et al. The electron-core interaction was handled by the projector augmented wave method (PAW), constructed by Kresse and Joubert. The electronic wave functions were expanded in a plane wave basis set with an energy of at least 500 eV.

For the calculations, we constructed several different supercells with a thickness of 4 atomic layers and approximately 20 A vacuum. The two most used unit cells contained stable adsorbate structures. These unit cells had 18 and 20 surface atoms, to calculate the 0.2 ML and 0.3 ML coverages of sulfate.

To consider solvent effects we used an implicit solvent model [68, 101, 153, 152], and for the permittivity of the acids we used the permittivity of clean water ($80 \frac{As}{Vm}$). Moreover fore these calculations, we raised the energy cutoff in any case to 700 eV to guaranty an accurate electronic density, since this is crucial for the solvent model.

4.6.4 Basic equations

The thermodynamically most stable adsorption structure of the co-adsorbed system under electrochemical conditions is given by the structure with the smallest Gibbs free energy of adsorption $\Delta\gamma$ per surface area A_S.

$$\Delta\gamma = \frac{1}{A_{\mathrm{S}}}\Big(G_{\mathrm{surf,ads}} - G_{\mathrm{surf,0}} - \sum_i n_i\tilde{\mu}_i(T,p,U)\Big), \tag{4.37}$$

where $G_{\mathrm{surf,ads}}$ is the Gibbs energy of the adsorbate covered surface in solution and $G_{\mathrm{surf,0}}$ is the Gibbs free energy of the clean surface in solution. The electrochemical potential of the adsorbates $\tilde{\mu}_i$ depends on temperature T and pressure p respectively the activity of ions in solution a_i. Unfortunately this is quite expensive to get, since a thermodynamic average over time needs to be calculated. A possible way out is the concept of the computational hydrogen electrode (CHE) introduced by Norskov et. al. [138]. This scheme combines thermodynamic quantities with $ab initio$ density functional theory calculations.

$$\tilde{\mu}_{\mathrm{H^+}} + \tilde{\mu}_{\mathrm{e^-}} = \frac{1}{2}\mu_{\mathrm{H_2}} - eU_{SHE} - k_BTln(10)pH, \tag{4.38}$$

where $\tilde{\mu}_{\mathrm{H^+}}$ is the electrochemical potential of protons on the surface, $\tilde{\mu}_{\mathrm{e^-}}$ the electrochemical potential of electrons at fermi level and $\mu_{\mathrm{H_2}}$ the chemical potential of hydrogen in the gas phase. We can calculate this value using DFT. The last two terms eU_{SHE} and $k_BTln(10)pH$ allow to consider particular thermodynamic conditions of the system. A similar concept can be applied for anions like chloride [73, 58, 59] or sulfate. However for other ions than H^+ a reduction couple is necessary. In the case of sulfate the reaction $SO_4^{2-} + 4H^+ + 2e^- \rightleftharpoons SO_2 + 2H_2O$ at a standard redox potential of U^0 = 0.17 V is suitable. The electrochemical potential of sulfate is therefore given by

$$\tilde{\mu}_{\mathrm{SO_4{}^{2-}}} + 2\tilde{\mu}_{\mathrm{e^-}} = \mu_{\mathrm{SO_2}} + 2\mu_{\mathrm{H_2O}} - 4\tilde{\mu}_{\mathrm{H^+}}\,. \tag{4.39}$$

The two electrons are energetically at the fermi level of the metal electrode, therefore its energy depends on the redox potential U and the electrode potential U_{SHE}.

$$\tilde{\mu}_{\mathrm{SO_4{}^{2-}}} + 2\mu_{\mathrm{e^-}} = \mu_{\mathrm{SO_2}} + 2\mu_{\mathrm{H_2O}} - 4\tilde{\mu}_{\mathrm{H^+}} + 2e(U - U_{SHE}) \tag{4.40}$$

The redox potential at standard condition U^0 can be separated from the redox potential at arbitrary conditions U, using

$$U = U^0 - \frac{kT}{2\mathrm{e}} ln\Big(\frac{\mathrm{p}_{\mathrm{SO_2}}/\mathrm{p}^0_{\mathrm{SO_2}}}{\alpha_{\mathrm{SO_4}^{2-}}\alpha^4_{\mathrm{H^+}}}\Big)\,. \tag{4.41}$$

Assuming standard conditions for the pressure of $\mathrm{SO_2}$ and inserting eq. 4.41 and eq. 4.38 into eq. 4.40 gives

$$\begin{aligned}\tilde{\mu}_{\mathrm{SO_4}^{2-}} - 2\mu_{\mathrm{e^-}} = \mu_{\mathrm{SO_2}} + 2\mu_{\mathrm{H_2O}} - 2\mu_{\mathrm{H_2}} + 2eU_{SHE} \\ +2eU^0 + k_B T ln(\alpha_{SO_4^{2-}})\,.\end{aligned} \tag{4.42}$$

This equation provides a way to get the electrochemical potential of adsorbed sulfate on the electrode surface, without calculating a thermal average. Instead we can calculate stability of arbitrary co-adsorbed structures on the metal surface by comparing their Gibbs free energies of adsorption.

$$\begin{aligned}\Delta\gamma &= \frac{1}{A_{\mathrm{S}}}\Big(G_{\mathrm{surf,ads}} - G_{\mathrm{surf},0} - n_{H^+}\tilde{\mu}_{H^+} - n_{SO_4^{2-}}\tilde{\mu}_{SO_4^{2-}}\Big) \\ &= \frac{1}{A_{\mathrm{S}}}\Big(E_{ads} - n_{H^+}\Delta\tilde{\mu}_{H^+} - n_{SO_4^{2-}}\Delta\tilde{\mu}_{SO_4^{2-}}\Big)\,,\end{aligned} \tag{4.43}$$

where

$$\begin{aligned}E_{ads} &= G_{\mathrm{surf,ads}} - G_{\mathrm{surf},0} - \frac{n_{\mathrm{H^+}}}{2}\mu_{H_2} \\ &\quad -n_{SO_4^{2-}}\Big(\mu_{\mathrm{SO_2}} + 2\mu_{\mathrm{H_2O}} - 2\mu_{\mathrm{H_2}}\Big)\,.\end{aligned} \tag{4.44}$$

Replacing the Gibbs energies by total energies from DFT calculations gives for the adsorption energy

$$\begin{aligned}E_{ads} &= E_{\mathrm{surf,ads}} - E_{\mathrm{surf},0} - \frac{n_{\mathrm{H^+}}}{2}E_{H_2} \\ &\quad -n_{SO_4^{2-}}\Big(E_{\mathrm{SO_2}} + 2E_{\mathrm{H_2O}} - 2E_{\mathrm{H_2}}\Big)\,.\end{aligned} \tag{4.45}$$

The two terms $\Delta\tilde{\mu}_{H^+}$ and $\Delta\tilde{\mu}_{SO_4^{2-}}$ are therefore given by

$$\Delta\tilde{\mu}_{H^+} = -eU_{SHE} - k_B T ln(10) pH \tag{4.46}$$

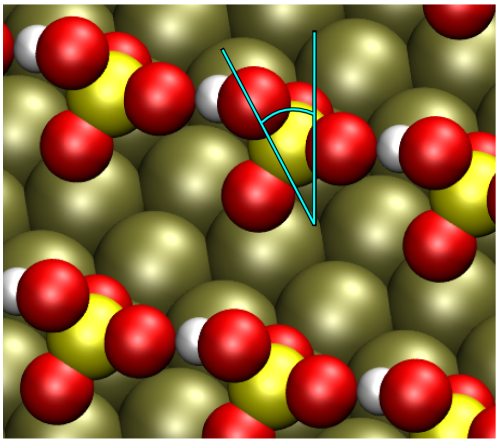

Figure 4.33: Bisulfate ions in the relaxed $\sqrt{3} \times \sqrt{7}$ structure are on the Pt(111) surface considerable rotated. The rotation angle is up to $\alpha = 32.3\,°$.

and

$$\Delta\tilde{\mu}_{SO_4^{2-}} = 2eU_{SHE} + 2eU^0 + k_B T ln(a_{SO_4^{2-}})\,. \tag{4.47}$$

However, a high surface-coverage of sulfate can only exist, when there is a larger concentration of sulfate respectively bisulfate in solution. This results in an distinctly larger permittivity. To take this into account we calculated some structures with a permittivity of concentrated sulfuric acid $(100\,\frac{As}{Vm})$ instead of the permittivity of clean water $(80\,\frac{As}{Vm})$. However there was almost no effect on the adsorption energy notable (about 0.01 eV per sulfate).

4.6.5 Sulfate on platinum

To get reliable phase diagrams it is crucial to consider all adsorbate structures which might exist on the electrode surface. Therefore we have investigated 66 different structures, most of them were arranged in the two mentioned distinct unit cells. For the sake of completeness additional structures where calculated in a $\sqrt{3} \times \sqrt{13}$ unit cell, which is similar than the row-like $\sqrt{3} \times \sqrt{7}$ structure, but with a slightly larger spacing inbetween the rows. The adsorption energies where calculated as described in eq. 4.45. For comparison most calculations where performed both without implicit solvent and with implicit solvent.

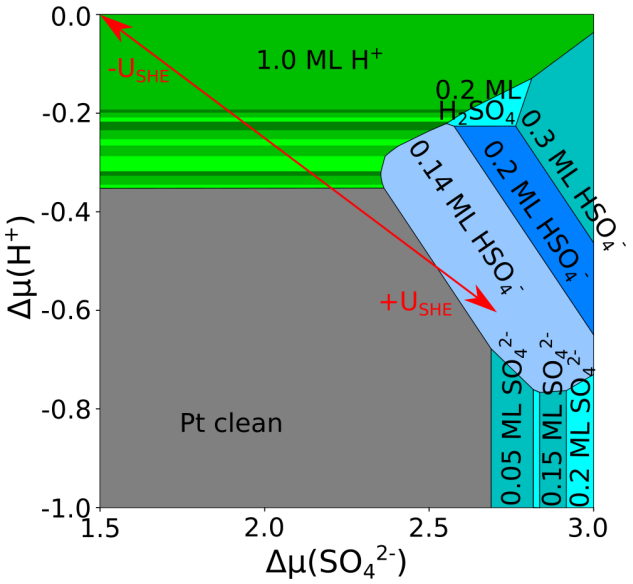

Figure 4.34: Phase diagram of co-adsorbed sulfate, bisulfate and hydrogen, but without any solvent interactions. gray: clean platinum surface; green: pure hydrogen coverages; blue: pure 0.3 ML sulfate or bisulfate coverages; cyan: sulfate or bisulfate $\sqrt{3} \times \sqrt{7}$ structures in 0.2 ML coverage. The artificial 0.14 ML $\sqrt{3} \times \sqrt{13}$ structure is similar to the $\sqrt{3} \times \sqrt{7}$ structure but with broader spacing in-between the bisulfate rows.

Without solvation

In the first approach, we did not use the implicit solvation model at all. Moreover, we omitted all water containing structures and calculated the Gibbs energies and the phase diagram only for adsorbed hydrogen and sulfate in various configurations (see fig. 4.34). Experiments have shown, that sulfate tends to adsorb in row-like structures at 0.2 ML coverage [46, 21, 115, 47]. The stability of these rows is usually explained by spacer molecules between them. This can be a water species, like OH^-, H_2O or H_3O^+, which are very difficult to see in STM experiments [187, 6, 95, 21, 22, 28]. Remarkable is that even without any solvent contribution or spacer molecules, sulfate seems to be rather stable in a row-like configuration. This is nothing that you would expect naively since sulfate ions are fairly spherical adsorbates. Therefore a symmetric, two-dimensional surface structure would be much more reasonable on the Pt(111) surface than ordered rows. Thus, another mechanism, then hidden spacer molecules, stabilizes the sulfate rows. Without hydrogen, the most stable adsorption position of sulfate

ions on the Pt(111) surface is always with three oxygen atoms down for both the fully covered platinum surface (0.3 ML) and the row-like coverage (0.2 ML) as well. But an increase in the hydrogen concentration changes the situation completely. The hydrogen atoms are ideally located at the topmost oxygen atom of sulfate. The resulting bisulfate ions (HSO_4^-) on the surface tilt, depending on the amount of hydrogen (see fig. 4.33). The maximum rotation was found when there is only bisulfate adsorbed, and no sulfate left. The rotation angle, in this case, was up to $32.3\,^\circ$ against the surface perpendicular. In this configuration, all sulfate ions in the rows are linked with bridging hydrogen atoms. Besides, sulfate adsorption with two oxygens down is nothing new, it was also proposed others, e.g., cluster calculations containing solvation[173] or IR-spectrum calculations[154].

Notable is that the tilted structures are so stable that only pure sulfate or pure bisulfate remains on the surface. Various concentrations of hydrogen in-between do not appear in the phase diagram at all. However, we calculated the mentioned row-like structure with a larger spacing in-between the rows as well. This artificial $\sqrt{3} \times \sqrt{13}$ structure with 0.14 ML coverage was not reported in any experimental papers. However, it is clearly a stable phase in the diagram, as long as no solvation was taken into account. Therefore the absence of this low coverage in experiments is due to solvent interactions, which stabilizes apparently higher coverages more.

Implicit solvation

In the next step, we performed the same calculations, but this time, we included solvation, realized by an implicit water model, but without any explicit solvation. The solvation weakens the hydrogen bond between the linked bisulfate ions considerably. Thus the rotation of the individual bisulfate ions is much less prominent. Furthermore, the high coverage structures of 0.3 ML were stabilized more than the row-like structures of 0.2 ML coverage. Both effects together result in the unrealistic situation, that only the high coverage structures were seen in the phase diagram and the row-like structures, which were observed by various STM experiments, vanished completely. Nevertheless, this result is reasonable, since the solvent screens charges, thus stronger polarized surface structures benefit more. However, this drastic change in stability highlights the importance of a proper solvation model, since different coverages of sulfate get stabilized by an entirely different extent. It additionally shows, that implicit solvation alone is not capable of computing sulfate adsorption correctly.

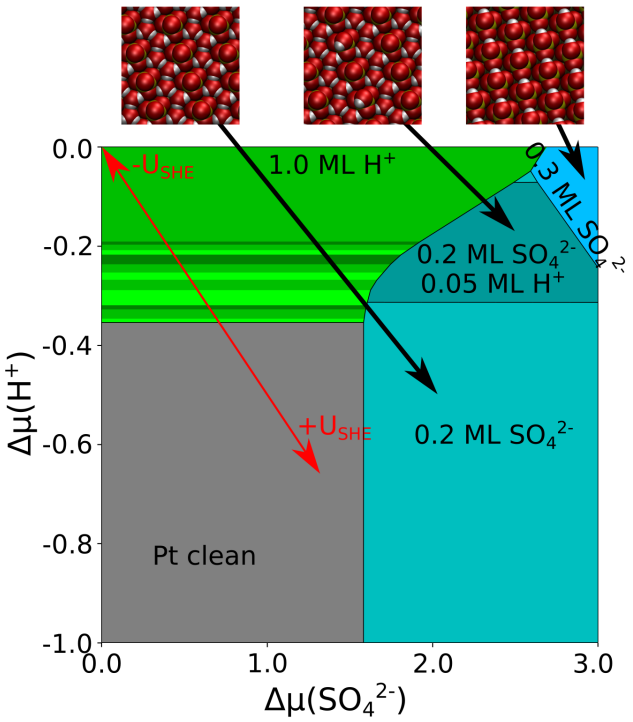

Figure 4.35: Phase diagram of co-adsorbed sulfate, bisulfate and water on Pt(111), all calculations performed with an implicit solvent method. gray: clean platinum surface; green: pure hydrogen coverage; blue: pure 0.3 ML sulfate coverage; cyan: sulfate or bisulfate row structures in 0.2 ML coverage with additional 0.4 ML explicit water.

Both Implicit and explicit solvation

To get an accurate description of the sulfate covered surface, we included explicit solvation as well by adding up to 3 molecules of water per sulfate molecule to the 0.2 ML coverages. The first molecule of water gains up to $-0.82\,eV$ adsorption energy when it adsorbs in-between the flat attached sulfate rows, and it gains up to $-0.72\,eV$ when it adsorbs in-between the tilted bisulfate rows, always with respect to a solvated molecule in bulk water. For comparison, the adsorption energy of a solvated water molecule in a solvated bilayer structure is just $-0.19\,eV$. This vast difference emphasizes moreover that it is crucial to add explicit solvation besides the implicit solvation model. The adsorption energy of the second molecule of water is still up to $-0.67\,eV$, which is also very considerable. However, the third molecule of water adsorbs with only $-0.17\,eV$. Thus it is not more stable than a bilayer anymore. The last adsorption energy is quite small because

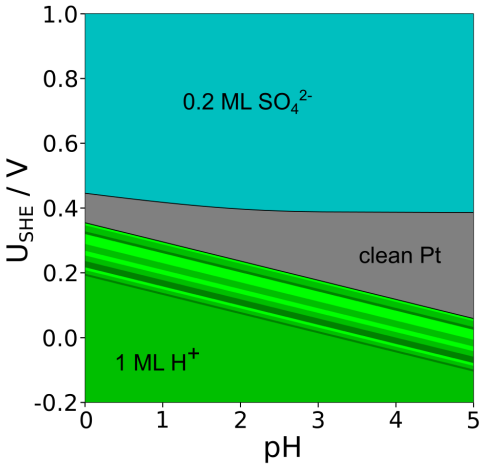

Figure 4.36: Pourbaix diagram of adsorbed SO_4^{2-}, HSO_4^- and H^+ on Pt(111), $T = 298\,K$ and $a(SO_4^{2-}) = 0.1$. The green area denotes a 1 ML coverage of H^+, whereas the blueish area denote the stable SO_4^{2-} structure.

the third molecule does not fit into the sulfate structure like the first and the second. Despite different initial configurations both the first and the second water molecule ended in all the energy minimum calculations flat adsorbed on the platinum surface in-between the (bi)sulfate rows. This strong interaction of (bi)sulfate and water in the $\sqrt{3} \times \sqrt{7}$ structure was also observed in TPD [187] and radioactive labeling studies [95]. Interestingly the explicit molecules of water destabilize the linked bisulfate rows even more so that the rotation becomes less prominent again. Therefore the strong interaction between the adsorbed bisulfate ions under vacuum conditions is by the extensive solvation dramatically decreased, so that the rotation is nearly not observable anymore. The corresponding phase diagram of the fully solvated (bi)sulfate coverages is shown in Fig. 4.35. It is obvious that the solvation of the (bi)sulfate structures changed the stability of these phases in the diagram entirely. Thus the improved phase diagram shows three prominent regions. On the left-hand side, the greenish region. There are different coverages of hydrogen stable on the platinum surface. These structures are stable at low electrode potentials and low pH value of the solution. At about 0.5 eV the hydrogen evolution reaction will start, however, this is not reflected by the DFT calculation. On the right-hand side of the diagram are the (bi)sulfate coverages, depicted in blueish colors. All the 0.2 ML coverages are (bi)sulfate rows, with additional two water molecules for each sulfate ion. The rows with a larger spacing

(0.1 ML) are not stable anymore. Interestingly the pure bisulfate 0.2 ML coverage, which was very stable without solvation does also not appear in the solvated phase diagram as well. Furthermore, the higher coverage structures with 0.3 ML are significantly less stable as well.

4.6.6 Pourbaix diagrams

Using the Gibbs free energies from the phase diagram we can plot electrode potential vs. pH to get a pourbaix diagram. Therefore we need to keep the remaining variable parameters constant. We chose for the pourbaix diagram $T = 298\,K$ and $a(SO_4^{2-}) = 0.1$. The resulting diagram is depicted in Fig. 4.36. The calculated Pourbaix diagram allows to identify the critical phase transition which is known as butterfly shape of cyclovoltammetry measurements. At negative potentials there is the hydrogen covered Pt(111) surface. In this region the coverage is about 1 ML. The surface concentration of protons decreases with rising electrode potential until the platinum surface is clean. Then adsorption of unordered (bi)sulfate starts, but these structures cannot be computed in DFT. Finally the pure sulfate coverage is reached at the spike of the cyclovoltammogram. Here the row-like 0.2 ML structure of sulfate is reached. A further increase of the electrode potential leads to the higher coverage of 0.3 ML sulfate. The additional adsorption of OH^- between the sulfate rows at about 0.7 V, which would happen for low sulfate concentrations, is not included in our calculations [52]. Dense 0.3 ML coverages of bisulfate or sulfate are apparently not stable at any conditions on the platinum surface. Note that this is the same information than if you follow the red arrow in Fig.4.35.

4.6.7 Sulfate on gold

Sulfate adsorption on the Au(111) surface shows qualitatively the same features than sulfate adsorption on Pt(111), albeit gold is a more noble metal. Therefore hydrogen adsorption happens at a significantly larger electrochemical potential. Note, that the scale of the phase diagram of platinum (Fig. 4.35) and gold (Fig. 4.37) is different. But also the sulfate adsorption occurs at a larger electrochemical potential. This shift in both potentials causes, that sulfate rows contain a much higher amount of hydrogen, respectively bisulfate, in comparison with

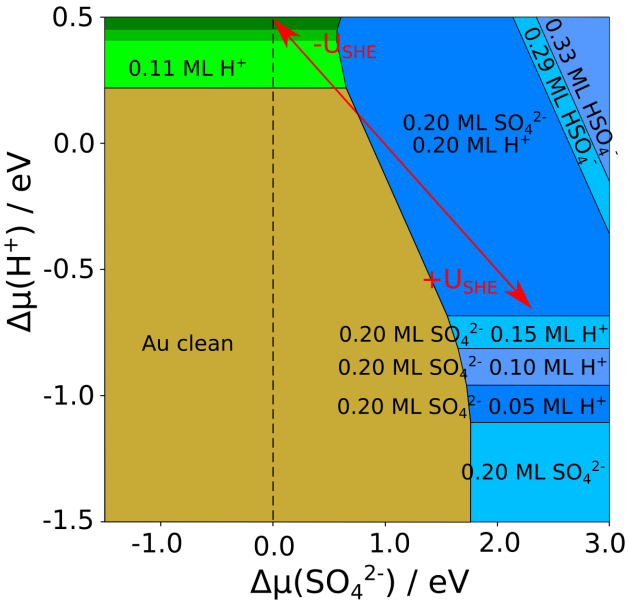

Figure 4.37: Phase diagram of co-adsorbed sulfate, bisulfate and water on Au(111), all calculations performed with an implicit solvent method. gold: clean gold surface; green: pure hydrogen coverages; blue: pure 0.3 ML sulfate or bisulfate coverages; cyan: sulfate or bisulfate row structures in 0.2 ML coverage with additional 0.4 ML explicit water.

adsorbed sulfate on platinum. This behavior can be observed in the pourbaix diagram of gold as well (Fig. 4.38).

4.6.8 Conclusion

Since sulfate containing electrolytes are widely used in electrochemistry a good understanding of the electrode surface is crucial. Using the approach of the computational hydrogen electrode (CHE) we provide phase diagrams of co-adsorbed sulfate, bisulfate and hydrogen on the platinum (111) surface. We confirm that structures at 0.2 ML coverage and 0.3 ML coverage built up stable phases on a wide range of electrode potential. Furthermore we explain the importance of a proper solvation for the 0.2 ML coverage.

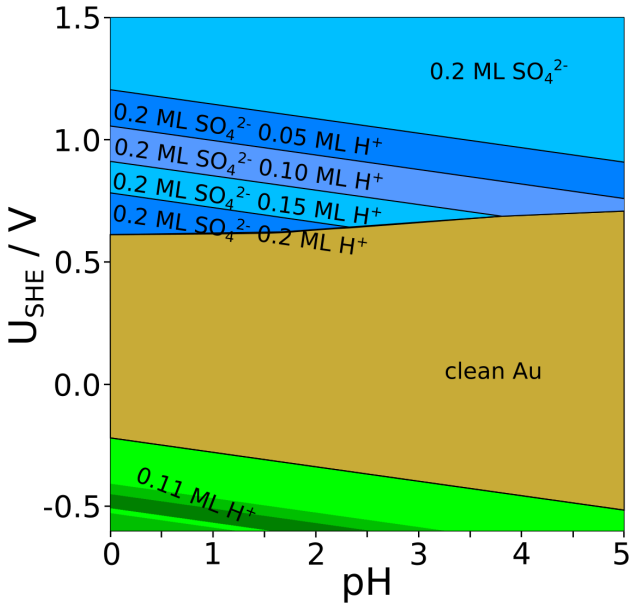

Figure 4.38: Pourbaix diagram of adsorbed SO_4^{2-}, HSO_4^- and H^+ on Pt(111), $T = 298\,K$ and $a(SO_4^{2-}) = 0.1$. The green area denotes various coverage of H^+, whereas the blueish area denote the 0.2 ML coverages of SO_4^{2-} respetively HSO_4^- structures.

4.6.9 Acknowledgments

The numerical work was performed on the computational resource bwUniCluster funded by the Ministry of Science, Research and Arts and the Universities of the State of Baden-Württemberg, Germany, within the framework program bwHPC.

5 Summary

The focus of the present dissertation was to get a better understanding of adsorbate structures at the solid/liquid interface of metal electrodes. Electrocatalytic reactions in this region depend essentially on the underlying atomistic structure. Ions coming from the electrolyte build up dense coverages on the electrode surface, which influence considerable its characteristics. Therefore the stability of these structures needs to be verified at various electrochemical conditions.

Halides are important candidates for the anionic species in electrolytes. However, low coverages of chloride, bromide or iodide on platinum decreases notably the work function of a platinum electrode. This behavior is the opposite of what one would expect for usual adsorption of anionic species on an electrode. Since a negatively charged adlayer always increases the surface dipole moment, which results in a larger instead of a smaller work function.

My calculations clarified the unexpected reduction in the work function, which appears when halides adsorb on platinum. The adsorption of Cl^-, Br^- or I^- causes a charge built up between the adatoms and the metal surface, which results in a significant polarization of the adlayer. This covalent bond like charge accumulation reduces the charge in the adlayer region away from the surface. Furthermore, the calculations proofed, that a Friedel oscillation like charge polarization in the metal slab itself exists, but it does not contribute to the total polarization of the unit-cell. When the adsorption reaction takes place, the charge of the adsorbed anions is to a large extent transferred to the metal slab. Adsorbed iodide is basically uncharged on the Pt(111) surface, whereas bromide and chloride are still slightly charged. Thus the work function decrease is clearly due to significant polarization effects in the adlayer and not due to a positively charged adlayer or even subsurface adsorption of halides.

However, for the case of fluoride, the situation is utterly different. Fluoride ions show almost no charge transfer to platinum during adsorption. Additional no indication of a covalent bond like structure is noticeable. Besides fluoride is the only halide, which tends to adsorb in the on-top position instead of the threefold-hollow

side position. Therefore it behaves on the platinum surface like an ordinary negative charged anion, and it increases the work function. However, on the Sr(111) surface, the results for fluoride seems to be opposed, since adsorbed fluoride decreases the work function remarkable there. But the mechanism for the work function change is entirely different, compared to platinum. Fluoride on strontium also does not show polarization at all, it is in the same way symmetrically negative charged like on platinum. However, fluoride ions are small and penetrate the vast electron spillout region of the strontium surface so deeply, that the adsorption results in a pullback of electronic density. This reduces the dipole moment of the surface, and therefore, it reduces the work function of the metal as well.

Since we identified these two independent mechanisms for the unexpected decrease of the work function on platinum and strontium, we investigated the impact of halide adsorption on eight additional fcc metals (Ca, Ni, Pd, Cu, Ag, Au, Al, and Pb). Thereby we confirmed first, that both mechanisms can be observed. Usually, one of these two different mechanisms is the dominant one. The mechanism due to electron spillout depletion by deeply adsorbed ions is favored if the adatoms are small, hardly polarizable and the work function of the underlying metal is rather small. The other mechanism due to polarization of the adatoms occurs for larger, more easily polarizable adatoms and metals with higher work functions. Especially the adsorption of halides on lead is a rather interesting example since both mechanisms occur here at once. Small fluoride ions adsorb deeply in the electron spillout region of lead. Therefore the work function of the fluoride covered surface is significantly lower than for the chloride or bromide covered lead surface. But although iodine ions are too large to penetrate the electron spillout region of lead, it reduces the work function more than chloride or bromide adsorption. However, in this case, it is due to the other mechanism, the polarization of the iodide adlayer.

But halide adsorption usually happens in an aqueous environment and rarely under vacuum conditions. Therefore it is constructive to enhance the ordinary density function calculation by a thermodynamic model, which enables to include the influence of different pH values, electrolyte concentrations, and electrode potentials. This was done by applying the concept of the computational hydrogen electrode. There we assume first an equilibrium between hydrogen in the gas phase and adsorbed protons at standard conditions (pH=0, p=1 bar, T=298 K), on the electrode surface. In the next step, we include the deviation of these thermodynamic parameters from standard conditions. The same approach can be used for halide adsorption as-well. Thus we can compare the stability of different adsorbate coverages by looking at the Gibbs free energy of adsorption at arbitrary

thermodynamic parameters. In the corresponding paper (chapter 3) we used this simple but efficient approach to get stable coverages of chloride, bromide, and iodide on Pt(111) and Cu(111), at different electrode potentials.

However, the stability of different halide coverages alone is important information, but it provides still an incomplete description of the electrode surface in an aqueous environment. At negative electrode potentials, the Pt(111) surface will certainly be covered with a large amount of protons. Since the electrochemical potential of hydrogen does not depend on the electrochemical potential of the halides, it is possible to extend the thermodynamic approach of the computational hydrogen electrode to compute a two-dimensional phase diagram involving two independent parameters. Thus it provides stable coverages at various pH-values, anion concentrations or electrode potential under experimental conditions. The calculations evidenced that the co-adsorption of hydrogen and halides show a competitive character, which means that at most conditions either a pure hydrogen coverage or a pure halide coverage is present on the platinum surface. Interestingly, from the chloride coverages, the 3×3-structure showed extraordinary stability. This particular structure is almost the only stable chloride structure over the whole range of electrochemical potential. Whereas for the case of iodide, we found five different coverages in the same range.

But anionic adsorption can also lead to a much more drastic structural change than just the buildup of different stable adsorbate coverages. When the nitrate coverage on lead becomes larger than a half monolayer, the topmost surface layers start to reconstruct. This salt-like reconstruction layer becomes in such an extent stable that lower coverages do not appear on this particular surface at all.

Another frequently used anion in electrochemistry is sulfate. However, in aqueous environment sulfate is in equilibrium with bisulfate $SO_4^{2-} + H^+ \rightleftharpoons HSO_4^-$, which is also the more stable ion in solution, under standard conditions. The chemical potentials of protons and sulfate/bisulfate are therefore not independent anymore. An increase in the electrochemical potential of protons, e.g. by a decrease of the pH value of the solution, will shift the equilibrium to the side of bisulfate. This increases the complexity of the system significantly. Moreover, strongly adsorbed water molecules govern the adsorbate patterns on platinum and gold. Unfortunately, both water and the difference between sulfate and bisulfate can hardly be observed in STM experiments clearly. Our DFT calculations confirmed that the sulfate rows were indeed stabilized through these water molecules. But these molecules cannot be captured by an implicit solvation scheme, that is why they have to be modeled explicitly. Besides the calculations have shown, that bisul-

fate hardly exists on the surface. The row-like 0.2 ML structure consists of only sulfate and water. In the corresponding paper, we provided phase diagrams and Pourbaix diagrams as well.

6 Zusammenfassung

Das Ziel dieser Dissertation war es, ein besseres Verständnis über Adsorbat Strukturen an der fest/flüssig Grenzfläche metallischer Elektroden zu erlangen. Elektrokatalytische Reaktionen, die in dieser Region ablaufen, hängen erheblich von der zugrunde liegenden atomaren Struktur ab. Die Ionen des Elektrolyts bilden auf der Elektrodenoberfläche dicht gepackte Strukturen, die erhelblich deren Eigenschaften beeinflussen. Deshalb ist es wichtig, die Stabilität dieser Bedeckungen bei unterschiedlichen elektrochemischen Bedingungen zu kennen.

Eine wichtige Gruppe von Anionen, die in Elektrolyten vorkommen, sind die Halogene. Kleinere Bedeckungen von Chlorid, Bromid oder Iodid können die Austrittsarbeit von einer Platinelektrode beträchtlich reduzieren. Dieses Verhalten ist noch dazu das Gegenteil von dem was man eigentlich von einer anionischen Adsorbatstruktur erwarten würde, da negativ geladene Adsorbatschichen immer das Oberflächendipolmoment verstärken, woraus eine Verstärkung anstelle einer Verringerung der Austrittsarbeit resultieren sollte.

Diese unerwartete Reduzierung der Austrittsarbeit, wie sie bei Halogenadsorption auf Platin auftritt, konnte ich mit Hilfe von dichtefunktionaltheoretischen Rechnungen erklären. Eine durch Adsorption von Cl^-, Br^- oder I^- Ionen verursachte Ladungsansammlung zwischen den Adsorbatatomen und der Metalloberfläche führt zu einer erheblichen Polarisation der Adsorbatschicht. Diese kovalente Bindungs- struktur reduziert im von der Oberfläche abgewandten Bereich, die Elektronendichte in der Adsorbat Schicht. Die Rechnungen haben zudem gezeigt, dass eine Polarisation der Metallschicht selbst, ähnlich wie bei Friedel Oszillationen, zwar existiert, sie aber nicht zur gesamten Polarisation der Einheitszelle beiträgt. Darüber hinaus wird die Ladung der adsorbierten Anionen fast vollständig auf die Metalloberfläche übertragen. Adsorbiertes Iodid ist auf der Pt(111) Oberfläche praktisch ungeladen, Chlorid und Bromid sind noch eine ein wenig geladen. Die Verringerung der Austrittsarbeit wird deshalb nur durch Polarisation der Adsorbatschicht hervorgerufen und nicht durch eine positive Ladung der Adatome oder durch Eindringen der Ionen unter die oberste Metallschicht.

Für die Adsorption von Fluorid ist die Situation jedoch vollkommen anders. Fluorid Ionen zeigen beinahe keine Ladungsübertragung auf Platin. Zudem ist kein Anzeichen einer kovalenten Bindung erkennbar. Abgesehen davon ist Fluorid das einzige der Halogenide, das auf Platin in on-top Position anstelle der threefold-hollow Position adsorbiert. Es verhält sich auf der Platin Oberfläche wie ein gewöhnliches negatives geladenes Anion und erhöht die Austrittsarbeit. Auf der Sr(111) Oberfläche ist jedoch das Gegenteil der Fall, hier reduziert adsorbiertes Fluorid die Austrittsarbeit erheblich. Allerdings ist der Mechanismus für die Änderung der Austrittsarbeit hier komplett verschieden. Auf Strontium zeigt Fluorid ebenfalls keine Polarisation, es ist wie auf Platin symmetrisch negativ geladen. Allerdings ist Fluorid klein und dringt daher so tief in die Elektronenhülle der Strontiumoberfläche ein, so dass durch die Adsorption Elektronendichte der Metallschicht zurück gezogen wird. Dies reduziert das Oberlfächendipolmoment und somit auch die Austrittsarbeit von Strontium.

Nachdem wir diese zwei unabhängigen Mechanismen der unerwarteten Reduzierung der Austrittsarbeit auf Platin und Strontium identifiziert hatten, untersuchten wir den Einfluss der Halogenid Adsorption auf acht weiteren fcc Metallen (Ca, Ni, Pd, Cu, Ag, Au, Al und Pb). Dabei konnten wir bestätigen, dass beide oben beschriebenen Mechanismen auftreten. Normalerweise dominiert jedoch einer davon. Der Mechanismus, bei dem die natürlichen Elektronendichte des Metalls durch tief eindringende Ionen zurück gezogen wird, tritt bevorzugt auf, wenn die Adsorbat Atome klein sind, schlecht polarisierbar und wenn die Austrittsarbeit des zugrunde liegenden Metalls eher klein ist. Der andere Mechanismus, der durch Polarisation der Adsorbat Atome entsteht, tritt bei größeren, leichter polarisierbaren Adsorbaten und Metallen mit einer eher großen Austrittsarbeit auf. Interessanterweise ist die Adsorption von Halogeniden auf Blei ein sehr schönes Beispiel, da hier beide Mechanismen gleichzeitig auftreten. Die kleine Fluorid Ionen adsorbieren tief in der Elektronendichte Schicht von Blei. Deshalb ist die Austrittsarbeit der Fluorid bedeckten Oberfläche erheblich kleiner, als die der Chlorid oder Bromid bedeckten Oberfläche. Obwohl Iodid Ionen sehr groß sind und nicht in die Oberflächenelektronendichte eindringen können, führen auch sie zu einer stärkeren Reduzierung der Austrittsarbeit als Chlorid oder Bromid. Diesmal liegt das jedoch an dem anderen Mechanismus, also an der Polarisation der Iodid Schicht.

Allerdings kommt die Adsorption von Halogenen normalerweise nur in einer wässrigen Umgebung vor und nur selten unter Vakuum Bedingungen. Deshalb ist es sinnvoll die gewöhnliche Dichtefunktional Rechnung um ein Thermodynamisches

Modell zu erweitern, welches es ermöglicht den Einfluss unterschiedlicher pH Werte, die Elektrolytkonzentration, und das Elektrodenpotenzial zu berücksichtigen. Dies ist mit dem Modell der theoretischen Wasserstoff Elektrode (CHE) möglich. Dabei wird unter Standard Bedingungen (pH=0, p=1 bar, T=298 K) zuerst ein Gleichgewicht zwischen Wasserstoffmolekülen in der Gas Phase und adsorbierten Protonen auf der Oberfläche angenommen. Im nächsten Schritt wird anschließend eine Abweichung der thermodynamischen Parameter zu den Standard Bedingungen mit einbezogen. Dieser Ansatz lässt sich auch für die Halogen Adsorption übernehmen. Dadurch lässt sich durch Vergleich der freien Gibbs Energie, die Stabilität verschiedener Adsorbat Strukturen für beliebige thermodynamische Parameter untersuchen. In der dazu gehörenden Veröffentlichung (Kapitel 3) haben wir dieses einfache aber effektive Model benutzt, um stabile Bedeckungen von Chlorid, Bromid und Iodid auf Pt(111) und Cu(111), bei verschiedenem Elektrodenpotenzial zu untersuchen.

Die Stabilität unterschiedlicher Halogen Bedeckungen allein erlaubt jedoch nur eine unvollständige Beschreibung der Elektrodenoberfläche im wässrigen Medium. Bei negativem Elektrodenpotential ist eine Pt(111) Oberfläche immer mit einer großen Menge an Protonen bedeckt. Da das elektrochemische Potential von Wasserstoff jedoch nicht vom elektrochemischen Potential der Halogene abhängt, ist es möglich mit dem thermodynamischen Ansatz der theoretischen Wasserstoffelektrode auch ein zwei dimensionales Phasendiagramm mit zwei unabhängigen Parametern zu berechnen. Dies ermöglicht es nun, stabile Bedeckungen bei beliebigem pH-Wert, Anionen Konzentration oder Elektrodenpotenzial unter experimentellen Bedingungen abzulesen. Die Rechnungen belegen, dass die Ko-Adsorption von Wasserstoff und Halogenen ein konkurrierendes Verhalten zeigt, das bedeutet dass meist nur reine Wasserstoffbedeckungen oder reine Halogenbedeckungen auf der Platinoberfläche stabil sind. Interessanterweise zeigt von den Chloridbedeckungen die 3×3-Struktur eine außerordentliche Stabilität. Diese Struktur ist beinahe die einzige stabile Struktur über den gesamten Bereich des elektrochemischen Potentials. Bei der Iodid Adsorption sind dagegen fünf unterschiedliche Bedeckungen über den selben Bereich stabil.

Die Adsorption von Anionen führt manchmal aber auch zu einer erheblich stärkeren Strukturänderung, als nur zum Entstehen von unterschiedlich stabilen Adsorbat Bedeckungen. Wird die Nitrat Bedeckung auf Blei größer als eine habe Monolage, so kommt es zu einer Oberflächenrekonstruktion der obersten Blei Schichten. Diese salzartige Rekonstruktion ist dabei dermaßen stabil, dass niedrigere Bedeckungen auf dieser Oberfläche gar nicht auftreten.

Ein anderes häufig verwendetes Anion in der Elektrochemie ist Sulfat. In wässriger Umgebung besteht jedoch immer ein Gleichgewicht aus Sulfat und Hydrogensulfat $SO_4^{2-} + H^+ \rightleftharpoons HSO_4^-$, welches unter Standard Bedingungen auch das stabilere der beiden Ionen ist. Die chemischen Potentiale von Protonen und Sulfat sind deshalb nicht mehr unabhängig. Durch eine Verringerung des elektrochemischen Potentials der Protonen, z.B. durch eine Verringerung des pH Wertes der Lösung, wird das Gleichgewicht auf die Seite von Hydrogensulfat verschoben. Zudem beeinflussen stark adsorbierte Wassermoleküle die Adsorbatstrukturen auf Platin und Gold, jedoch ist es experimentell weder möglich diese Moleküle, noch den Unterschied zwischen Hydrogensulfat und Sulfat deutlich in STM Experimenten zu erkennen. Unsere Rechnungen bestätigten, dass Reihen aus Sulfat in der Tat durch Wassermoleküle stabilisiert werden. Diese Moleküle können jedoch nicht mit einem impliziten Wassermodel berücksichtigt werden, daher müssen sie explizit simuliert werden. Zudem zeigten die Rechnungen, dass Hydrogensulfat auf der Platinoberfläche kaum stabil ist. Die 0.2 ML Bedeckung ist eine Struktur nur aus Sulfat und Wasser. In der dazu gehörenden Veröffentlichung zeigen wir Phasen Diagramme und Pourbaix Diagramme.

Bibliography

[1] A. STROPPA, G. K.: The shortcomings of semi-local and hybrid functionals: what we can learn from surface science studies. In: *New J. Phys.* 10 (2008), S. 063020

[2] ANDRYUSHECHKIN, B. ; ELTSOV, K. ; SHEVLYUGA, V. : Atomic scale observation of iodine layer compression on Cu(111). In: *Surf. Sci.* 472 (2001), S. 80 – 88. http://dx.doi.org/http://dx.doi.org/10.1016/S0039-6028(00)00926-2. – DOI http://dx.doi.org/10.1016/S0039–6028(00)00926–2

[3] ARENZ, M. ; STAMENKOVIC, V. ; SCHMIDT, T. ; WANDELT, K. ; ROSS, P. ; MARKOVIC, N. : The effect of specific chloride adsorption on the electrochemical behavior of ultrathin Pd films deposited on Pt(111) in acid solution. In: *Surf. Sci.* 523 (2003), S. 199–209. http://dx.doi.org/10.1016/S0039-6028(02)02456-1. – DOI 10.1016/S0039–6028(02)02456–1

[4] ASHCROFT, N. W. ; MERMIN, N. D.: *Solid State Physics*. Saunders College Publishing, 1976

[5] ASIRI, H. A. ; ANDERSON, A. B.: Using Gibbs Energies to Calculate the Pt(111) H_{upd} Cyclic Voltammogram. In: *J. Phys. Chem. C* 117 (2013), Nr. 34, S. 17509–17513. http://dx.doi.org/10.1021/jp401909n. – DOI 10.1021/jp401909n

[6] ATAKA, K.-i. ; OSAWA, M. : In Situ Infrared Study of WaterSulfate Coadsorption on Gold(111) in Sulfuric Acid Solutions. In: *Langmuir* 14 (1998), Nr. 4, 951-959. http://dx.doi.org/10.1021/la971110v. – DOI 10.1021/la971110v

[7] BADESCU, S. C. ; SALO, P. ; ALA-NISSILA, T. ; YING, S. C. ; JACOBI, K. ; WANG, Y. ; BEDÜRFTIG, K. ; ERTL, G. : Energetics and Vibrational States for Hydrogen on Pt(111). 88 (2002), S. 136101

[8] BAGOTZKY, V. S. ; VASSILYEV, Y. B. ; WEBER, J. ; PIRTSKHALAVA, J. N.: In: *J. Electroanal. Chem.* 27 (1970), 31 S.

[9] BAGUS, P. S. ; KAEFER, D. ; WITTE, G. ; WÖLL, C. : In: *Phys. Rev. Lett.* 100 (2008), 126101 S.

[10] BAGUS, P. S. ; STAEMMLER, V. ; WÖLL, C. : In: *Phys. Rev. Lett.* 89 (2002), 096104 S.

[11] BAGUS, P. S. ; WÖLL, C. ; WIECKOWSKI, A. : Dependence of surface properties on adsorbate-substrate distance: Work function changes and binding energy shifts for I/Pt(111). In: *Surf. Sci.* 603 (2009), S. 273–283

[12] BAKER, T. A. ; FRIEND, C. M. ; KAXIRAS, E. : Nature of Cl Bonding on the Au(111) Surface: Evidence of a Mainly Covalent Interaction. In: *J. Am. Chem. Soc.* 130 (2008), Nr. 12, S. 3720–3721

[13] BARTH, U. von ; HEDIN, L. : A local exchange-correlation potential for the spin polarized case. i. In: *Journal of Physics C: Solid State Physics* 5 (1972), Nr. 13, 1629. http://stacks.iop.org/0022-3719/5/i=13/a=012

[14] BENEDIKT, U. ; SCHNEIDER, W. B. ; AUER, A. A.: Modelling electrified interfaces in quantum chemistry: constant charge vs. constant potential. In: *Phys. Chem. Chem. Phys.* 15 (2013), S. 2712–2724. http://dx.doi.org/10.1039/C2CP42675G. – DOI 10.1039/C2CP42675G

[15] BERTEL, E. ; SCHWAHA, K. ; NETZER, F. : The adsorption of bromine on Pt(111): Observation of an irreversible order-disorder transition. In: *Surf. Sci.* 83 (1979), Nr. 2, 439-452. http://dx.doi.org/10.1016/0039-6028(79)90055-4. – DOI 10.1016/0039–6028(79)90055–4. – ISSN 0039–6028

[16] BITTNER, A. ; WINTTERLIN, J. ; BERAN, B. ; ERTL, G. : Bromine adsorption on Pt(111), (100), and (110) — an {STM} study in air and in electrolyte. In: *Surf. Sci.* 335 (1995), Nr. 0, 291–299. http://dx.doi.org/10.1016/0039-6028(95)00447-5. – DOI 10.1016/0039–6028(95)00447–5. – ISSN 0039–6028. – Proceedings of the {IUVSTA} Workshop on Surface Science and Electrochemistry

[17] BJÖRKETUN, M. E. ; ZENG, Z. ; AHMED, R. ; TRIPKOVIC, V. ; THYGESEN, K. S. ; ROSSMEISL, J. : Avoiding pitfalls in the modeling of electrochemical interfaces. In: *Chem. Phys. Lett.* 555 (2013), S. 145 – 148. http://dx.doi.org/10.1016/j.cplett.2012.11.025. – DOI 10.1016/j.cplett.2012.11.025

[18] BLÖCHL, P. E.: In: *Phys. Rev. B* 50 (1994), 17953 S.

[19] BONNET, N. ; MORISHITA, T. ; SUGINO, O. ; OTANI, M. : First-principles molecular dynamics at a constant electrode potential. In: *Phys. Rev. Lett.* 109 (2012), Dez., Nr. 26, S. 266101

[20] BONZEL, H. P.: In: *Surf. Sci. Rep.* 8 (1988), 43 S.

[21] BRAUNSCHWEIG, B. ; DAUM, W. : Superstructures and Order-Disorder Transition of Sulfate Adlayers on Pt(111) in Sulfuric Acid Solution. In: *Langmuir* 25 (2009), Nr. 18, 11112-11120. http://dx.doi.org/10.1021/la901399j. – DOI 10.1021/la901399j. – PMID: 19456179

[22] BRAUNSCHWEIG, B. ; MUKHERJEE, P. ; DLOTT, D. D. ; WIECKOWSKI, A. : Real-Time Investigations of Pt(111) Surface Transformations in Sulfuric Acid Solutions. In: *Journal of the American Chemical Society* 132 (2010), Nr. 40, S. 14036–14038. http://dx.doi.org/10.1021/ja106618z. – DOI 10.1021/ja106618z

[23] BROEKMANN, P. ; WILMS, M. ; KRUFT, M. ; STUHLMANN, C. ; WANDELT, K. : In-situ STM investigation of specific anion adsorption on Cu(111). In: *J. Electroanal. Chem.* 467 (1999), S. 307–324

[24] CARRASCO, J. ; KLIMEŠ, J. ; MICHAELIDES, A. : The role of van der Waals forces in water adsorption on metals. 138 (2013), S. 024708. http://dx.doi.org/10.1063/1.4773901. – DOI 10.1063/1.4773901

[25] CARRASCO, J. ; SANTRA, B. ; KLIMEŠ, J. ; MICHAELIDES, A. : To Wet or Not to Wet? Dispersion Forces Tip the Balance for Water Ice on Metals. In: *Phys. Rev. Lett.* 106 (2011), S. 026101. http://dx.doi.org/10.1103/PhysRevLett.106.026101. – DOI 10.1103/PhysRevLett.106.026101

[26] CHANG, S. C. ; YAU, S. L. ; SCHARDT, B. C. ; WEAVER, M. J.: Comparisons between scanning tunneling microscopy and outer-sphere electron-transfer rates at platinum (111) surfaces coated with ordered iodine adlayers. In: *J. Phys. Chem.* 95 (1991), Nr. 12, 4787–4794. http://dx.doi.org/10.1021/j100165a036. – DOI 10.1021/j100165a036

[27] COLLINS, D. ; SPICER, W. : The adsorption of CO, O2, and {H2} on Pt: II. Ultraviolet photoelectron spectroscopy studies. In: *Surf. Sci.* 69 (1977), Nr. 1, S. 114 – 132. – ISSN 0039–6028

[28] COMAS-VIVES, A. ; BANDLOW, J. ; JACOB, T. : Ab initio study of the elec-

trochemical H 2 SO 4/Pt (111) interface. In: *Physical Chemistry Chemical Physics* 15 (2013), Nr. 3, S. 992–997

[29] DERRY, G. N. ; JI-ZHONG, Z. : Work function of Pt(111). In: *Phys. Rev. B* 39 (1989), Jan, S. 1940–1941

[30] DION, M. ; RYDBERG, H. ; SCHRÖDER, E. ; LANGRETH, D. C. ; LUNDQVIST, B. I.: Van der Waals Density Functional for General Geometries. In: *Phys. Rev. Lett.* 92 (2004), Jun, 246401. http://dx.doi.org/10.1103/PhysRevLett.92.246401. – DOI 10.1103/PhysRevLett.92.246401

[31] DRONSKOWSKI, R. : *Computational Chemistry of Solid State Materials*. First. Wiley-VCH, 2005

[32] ERISMAN, J. W. ; SUTTON, M. A. ; GALLOWAY, J. ; KLIMONT, Z. ; WINIWARTER, W. : How a century of ammonia synthesis changed the world. In: *Nature Geoscience* 1 (2008), Sep, 636 EP -. https://doi.org/10.1038/ngeo325

[33] ERLEY, W. : Chlorine adsorption on the (111) faces of Pd and Pt. In: *Surf. Sci.* 94 (1980), S. 281–292

[34] ERNZERHOF, M. ; SCUSERIA, G. E.: Assessment of the Perdew?Burke?Ernzerhof exchange-correlation functional. In: *The Journal of Chemical Physics* 110 (1999), Nr. 11, 5029-5036. http://dx.doi.org/10.1063/1.478401. – DOI 10.1063/1.478401

[35] FAISAL, F. ; STUMM, C. ; BERTRAM, M. ; WAIDHAS, F. ; LYKHACH, Y. ; CHEREVKO, S. ; XIANG, F. ; AMMON, M. ; VOROKHTA, M. ; SMÍD, B. ; SKÁLA, T. ; TSUD, N. ; NEITZEL, A. ; BERANOVÁ, K. ; PRINCE, K. C. ; GEIGER, S. ; KASIAN, O. ; WÄHLER, T. ; SCHUSTER, R. ; SCHNEIDER, M. A. ; MATOLÍN, V. ; MAYRHOFER, K. J. J. ; BRUMMEL, O. ; LIBUDA, J. : Electrifying model catalysts for understanding electrocatalytic reactions in liquid electrolytes. In: *Nature Materials* 17 (2018), Nr. 7, 592-598. http://dx.doi.org/10.1038/s41563-018-0088-3. – DOI 10.1038/s41563–018–0088–3. – ISSN 1476–4660

[36] FARRELL, H. : The coadsorption of I and Cl on Pt(111). In: *Surf. Sci.* 100 (1980), Nr. 3, 613–625. http://dx.doi.org/10.1016/0039-6028(80)90427-6. – DOI 10.1016/0039–6028(80)90427–6. – ISSN 0039–6028

[37] FATTEBERT, J.-L. ; GYGI, F. : Density functional theory for efficient ab initio molecular dynamics simulations in solution. In: *Journal of Computational*

Chemistry 23 (2002), Nr. 6, 662-666. http://dx.doi.org/10.1002/jcc.10069. – DOI 10.1002/jcc.10069

[38] FELTER, T. E. ; HUBBARD, A. T.: LEED and electrochemistry of iodine on Pt(100) and Pt(111) single-crystal surfaces. In: *J. Electroanal. Chem.* 100 (1979), Nr. 1–2, 473–491. http://dx.doi.org/10.1016/S0022-0728(79)80179-5. – DOI 10.1016/S0022–0728(79)80179–5. – ISSN 0022–0728

[39] FERRIN, P. ; KANDOI, S. ; NILEKAR, A. U. ; MAVRIKAKIS, M. : Hydrogen adsorption, absorption and diffusion on and in transition metal surfaces: A DFT study. In: *Surf. Sci.* 606 (2012), S. 679 – 689. http://dx.doi.org/10.1016/j.susc.2011.12.017. – DOI 10.1016/j.susc.2011.12.017

[40] FERRIS, L. M.: Lead Nitrate-Nitric Acid-Water System. In: *Journal of Chemical & Engineering Data* 5 (1960), Nr. 3, 242-242. http://dx.doi.org/10.1021/je60007a002. – DOI 10.1021/je60007a002

[41] FILHOL, J. S. ; NEUROCK, M. : Elucidation of the electrochemical activation of water over Pd by first principles. In: *Angew. Chem. Int. Ed.* 45 (2006), S. 402

[42] FISHER, G. B.: The electronic structure of two forms of molecular ammonia adsorbed on Pt(111). In: *Chem. Phys. Lett.* 79 (1981), Nr. 3, S. 452 – 458. – ISSN 0009–2614

[43] FORESTI, M. L. ; INNOCENTI, M. ; FORNI, F. ; GUIDELLI, R. : Electrosorption Valency and Partial Charge Transfer in Halide and Sulfide Adsorption on Ag(111). In: *Langmuir* 14 (1998), S. 7008–7016. http://dx.doi.org/10.1021/la980692t. – DOI 10.1021/la980692t

[44] FORSTER-TONIGOLD, K. ; GROSS, A. : Dispersion corrected RPBE studies of liquid water. In: *The Journal of Chemical Physics* 141 (2014), Nr. 6, 064501. http://dx.doi.org/10.1063/1.4892400. – DOI 10.1063/1.4892400

[45] FUKUSHIMA, T. ; SONG, M.-B. ; ITO, M. : Local work-function changes of Pt(111) studied by {STM} and IRAS: coadsorption of Cl- with H3O+, NO, and {CO} molecules. In: *Surf. Sci.* 464 (2000), Nr. 2–3, 193–199. http://dx.doi.org/10.1016/S0039-6028(00)00665-8. – DOI 10.1016/S0039–6028(00)00665–8. – ISSN 0039–6028

[46] FUNTIKOV, A. ; LINKE, U. ; STIMMING, U. ; VOGEL, R. : An in-situ STM study of anion adsorption on Pt(111) from sulfuric acid solu-

tions. In: *Surface Science* 324 (1995), Nr. 1, L343 - L348. http://dx.doi.org/http://dx.doi.org/10.1016/0039-6028(94)00774-8. – DOI http://dx.doi.org/10.1016/0039–6028(94)00774–8. – ISSN 0039–6028

[47] FUNTIKOV, A. ; STIMMING, U. ; VOGEL, R. : Anion adsorption from sulfuric acid solutions on Pt(111) single crystal electrodes. In: *Journal of Electroanalytical Chemistry* 428 (1997), Nr. 1, 147 - 153. http://dx.doi.org/https://doi.org/10.1016/S0022-0728(96)05051-6. – DOI https://doi.org/10.1016/S0022–0728(96)05051–6. – ISSN 1572–6657

[48] GARCIA-ARAEZ, N. ; KOPER, M. T. M.: A sublattice-model isotherm for the competitive coadsorption of hydrogen and bromide on a Pt(100) electrode. In: *Phys. Chem. Chem. Phys.* 12 (2010), S. 143–148. http://dx.doi.org/10.1039/B912091B. – DOI 10.1039/B912091B

[49] GARCIA-ARAEZ, N. ; CLIMENT, V. ; HERRERO, E. ; FELIU, J. ; LIPKOWSKI, J. : Thermodynamic studies of chloride adsorption at the Pt(111) electrode surface from 0.1 M {HClO4} solution. In: *J. Electroanal. Chem.* 576 (2005), Nr. 1, 33–41. http://dx.doi.org/10.1016/j.jelechem.2004.10.003. – DOI 10.1016/j.jelechem.2004.10.003. – ISSN 1572–6657

[50] GARCIA-ARAEZ, N. ; CLIMENT, V. ; HERRERO, E. ; FELIU, J. ; LIPKOWSKI, J. : Thermodynamic studies of bromide adsorption at the Pt(111) electrode surface perchloric acid solutions: Comparison with other anions. In: *J. Electroanal. Chem.* 591 (2006), S. 149 – 158. http://dx.doi.org/http://dx.doi.org/10.1016/j.jelechem.2006.04.008. – DOI http://dx.doi.org/10.1016/j.jelechem.2006.04.008

[51] GARCIA-ARAEZ, N. ; CLIMENT, V. ; HERRERO, E. ; FELIU, J. M. ; LIPKOWSKI, J. : Determination of the Gibbs excess of H adsorbed at a Pt(111) electrode surface in the presence of co-adsorbed chloride. In: *J. Electroanal. Chem.* 582 (2005), Nr. 1–2, 76–84. http://dx.doi.org/10.1016/j.jelechem.2005.01.031. – DOI 10.1016/j.jelechem.2005.01.031. – ISSN 1572–6657

[52] GARCIA-ARAEZ, N. ; CLIMENT, V. ; RODRIGUEZ, P. ; FELIU, J. M.: Thermodynamic analysis of (bi)sulphate adsorption on a Pt(111) electrode as a function of pH. In: *Electrochimica Acta* 53 (2008), Nr. 23, 6793 - 6806. http://dx.doi.org/https://doi.org/10.1016/j.electacta.2007.12.086. – DOI https://doi.org/10.1016/j.electacta.2007.12.086. – ISSN 0013–4686. – EXPLORING FRONTIERS OF ELECTROCHEM-

ISTRY Selection of papers from the 58th Annual Meeting of the International Society of Electrochemistry 10-14 September 2007, Banff, Canada

[53] GARCIA-ARAEZ, N. ; CLIMENT, V. ; RODRIGUEZ, P. ; FELIU, J. M.: Elucidation of the Chemical Nature of Adsorbed Species for Pt(111) in H2SO4 Solutions by Thermodynamic Analysis. In: *Langmuir* 26 (2010), Nr. 14, S. 12408–12417. http://dx.doi.org/10.1021/la101112b. – DOI 10.1021/la101112b

[54] GARCIA-ARAEZ, N. ; LUKKIEN, J. J. ; KOPER, M. T. ; FELIU, J. M.: Competitive adsorption of hydrogen and bromide on Pt(1 0 0): Mean-field approximation vs. Monte Carlo simulations. In: *J. Electroanal. Chem.* 588 (2006), S. 1 – 14. http://dx.doi.org/http://dx.doi.org/10.1016/j.jelechem.2005.11.034. – DOI http://dx.doi.org/10.1016/j.jelechem.2005.11.034

[55] GASTEIGER, H. ; MARKOVIĆ, N. ; ROSS, P. : Bromide adsorption on Pt(111): Adsorption Isotherm and Electrosorption Valency Deduced from RRDE Measurements. In: *Langmuir* 12 (1996), Nr. 6, 1414–1418. http://dx.doi.org/10.1021/la950826s. – DOI 10.1021/la950826s

[56] GOHDA, Y. ; SCHNUR, S. ; GROSS, A. : Influence of water on elementary reaction steps in electrocatalysis. In: *Faraday Discuss.* 140 (2008), S. 233–244

[57] GOSSENBERGER, F. ; ROMAN, T. ; FORSTER-TONIGOLD, K. ; GROSS, A. : Change of the work function of platinum electrodes induced by halide adsorption. In: *Beilstein J. of Nanotechnol.* 5 (2014), S. 152

[58] GOSSENBERGER, F. ; ROMAN, T. ; GROSS, A. : Equilibrium coverage of halides on metal electrodes. In: *Surf. Sci.* 631 (2015), S. 17–22

[59] GOSSENBERGER, F. ; ROMAN, T. ; GROSS, A. : Hydrogen and halide co-adsorption on Pt(111) in an electrochemical environment: a computational perspective. In: *Electrochimica Acta* 216 (2016), 152 - 159. http://dx.doi.org/http://dx.doi.org/10.1016/j.electacta.2016.08.117. – DOI http://dx.doi.org/10.1016/j.electacta.2016.08.117. – ISSN 0013–4686

[60] GRIMME, S. ; ANTONY, J. ; EHRLICH, S. ; KRIEG, H. : A consistent and accurate ab initio parametrization of density functional dispersion correction (DFT-D) for the 94 elements H-Pu. In: *The Journal of Chemical Physics*

132 (2010), Nr. 15, –. http://dx.doi.org/10.1063/1.3382344. – DOI 10.1063/1.3382344

[61] GROSS, A. ; GOSSENBERGER, F. ; LIN, X. ; NADERIAN, M. ; SAKONG, S. ; ROMAN, T. : In: *J. Electrochem. Soc.* 161 (2014), E3015 S.

[62] GROSS, A. ; SCHEFFLER, M. : Role of zero-point effects in catalytic reactions involving hydrogen. In: *J. Vac. Sci. Technol. A* 15 (1997), S. 1624

[63] GROSS, A. : *Theoretical Surface Science*. Second. Springer, 2009

[64] GROSS, A. : Ab initio molecular dynamics study of H2 adsorption on sulfur- and chlorine-covered Pd(100). In: *Surf. Sci.* 608 (2013), S. 249–254. http://dx.doi.org/10.1016/j.susc.2012.10.015. – DOI 10.1016/j.susc.2012.10.015

[65] GROSSMAN, J. C. ; SCHWEGLER, E. ; DRAEGER, E. W. ; GYGI, F. ; GALLI, G. : Towards an assessment of the accuracy of density functional theory for first principles simulations of water. In: *The Journal of Chemical Physics* 120 (2004), Nr. 1, 300-311. http://dx.doi.org/10.1063/1.1630560. – DOI 10.1063/1.1630560

[66] GRÜNDER, Y. ; DRÜNKLER, A. ; GOLKS, F. ; WIJTS, G. ; STETTNER, J. ; ZEGENHAGEN, J. ; MAGNUSSEN, O. M.: Structure and electrocompression of chloride adlayers on Cu(111). In: *Surf. Sci.* 605 (2011), S. 1732–1737. http://dx.doi.org/10.1016/j.susc.2011.06.009. – DOI 10.1016/j.susc.2011.06.009

[67] GUIDELLI, R. ; SCHMICKLER, W. : Recent developments in models for the inter-face between a metal and an aqueous solution. In: *Electrochim. Acta* 45 (2000), S. 2317

[68] GUNCELER, D. ; LETCHWORTH-WEAVER, K. ; SUNDARARAMAN, R. ; SCHWARZ, K. A. ; ARIAS, T. A.: The importance of nonlinear fluid response in joint density-functional theory studies of battery systems. In: *Modelling and Simulation in Materials Science and Engineering* 21 (2013), Nr. 7, 074005. http://stacks.iop.org/0965-0393/21/i=7/a=074005

[69] HALCK, N. B. ; PETRYKIN, V. ; KRTIL, P. ; ROSSMEISL, J. : Beyond the volcano limitations in electrocatalysis - oxygen evolution reaction. In: *Phys. Chem. Chem. Phys.* 16 (2014), 13682-13688. http://dx.doi.org/10.1039/C4CP00571F. – DOI 10.1039/C4CP00571F

[70] HAMANN, D. R. ; SCHLÜTER, M. ; CHIANG, C. : Norm-Conserving Pseudopotentials. In: *Phys. Rev. Lett.* 43 (1979), Nov, 1494–1497. http://dx.doi.org/10.1103/PhysRevLett.43.1494. – DOI 10.1103/PhysRevLett.43.1494

[71] HAMMER, B. : Coverage dependence of N_2 dissociation at an N, O, or H precovered Ru(0001) surface investigated with density functional theory. In: *Phys. Rev. B* 63 (2001), S. 205423

[72] HAMMER, B. ; HANSEN, L. B. ; NØRSKOV, J. K.: Improved adsorption energetics within density-functional theory using revised Perdew-Burke-Ernzerhof functionals. In: *Phys. Rev. B* 59 (1999), Mar, 7413-7421. http://dx.doi.org/10.1103/PhysRevB.59.7413. – DOI 10.1103/PhysRevB.59.7413

[73] HANSEN, H. A. ; MAN, I. C. ; STUDT, F. ; ABILD-PEDERSEN, F. ; BLIGAARD, T. ; ROSSMEISL, J. : Electrochemical chlorine evolution at rutile oxide (110) surfaces. In: *Phys. Chem. Chem. Phys.* 12 (2010), S. 283–290. http://dx.doi.org/10.1039/B917459A. – DOI 10.1039/B917459A

[74] HERRERO, E. ; MOSTANY, J. ; FELIU, J. M. ; LIPKOWSKI, J. : Thermodynamic studies of anion adsorption at the Pt(111) electrode surface in sulfuric acid solutions. In: *Journal of Electroanalytical Chemistry* 534 (2002), Nr. 1, 79 - 89. http://dx.doi.org/http://dx.doi.org/10.1016/S0022-0728(02)01101-4. – DOI http://dx.doi.org/10.1016/S0022–0728(02)01101–4. – ISSN 1572–6657

[75] HOHENBERG, P. ; KOHN, W. : Inhomogeneous Electron Gas. In: *Phys. Rev.* 136 (1964), Nov, B864–B871. http://dx.doi.org/10.1103/PhysRev.136.B864. – DOI 10.1103/PhysRev.136.B864

[76] HONG WENJING ; VALKENIER HENNIE ; MÉSZÁROS GÁBOR ; MANRIQUE DAVID ZSOLT ; MISHCHENKO ARTEM ; PUTZ ALEXANDER ; GARCÍA PAVEL MORENO ; LAMBERT COLIN J ; HUMMELEN JAN C ; WANDLOWSKI THOMAS: An MCBJ case study: The influence of pi-conjugation on the single-molecule conductance at a solid/liquid interface. In: *Beilstein Journal of Nanotechnology* 2 (2011), sep, 699–713. http://www.ncbi.nlm.nih.gov/pmc/articles/PMC3201624/. – ISSN 2190–4286

[77] IGNACZAK, A. ; GOMES, J. : Quantum calculations on the adsorption of halide ions on the noble metals. In: *J. Electroanal. Chem.* 420 (1997), S. 71 – 78. – ISSN 1572–6657

[78] INUKAI, J. ; OSAWA, Y. ; ITAYA, K. : Adlayer Structures of Chlorine, Bromine, and Iodine on Cu(111) Electrode in Solution: In-Situ STM and ex-Situ LEED Studies. In: *J. Phys. Chem. B* 102 (1998), S. 10034

[79] INUKAI, J. ; OSAWA, Y. ; WAKISAKA, M. ; SASHIKATA, K. ; KIM, Y.-G. ; ITAYA, K. : Underpotential Deposition of Copper on Iodine-Modified Pt(111): In Situ STM and ex Situ LEED Studies. In: *J. Phys. Chem. B* 102 (1998), Nr. 18, 3498–3505. http://dx.doi.org/10.1021/jp9804143. – DOI 10.1021/jp9804143

[80] ISRAELACHVILI, J. N.: *Intermolecular and Surface Forces*. Third. Academic Press, 2011

[81] JINNOUCHI, R. ; ANDERSON, A. B.: Aqueous and Surface Redox Potentials from Self-Consistently Determined Gibbs Energies. In: *J. Phys. Chem. C* 112 (2008), S. 8747–8750. http://dx.doi.org/10.1021/jp802627s. – DOI 10.1021/jp802627s

[82] JINNOUCHI, R. ; HATANAKA, T. ; MORIMOTO, Y. ; OSAWA, M. : First principles study of sulfuric acid anion adsorption on a Pt(111) electrode. In: *Phys. Chem. Chem. Phys.* 14 (2012), 3208-3218. http://dx.doi.org/10.1039/C2CP23172G. – DOI 10.1039/C2CP23172G

[83] JINNOUCHI, R. ; KODAMA, K. ; MORIMOTO, Y. : {DFT} calculations on H, {OH} and O adsorbate formations on Pt(111) and Pt(332) electrodes. In: *J. Electroanal. Chem.* 716 (2014), S. 31 – 44. http://dx.doi.org/http://dx.doi.org/10.1016/j.jelechem.2013.09.031. – DOI http://dx.doi.org/10.1016/j.jelechem.2013.09.031

[84] JO, S. K. ; WHITE, J. M.: Characterization of adsorption states of atomic iodine on Pt(111). In: *Surf. Sci.* 261 (1992), S. 111–117

[85] KARLBERG, G. S. ; ROSSMEISL, J. ; NØRSKOV, J. K.: Estimations of electric field effects on the oxygen reduction reaction based on the density functional theory. 9 (2007), S. 5158

[86] KEITH, J. A. ; JACOB, T. : Theoretical Studies of Potential-Dependent and Competing Mechanisms of the Electrocatalytic Oxygen Reduction Reaction on Pt(111). In: *Angew. Chem. Int. Ed.* 49 (2010), S. 9521–9525. http://dx.doi.org/10.1002/anie.201004794. – DOI 10.1002/anie.201004794

[87] KEMP, D. D. ; GORDON, M. S.: Theoretical Study of the Solvation of Fluorine and Chlorine Anions by Water. In: *The Journal of Physical Chem-*

istry A 109 (2005), Nr. 34, 7688-7699. http://dx.doi.org/10.1021/jp058086b. – DOI 10.1021/jp058086b. – PMID: 16834143

[88] KIM, H. ; BOYSEN, D. A. ; OUCHI, T. ; SADOWAY, D. R.: Calcium–bismuth electrodes for large-scale energy storage (liquid metal batteries). In: *J. Power Sources* 241 (2013), S. 239–248. http://dx.doi.org/10.1016/j.jpowsour.2013.04.052. – DOI 10.1016/j.jpowsour.2013.04.052. – ISSN 0378–7753

[89] KITTEL, C. : *Introduction to Solid State Physics*. Seventh. John Wiley & Sons, 1996

[90] KITTEL, C. : *Introduction to Solid State Physics*. Eight. John Wiley & Sons, 2004

[91] KLÖTZER, B. ; BECHTOLD, E. : Reaction of adsorbed chlorine with hydrogen on a Pt(100) face. In: *Surf. Sci.* 326 (1995), Nr. 3, 218–228. http://dx.doi.org/10.1016/0039-6028(94)00796-9. – DOI 10.1016/0039–6028(94)00796–9. – ISSN 0039–6028

[92] KOHN, W. : Nobel Lecture: Electronic structure of matter—wave functions and density functionals. In: *Rev. Mod. Phys.* 71 (1999), Oct, 1253–1266. http://dx.doi.org/10.1103/RevModPhys.71.1253. – DOI 10.1103/RevModPhys.71.1253

[93] KOHN, W. ; SHAM, L. J.: Self-Consistent Equations Including Exchange and Correlation Effects. In: *Phys. Rev.* 140 (1965), Nov, A1133–A1138. http://dx.doi.org/10.1103/PhysRev.140.A1133. – DOI 10.1103/PhysRev.140.A1133

[94] KOLB, D. M.: An atomistic view of electrochemistry. In: *Surf. Sci.* 500 (2002), S. 722

[95] KOLICS, A. ; WIECKOWSKI, A. : Adsorption of Bisulfate and Sulfate Anions on a Pt(111) Electrode. In: *The Journal of Physical Chemistry B* 105 (2001), Nr. 13, 2588-2595. http://dx.doi.org/10.1021/jp003536f. – DOI 10.1021/jp003536f

[96] KRESSE, G. ; FURTHMÜLLER, J. : Efficient iterative schemes for ab initio total-energy calculations using a plane-wave basis set. In: *Phys. Rev. B* 54 (1996), S. 11169

[97] KRESSE, G. ; JOUBERT, D. : From ultrasoft pseudopotentials to the projector augmented-wave method. In: *Phys. Rev. B* 59 (1999), S. 1758

[98] KRUFT, M. ; WOHLMANN, B. ; STUHLMANN, C. ; WANDELT, K. : Chloride adsorption on Cu(111) electrodes in dilute {HCl} solutions. In: *Surf. Sci.* 377-379 (1997), S. 601–604

[99] LANG, N. D.: Small adsorbate dipole moments need not imply small charge transfers. In: *Surf. Sci.* 127 (1983), Nr. 2, S. L118 – L122

[100] LEACH, A. R.: *Molecular Modelling: Principles and Applications*. 2nd. Harlow : Pearson, 2001

[101] LETCHWORTH-WEAVER, K. ; ARIAS, T. A.: Joint density functional theory of the electrode-electrolyte interface: Application to fixed electrode potentials, interfacial capacitances, and potentials of zero charge. In: *Phys. Rev. B* 86 (2012), Aug, 075140. http://dx.doi.org/10.1103/PhysRevB.86.075140. – DOI 10.1103/PhysRevB.86.075140

[102] LEUNG, T. C. ; KAO, C. L. ; SU, W. S. ; FENG, Y. J. ; CHAN, C. T.: Relationship between surface dipole, work function and charge transfer: Some exceptions to an established rule. In: *Phys. Rev. B* 68 (2003), Nov, S. 195408. http://dx.doi.org/10.1103/PhysRevB.68.195408. – DOI 10.1103/PhysRevB.68.195408

[103] LEVIE, R. de: The electrolysis of water. In: *J. Electroanal. Chem.* 476 (1999), Nr. 1, S. 92–93. http://dx.doi.org/10.1016/S0022-0728(99)00365-4. – DOI 10.1016/S0022–0728(99)00365–4

[104] LI, N. ; LIPKOWSKI, J. : Chronocoulometric studies of chloride adsorption at the Pt(111) electrode surface. In: *J. Electroanal. Chem.* 491 (2000), S. 95

[105] LIN, I.-C. ; SEITSONEN, A. P. ; TAVERNELLI, I. ; ROTHLISBERGER, U. : Structure and Dynamics of Liquid Water from ab Initio Molecular Dynamics?Comparison of BLYP, PBE, and revPBE Density Functionals with and without van der Waals Corrections. In: *Journal of Chemical Theory and Computation* 8 (2012), Nr. 10, 3902-3910. http://dx.doi.org/10.1021/ct3001848. – DOI 10.1021/ct3001848. – PMID: 26593030

[106] LIN, X. ; DASGUPTA, A. ; XIE, F. ; SCHIMMEL, T. ; EVERS, F. ; GROSS, A. : Exchange processes in the contact formation of Pb electrodes. In: *Electrochimica Acta* 140 (2014), 505 - 510. http://dx.doi.org/https://doi.org/10.1016/j.electacta.2014.05.160. – DOI https://doi.org/10.1016/j.electacta.2014.05.160. – ISSN 0013–4686. – Electrochemistry for a New Era

[107] LIN, X. ; GOSSENBERGER, F. ; GROSS, A. : Ionic Adsorbate Structures on Metal Electrodes Calculated from First-Principles. In: *Industrial & Engineering Chemistry Research* 55 (2016), Nr. 42, 11107-11113. http://dx.doi.org/10.1021/acs.iecr.6b03087. – DOI 10.1021/acs.iecr.6b03087

[108] LIN, X. ; GROSS, A. : First-principles study of the water structure on flat and stepped gold surfaces. In: *Surf. Sci.* 606 (2012), S. 886–891

[109] LIN XIAOHANG ; EVERS FERDINAND ; GROSS AXEL: First-principles study of the structure of water layers on flat and stepped Pb electrodes. In: *Beilstein Journal of Nanotechnology* 7 (2016), mar, 533–543. http://www.ncbi.nlm.nih.gov/pmc/articles/PMC4901556/. – ISSN 2190–4286

[110] LIPKOWSKI, J. ; SHI, Z. ; CHEN, A. ; PETTINGER, B. ; BILGER, C. : Ionic adsorption at the Au(111) electrode. In: *Electrochim. Acta* 43 (1998), S. 2875 – 2888. http://dx.doi.org/http://dx.doi.org/10.1016/S0013-4686(98)00028-0. – DOI http://dx.doi.org/10.1016/S0013–4686(98)00028–0

[111] LISCHKA, M. ; GROSS, A. : Hydrogen adsorption on an open metal surface: H_2/Pd(210). In: *Phys. Rev. B* 65 (2002), S. 075420

[112] LISCHKA, M. ; MOSCH, C. ; GROSS, A. : CO and hydrogen adsorption on Pd(210). In: *Surf. Sci.* 570 (2004), S. 227

[113] LU, F. ; SALAITA, G. N. ; BALTRUSCHAT, H. ; HUBBARD, A. T.: Adlattice structure and hydrophobicity of Pt (111) in aqueous potassium iodide solutions: Influence of pH and electrode potential. In: *J. Electroanal. Chem.* 222 (1987), Nr. 1–2, 305–320. http://dx.doi.org/10.1016/0022-0728(87)80295-4. – DOI 10.1016/0022–0728(87)80295–4. – ISSN 0022–0728

[114] LUCAS, C. A. ; MARKOVIĆ, N. M. ; ROSS, P. N.: Adsorption of halide anions at the Pt(111)-solution interface studied by in situ surface x-ray scattering. In: *Phys. Rev. B* 55 (1997), Mar, 7964–7971. http://dx.doi.org/10.1103/PhysRevB.55.7964. – DOI 10.1103/PhysRevB.55.7964

[115] MADRY, B. ; WANDELT, K. ; NOWICKI, M. : Deposition of copper multilayers on Au(111) in sulfuric acid solution: An electrochemical scanning tunneling microscopy study. In: *Surface Science* 637-638 (2015), Nr. Supplement C, 77 - 84. http://dx.doi.org/https://doi.org/10.1016/j.susc.2015.03.017. – DOI https://doi.org/10.1016/j.susc.2015.03.017. – ISSN 0039–6028

[116] MAGNUSSEN, O. M.: Ordered anion adlayers on metal electrode surfaces. In: *Chem. Rev.* 107 (2002), S. 679–725

[117] MAN, I. C. ; SU, H.-Y. ; CALLE-VALLEJO, F. ; HANSEN, H. A. ; MARTINEZ, J. I. ; INOGLU, N. G. ; KITCHIN, J. ; JARAMILLO, T. F. ; NØRSKOV, J. K. ; ROSSMEISL, J. : Universality in Oxygen Evolution Electrocatalysis on Oxide Surfaces. In: *ChemCatChem* 3 (2011), S. 1159–1165. http://dx.doi.org/10.1002/cctc.201000397. – DOI 10.1002/cctc.201000397

[118] MARKOVIĆ, N. M. ; ROSS JR., P. N.: Surface science studies of model fuel cell electrocatalysts. In: *Surf. Sci. Rep.* 45 (2002), S. 117

[119] MARKOVIĆ, N. M. ; SCHMIDT, T. J. ; GRGUR, B. N. ; GASTEIGER, H. A. ; BEHM, R. J. ; ROSS, P. N.: Effect of Temperature on Surface Processes at the Pt(111)-Liquid Interface: Hydrogen Adsorption, Oxide Formation, and CO Oxidation. In: *J. Phys. Chem. B* 103 (1999), S. 8568–8577. http://dx.doi.org/10.1021/jp991826u. – DOI 10.1021/jp991826u

[120] MARKOVIĆ, N. ; GASTEIGER, H. ; GRGUR, B. ; ROSS, P. : Oxygen reduction reaction on Pt(111): effects of bromide. In: *J. Electroanal. Chem.* 467 (1999), Nr. 1–2, 157 - 163. http://dx.doi.org/http://dx.doi.org/10.1016/S0022-0728(99)00020-0. – DOI http://dx.doi.org/10.1016/S0022–0728(99)00020–0. – ISSN 1572–6657

[121] MARSHALL, S. T. ; MEDLIN, J. W.: Surface-level mechanistic studies of adsorbate–adsorbate interactions in heterogeneous catalysis by metals. In: *Surf. Sci. Rep.* 66 (2011), Nr. 5, 173–184. http://dx.doi.org/10.1016/j.surfrep.2011.03.001. – DOI 10.1016/j.surfrep.2011.03.001. – ISSN 0167–5729

[122] MCCRUM, I. T. ; AKHADE, S. A. ; JANIK, M. J.: Electrochemical specific adsorption of halides on Cu(111), (100), and (211): A Density Functional Theory study. In: *Electrochim. Acta* 173 (2015), S. 302–309. http://dx.doi.org/http://dx.doi.org/10.1016/j.electacta.2015.05.036. – DOI http://dx.doi.org/10.1016/j.electacta.2015.05.036

[123] METHFESSEL, M. ; PAXTON, A. T.: High-precision sampling for Brillouin-zone integration in metals. In: *Phys. Rev. B* 40 (1989), S. 3616

[124] MICHAELIDES, A. : Density functional theory simulations of water–metal interfaces: waltzing waters, a novel 2D ice phase, and more. In: *Applied Physics A* 85 (2006), Nr. 4, 415–425. http://dx.doi.org/10.1007/

s00339-006-3695-9. – DOI 10.1007/s00339–006–3695–9. – ISSN 0947–8396

[125] MICHAELIDES, A. ; HU, P. ; LEE, M. H. ; ALAVI, A. ; KING, D. A.: Resolution of an Ancient Surface Science Anomaly: Work Function Change Induced by N Adsorption on W100. In: *Phys. Rev. Lett.* 90 (2003), Nr. 24, S. 246103

[126] MICHAELIDES, A. ; RANEA, V. A. ; ANDRES, P. L. ; KING, D. A.: General Model for Water Monomer Adsorption on Close-Packed Transition and Noble Metal Surfaces. In: *Phys. Rev. Lett.* 90 (2003), S. 216102. http://dx.doi.org/10.1103/PhysRevLett.90.216102. – DOI 10.1103/PhysRevLett.90.216102

[127] MIGANI, A. ; SOUSA, C. ; ILLAS, F. : Chemisorption of atomic chlorine on metal surfaces and the interpretation of the induced work function changes. In: *Surf. Sci.* 574 (2005), Nr. 2-3, S. 297–305. http://dx.doi.org/10.1016/j.susc.2004.10.041. – DOI 10.1016/j.susc.2004.10.041. – ISSN 0039–6028

[128] MIGANI, A. ; ILLAS, F. : A Systematic Study of the Structure and Bonding of Halogens on Low-Index Transition Metal Surfaces. In: *J. Phys. Chem. B* 110 (2006), Nr. 24, 11894-11906. http://dx.doi.org/10.1021/jp060400u. – DOI 10.1021/jp060400u

[129] MOLL, N. ; KLEY, A. ; PEHLKE, E. ; SCHEFFLER, M. : GaAs equilibrium crystal shape from first principles. In: *Phys. Rev. B* 54 (1996), Sep, 8844–8855. http://dx.doi.org/10.1103/PhysRevB.54.8844. – DOI 10.1103/PhysRevB.54.8844

[130] MONKHORST, H. J. ; PACK, J. D.: Special points for Brillouin-zone integrations. In: *Phys. Rev. B* 13 (1976), S. 5188

[131] NEUGEBAUER, J. ; SCHEFFLER, M. : Adsorbate-substrate and adsorbate-adsorbate interactions of Na and K adlayers on Al(111). In: *Phys. Rev. B* 46 (1992), Dec, 16067–16080. http://dx.doi.org/10.1103/PhysRevB.46.16067. – DOI 10.1103/PhysRevB.46.16067

[132] NIE, S. ; FEIBELMAN, P. J. ; BARTELT, N. C. ; THÜRMER, K. : Pentagons and Heptagons in the First Water Layer on Pt(111). In: *Phys. Rev. Lett.* 105 (2010), Jul, 026102. http://dx.doi.org/10.1103/PhysRevLett.105.026102. – DOI 10.1103/PhysRevLett.105.026102

[133] NIE, X. ; LUO, W. ; JANIK, M. J. ; ASTHAGIRI, A. : Reaction mechanisms of

CO2 electrochemical reduction on Cu(111) determined with density functional theory. In: *Journal of Catalysis* 312 (2014), 108 - 122. http://dx.doi.org/https://doi.org/10.1016/j.jcat.2014.01.013. – DOI https://doi.org/10.1016/j.jcat.2014.01.013. – ISSN 0021–9517

[134] NIEUWENHUYS, B. E. ; MEIJER, D. T. ; SACHTLER, W. M. H.: Adsorption of Xenon on platinum studied by field emission microscopy. In: *physica status solidi (a)* 24 (1974), Nr. 1, S. 115–122. – ISSN 1521–396X

[135] NIEUWENHUYS, B. : Influence of the surface structure on the adsorption of hydrogen on platinum, as studied by field emission probe-hole microscopy. In: *Surf. Sci.* 59 (1976), Nr. 2, S. 430 – 446. – ISSN 0039–6028

[136] NIEUWENHUYS, B. ; SACHTLER, W. : Crystal face specificity of nitrogen adsorption on a platium field emission tip. In: *Surf. Sci.* 34 (1973), Nr. 2, S. 317 – 336. – ISSN 0039–6028

[137] NØRSKOV, J. K. ; BLIGAARD, T. ; LOGADOTTIR, A. ; KITCHIN, J. R. ; CHEN, J. G. ; PANDELOV, S. ; STIMMING, U. : Trends in the Exchange Current for Hydrogen Evolution. In: *J. Electrochem. Soc.* 152 (2005), S. J23

[138] NØRSKOV, J. K. ; ROSSMEISL, J. ; LOGADOTTIR, A. ; LINDQVIST, L. ; KITCHIN, J. R. ; BLIGAARD, T. ; JÓNSSON, H. : Origin of the Overpotential for Oxygen Reduction at a Fuel-Cell Cathode. In: *J. Phys. Chem. B* 108 (2004), S. 17886–17892. http://dx.doi.org/10.1021/jp047349j. – DOI 10.1021/jp047349j

[139] OBLIERS, B. ; BROEKMANN, P. ; WANDELT, K. : Uniaxial compression of iodide adlayers on Cu(111) studied under electrochemical conditions. In: *J. Electroanal. Chem.* 554-555 (2003), S. 183 – 189. http://dx.doi.org/http://dx.doi.org/10.1016/S0022-0728(03)00212-2. – DOI http://dx.doi.org/10.1016/S0022–0728(03)00212–2. – ISSN 1572–6657

[140] OELGEKLAUS, R. ; ROSE, J. ; BALTRUSCHAT, H. : On the rate of hydrogen and iodine adsorption on polycrystalline Pt and Pt(111). In: *J. Electroanal. Chem.* 376 (1994), S. 127 – 133. http://dx.doi.org/http://dx.doi.org/10.1016/0022-0728(94)03439-7. – DOI http://dx.doi.org/10.1016/0022–0728(94)03439–7

[141] ORTS, J. M. ; GÓMEZ, R. ; FELIU, J. M. ; ALDAZ, A. ; CLAVILIER, J. : Nature of Br Adlayers on Pt(111) Single-Crystal Surfaces. Voltammetric, Charge Displacement, and ex Situ STM Experiments. In: *J. Phys. Chem.*

100 (1996), Nr. 6, 2334–2344. http://dx.doi.org/10.1021/jp952989v. – DOI 10.1021/jp952989v

[142] OTANI, M. ; HAMADA, I. ; SUGINO, O. ; MORIKAWA, Y. ; OKAMOTO, Y. ; IKESHOJI, T. : Structure of the water/platinum interface – a first principles simulation under bias potential. 10 (2008), S. 3609. http://dx.doi.org/10.1039/b803541e. – DOI 10.1039/b803541e

[143] PAIER, J. ; HIRSCHL, R. ; MARSMAN, M. ; KRESSE, G. : The Perdew-Burke-Ernzerhof exchange-correlation functional applied to the G2-1 test set using a plane-wave basis set. In: *J. Chem. Phys.* 122 (2005), Nr. 23, S. 234102

[144] PARR, R. G. ; YANG, W. : *Density-Functional Theory of Atoms and Molecules*. Oxford University Press, 1989

[145] PAULEY, J. L. ; TESTERMAN, M. K.: Basic Salts of Lead Nitrate Formed in Aqueous Media1. In: *Journal of the American Chemical Society* 76 (1954), Nr. 16, 4220-4222. http://dx.doi.org/10.1021/ja01645a062. – DOI 10.1021/ja01645a062

[146] PAŠTI, I. A. ; MENTUS, S. V.: Halogen adsorption on crystallographic (111) planes of Pt, Pd, Cu and Au, and on Pd-monolayer catalyst surfaces: First-principles study. In: *Electrochim. Acta* 55 (2010), Nr. 6, S. 1995–2003. – ISSN 0013–4686

[147] PAŠTI, I. A. ; MENTUS, S. V.: Halogen adsorption on crystallographic (111) planes of Pt, Pd, Cu and Au, and on Pd-monolayer catalyst surfaces: First-principles study. In: *Electrochim. Acta* 55 (2010), Nr. 6, S. 1995 – 2003. – ISSN 0013–4686

[148] PELJHAN, S. ; KOKALJ, A. : Adsorption of Chlorine on Cu(111): A Density-Functional Theory Study. In: *J. Phys. Chem. C* 113 (2009), Nr. 32, S. 14363–14376

[149] PERDEW, J. P. ; BURKE, K. ; ERNZERHOF, M. : Generalized gradient approximation made simple. In: *Phys. Rev. Lett.* 77 (1996), S. 3865

[150] PERDEW, J. P. ; RUZSINSZKY, A. ; CONSTANTIN, L. A. ; SUN, J. ; CSONKA, G. I.: Some Fundamental Issues in Ground-State Density Functional Theory: A Guide for the Perplexed. In: *Journal of Chemical Theory and Computation* 5 (2009), Nr. 4, 902-908. http://dx.doi.org/10.1021/ct800531s. – DOI 10.1021/ct800531s. – PMID: 26609599

[151] PERDEW, J. P. ; YUE, W. : Accurate and simple density functional for the electronic exchange energy: Generalized gradient approximation. In: *Phys. Rev. B* 33 (1986), Jun, 8800–8802. http://dx.doi.org/10.1103/PhysRevB.33.8800. – DOI 10.1103/PhysRevB.33.8800

[152] PETROSYAN, S. A. ; BRIERE, J.-F. ; ROUNDY, D. ; ARIAS, T. A.: Joint density-functional theory for electronic structure of solvated systems. In: *Phys. Rev. B* 75 (2007), May, 205105. http://dx.doi.org/10.1103/PhysRevB.75.205105. – DOI 10.1103/PhysRevB.75.205105

[153] PETROSYAN, S. A. ; RIGOS, A. A. ; ARIAS, T. A.: Joint Density-Functional Theory: Ab Initio Study of Cr2O3 Surface Chemistry in Solution. In: *The Journal of Physical Chemistry B* 109 (2005), Nr. 32, 15436-15444. http://dx.doi.org/10.1021/jp044822k. – DOI 10.1021/jp044822k. – PMID: 16852958

[154] QIAN, Y. ; IKESHOJI, T. ; ZHAO, Y.-y. ; OTANI, M. : Vibrational Dynamics of Sulfate Anion Adsorption on Pt(111) Surface: Ab Initio Molecular Dynamics Simulations. In: *ChemElectroChem* 1 (2014), Nr. 10, 1632–1635. http://dx.doi.org/10.1002/celc.201402205. – DOI 10.1002/celc.201402205. – ISSN 2196–0216

[155] QUAINO, P. ; LUQUE, N. ; SOLDANO, G. ; NAZMUTDINOV, R. ; SANTOS, E. ; ROMAN, T. ; LUNDIN, A. ; GROSS, A. ; SCHMICKLER, W. : Solvated protons in density functional theory - a few examples. In: *Electrochim. Acta* 105 (2013), S. 248 – 253. – ISSN 0013–4686

[156] REUTER, K. ; SCHEFFLER, M. : Composition, structure, and stability of RuO_2(110) as a function of oxygen pressure. In: *Phys. Rev. B* 65 (2001), S. 035406

[157] ROGAL, J. ; REUTER, K. ; SCHEFFLER, M. : CO oxidation at Pd(100): A first-principles constrained thermodynamics study. In: *Phys. Rev. B* 75 (2007), S. 205433

[158] ROMAN, T. ; GOSSENBERGER, F. ; FORSTER-TONIGOLD, K. ; GROSS, A. : Halide adsorption on close-packed metal electrodes. In: *Phys. Chem. Chem. Phys.* 16 (2014), S. 13630–13634

[159] ROMAN, T. ; GROSS, A. : Periodic density-functional calculations on work function change induced by adsorption of halogens on Cu(111). In: *Phys. Rev. Lett.* 110 (2013), S. 156804

[160] ROMAN, T. ; NAKANISHI, H. ; DINO, W. ; KASAI, H. : Hydrogen atom quantum migration on platinum. In: *e-Journal of Surface Science and Nanotechnology* 4 (2006), S. 619–623. http://dx.doi.org/10.1380/ejssnt.2006.619. – DOI 10.1380/ejssnt.2006.619

[161] ROMAN, T. ; GROSS, A. : Structure of water layers on hydrogen-covered Pt electrodes. In: *Catal. Today* 202 (2013), S. 183–190

[162] ROMAN, T. ; NAKANISHI, H. ; KASAI, H. : Coadsorbed H and CO interaction on platinum. In: *Phys. Chem. Chem. Phys.* 10 (2008), 6052–6057. http://dx.doi.org/10.1039/B806186F. – DOI 10.1039/B806186F

[163] ROQUES, J. ; ANDERSON, A. B.: Theory for the Potential Shift for OHads Formation on the Pt Skin on Pt3Cr(111) in Acid. In: *Journal of The Electrochemical Society* 151 (2004), Nr. 3, E85-E91. http://dx.doi.org/10.1149/1.1645265. – DOI 10.1149/1.1645265

[164] ROQUES, J. ; ANDERSON, A. B.: Pt3Cr(111) Alloy Effect on the Reversible Potential of OOH(ads) Formation from O2(ads) relative to Pt(111). In: *Journal of Fuel Cell Science and Technology* 2 (2005), S. 86–93. http://dx.doi.org/10.1115/1.1867972. – DOI 10.1115/1.1867972

[165] ROSSMEISL, J. ; NØRSKOV, J. K. ; TAYLOR, C. D. ; JANIK, M. J. ; NEUROCK, M. : Calculated Phase Diagrams for the Electrochemical Oxidation and Reduction of Water over Pt(111). In: *J. Phys. Chem. B* 110 (2006), S. 21833–21839. http://dx.doi.org/10.1021/jp0631735. – DOI 10.1021/jp0631735

[166] ROUDGAR, A. ; GROSS, A. : Hydrogen adsorption energies on bimetallic overlayer systems at the solid-vacuum and the solid-liquid interface. In: *Surf. Sci.* 597 (2005), S. 42

[167] ROUDGAR, A. ; GROSS, A. : Water bilayer on the Pd/Au(111) overlayer system: coadsorption and electric field effects. In: *Chem. Phys. Lett.* 409 (2005), S. 157

[168] SAKONG, S. ; FORSTER-TONIGOLD, K. ; GROSS, A. : The structure of water at a Pt(111) electrode and the potential of zero charge studied from first principles. In: *The Journal of Chemical Physics* 144 (2016), Nr. 19, 194701. http://dx.doi.org/10.1063/1.4948638. – DOI 10.1063/1.4948638

[169] SAKONG, S. ; GROSS, A. : The Importance of the Electrochemical Environment in the Electro-Oxidation of Methanol on Pt(111). In: *ACS Cataly-*

sis 6 (2016), Nr. 8, 5575-5586. http://dx.doi.org/10.1021/acscatal.6b00931. – DOI 10.1021/acscatal.6b00931

[170] SAKONG, S. ; NADERIAN, M. ; MATHEW, K. ; HENNIG, R. G. ; GROSS, A. : Density functional theory study of the electrochemical interface between a Pt electrode and an aqueous electrolyte using an implicit solvent method. In: *J. Chem. Phys.* 142 (2015), S. 234107. http://dx.doi.org/http://dx.doi.org/10.1063/1.4922615. – DOI http://dx.doi.org/10.1063/1.4922615

[171] SALAITA, G. N. ; STERN, D. A. ; LU, F. ; BALTRUSCHAT, H. ; SCHARDT, B. C. ; STICKNEY, J. L. ; SORIAGA, M. P. ; FRANK, D. G. ; HUBBARD, A. T.: Structure and composition of a platinum(111) surface as a function of pH and electrode potential in aqueous bromide solutions. In: *Langmuir* 2 (1986), Nr. 6, 828–835. http://dx.doi.org/10.1021/la00072a031. – DOI 10.1021/la00072a031

[172] SALMERÓN, M. ; FERRER, S. ; JAZZAR, M. ; SOMORJAI, G. A.: Photoelectron-spectroscopy study of the electronic structure of Au and Ag overlayers on Pt(100), Pt(111), and Pt(997) surfaces. In: *Phys. Rev. B* 28 (1983), Dec, S. 6758–6765

[173] SANTANA, J. A. ; CABRERA, C. R. ; ISHIKAWA, Y. : A density-functional theory study of electrochemical adsorption of sulfuric acid anions on Pt(111). In: *Phys. Chem. Chem. Phys.* 12 (2010), 9526-9534. http://dx.doi.org/10.1039/C000981D. – DOI 10.1039/C000981D

[174] SANTOS, E. ; HINDELANG, P. ; QUAINO, P. ; SCHULZ, E. N. ; SOLDANO, G. ; SCHMICKLER, W. : Hydrogen Electrocatalysis on Single Crystals and on Nanostructured Electrodes. In: *ChemPhysChem* 12 (2011), S. 2274–2279. http://dx.doi.org/10.1002/cphc.201100309. – DOI 10.1002/cphc.201100309

[175] SARACINO, M. ; BROEKMANN, P. ; GENTZ, K. ; BECKER, M. ; KELLER, H. ; JANETZKO, F. ; BREDOW, T. ; WANDELT, K. ; DOSCH, H. : Surface relaxation phenomena at electrified interfaces: Revealing adsorbate, potential, and solvent effects by combined x-ray diffraction, STM and DFT studies. In: *Phys. Rev. B* 79 (2009), S. 115448. http://dx.doi.org/10.1103/PhysRevB.79.115448. – DOI 10.1103/PhysRevB.79.115448

[176] SATO, K. ; YOSHIMOTO, S. ; INUKAI, J. ; ITAYA, K. : Effect of sulfuric acid

concentration on the structure of sulfate adlayer on Au(1 1 1) electrode. 8 (2006), 05, S. 725–730

[177] SCHARDT, B. C. ; STICKNEY, J. L. ; STERN, D. A. ; WIECKOWSKI, A. ; ZAPIEN, D. C. ; HUBBARD, A. T.: Electrodeposition of lead onto platinum(111) in aqueous bromide solutions. Studies by LEED and Auger spectroscopy. In: *Langmuir* 3 (1987), Nr. 2, 239–244. http://dx.doi.org/10.1021/la00074a017. – DOI 10.1021/la00074a017

[178] SCHARDT, B. C. ; YAU, S.-L. ; RINALDI, F. : Atomic Resolution Imaging of Adsorbates on Metal Surfaces in Air: Iodine Adsorption on Pt(111). In: *Science* 243 (1989), Nr. 4894, 1050–1053. http://dx.doi.org/10.1126/science.243.4894.1050. – DOI 10.1126/science.243.4894.1050

[179] SCHENNACH, R. ; BECHTOLD, E. : Chlorine adsorption on Pt(111) and Pt(110). In: *Surf. Sci.* 380 (1997), Nr. 1, 9–16. http://dx.doi.org/10.1016/S0039-6028(96)01593-2. – DOI 10.1016/S0039–6028(96)01593–2. – ISSN 0039–6028

[180] SCHMICKLER, W. : Electronic Effects in the Electric Double Layer. In: *Chem. Rev.* 96 (1996), S. 3177–3200. http://dx.doi.org/10.1021/cr940408c. – DOI 10.1021/cr940408c

[181] SCHMICKLER, W. ; GUIDELLI, R. : The partial charge transfer. In: *Electrochim. Acta* 127 (2014), S. 489 – 505. http://dx.doi.org/http://dx.doi.org/10.1016/j.electacta.2014.02.057. – DOI http://dx.doi.org/10.1016/j.electacta.2014.02.057

[182] SCHMICKLER, W. ; SANTOS, E. : *Interfacial Electrochemistry*. 2nd. Berlin : Springer, 2010

[183] SCHMIDT, T. ; JR., P. R. ; MARKOVIC, N. : Temperature dependent surface electrochemistry on Pt single crystals in alkaline electrolytes: Part 2. The hydrogen evolution/oxidation reaction. In: *J. Electroanal. Chem.* 524 (2002), S. 252–260. http://dx.doi.org/10.1016/S0022-0728(02)00683-6. – DOI 10.1016/S0022–0728(02)00683–6. – ISSN 1572–6657

[184] SCHNUR, S. ; GROSS, A. : Properties of metal-water interfaces studied from first principles. In: *New J. Phys.* 11 (2009), S. 125003

[185] SCHNUR, S. ; GROSS, A. : Challenges in the first-principles description of reactions in electrocatalysis. In: *Catal. Today* 165 (2011), S. 129–137. http://dx.doi.org/10.1016/j.cattod.2010.11.071. – DOI 10.1016/j.cattod.2010.11.071

[186] SHI, Z. ; WU, S. ; LIPKOWSKI, J. : Coadsorption of metal atoms and anions: Cu upd in the presence of SO_4^{2-}, Cl^- and Br^-. In: *Electrochim. Acta* 40 (1995), S. 9–15. http://dx.doi.org/http://dx.doi.org/10.1016/0013-4686(94)00244-U. – DOI http://dx.doi.org/10.1016/0013–4686(94)00244–U

[187] SHINGAYA, Y. ; ITO, M. : Interconversion of a bisulfate anion into a sulfuric acid molecule on a Pt(111) electrode in a 0.5 M H2SO4 solution. In: *Chemical Physics Letters* 256 (1996), Nr. 4, 438 - 444. http://dx.doi.org/http://dx.doi.org/10.1016/0009-2614(96)00465-4. – DOI http://dx.doi.org/10.1016/0009–2614(96)00465–4. – ISSN 0009–2614

[188] SKÚLASON, E. ; KARLBERG, G. S. ; ROSSMEISL, J. ; BLIGAARD, T. ; GREELEY, J. ; JÓNSSON, H. ; NØRSKOV, J. K.: Density functional theory calculations for the hydrogen evolution reaction in an electrochemical double layer on the Pt(111) electrode. In: *Phys. Chem. Chem. Phys.* 9 (2007), S. 3241

[189] SONG, M. ; ITO, M. : STM observation of Pt111(3x3)-Cl and c(4x2)-Cl structures. In: *Bull. Korean Chem. Soc.* 22 (2001), S. 267

[190] SPOHR, E. ; TOTH, G. ; HEINZINGER, K. : Structure and dynamics of water and hydrated ions near platinum and mercury surfaces as studied by {MD} simulations. In: *Electrochim. Acta* 41 (1996), S. 2131–2144. http://dx.doi.org/http://dx.doi.org/10.1016/0013-4686(96)00045-X. – DOI http://dx.doi.org/10.1016/0013–4686(96)00045–X

[191] STERN, D. A. ; BALTRUSCHAT, H. ; MARTINEZ, M. ; STICKNEY, J. L. ; SONG, D. ; LEWIS, S. K. ; FRANK, D. G. ; HUBBARD, A. T.: Characterization of single-crystal electrode surfaces as a function of potential and pH by Auger spectroscopy and LEED: Pt (111) in aqueous CaCl2 and {HCl} solutions. In: *J. Electroanal. Chem.* 217 (1987), Nr. 1, 101–110. http://dx.doi.org/10.1016/0022-0728(87)85067-2. – DOI 10.1016/0022–0728(87)85067–2. – ISSN 0022–0728

[192] STICKNEY, J. ; ROSASCO, S. ; HUBBARD, A. : Electrodeposition of copper on platinum (111) surfaces pretreated with iodine. In: *J. Electrochem. Soc.* 131 (1984), S. 260

[193] STICKNEY, J. L. ; ROSASCO, S. D. ; SALAITA, G. N. ; HUBBARD, A. T.: Ordered ionic layers formed on platinum(111) from aqueous solutions. In: *Langmuir* 1 (1985), Nr. 1, 66–71. http://dx.doi.org/10.1021/la00061a009. – DOI 10.1021/la00061a009

[194] STRMCNIK, D. ; TRIPKOVIC, D. ; VLIET, D. van d. ; STAMENKOVIC, V. ; MARKOVIC, N. : Adsorption of hydrogen on Pt(111) and Pt(100) surfaces and its role in the {HOR}. In: *Electrochem. Comm.* 10 (2008), S. 1602 – 1605. http://dx.doi.org/http://dx.doi.org/10.1016/j.elecom.2008.08.019. – DOI http://dx.doi.org/10.1016/j.elecom.2008.08.019

[195] TANAKA, S. ; YAU, S.-L. ; ITAYA, K. : In-situ scanning tunneling microscopy of bromine adlayers on Pt(111). In: *J. Electroanal. Chem.* 396 (1995), Nr. 1–2, 125–130. http://dx.doi.org/10.1016/0022-0728(95)04062-S. – DOI 10.1016/0022–0728(95)04062–S. – ISSN 1572–6657

[196] TAYLOR, C. D. ; WASILESKI, S. A. ; FILHOL, J.-S. ; NEUROCK, M. : First principles reaction modeling of the electrochemical interface: Consideration and calculation of a tunable surface potential from atomic and electronic structure. 73 (2006), S. 165402

[197] TKATCHENKO, A. ; SCHEFFLER, M. : Accurate Molecular Van Der Waals Interactions from Ground-State Electron Density and Free-Atom Reference Data. In: *Phys. Rev. Lett.* 102 (2009), Feb, 073005. http://dx.doi.org/10.1103/PhysRevLett.102.073005. – DOI 10.1103/PhysRevLett.102.073005

[198] TOMÁNEK, D. ; WILKE, S. ; SCHEFFLER, M. : Hydrogen-Induced Polymorphism of the Pd(110) Surface. In: *Phys. Rev. Lett.* 79 (1997), Aug, 1329–1332. http://dx.doi.org/10.1103/PhysRevLett.79.1329. – DOI 10.1103/PhysRevLett.79.1329

[199] TONIGOLD, K. ; GROSS, A. : Dispersive interactions in water bilayers at metallic surfaces: A comparison of the PBE and RPBE functional including semiempirical dispersion corrections. In: *Journal of Computational Chemistry* 33 (2012), Nr. 6, 695–701. http://dx.doi.org/10.1002/jcc.22900. – DOI 10.1002/jcc.22900. – ISSN 1096–987X

[200] TRASATTI, S. : The absolute electrode potential: an explanatory note. In: *Pure Appl. Chem.* 58 (1986), S. 955–966. http://dx.doi.org/10.1351/pac198658070955. – DOI 10.1351/pac198658070955

[201] TRIPKOVIC, D. V. ; STRMCNIK, D. ; VLIET, D. van d. ; STAMENKOVIC, V. ; MARKOVIC, N. M.: The role of anions in surface electrochemistry. In: *Faraday Discuss.* 140 (2009), S. 25–40. http://dx.doi.org/10.1039/B803714K. – DOI 10.1039/B803714K

[202] VANDERBILT, D. : Soft self-consistent pseudopotentials in a generalized eigenvalue formalism. In: *Phys. Rev. B* 41 (1990), Apr, 7892–7895. http://dx.doi.org/10.1103/PhysRevB.41.7892. – DOI 10.1103/PhysRevB.41.7892

[203] VILLEGAS, I. ; WEAVER, M. J.: Infrared Spectroscopy of Model Electrochemical Interfaces in Ultrahigh Vacuum: Evidence for Coupled Cation-Anion Hydration in the Pt(111)/K,Cl System. In: *J. Phys. Chem.* 100 (1996), Nr. 50, 19502–19511. http://dx.doi.org/10.1021/jp9616270. – DOI 10.1021/jp9616270

[204] WAGNER, F. T. ; MOYLAN, T. E.: Hydrogen chloride adsorption and coadsorption with hydrogen or water on platinum (111). In: *Surf. Sci.* 216 (1989), Nr. 3, 361–385. http://dx.doi.org/10.1016/0039-6028(89)90381-6. – DOI 10.1016/0039–6028(89)90381–6. – ISSN 0039–6028

[205] WANG, H.-F. ; LIU, Z.-P. : Formic Acid Oxidation at Pt/H_2O Interface from Periodic DFT Calculations Integrated with a Continuum Solvation Model. In: *J. Phys. Chem. C* 113 (2009), S. 17502–17508. http://dx.doi.org/10.1021/jp9059888. – DOI 10.1021/jp9059888

[206] WANG, Y. ; PERDEW, J. P.: Spin scaling of the electron-gas correlation energy in the high-density limit. In: *Phys. Rev. B* 43 (1991), Apr, 8911–8916. http://dx.doi.org/10.1103/PhysRevB.43.8911. – DOI 10.1103/PhysRevB.43.8911

[207] WASILESKI, S. A. ; JANIK, M. J.: A first-principles study of molecular oxygen dissociation at an electrode surface: a comparison of potential variation and coadsorption effects. 10 (2008), S. 3613

[208] WEI, C. M. ; GROSS, A. ; SCHEFFLER, M. : Ab initio calculation of the potential energy surface for the dissociation of H_2 on the sulfur-covered Pd(100) surface. In: *Phys. Rev. B* 57 (1998), S. 15572

[209] XIE, F.-Q. ; HÜSER, F. ; PAULY, F. ; OBERMAIR, C. ; SCHÖN, G. ; SCHIMMEL, T. : Conductance of atomic-scale Pb contacts in an electrochemical environment. In: *Phys. Rev. B* 82 (2010), Aug, 075417. http://dx.doi.org/10.1103/PhysRevB.82.075417. – DOI 10.1103/PhysRevB.82.075417

[210] XIE, F.-Q. ; MAUL, R. ; BRENDELBERGER, S. ; OBERMAIR, C. ; STARIKOV, E. B. ; WENZEL, W. ; SCHÖN, G. ; SCHIMMEL, T. : Preselectable integer quantum conductance of electrochemically fabricated silver point contacts.

In: *Applied Physics Letters* 93 (2008), Nr. 4, 043103. http://dx.doi.org/10.1063/1.2955521. – DOI 10.1063/1.2955521

[211] XIE, F.-Q. ; NITTLER, L. ; OBERMAIR, C. ; SCHIMMEL, T. : Gate-Controlled Atomic Quantum Switch. In: *Phys. Rev. Lett.* 93 (2004), Sep, 128303. http://dx.doi.org/10.1103/PhysRevLett.93.128303. – DOI 10.1103/PhysRevLett.93.128303

[212] XIE, F. ; MAUL, R. ; OBERMAIR, C. ; WENZEL, W. ; SCHÖN, G. ; SCHIMMEL, T. : Multilevel Atomic-Scale Transistors Based on Metallic Quantum Point Contacts. In: *Advanced Materials* 22 (2010), Nr. 18, 2033–2036. http://dx.doi.org/10.1002/adma.200902953. – DOI 10.1002/adma.200902953. – ISSN 1521–4095

[213] XIN, H. ; VOJVODIC, A. ; VOSS, J. ; NØRSKOV, J. K. ; ABILD-PEDERSEN, F. : Effects of d-band shape on the surface reactivity of transition-metal alloys. In: *Phys. Rev. B* 89 (2014), Mar, 115114. http://dx.doi.org/10.1103/PhysRevB.89.115114. – DOI 10.1103/PhysRevB.89.115114

[214] YAU, S. L. ; VITUS, C. M. ; SCHARDT, B. C.: In situ scanning tunneling microscopy of adsorbates on electrode surfaces: images of the (.sqroot.3.times..sqroot.3)R30.degree.-iodine adlattice on platinum(111). In: *J. Am. Chem. Soc.* 112 (1990), Nr. 9, 3677–3679. http://dx.doi.org/10.1021/ja00165a073. – DOI 10.1021/ja00165a073

[215] YEH, K.-Y. ; RESTAINO, N. A. ; ESOPI, M. R. ; MARANAS, J. K. ; JANIK, M. J.: The adsorption of bisulfate and sulfate anions over a Pt(1 1 1) electrode: A first principle study of adsorption configurations, vibrational frequencies and linear sweep voltammogram simulations. In: *Catalysis Today* 202 (2013), 20 - 35. http://dx.doi.org/https://doi.org/10.1016/j.cattod.2012.03.011. – DOI https://doi.org/10.1016/j.cattod.2012.03.011. – ISSN 0920–5861. – Electrocatalysis

[216] YOO, S. ; ZENG, X. C. ; XANTHEAS, S. S.: On the phase diagram of water with density functional theory potentials: The melting temperature of ice Ih with the Perdew-Burke-Ernzerhof and Becke-Lee-Yang-Parr functionals. In: *The Journal of Chemical Physics* 130 (2009), Nr. 22, 221102. http://dx.doi.org/10.1063/1.3153871. – DOI 10.1063/1.3153871

A Abbreviations

AIMD	ab-initio molecular dynamic (simulation)
DFT	density functional theory
DOS	density of states
fcc	face-centered cubic, a unit cell type
GGA	generalized gradient approximation
KMC	kinetic Monte Carlo
KRR	kernel ridge regression
LDA	local density approximation
LSDA	local spin density approximation
PBE	Perdew Burke Ernzerhof functional
RPBE	revised PBE functional
STM	scanning tunneling microscope
VASP	Vienna ab-initio Simulation Package, a dft program
UHV	ultra high vacuum

B Conference contributions

1. Florian Gossenberger, and Axel Groß, Halogen adsorption-induced work function changes on Pt(111), DPG-Frühjahrstagung (2013), poster.
2. Florian Gossenberger, Tanglaw Roman and Axel Groß, Adsorbate coverage-dependent work function changes on platinum, summer school Norderney (2013), poster.
3. Florian Gossenberger, and Axel Groß, Halogen and water adsorption-induced work function changes on Pt(111), Max-Planck Gesellschaft, Schloß Ringberg (2013), poster.
4. Florian Gossenberger, and Axel Groß, Simulation of equilibrium structures of halogens and hydrogen on Pt(111), summer school Villars (2014), poster.
5. Florian Gossenberger, and Axel Groß, Adsorption of halides on metal electrodes, DTU Copenhagen/Denmark (2015), talk.
6. Florian Gossenberger, and Axel Groß, Adsorption of halides on metal electrodes, DPG-Frühjahrstagung (2015), talk.
7. Florian Gossenberger, and Axel Groß, Simulation of equilibrium structures of halogens and hydrogen on Pt(111), Reisensburg (2015) ,poster.
8. Florian Gossenberger, and Axel Groß, Adsorption of halides on metal electrodes, Ulm Electrochemistry Symposium (2015), talk.
9. Florian Gossenberger, and Axel Groß, Adsorption of halides on metal electrodes, DPG-Frühjahrstagung (2016), talk.
10. Florian Gossenberger, and Axel Groß, Coadsorption of anions and cations on platinum, DPG-Frühjahrstagung (2017), talk.
11. Florian Gossenberger, and Axel Groß, Modeling the electrochemical electrode-electrolyte interface, 7th Bonn Humboldt Award Winners' Forum "Fundamental Concepts and Principles of Chemical Energy Conversion" (2017), poster.

12. Florian Gossenberger, and Axel Groß, Modeling the electrochemical electrode-electrolyte interface, Ulm (2018), poster.

C Curriculum vitae

The CV is not published for reasons of data protection.

D Acknowledgment

Acknowledgment is not published for reasons of data protection.

E Publications

E.1 Publication in chapter 4.1

The following article is used in chapter 4.1, it is reprinted and adapted from F. Gossenberger, T. Roman, K. Forster-Tonigold, and A. Gross, Beilstein J. of Nanotechnol. 5 (2014), 152.

Beilstein Journal of Nanotechnology

Change of the work function of platinum electrodes induced by halide adsorption

Florian Gossenberger[1], Tanglaw Roman[*1], Katrin Forster-Tonigold[2] and Axel Groß[1,2]

Full Research Paper

Open Access

Address:
[1]Institute of Theoretical Chemistry, Ulm University, 89069 Ulm, Germany and [2]Helmholtz Institute Ulm (HIU) for Electrochemical Energy Storage, 89069 Ulm, Germany

Email:
Tanglaw Roman[*] - tanglaw.roman@uni-ulm.de

* Corresponding author

Keywords:
density functional theory; ionicity; polarizability; surface dipole; work function

Beilstein J. Nanotechnol. **2014,** *5,* 152–161.
doi:10.3762/bjnano.5.15

Received: 22 August 2013
Accepted: 21 January 2014
Published: 10 February 2014

This article is part of the Thematic Series "Electrocatalysis on the nm scale".

Guest Editor: R. J. Behm

Abstract

The properties of a halogen-covered platinum(111) surface have been studied by using density functional theory (DFT), because halides are often present at electrochemical electrode/electrolyte interfaces. We focused in particular on the halogen-induced work function change as a function of the coverage of fluorine, chlorine, bromine and iodine. For electronegative adsorbates, an adsorption-induced increase of the work function is usually expected, yet we find a decrease of the work function for Cl, Br and I, which is most prominent at a coverage of approximately 0.25 ML. This coverage-dependent behavior can be explained by assuming a combination of charge transfer and polarization effects on the adsorbate layer. The results are contrasted to the adsorption of fluorine on calcium, a system in which a decrease in the work function is also observed despite a large charge transfer to the halogen adatom.

Introduction

In electrochemistry, processes at the interface between an electron conductor, the electrode, and an ion conductor, the electrolyte, are studied [1]. In order to be charge neutral, the electrolyte contains equal amounts of anions and cations. In aqueous electrolytes, protons acting as cations are always present [2] whereas halides are often chosen as anions. The contact of a particular solvent with an electrode surface can lead to a rather complex situation at the electrode surface [3,4]. The characteristics of the solvent significantly affects processes such as adsorption and desorption. Because of the strong interaction of halogen atoms with metal electrodes, the metal electrodes typically become halogen-covered through specific adsorption. These adsorbed anions are not only part of the electrochemical double layer, in general they also change the work function of

the electrode, which is directly related to the electrode potential [5]. Furthermore, they also affect the chemical properties of the electrodes [6].

In spite of the importance of the specific adsorption of anions in electrochemistry, atomistic details of the role of anions in surface electrochemistry are still poorly understood [7]. Here, surface science studies focusing on the change of the properties of metal surfaces upon halide adsorption can help to elucidate the role of anionic specific adsorption at electrode/electrolyte interfaces, in particular with respect to the adsorption-induced change of the work function. It is known that the work function is strongly influenced by the adsorption of ions, which can lead to both an increase and a decrease of the work function [8-17]. In a previous study, we have addressed the adsorption of iodine and chlorine on Cu(111) [9] by using periodic density functional theory (DFT) calculations. Whereas chlorine causes the expected increase of the work function upon adsorption of an electronegative adsorbate, iodine leads to a surprising decrease of the work function for coverages up to approximately 0.4 ML. By analyzing the underlying electronic structure, we were able to show that this behavior can be explained through a combination of charge transfer and polarization effects of the adsorbate layer.

We have now extended this previous study by considering the adsorption of fluorine, chlorine, bromine and iodine on Pt(111) in order to check whether the findings for halogen adsorption on Cu(111) are also valid for the technologically important electrode material platinum. It has already been observed experimentally [18-20] as well as theoretically [11,13,17] that the adsorption of chlorine, bromine and iodine on Pt(111) leads to an unexpected decrease of the work function. Based on calculations for several adsorbates on tungsten surfaces, Leung, Kao and Su pointed out that it is possible to relate the electronegativity scale to the direction of the charge transfer but not necessarily to the induced work function change. It has also been shown that the formation of halogen oxides at the surface of a metal oxide leads to a decrease in the work function [21]. The problem of the unexpected decrease of the work function was also tackled by Michaelides et al. [8] for a system of nitrogen adsorbed on a tungsten (100) surface. They showed that the decrease of the work function depends strongly on the length of the chemisorption bond. If the adatom is located close to the surface, it is in the region of the overspill electron density of the metal. This leads to an area of electron depletion far from the surface, and in combination with an electron buildup in the area around the adsorbed ion, to a decrease of the work function.

In this paper we present a detailed study of the halogen-induced change of the work function on Pt(111) as a function of the halogen coverage, which has still been missing. We will show that the observed decrease of the work function upon the adsorption of chlorine, bromine and iodine on Pt(111) at low coverages can be explained by the strong polarization of the adsorbed halogen atoms, as in the case of I/Cu(111) [9]. We contrast these results with findings obtained for fluorine adsorption on calcium, for which an adsorption-induced decrease of the work function is also observed. However, due to the particular geometric conditions in this system, the spillout mechanism [8,22] is operative.

Methods

For the following calculations, the periodic density functional theory (DFT) program Vienna Ab initio Simulation Package (VASP) was used. The exchange and correlation energy was calculated by using the generalized gradient approximation (GGA) with the PBE functional, developed by Perdew, Burke and Ernzerhof [23]. This functional is widely used, as it has been shown to give reliable results in terms of atomization energy, chemisorption energies [24,25], work function changes [26], and good estimates of bulk properties of metals [27]. Hybrid functionals are not necessarily improvements to PBE; for example they do not yield a satisfactory description of the characteristics of transition metals [27].

To describe the ionic cores of the atoms, we used the projector augmented wave potentials (PAW) constructed by Kresse and Joubert [28]. The electronic wave functions were expanded in a plane wave basis set up to an energy cutoff of 400 eV. For the calculations, a periodic slab with a thickness of 7 atomic layers and 4 × 4 lateral periodicity was chosen. All calculations were done by using a symmetric setup of the slab, i.e., the halogen atoms were adsorbed on both sides of the slab, the middle three layers of the slab were kept fixed and the outermost two layers of both sides of the slab together with the adatoms were relaxed. Thus no dipole correction was necessary in order to derive the work function of the surface terminations. The unit cell was computed with a gamma-centered 4 × 4 × 1 *k*-point mesh.

The optimized lattice constant for platinum was found to be $a = 3.98$ Å, which is only 1.48% larger than the standard experimental value [29]. For low coverages the halogens iodine, bromine and chlorine adsorb most stably at the fcc threefold-hollowsite position on a platinum (111) surface. Since the hcp threefold-hollow position is also quite stable, the halogens were ordered in symmetric patterns on the surface with the highest possible nearest neighbor distance to other adsorbed atoms in hcp and fcc positions. The threefold-hollow adsorption positions are considered as the most probable adsorption sites for halogens on metals [9,10,14,30]. In this manner, six different coverages – 1/16 ML, 2/16 ML, 3/16 ML, 4/16 ML, 6/16 ML

and 8/16 ML – were created, which are illustrated in Figure 1. The structures of iodine, bromine and chlorine were relaxed completely.

Interestingly enough, fluorine atoms adsorb more stably at the on-top position of platinum. At this position, the average distance to the topmost surface layer is larger than on the threefold-hollow sites. Since we are interested in getting trends among the halogen atoms in order to understand and predict adsorption processes, we kept the fluorine in the threefold-hollow site positions, but allowed for vertical relaxation, which made a better comparison with the results for the chlorine, bromine and iodine adsorption structures possible.

Results and Discussion

Of central importance for this particular work is the determination of the change of the work function as a function of the halogen coverage. In periodic slab calculations, the work function is given by the difference between the Fermi energy and the value of the one-electron potential in vacuum. Vacuum is reached when the potential does not change anymore with increasing distance from the surface.

Figure 2 shows the work function of halogen-covered Pt(111) as a function of the halogen coverage. For clean Pt(111), the calculations yield a value of 5.71 eV. Various experimental measurements in the last decades do not agree well with each other. They are in the range of 5.6 eV to 6.1 eV [20,31-37]. The presence of fluorine on Pt(111) always increases the work function, which is qualitatively consistent with what one expects from a dipole involving a negative charge on the adsorbate. The adsorption of chlorine, bromine or iodine on a platinum (111) surface reduces the work function at low coverages. While the trend reverses at 0.25 ML, ΔΦ becomes positive not until the coverage reaches half a monolayer. The experimental trends [18-20] as well as theoretical values by Migani et al. [10] agree with the calculated results.

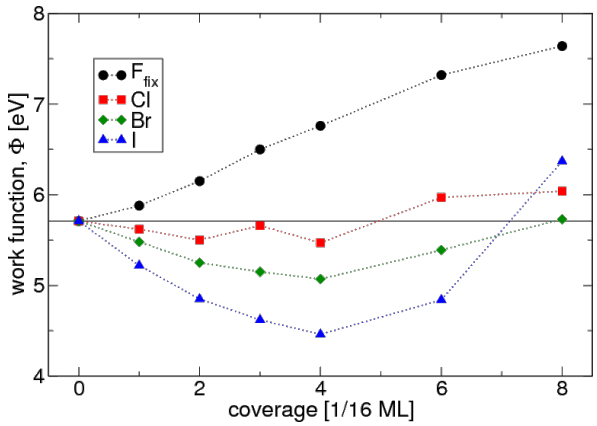

Figure 2: Calculated change of the work function vs coverage for the adsorption of fluorine, chlorine, bromine and iodine on Pt(111). The high value for the 0.5 ML calculation of iodine is due to a double layer structure of the adsorbates, caused by the larger size of iodine atoms.

Aside from the sign of the work function change, the dependence of ΔΦ on the halogen coverage is another aspect that needs

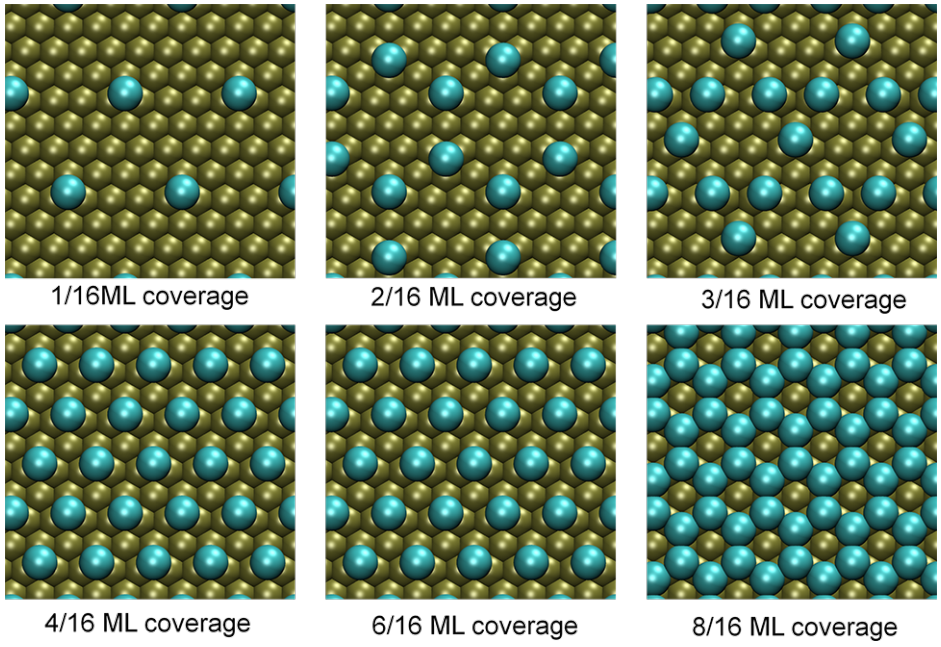

Figure 1: The figures show the relaxed structures of different coverages of chlorine on a Pt(111) surface.

to be clarified. In a simple model, one may completely neglect the interaction between the adsorbates. In this case, a linear trend $\Delta\Phi(\theta) \propto -\theta\Delta\mu$ would be expected, where θ is the surface coverage and Δμ is the change in the surface dipole moment brought about by the adsorption of a halogen atom. Obviously, this model is applicable only at low coverages in Figure 2. In a more advanced model, the electrostatic interaction between adjacent dipoles is taken into account by assuming that the mutual repulsion of the dipoles leads to a decrease in the polarity of the halogen–metal bond. The term Δμ thus becomes dependent on the halogen coverage, which causes a saturation of ΔΦ at high coverages. However, this does not explain the observed non-monotonic behavior of the work function change and so a more comprehensive explanation is needed.

In general, an adsorbate layer that involves charge transfer in the adsorption reaction can produce an observable change in the work function of the metal surface since electrons, in leaving the metal surface, will have to pass through the resulting interface dipole layer. Depending on the orientation of the dipole, this can either make removing electrons easier or harder. More precisely, the connection between work function change and surface dipole moment change is given by

$$\Delta\Phi = -\frac{e}{\varepsilon_0}\left(\mu_z - \mu_{z,0}\right) = -\frac{e}{\varepsilon_0}\Delta\mu\,, \qquad (1)$$

where $\mu_{z,0}$ is the surface-normal dipole moment per unit area of the clean surface, μ_z is the surface-normal dipole moment per unit area for the adsorbate-covered surface. A positive value of μ has traditionally been assigned to a dipole pointing away from the bulk, which leads to a decrease of the work function ($\Delta\Phi < 0$). Conversely, a negative μ points into the bulk and increases the work function ($\Delta\Phi > 0$). The surface dipole moment changes when the electron density close to the surface becomes redistributed upon bond formation. The most straightforward description of this redistribution is through the electron density difference that is given by the difference of the electron density of the interacting system with the total electron density of the non-interacting metal slab and halogen layer at the same atomic positions, $\rho_{\text{diff}} = \rho_{\text{Hal+Pt}} - (\rho_{\text{Hal}} + \rho_{\text{Pt}})$. The electron density difference profile $\Delta\lambda(z)$ along the z direction corresponds to the lateral sum of the electron density difference in the x and y directions,

$$\Delta\lambda = \frac{1}{N}\iint_{\text{cell}} \rho_{\text{diff}}\, dx\, dy\,, \qquad (2)$$

where N is the number of halogen atoms adsorbed on one side of the slab per unit cell. The Δλ profiles for a coverage of 1/16 ML of the four halogens are shown in Figure 3. The shape of the diagrams for higher coverages look similar. The profiles illustrate how the electron density is reorganized along the z direction when the adatoms adsorb. The gray area on the left hand side denotes the metal slab. The topmost metal atoms are centered at z = 0 Å. The electron density difference profile shows a significant electron depletion far from the surface for the case of chlorine, bromine and iodine, followed by an electron buildup close to the surface, and oscillations in the metal. In the case of fluorine, there is just an electron buildup around the fluorine atom, followed by oscillations into the bulk. This electron buildup around the fluorine atom indicates an ionic state. Fluorine is partially constrained to remain at the threefold-hollow sites, where the average distance from the center of the adsorbates to the topmost surface layer is smaller than for fluorine adsorbed at the on-top position. Calculations for F atoms at the most stable adsorption site may give slightly different results in charge transfer and dipole moments.

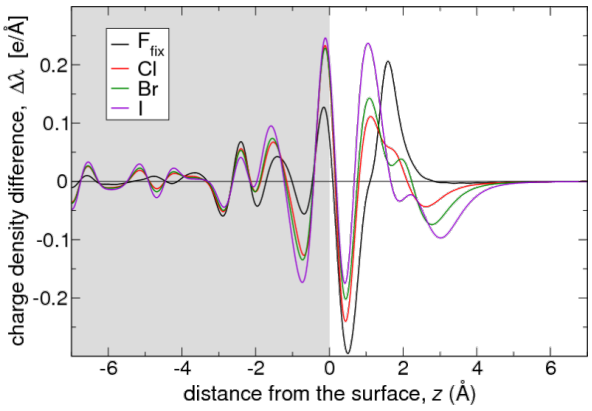

Figure 3: Charge density difference Δλ(z) for the adsorption of fluorine, chlorine, bromine, and iodine on Pt(111) at the fcc hollow position for a coverage of 1/16 ML. The subsurface region corresponds to the gray-shaded area at z < 0.

In the next step, the resulting surface dipole moment change $\Delta\mu_N$ can be determined by analyzing Δλ, as in [9] for the adsorption of iodine and chlorine on Cu(111). The N indicates that this is the total surface dipole moment of N atoms adsorbed in the unit cell. The dipole moment change due to the adsorption process can be calculated by integration of $\Delta\lambda_N(z) = N\Delta\lambda(z)$ along the z direction, perpendicular to the surface,

$$\Delta\mu_N = -\int_{\text{bulk}}^{\text{vac}} z\Delta\lambda_N(z)\, dz \qquad (3)$$

where the negative sign is introduced because positive regions of $\Delta\lambda_N$ (i.e., electron buildup) are in fact negatively charged. The integration runs from the central layer of the platinum slab

to the middle of the vacuum. Figure 4 shows the good correlation between the calculated work function and the dipole moment derived from the charge distribution, which verifies the assumptions that underlie Equation 3.

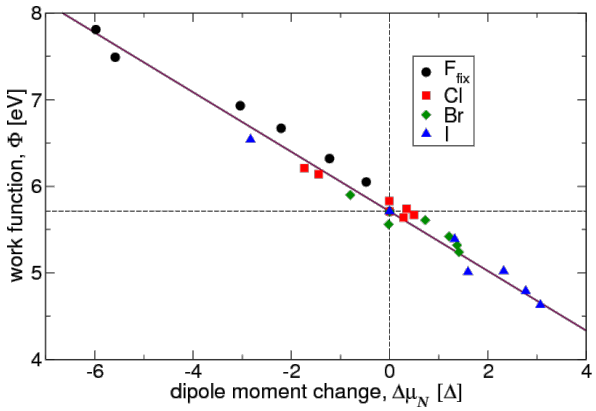

Figure 4: Calculated work function versus dipole moment. The solid line corresponds to the expectation according to Equation 1.

Since Δλ of the fluorine-covered platinum slab shows for all coverage values the structure of an electron buildup far from the surface, followed by an electron depletion close to the surface, the dipole moment on each face of the slab becomes more negative as a function of the coverage, which is consistent with a work function increase. For the other three halogens, the electron density difference profile looks more complicated. There is an electron depletion far from the surface, followed by an electron buildup. This structure is sufficiently strong to invert the dipole moment, so that $\Delta\mu_N$ changes sign as a function of the coverage.

It has been suggested that adsorbates that are located rather close to a surface can decrease the electron spillout at the surface. This can cause unexpected changes of the work function, such as the decrease of the work function observed for N on the W(100) surface [8] or the small dipole moment for O on Al(111) [22]. However, the area of electron depletion for chlorine, bromine and iodine is approximately 2.5–4.0 Å away from the center of the topmost platinum atoms, far beyond the region of a sizable electron spillout for the uncovered surface. This electron density shift rather corresponds to a redistribution of the electron density in the adatom layer, which can be associated with a covalent character of the chemisorption bond. This rearrangement is particularly strong for the adsorption of iodine, and slightly weaker for bromine and chlorine. The character of the chemisorption bond between iodine and platinum was discussed in the past [10,17] and conflicting results in terms of the charge of the adatom were presented. In this study, we find that the charge buildup between the iodine and the Pt surface indicates the presence of a covalent bond. Similar conclusions have been found, for example for the adsorption of I on Cu [9] or Cl on Au [14]. Furthermore, in a chronocoulometric study [38] it was found that the adsorbed species is basically a neutral chlorine atom which agrees nicely with our findings. Fluorine, on the other hand, tends to adsorb to the Pt(111) surface mainly in the ionic form.

Coverage trends

Our calculations confirm the experimental observations [18-20] of a work function minimum as a function of the halogen coverage. Several mechanisms have been proposed to explain its occurrence. For cationic adsorbates, the subsequent increase of Φ beyond the work function minimum was attributed to a reduction of the ionicity of the cationic adsorbate [39]. This explanation, however, does not apply to the halogen adsorption considered here as we still find no indication of cationic adsorption.

The work function minimum has also been explained through differences in site occupancies that occur as halogen coverage increases. Subsurface penetration followed by surface adsorption was one of the possibilities considered in explaining the work function minimum for chlorine on platinum [18]. This was based on the assumption that subsurface penetration and surface adsorption lead to opposite dipole moments at the surface. In contrast, for iodine on platinum, an adsorption site effect was suggested under the assumption that threefold-site adsorption decreases the work function, while adding iodine to top sites increases it [20]. As the coverage increases, more top sites get occupied by iodine, which leads to the increase in Φ beyond the minimum. Still, the change of the surface work function remained negative over the entire coverage range that was considered.

A more recent computational study has shown that the adsorption of isolated iodine atoms at the hollow or top sites both lead to $\Delta\Phi < 0$, although the decrease in the work function is larger for the adsorption of iodine at the hollow site [17]. Another explanation for the minimum of the work function was proposed, namely changes in the polarization of the metal substrate. The authors found that the polarization in the platinum substrate that is induced by the presence of the iodine anion adsorbate is reduced with increasing coverage, hence explaining the non-monotonic behavior in ΔΦ.

While changing site occupancy with increasing coverage can and will lead to observable changes in the work function, in this study we focus on changes of the work function that are caused by effects that are primarily electronic in nature, i.e., that are not due to changes in the adsorption or absorption site. Hence a

deeper analysis of charge transfer, internal redistribution of charge in the metal substrate, and redistribution of charge on the halogen adatoms is needed. To analyze the surface dipole moments in detail, we use the total surface dipole moment per unit cell normalized to the number of adatoms to define the dipole moment change created per adsorbed atom,

$$\Delta\mu_{\mathrm{q}} = -\bar{z}_{\mathrm{X}} \int_{z_{\mathrm{q}}}^{\mathrm{vac}} \Delta\lambda(z)dz\,, \tag{4}$$

The normalized dipole moments are shown in Figure 5. The plots are nowhere flat, suggesting the presence of considerable neighboring adatom interactions even at the lowest coverages. There is also a clear tendency for the dipole moment induced by the adsorption of a single halogen atom to be reduced as the concentration of adatoms increases at the Pt surface. Note that the 0.5 ML coverage of iodine is so closely packed that the repulsion of the electron shells induces a two-layer structure of the adsorbate layer. Every second iodine atom becomes a part of a second adsorbate layer, which is positioned about 1.7 Å farther from the surface than the first layer of iodine atoms.

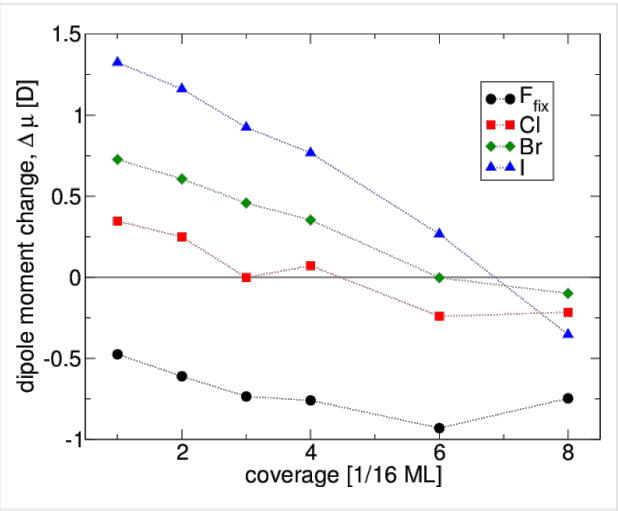

Figure 5: Calculated normalized dipole moment as a function of the coverage of fluorine, chlorine, bromine and iodine on Pt(111).

Looking at the charge transfer as a function of the coverage is useful to understand the negative slopes of Δμ for the adsorption of halogens. Quantifying charge transfer between atoms however always involves a more or less ambivalent choice as far as associating the electron density to a particular atom is concerned. We have therefore considered two limits: a maximum-charge-transfer picture, and a zero-charge-transfer picture of halogen adsorption on platinum.

The maximum charge transfer is obtained by assuming that the complete electron buildup between an adatom and the surface is always counted to the adsorbate. In practice, this is done by determining the plane $z = z_q$ between the metal and the adatom that maximizes the area under $\Delta\lambda(z)$ at the halogen side. The charge transfer from the metal surface to the adatoms gives rise to a change of the dipole moment, $\Delta\mu_{\mathrm{q}}$. By using a simple model that assumes charge transfer from the topmost Pt layer to the halogen adlayer, the contribution of the electron transfer to the surface dipole moment can be quantified,

$$\Delta\mu_{\mathrm{q}} = -\bar{z}_{\mathrm{X}} \int_{z_{\mathrm{q}}}^{\mathrm{vac}} \Delta\lambda(z)dz\,, \tag{5}$$

where $\bar{z}_{\mathrm{X}}$ is the average distance of the halogen adatoms from the metal surface. We combine all other parts contributing to the total dipole moment in the term $\Delta\mu_{\mathrm{pol}}$, because it involves polarization effects in the metal and in the adlayer. The combination of both contributions leads to the total dipole moment change,

$$\Delta\mu = \Delta\mu_{\mathrm{q}} + \Delta\mu_{\mathrm{pol}}\,. \tag{6}$$

These contributions are plotted in Figure 6a and Figure 6b, respectively. The effect of the charge transfer $\Delta\mu_{\mathrm{q}}$ to the surface dipole is nearly zero for iodine. For fluorine, however, charge transfer plays a significant role, which can be expected since it is more electronegative than the other halogens, as also reported by Migani et al. [10]. Moreover, the negative dipole moment change for the adsorption of fluorine decreases even more with increasing coverage, which is due to the fact that the adsorption distance and charge transfer to the F adatoms increase with increasing coverage.

The results also suggest that higher surface concentrations of adatoms decrease the dipole moment change per adatom through mutual depolarization. This effect is most pronounced for iodine, as well as for a low-coverage adsorption of bromine and chlorine, but not for fluorine because of the low polarizability of small atoms. Besides the repulsion of the dipoles, the electron shells of adsorbed atoms at a higher coverage start to repel.

Another interesting question concerns the importance of the electron density oscillations in the subsurface, as shown in Figure 3. It might be speculated that these oscillations could be responsible for the significant polarization part, $\Delta\mu_{\mathrm{pol}}$, of the total dipole moment Δμ. To answer this question, we have divided Δλ into two parts, one representing the dipole moment change due to polarization in the adsorbate layer and the other part representing the dipole moment change due to polarization in the substrate,

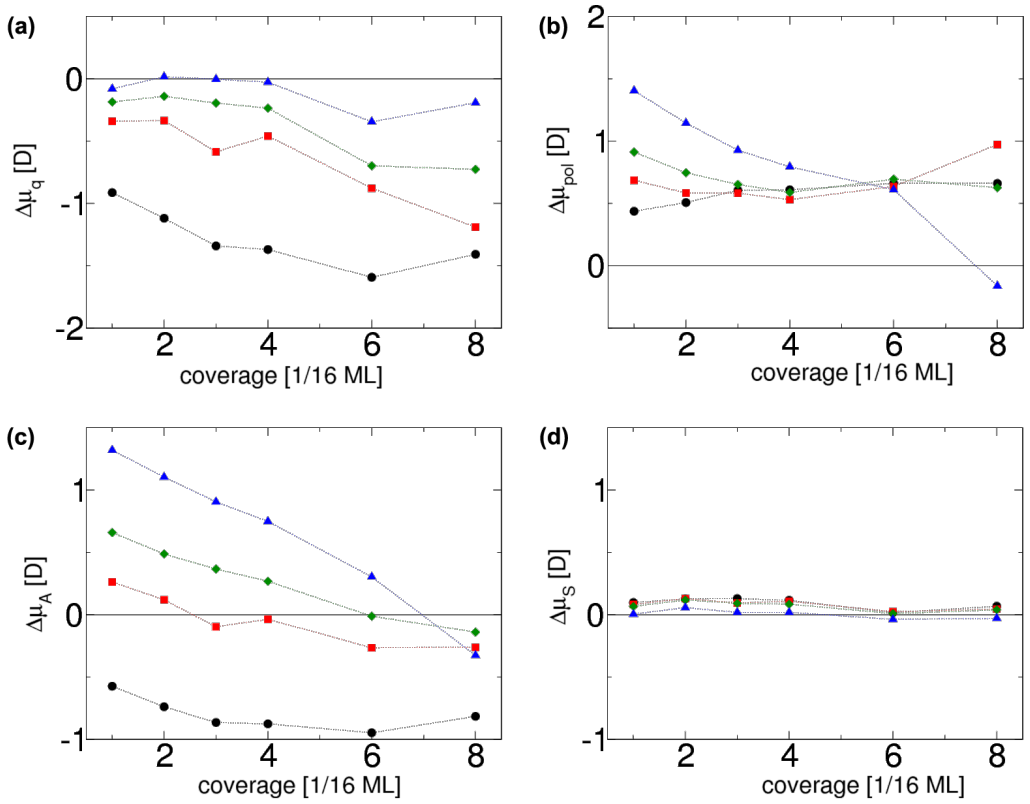

Figure 6: Contributions to the total dipole moment change $\Delta\mu$ according to Equation 6 and Equation 7 as a function of halogen coverage. The term $\Delta\mu_q$ describes the purely charge transfer induced dipole moment and $\Delta\mu_{pol}$ the polarization induced dipole moment; $\Delta\mu_A$ shows the effect of the adsorbate layer on the total dipole moment and $\Delta\mu_S$ indicates substrate effects. The color code denoting the different halogen atoms is the same as used in the previous figures.

$$\Delta\mu = \Delta\mu_A + \Delta\mu_S \,. \tag{7}$$

This zero-charge transfer picture for breaking down polarization is especially effective for iodine adsorption on platinum. Such a distinction between pure substrate and adsorbate contributions is again an arbitrary choice. In order to obtain trends, the integration was started from the point z_0, at which the unit cell is divided exactly into the charge neutral part of the adlayer and the charge neutral part of the platinum slab, defined by the condition

$$\int_{z_0}^{\text{vac}} \Delta\lambda(z)\,dz = 0 \,. \tag{8}$$

For this choice, the analogous integral on the metal side is also zero due to the overall charge neutrality of the supercell. It is then possible to estimate the surface dipole moment μ_S and the adsorbate dipole moment μ_A by using

$$\Delta\mu_S = \int_{\text{bulk}}^{z_0} z\Delta\lambda(z)\,dz \tag{9}$$

and

$$\Delta\mu_A = \int_{z_0}^{\text{vac}} z\Delta\lambda(z)\,dz \,. \tag{10}$$

We briefly summarize the difference in the integration limits z_q and z_0 of Equation 5 and Equation 9, respectively: These equations have the purpose of dividing the unit cell into two parts, but it is not clear where exactly the adatom ends and where the platinum begins or vice versa. The two integration limits mark special points in the graph of $\Delta\lambda$. The limit z_q divides the unit cell at the point of maximum charge at the adatom, in contrast to z_0 which divides at the point of zero charge at the adatom.

The adsorbate and the substrate dipole moments, which are plotted in Figure 6c and Figure 6d, respectively, indicate that the contribution of the change of the metal substrate dipole moment $\Delta\mu_S$ to the total change of the dipole moment $\Delta\mu$ is minor compared with the impact of adsorbate polarization $\Delta\mu_A$, which affects the total dipole moment change quite dramatically. This also means that our analysis does not support the

view [17] that substrate polarization plays an important role in explaining the halogen-induced work function decrease.

Additionally, it is noticeable that the decrease in the total change of the dipole moment in the case of iodine and chlorine at around 0.25 ML is much more significant on platinum compared with the total change of the dipole moment of copper [9]. The work function of the copper surface is about 1 eV smaller, thus the charge transfer is larger from copper than from the platinum surface to the halogen adatom. It is for this reason that the adsorption of chlorine on copper does not exhibit a work function minimum with increasing adsorption coverage [9,40], similar to the work function plot of F on Pt in the current study.

Fluorine on calcium

We have shown that the strong polarizability of large atoms such as iodine leads to a considerable buildup of charge in the adatom–surface bonding regions, which is consistent with covalent bonding, and an accompanying electron depletion region far from the surface which creates a net dipole on the adatom that in turn promotes a decrease in the work function. Here we show that the adsorption of fluorine can also decrease the work function of a metal surface, namely calcium, but through a different mechanism. Calcium is considered to be an attractive electrode material in electrochemical energy storage because of its low electronegativity, earth abundance, and low cost [41]. Fluorine adsorbs stably at a threefold hollow site on calcium, which is a metal with fcc structure and a calculated lattice constant that is 39% larger than that of platinum. At its equilibrium adsorption position, fluorine is only 0.73 Å from the topmost layer of Ca atoms. In contrast, iodine adsorbs 2.07 Å from the platinum surface.

In Figure 7, we compare two systems, in which halogen adsorption decreases the work function of the metal substrate. The left panel shows the adsorption of iodine on Pt(111) at a coverage of 1/9 ML. The right panel shows fluorine adsorption on Ca(111) at a coverage of 1/4 ML. This yields similar absolute values for the coverage per area for the two systems given the stark difference between the lattice constants of Pt and Ca. At these adsorption coverages, iodine reduces the platinum work function by 0.79 eV, while fluorine reduces the calcium work function by 0.20 eV.

Figure 7 shows that halogen adsorption can create a surface dipole that reduces the work function in two very distinct mechanisms, namely adatom polarization and spillout depletion. Iodine on platinum is characterized by a negligible charge transfer, covalent bonding, and polarization on the adatom. There is no evidence for a dominantly ionic bond for I/Pt(111)

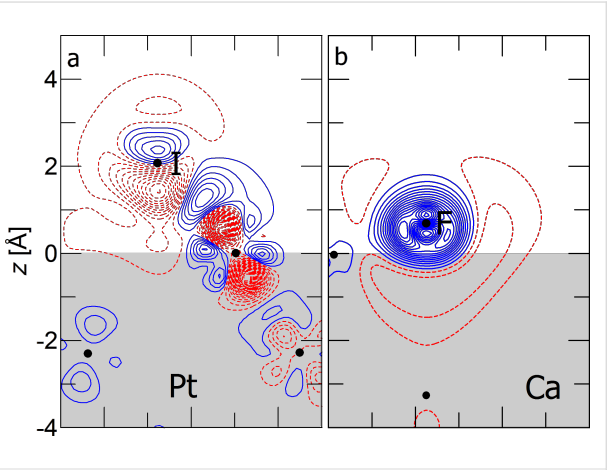

Figure 7: Cross sections of electron density difference $\rho_{diff}(\mathbf{r})$ at the surface. Solid-blue (dashed-red) contours denote regions of electron buildup (depletion). The interval between contours of constant electron density is 0.01 electrons/Å^3. The region of the metal slab is shaded gray as a visual aid.

reported in [17]. Fluorine adsorption on calcium on the other hand is characterized by a large charge transfer to the adatom with negligible polarization, creating a system, which is comprised of a negative ion enveloped by electron depletion. Since fluorine is adsorbed very close to the surface, it is embedded within the electron spillout region of calcium. The depletion of electron density in the spillout region not only reduces the effect of the strongly negative fluorine on the net dipole, but even overcompensates it, resulting in a decrease of the work function.

Conclusion

The change of the work function induced by halogen adsorption on Pt(111) as a function of the coverage was studied by electronic structure calculations. In general, because of their electronegativity, the adsorption of halogens is associated with a charge transfer from the metal substrate to the adsorbate layer. In the case of fluorine adsorption, this leads to the expected increase in the work function. However, for chlorine, bromine and iodine adsorption on Pt(111), the charge transfer effect is overcompensated by a significant polarization of the adsorbate, causing a work function decrease. The decreasing change of the dipole moment per adatom with an increasing adsorption coverage leads to a maximum in the total surface dipole moment and a minimum in the work function at a coverage of approximately 0.25 ML. The mutual depolarization within the adsorbate layer contributes to the eventual work function increase.

The anomalous work function change on platinum is large because of the high work function of clean platinum, which favors only a small electron transfer to the halogen adatoms

compared with other metals. Therefore, polarization effects that reverse the dipole moment attributed to charge transfer are more pronounced than on metals with smaller work functions such as copper.

Furthermore, we showed that fluorine adsorption can also lead to an anomalous work function decrease, but through a different mechanism. On calcium, fluorine is adsorbed close to the surface because of the large spacing between the calcium atoms. This causes a depletion of the electron density in the spillout region, which results in a decrease of the work function.

Acknowledgements

This research has been supported by the German Science Foundation (DFG) through the research unit FOR 1376 (DFG contract GR 1503/21-1). Computer time has been provided by the BW-Grid of the federal state of Baden-Württemberg and by a computer cluster financed through the stimulus programme "Electrochemistry for Electromobility" of the German Ministry of Education and Science (BMBF).

References

1. Kolb, D. M. *Surf. Sci.* **2002,** *500,* 722–740. doi:10.1016/S0039-6028(01)01583-7
2. Quaino, P.; Luque, N. B.; Soldano, G.; Nazmutdinov, R.; Santos, E.; Roman, T.; Lundin, A.; Groß, A.; Schmickler, W. *Electrochim. Acta* **2013,** *105,* 248–253. doi:10.1016/j.electacta.2013.04.084
3. Schnur, S.; Groß, A. *Catal. Today* **2011,** *165,* 129–137. doi:10.1016/j.cattod.2010.11.071
4. Roman, T.; Groß, A. *Catal. Today* **2013,** *202,* 183–190. doi:10.1016/j.cattod.2012.06.001
5. Trasatti, S. *Pure Appl. Chem.* **1986,** *58,* 955–966. doi:10.1351/pac198658070955
6. Groß, A. *Surf. Sci.* **2013,** *608,* 249–254. doi:10.1016/j.susc.2012.10.015
7. Tripkovic, D. V.; Strmcnik, D.; van der Vliet, D.; Stamenkovic, V.; Markovic, N. M. *Faraday Discuss.* **2009,** *140,* 25–40. doi:10.1039/B803714K
8. Michaelides, A.; Hu, P.; Lee, M.-H.; Alavi, A.; King, D. A. *Phys. Rev. Lett.* **2003,** *90,* 246103. doi:10.1103/PhysRevLett.90.246103
9. Roman, T.; Groß, A. *Phys. Rev. Lett.* **2013,** *110,* 156804. doi:10.1103/PhysRevLett.110.156804
10. Migani, A.; Illas, F. *J. Phys. Chem. B* **2006,** *110,* 11894–11906. doi:10.1021/jp060400u
11. Migani, A.; Sousa, C.; Illas, F. *Surf. Sci.* **2005,** *574,* 297–305. doi:10.1016/j.susc.2004.10.041
12. Leung, T. C.; Kao, C. L.; Su, W. S.; Feng, Y. J.; Chan, C. T. *Phys. Rev. B* **2003,** *68,* 195408. doi:10.1103/PhysRevB.68.195408
13. Pašti, I. A.; Mentus, S. V. *Electrochim. Acta* **2010,** *55,* 1995–2003. doi:10.1016/j.electacta.2009.11.021
14. Baker, T. A.; Friend, C. M.; Kaxiras, E. *J. Am. Chem. Soc.* **2008,** *130,* 3720–3721. doi:10.1021/ja7109234
15. Bagus, P. S.; Staemmler, V.; Wöll, C. *Phys. Rev. Lett.* **2002,** *89,* 096104. doi:10.1103/PhysRevLett.89.096104
16. Bagus, P. S.; Käfer, D.; Witte, G.; Wöll, C. *Phys. Rev. Lett.* **2008,** *100,* 126101. doi:10.1103/PhysRevLett.100.126101
17. Bagus, P. S.; Wöll, C.; Wieckowski, A. *Surf. Sci.* **2009,** *603,* 273–283. doi:10.1016/j.susc.2008.11.021
18. Erley, W. *Surf. Sci.* **1980,** *94,* 281–292. doi:10.1016/0039-6028(80)90007-2
19. Bertel, E.; Schwaha, K.; Netzer, F. P. *Surf. Sci.* **1979,** *83,* 439–452. doi:10.1016/0039-6028(79)90055-4
20. Jo, S. K.; White, J. M. *Surf. Sci.* **1992,** *261,* 111–117. doi:10.1016/0039-6028(92)90222-R
21. Hansen, H. A.; Man, I. C.; Studt, F.; Abild-Pedersen, F.; Bligaard, T.; Rossmeisl, J. *Phys. Chem. Chem. Phys.* **2010,** *12,* 283–290. doi:10.1039/B917459A
22. Lang, N. D. *Surf. Sci.* **1983,** *127,* L118–L122. doi:10.1016/0039-6028(83)90409-0
23. Perdew, J. P.; Burke, K.; Ernzerhof, M. *Phys. Rev. Lett.* **1996,** *77,* 3865–3868. doi:10.1103/PhysRevLett.77.3865
24. Paier, J.; Hirschl, R.; Marsman, M.; Kresse, G. *J. Chem. Phys.* **2005,** *122,* 234102. doi:10.1063/1.1926272
25. Hammer, B.; Hansen, L. B.; Nørskov, J. K. *Phys. Rev. B* **1999,** *59,* 7413–7421. doi:10.1103/PhysRevB.59.7413
26. Lischka, M.; Groß, A. *Phys. Rev. B* **2002,** *65,* 075420. doi:10.1103/PhysRevB.65.075420
27. Stroppa, A.; Kresse, G. *New J. Phys.* **2008,** *10,* 063020. doi:10.1088/1367-2630/10/6/063020
28. Kresse, G.; Joubert, D. *Phys. Rev. B* **1999,** *59,* 1758–1775. doi:10.1103/PhysRevB.59.1758
29. Kittel, C. *Introduction to Solid State Physics,* 7th ed.; John Wiley & Sons, 1996.
30. Ignaczak, A.; Gomes, J. A. N. F. *J. Electroanal. Chem.* **1997,** *420,* 71–78. doi:10.1016/S0022-0728(96)04815-2
31. Collins, D. M.; Spicer, W. E. *Surf. Sci.* **1977,** *69,* 114–132. doi:10.1016/0039-6028(77)90164-9
32. Fisher, G. B. *Chem. Phys. Lett.* **1981,** *79,* 452–458. doi:10.1016/0009-2614(81)85013-0
33. Nieuwenhuys, B. E.; Sachtler, W. M. H. *Surf. Sci.* **1973,** *34,* 317–336. doi:10.1016/0039-6028(73)90121-0
34. Nieuwenhuys, B. E.; Meijer, D. T.; Sachtler, W. M. H. *Phys. Status Solidi A* **1974,** *24,* 115–122. doi:10.1002/pssa.2210240108
35. Nieuwenhuys, B. E. *Surf. Sci.* **1976,** *59,* 430–446. doi:10.1016/0039-6028(76)90027-3
36. Salmerón, M.; Ferrer, S.; Jazzar, M.; Somorjai, G. A. *Phys. Rev. B* **1983,** *28,* 6758–6765. doi:10.1103/PhysRevB.28.6758
37. Derry, G. N.; Ji-Zhong, Z. *Phys. Rev. B* **1989,** *39,* 1940–1941. doi:10.1103/PhysRevB.39.1940
38. Garcia-Araez, N.; Climent, V.; Herrero, E.; Feliu, J.; Lipkowski, J. *J. Electroanal. Chem.* **2005,** *576,* 33–41. doi:10.1016/j.jelechem.2004.10.003
39. Bonzel, H. P. *Surf. Sci. Rep.* **1988,** *8,* 43–125. doi:10.1016/0167-5729(88)90007-6
40. Peljhan, S.; Kokalj, A. *J. Phys. Chem. C* **2009,** *113,* 14363–14376. doi:10.1021/jp902273k
41. Kim, H.; Boysen, D. A.; Ouchi, T.; Sadoway, D. R. *J. Power Sources* **2013,** *241,* 239–248. doi:10.1016/j.jpowsour.2013.04.052

E.2 Publication in chapter 4.2

The following article is used in chapter 4.2, it is reprinted and adapted from T. Roman, F. Gossenberger, K. Forster-Tonigold, and A. Gross, Phys. Chem. Chem. Phys. 16 (2014), 13630-13634, with the permission from Physical Chemistry Chemical Physics.

PCCP

PAPER

View Article Online
View Journal | View Issue

Halide adsorption on close-packed metal electrodes

Cite this: *Phys. Chem. Chem. Phys.*, 2014, **16**, 13630

Tanglaw Roman,*[a] Florian Gossenberger,[a] Katrin Forster-Tonigold[ab] and Axel Groß[ab]

Received 16th January 2014,
Accepted 24th February 2014

DOI: 10.1039/c4cp00237g

www.rsc.org/pccp

Two mechanisms have been cited as the reason for unexpected work function decrease upon adsorption of electronegative adatoms: electron spillout depletion [Michaelides *et al.*, *Phys. Rev. Lett.*, 2003, **90**, 246103] and polarization of the adatom [Roman *et al.*, *Phys. Rev. Lett.*, 2013, **110**, 156804]. We attempt to bridge the two pictures in this work. Work function changes due to the adsorption of halides on (111) surfaces of fcc metals (Ca, Sr, Ni, Pd, Pt, Cu, Ag, Au, Al and Pb) were studied using periodic density functional theory. The two mechanisms were found to be clearly independent of each other because of the opposite factors that lead to the work function decrease, and are therefore easy to distinguish. A more general picture of interpreting bond ionicity based on observed work function changes is discussed.

1 Introduction

Electrochemical processes typically occur at the interface between an electron conductor, the electrode, and an ion conductor, the electrolyte.[1] Therefore the structure of the electrode/electrolyte interface is of strong interest in electrochemistry. At this interface, an electric double layer is formed, consisting of an electronic charge on the electrode and a corresponding ionic counter charge in the electrolyte. Of particular importance is the adsorption of anions on metal electrodes.[2,3] Often they adsorb specifically, *i.e.*, they form chemical bonds with the metal surface. These adsorbed anions not only affect the chemical properties of electrodes,[4] but in general they also change the work function of the electrode, which is directly related to the electrode potential.[5]

As part of a systematic effort to model electrode/electrolyte interfaces using first-principles,[6–9] we have recently addressed the work function change induced by the adsorption of halides on Cu(111)[10] and on Pt(111) and Ca(111).[11] Cu and Pt are metals well-studied in electrochemistry,[12,13] whereas calcium is considered to be an attractive electrode material in electrochemical energy storage because of its low electronegativity, earth abundance, and low cost.[14] The equilibrium coverage of halides as a function of the electrode potential using a simple thermodynamical model was also investigated.[15,16]

An adsorbed halogen layer is expected to produce an observable increase in the work function Φ of the metal surface since electrons, on leaving the metal surface, will have to pass through the resulting interface dipole layer comprised of a positively-charged metal substrate and a negatively-charged halogen layer. However, it has already been observed experimentally[17–19] as well as theoretically[20–22] that the adsorption of chlorine, bromine and iodine on metal surfaces can lead to an unexpected decrease of the work function.

In our previous work,[10,11] we have identified two different mechanisms that can explain the unexpected negative work function change if a halogen is adsorbed on a metal substrate: polarization of the adatom,[10] and reduction in the surface spillout electron density.[11,23] In the former mechanism, the strong polarizability of large atoms like iodine leads to a considerable charge accumulation in the adatom–surface bonding regions, consistent with covalent bonding, and an accompanying charge depletion region far from the surface. This creates a dipole on the adatom that in turn promotes a decrease in the work function. Fluorine adsorption on calcium, on the other hand, is characterized by a large charge transfer to the adatom with negligible polarization, creating a system comprised of a negative ion enveloped by an electron density depletion region. Since fluorine is adsorbed very close (*ca.* 0.7 Å) to the surface, it is embedded within the electron spillout region of calcium. The depletion of electron density in the spillout region not only reduces the effect of the negatively-charged fluorine on the overall dipole, but overcompensates it, resulting in a work function decrease.

A complete picture of the factors leading to a decrease in the work function is however still missing. It is for instance not

[a] *Institute of Theoretical Chemistry, Ulm University, 89069 Ulm, Germany. E-mail: tanglaw.roman@uni-ulm.de; Fax: +49 (0)731 50 22819; Tel: +49 (0)731 50 22817*
[b] *Helmholtz Institute Ulm (HIU) Electrochemical Energy Storage, 89069 Ulm, Germany*

clear as to which particular circumstances would make one specific mechanism dominant, or perhaps in which situations would these two independent mechanisms contribute on an equal footing to the decrease in the work function. In the present study we have therefore extended our previous work by systematically studying the adsorption properties of halogens at (111) surfaces of several fcc metals (Ca, Sr, Ni, Pd, Pt, Cu, Ag, Au, Al, and Pb). We will show that halogen atoms can lower the work function on most of the considered metals, and we will discuss the mechanisms leading to this still unexpected work function decrease.

2 Computational details

Periodic DFT calculations that employ the exchange–correlation functional of Perdew, Burke, and Ernzerhof (PBE)[24] were done using the Vienna *ab initio* simulation package (VASP).[25] Electron–core interactions were accounted for by the projector augmented wave method.[26,27] The electronic one-particle wavefunctions were expanded in a plane-wave basis set up to an energy cutoff of 500 eV. The metal substrates were represented by slabs of seven atomic layers, of which the inner three layers were kept fixed in the bulk position during geometry optimizations while the rest of the system was allowed to relax. Halogen atoms were placed symmetrically on both sides of the slab.

For these systems, it is possible to quantify work function changes brought about by adatoms through two methods: straightforwardly from the local potential of electrons, and from the dipole moment (multiplied by a factor $-e/\varepsilon_0$) based on changes in electronic density. We have already shown and discussed in detail that these two methods lead to in principle identical findings.[11] In this study we use only the former, in which the work function is obtained from the difference between the Fermi energy and the average local potential of electrons in the vacuum, where the potential does not change anymore with increasing distance from the surface.

The coverage has a strong impact on the work function change.[10,11] Since the various fcc metals studied span a broad range of lattice constants, the absolute coverage (adatoms per unit area) and not the relative coverage per surface atom has to be similar in order to allow a fair comparison among the different substrates. The coverages used within this study are shown in Table 1. For the integration over the first Brillouin zone we used a mesh of 5 × 5 × 1 special *k*-points[28] with a Methfessel–Paxton smearing[29] of 0.1 eV.

Table 1 Computed lattice constants *a*, work function Φ of the clean (111) surface, and halogen relative and absolute coverages (Θ_{rel} and Θ_{abs}, respectively) on (111) surfaces of fcc metals used in this study

	a (Å)	Φ (eV)	Θ_{rel} (ML)	Θ_{abs} (1/Å^2)
Ni	3.524	5.03	1/9	2.067×10^{-2}
Cu	3.636	4.77	1/9	1.941×10^{-2}
Pd	3.964	5.23	1/9	1.633×10^{-2}
Pt	3.978	5.71	1/9	1.622×10^{-2}
Al	4.051	4.04	1/9	1.564×10^{-2}
Ag	4.164	4.35	1/9	1.480×10^{-2}
Au	4.174	5.07	1/9	1.473×10^{-2}
Pb	5.040	3.69	1/4	2.273×10^{-2}
Ca	5.531	2.96	1/4	1.887×10^{-2}
Sr	6.030	2.59	1/4	1.588×10^{-2}

3 Results and discussion

The differences in the energies between fcc and hcp hollow site-adsorption of halogens on fcc metals are shown in Fig. 1. Aluminum is not included here because of its unique preference for top-site adsorption. The top position is also the most stable in the case of F/Pt(111). Halogens mostly favor fcc hollow site adsorption on the transition metals, whereas adsorption on the hcp hollow site is more favored on the alkaline earth metals. The copper group of coinage metals (Cu, Ag, and Au) shows the least absolute difference between fcc and hcp adsorption, which implies that the occupancies of hcp and fcc sites are similarly probable. The energetic difference between the adsorption energies on the two threefold-hollow sites decreases with increasing adatom size, *i.e.* fluorine discriminates between the hcp and fcc sites more strongly than iodine. Also, the figure shows that fcc metals with higher work functions generally have more stable fcc-site adsorption of halogens. There is no simple explanation for these trends.

Adsorption energies of halogen atoms with respect to the free halogen molecule are shown in Fig. 2. Most metals interact strongly with F and more weakly with Cl, Br and the least with I. However, Pd, Pt and Au do not follow this trend, which can be rationalized as a transition from predominantly ionic bonding to predominantly covalent bonding. Surfaces with low work functions such as Ca and Sr easily transfer electronic charge to electronegative adsorbates such as halogen atoms, resulting in a more ionic bonding situation. Hence the more electronegative (*i.e.*, smaller) halogen atoms exhibit the strongest bonding. On the other hand, surfaces such as Pt, Pd and Au which have large work functions exhibit a smaller charge transfer to electronegative adsorbates so that the bonding becomes mostly covalent in nature, as we have already shown.[10,11] And here

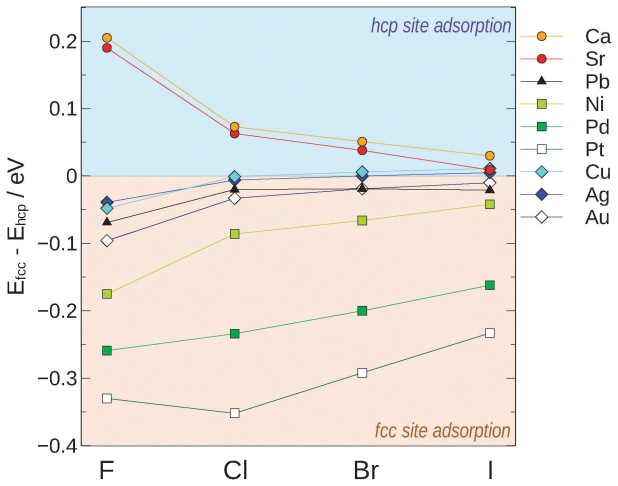

Fig. 1 Relative stability of fcc-site adsorption compared with hcp-site adsorption.

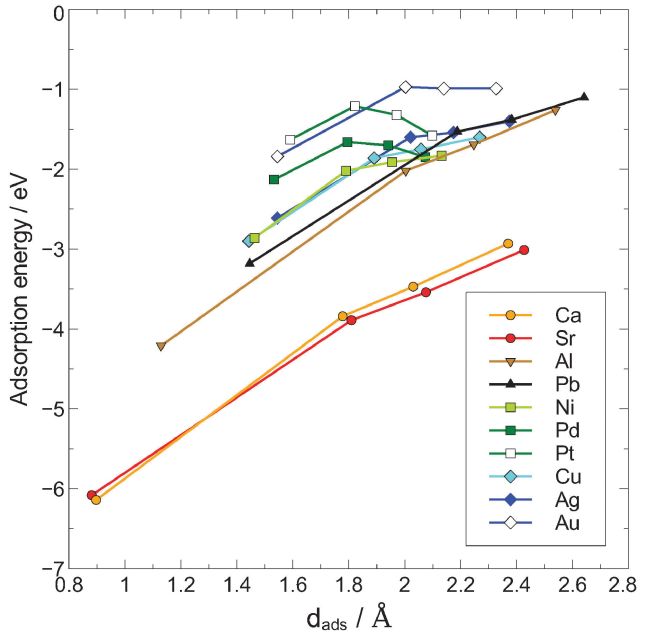

Fig. 2 Adsorption energies of halogens on the (111) surface of different fcc metals as a function of the adsorption distance of the halogen to the surface. The four data points shown for each substrate correspond to the adsorption of F (smallest adsorption distances), Cl, Br and I (with increasing adsorption distance, respectively).

the more polarizable (*i.e.*, larger) halogen atoms then bind most strongly.

In Fig. 3 the work function changes due to the adsorption of halogen atoms on different fcc metal surfaces is shown as a function of the adsorption distance d_{ads} of the halogen atom to the surface. From the knowledge that halogens mostly prefer fcc-site adsorption, we have used the fcc adsorption site for all metals in order to calculate comparable work function changes. We note that adsorption on a substrate with a larger lattice constant does not necessarily mean that the adatom will adsorb more closely to the surface. This is visible for iodine adsorption on Ca, Sr and Pb, in contrast to Pt, Pd and Ni. Strong covalent bonding on the nickel group of elements leads to this trend.

We find rather short adsorption distances for a fluorine atom adsorbing on Ca(111), Sr(111) and Al(111). The work function change in these systems is negative due to a reduction of the electron spillout of the metal. On the other hand, the larger adsorption distances of Cl, Br and I lead to the expected increase of the work function, in accordance with the jellium model. They adsorb at distances that are larger than a certain critical distance that determines whether a negative work function change due to a reduction of the electron spillout occurs. The critical distance is the distance at which the work function change is zero in Fig. 4. The metal atoms were fixed at the structure of the clean surface in these calculations. This figure excludes the work function change curve on nickel because of challenges in correctly describing the spin-polarized electronic structure of the adsorption energy minimum.

Depending on the nature of the metallic substrate, a weaker or stronger polarization of the halogen atom occurs. On surfaces with low work functions (*i.e.*, alkaline earth metals), the work function change increases with increasing adatom size because a larger halogen–metal separation increases the magnitude of the dipole moment associated with the negative charge on the halogen and positive charge on the surface. On the other hand, for surfaces with large work functions (*i.e.*, transition metals), the work function decreases with increasing adatom size because larger atoms have lower electronegativities and are more polarizable.

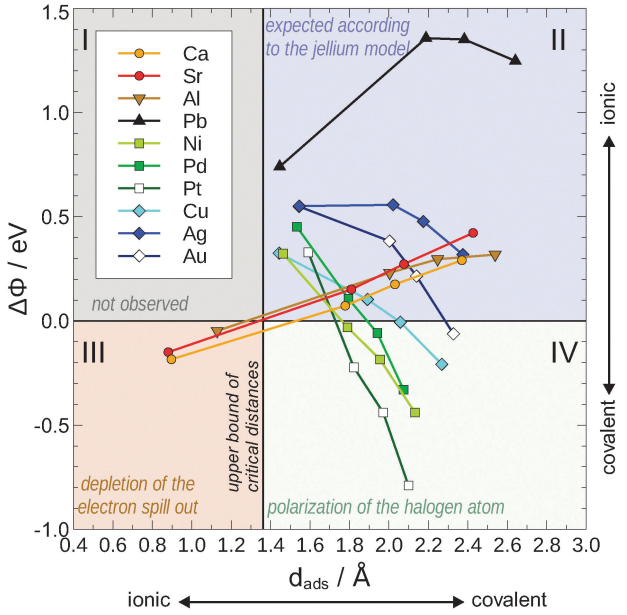

Fig. 3 Work function changes due to the adsorption of halogens on the (111) surface of different fcc metals as a function of the adsorption distance. The four data points shown for each substrate correspond to the adsorption of F (smallest adsorption distances), Cl, Br and I (with increasing adsorption distance, respectively).

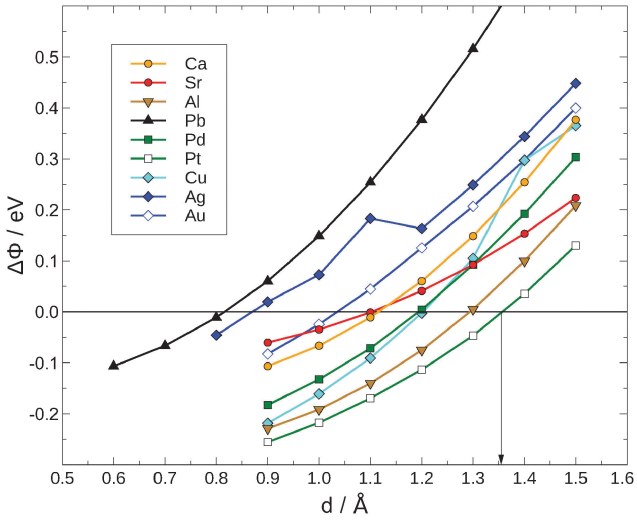

Fig. 4 Determination of the critical distance: it is defined as the distance of a fluorine atom to the surface at which the work function of the metal surface does not change due to the presence of the adatoms. The upper bound of critical distances is indicated by the arrow.

Now while the work function change increases monotonously for halogens adsorbed on Ca(111), and decreases monotonously on Pt(111), there is a kink in the plot of work function change for halogens adsorbed on Pb(111): while the adsorption of Cl leads to a larger work function change than the adsorption of F, the adsorption of I induces a lower work function change than Cl. Such a trend can be interpreted as the result of the two opposing mechanisms acting on an equal footing.

Based on an analysis of how the electron distribution rearranges because of the adsorption, a correlation between the observed change in the work function, the adsorption distance, and the bonding mechanism is summarized in Fig. 3. Systems that fall under quadrants II and III of Fig. 3 show dominantly ionic bonding, while all dominantly covalent systems lie in quadrant IV.

The adsorption of iodine decreases the work function of clean Pt by 0.79 eV, while chlorine increases the work function of Pb(111) by 1.36 eV. This contrast emphasizes how starkly different the effects of halogen adsorption are on the work function of metals. The adsorption of iodine on platinum yields the largest decrease in the work function because Pt has the largest work function among the fcc metals considered, and I has the lowest electronegativity. Ionic bonding is hence weak. Calcium on the other hand has the lowest work function, and F has the highest electronegativity among the halogens, and so one can expect that the adsorption of fluorine on calcium should give the strongest work function increase. This is however not seen due to the fact that F adsorbs within the metal's electron spillout region. The work function of Pb is lower compared with the transition metals, and Cl has a high electronegativity. Thus one can expect the Cl–Pb bond to have a strong ionic character. The Cl–Pb bond is much longer compared to the F–Ca bond, and so the adatom is outside the spillout region of Pb. This therefore leads to a large work function increase.

Furthermore, a more strongly charged atom that is adsorbed/absorbed into a metal induces a stronger screening charge surrounding it. It is then no surprise that fluorine, the most electronegative element, adsorbs on calcium with an accompanying electron density depletion region envelope.[11] Together with their small sizes, this explains why the electronegative second row elements have been observed to create anomalous surface dipole moments[23,30] upon adsorption onto metals.

Finally, Fig. 5 shows the dependence of the work function changes on the electronic properties of the various metal surfaces: the work function changes due to the adsorption of I on different fcc metal surfaces are plotted *versus* the work function of the bare metals. The trend is obvious. The higher the work function of the bare metal, the lower the work function change. For transition metals, the adsorption of I leads to a decrease of the work function. The exception is Ag, due the high charge transfer to iodine, given the low work function of silver. A similar dependence has been reported by Migani *et al.*:[21] they looked at the halogen charge transfer as a function of the work function of the metal. They observed that the higher the work function, the less the charge transfer. This also means that the higher the work function, the less ionic and the more covalent is the bond. Additionally, it can be said that the more covalent the metal–halogen bond, the stronger the polarization of the halogen atom. Finally, a stronger polarization leads to a more negative work function change.

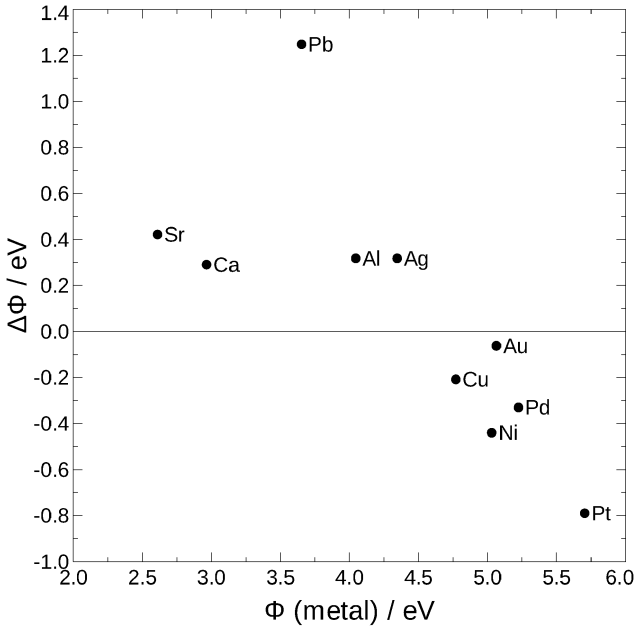

Fig. 5 The polarization mechanism: the work function change due to the adsorption of I on different metal substrates is plotted against the work function of the respective metal.

4 Conclusions

We have discussed the role of the substrate in promoting a decrease in the work function upon halogen adsorption, governed by two mechanisms: electron spillout depletion associated with ionic interaction, and polarization on the adatom associated with covalent bonding. These two mechanisms are clearly independent of each other because of the opposite factors that lead to the work function decrease. With the exception of adsorption on Pb and Ag, we have shown that halogen adsorption can decrease the work function on (111) faces of fcc metals.

The two mechanisms are well-distinguishable. A work function decrease due to electron spillout depletion is favored for (1) small adatoms, which adsorb more closely to the metal surface, are more strongly charged, and are less polarizable, and (2) substrates with small work functions, which promote a more ionic and less covalent character to the adsorption interaction. Consequently, a decrease in the work function due to adatom polarization is seen more for large adatoms and substrates with large work functions. The fact that iodine adsorption does not decrease the work function of calcium, as well as fluorine on platinum, suggest that both conditions have to be met. The stark difference between the two mechanisms suggest that a system in which both of them operate together to decrease the work function of the metal may not exist.

Acknowledgements

This research has been supported by the German Science Foundation (DFG) through the research unit FOR 1376 (DFG contract GR 1503/21-1). Generous supply of computer time at the Leibniz Rechenzentrum is gratefully acknowledged.

References

1 D. M. Kolb, *Surf. Sci.*, 2002, **500**, 722.
2 O. M. Magnussen, *Chem. Rev.*, 2002, **107**, 679–725.
3 D. V. Tripkovic, D. Strmcnik, D. van der Vliet, V. Stamenkovic and N. M. Markovic, *Faraday Discuss.*, 2009, **140**, 25–40.
4 A. Groß, *Surf. Sci.*, 2013, **608**, 249–254.
5 S. Trasatti, *Pure Appl. Chem.*, 1986, **58**, 955–966.
6 S. Schnur and A. Groß, *New J. Phys.*, 2009, **11**, 125003.
7 S. Schnur and A. Groß, *Catal. Today*, 2011, **165**, 129–137.
8 X. Lin and A. Groß, *Surf. Sci.*, 2012, **606**, 886–891.
9 T. Roman and A. Groß, *Catal. Today*, 2013, **202**, 183–190.
10 T. Roman and A. Groß, *Phys. Rev. Lett.*, 2013, **110**, 156804.
11 F. Gossenberger, T. Roman, K. Forster-Tonigold and A. Groß, *Beilstein J. Nanotechnol.*, 2014, **5**, 152.
12 P. Broekmann, M. Wilms, M. Kruft, C. Stuhlmann and K. Wandelt, *J. Electroanal. Chem.*, 1999, **467**, 307–324.
13 N. M. Marković, T. J. Schmidt, B. N. Grgur, H. A. Gasteiger, R. J. Behm and P. N. Ross, *J. Phys. Chem. B*, 1999, **103**, 8568–8577.
14 H. Kim, D. A. Boysen, T. Ouchi and D. R. Sadoway, *J. Power Sources*, 2013, **241**, 239–248.
15 F. Gossenberger, T. Roman and A. Groß, *Surf. Sci.*, DOI: 10.1016/j.susc.2014.01.021.
16 S. Peljhan and A. Kokalj, *J. Phys. Chem. C*, 2009, **113**, 14363–14376.
17 W. Erley, *Surf. Sci.*, 1980, **94**, 281–292.
18 E. Bertel, K. Schwaha and F. P. Netzer, *Surf. Sci.*, 1979, **83**, 439.
19 S. K. Jo and J. M. White, *Surf. Sci.*, 1992, **261**, 111.
20 P. S. Bagus, C. Wöll and A. Wieckowski, *Surf. Sci.*, 2009, **603**, 273.
21 A. Migani, C. Sousa and F. Illas, *Surf. Sci.*, 2005, **574**, 297–305.
22 I. A. Pašti and S. V. Mentus, *Electrochim. Acta*, 2010, **55**, 1995–2003.
23 A. Michaelides, P. Hu, M. H. Lee, A. Alavi and D. A. King, *Phys. Rev. Lett.*, 2003, **90**, 246103.
24 J. P. Perdew, K. Burke and M. Ernzerhof, *Phys. Rev. Lett.*, 1996, **77**, 3865.
25 G. Kresse and J. Furthmüller, *Phys. Rev. B: Condens. Matter Mater. Phys.*, 1996, **54**, 11169.
26 P. E. Blöchl, *Phys. Rev. B: Condens. Matter Mater. Phys.*, 1994, **50**, 17953.
27 G. Kresse and D. Joubert, *Phys. Rev. B: Condens. Matter Mater. Phys.*, 1999, **59**, 1758.
28 H. J. Monkhorst and J. D. Pack, *Phys. Rev. B: Condens. Matter Mater. Phys.*, 1976, **13**, 5188.
29 M. Methfessel and A. T. Paxton, *Phys. Rev. B: Condens. Matter Mater. Phys.*, 1989, **40**, 3616.
30 N. D. Lang, *Surf. Sci.*, 1983, **127**, L118.

E.3 Publication in chapter 4.3

The following article is used in chapter 4.3, it is reprinted and adapted from F. Gossenberger, T. Roman, and A. Gross, Surf. Sci. 631 (2015), 17-22, with the permission from Elsevier.

Surface Science 631 (2015) 17–22

Contents lists available at ScienceDirect

Surface Science

journal homepage: www.elsevier.com/locate/susc

Equilibrium coverage of halides on metal electrodes

Florian Gossenberger [a], Tanglaw Roman [a], Axel Groß [a,b,*]

[a] Institute of Theoretical Chemistry, Ulm University, D-89069 Ulm, Germany
[b] Helmholtz Institute Ulm (HIU) Electrochemical Energy Storage, 89069 Ulm, Germany

ARTICLE INFO

Available online 10 February 2014

Keywords:
Electrochemistry
Density functional theory
Halide adsorption
Coverage

ABSTRACT

The adsorption of halides on Cu(111) and Pt(111) has been studied using periodic density functional theory calculations. The equilibrium coverage of the halides as a function of the electrode potential was determined using a thermodynamic approach in which the electrochemical environment is not explicitly taken into account. For all considered systems, halide coverages between 1/3 and 3/8 should be stable over a wide potential range. Although some quantitative discrepancies with experiment are obtained, the qualitative trends derived from the calculations are consistent with experimental observations. The reasons for the remaining discrepancies with the experiment are discussed.

1. Introduction

The adsorption of anions on metal electrodes is of particular interest in electrochemistry [1,2]. At the electrochemical interface between the electrode and the electrolyte an electric double layer is formed consisting of an electronic charge on the electrode and a corresponding ionic counter charge in the electrolyte [3,4]. Anions such as halides often adsorb specifically, i.e., they form chemical bonds with the metal surface. These adsorbed anions not only affect the chemical properties of electrodes [5] by either directly participating in reactions at the surface or by modifying the electronic properties of the electrodes or by simply blocking adsorption and reaction sites [1], but in general they also change the work function of the electrode, which is directly related to the electrode potential [6].

As part of a systematic effort to model electrode/electrolyte interfaces from first-principles [7–10], we have recently addressed the work function change induced by the adsorption of halides on Cu(111) [11] and on Pt(111) and Ca(111) [12]. In particular, we focused on the anomalous work function change observed at low coverages for some halide/metal systems [13–18] which could be explained either by a polarization of the adatom [11] or a reduction in the surface overspill electron density [12,19].

Here we extend our previous studies in order to determine the equilibrium coverage of halides on Cu(111) and Pt(111). Although recently there is a growing number of first-principles studies addressing structures and processes at electrochemical metal/liquid interfaces [20–28], there have been only few computational attempts to focus on the role of anions on metal electrodes [17,29,30], and it is certainly fair to say that a systematic approach to study anion adsorption on metal electrodes from first-principles in an electrochemical setup is still missing. In an electrochemical situation, the anion coverage on the electrodes is a function of the electrode potential. Although the concentration of anions in the electrolyte is typically relatively low, their concentration on the electrode can be rather high because of their strong interaction with metal electrodes [10,16–18]. However, the exact coverage is often not known.

The realistic modeling of electrochemical metal/liquid interfaces is hampered by three facts: i) In electrochemistry, structures and properties of the electrode–electrolyte interfaces are governed by the electrode potential, which adds considerable complexity to the theoretical treatment since charged surfaces have to be considered [7]. ii) The theoretical treatment of processes at solid–liquid interfaces includes a proper description of the liquid which requires to determine free energies instead of just total energies. This means that computationally expensive statistical averages have to be performed [7,10]. iii) Electronic structure methods based on density functional theory (DFT) combine numerical efficiency with a satisfactory accuracy. However, there are severe shortcomings of the DFT description of liquids, in particular water, using current functionals [31–33].

These problems can be avoided if the electrochemical environment is not explicitly but only implicitly taken into account. In a very elegant approach [34,35] that is now termed “Computational hydrogen electrode” and that is similar to the ab initio thermodynamics approach used in heterogeneous catalysis [36], the electrochemical environment is just considered as a reservoir the adsorbates come from, but the explicit influence of the electrochemical environment on the adsorption properties is not taken into account. This is of course a severe approximation, but it is computationally very attractive, and it allows to establish trends in electrochemistry and electrocatalysis [37].

Here we also use this approach to determine the equilibrium coverage of halides on Cu(111) and Pt(111) in the spirit of the work by Hansen et al. [38]. We will show that the trends in the electrochemical halide coverage observed experimentally can be well reproduced using this approach. Still, discrepancies remain whose possible reasons will be discussed.

* Corresponding author.
E-mail address: axel.gross@uni-ulm.de (A. Groß).

http://dx.doi.org/10.1016/j.susc.2014.01.021
0039-6028

2. Computational details

Periodic DFT calculations that employ the exchange-correlation functional of Perdew, Burke, and Ernzerhof (PBE) [39] were done using the Vienna ab initio program package (VASP) [40]. Electron–core interactions were accounted for by the projector augmented wave method [41,42]. The electronic one-particle wave functions were expanded in a plane-wave basis set up to an energy cutoff of 500 eV.

The metal substrates were represented by slabs of seven atomic layers, of which the inner three layers were kept fixed in the bulk position during geometry optimizations while the rest of the system was allowed to relax. Halogen atoms were placed symmetrically at both sides of the slab. Most of the calculations were performed in a 4×4 surface unit cell for halide coverages between 1/16 and 1/2. The corresponding energy minimum structures for chlorine on Cu(111) are illustrated in Fig. 1. For the integration over the first Brillouin zone we used a mesh of at least $4 \times 4 \times 1$ special k-points [43] with a Methfessel–Paxton smearing [44] of 0.1 eV. In addition, $\sqrt{3} \times \sqrt{3}$ unit cells were used to study different halide coverage of 1/3. Experimentally, halide adsorbate structures with other geometries than those considered in our computational study have been found (see the discussion below). Still, we are mainly interested in qualitative trends and the characteristic differences between the studied systems. Hence we made no effort to address further geometries.

3. Results and discussion

3.1. Theoretical background

The calculated adsorption energies per halogen atom referred to the corresponding free halogen molecule for the considered systems are shown in Fig. 2. The results are in satisfactory agreement with previous computational studies using similar setups (see, e.g., [45]). As a general trend, it can be seen that the adsorption on Cu(111) is stronger than that on Pt(111) although for iodine adsorption the effect is rather small. The trend among the halides is not identical: on Cu(111) chlorine adsorption is stronger than iodine adsorption, while on Pt(111) it is the other way around.

In order to understand these trends, we determined the adsorption energies of the halogen atoms at a coverage of 1/9 on (111) surfaces of Ag, Cu, Ni, Au, Pd, and Pt, where we have ordered the substrates according to increasing work function (see Table 1). In fact, we find a

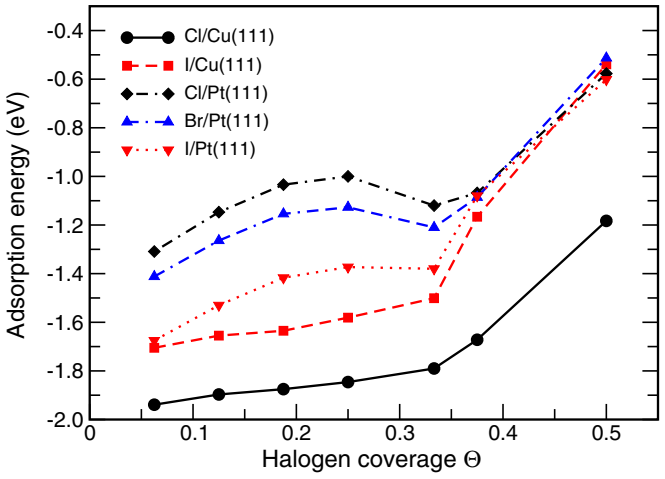

Fig. 2. Adsorption energies of halogen atoms on Cu(111) and Pt(111) with respect to the free halogen molecule as a function of the coverage.

gradual change in the trend in the adsorption energies of Cl, Br, and I. Whereas on Ag and Cu, Cl exhibits the strongest adsorption on Pd and Pt it is I. Thus there is a strong correlation between the work function and the trend in the adsorption energies among the halogen atoms, except for fluorine which exhibits the strongest adsorption of the halogen atoms on all surfaces.

The trend in the adsorption energies, except for fluorine, can then be rationalized as a transition from predominantly ionic bonding to predominantly covalent bonding. Surfaces with low work function such as Ag and Cu easily transfer electronic charge to electronegative adsorbates such as halogen atoms resulting in a more ionic bonding situation. And then the more electronegative (i.e., smaller) halogen atoms exhibit the strongest bonding.

On the other hand, the surfaces with large work function such as Pd and Pt exhibit a smaller charge transfer to electronegative adsorbates so that the bonding becomes mostly covalent in nature, as we already showed [11,12]. And here the more polarizable (i.e., larger) halogen atoms then bind most strongly.

In general, binding to the metal substrates becomes weaker at higher coverage, indicating a repulsive interaction between the adsorbed halogen atoms which becomes particularly evident for coverages $\Theta \geq 1/3$. It

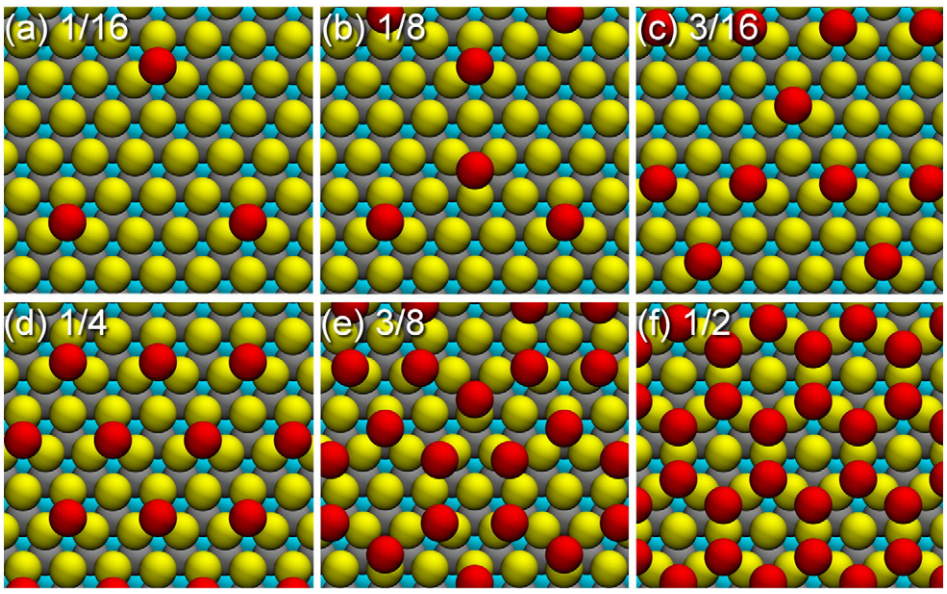

Fig. 1. Relaxed structures of chlorine atoms in a 4×4 geometry on Cu(111) for coverages between 1/16 and 1/2.

Table 1
Adsorption energies in eV of halogen atoms with respect to the free halogen molecule on (111) metal surfaces at a coverage of 1/9. The metal surfaces are ordered according to increasing work function.

E_{ads} (eV)	Ag	Cu	Ni	Au	Pd	Pt
F	−2.61	−2.90	−2.86	−1.84	−2.13	−1.63
Cl	−1.60	−1.86	−2.02	−0.97	−1.66	−1.21
Br	−1.54	−1.75	−1.91	−0.99	−1.70	−1.32
I	−1.40	−1.60	−1.83	−0.99	−1.85	−1.58

is also obvious that the halogen coverage 1/3 corresponding to a $\sqrt{3}\times\sqrt{3}$ structure is rather stable, especially for chlorine and bromine on Pt(111). Note that the $\sqrt{3}\times\sqrt{3}$ structure corresponds to the two-dimensional close-packed structure, but at the same time it is the structure with the largest mutual distances among the adsorbates for a given density. This might explain its stability for adsorbates that repel each other such as halides.

From the adsorption energies shown in Fig. 2 it is, however, not directly clear what the thermodynamically stable structures under specific conditions are. In order to address this issue, we will first briefly recall the theoretical background for the determination of an adsorbate coverage in thermal equilibrium. It is important to note that in equilibrium, every species is characterized by its chemical potential which is constant throughout the whole system. At gas/solid interfaces – as they occur in heterogeneous catalysis – the Gibbs free energy of adsorption $\Delta\gamma$ for N_{ads} adsorbates bound to a surface area A_s at a given temperature T and pressure p can be expressed [36] as

$$\Delta\gamma(T,p)=\gamma(T,p,N_{ads})-\gamma_{clean}(T,p,0) \tag{1}$$

$$=\frac{1}{A_s}\Delta G^{ads}(T,p) \tag{2}$$

$$=\frac{N_{ads}}{A_s}(E_{ads}-\mu_{ads}(T,p))\ . \tag{3}$$

Here, $\Delta G^{ads}(T,p)$ is the difference in free energy and $\mu_{ads}(T,p)$ is the chemical potential of the adsorbate. In the last Eq. (3) above, E_{ads} is the total adsorption energy per particle, and any change in entropy and zero-point energies upon adsorption is neglected, as often done in theoretical studies addressing systems in heterogeneous catalysis and surface science [36].

In the adsorption at electrochemical interfaces, the reference state corresponds to species in solution in the presence of an electrode potential U. This means that the chemical potential μ has to be replaced by the electrochemical potential

$$\tilde{\mu}=\mu+neU\ , \tag{4}$$

where n is the charge of the particle. Still the problem remains that the electrochemical potential includes all solvation effects of the species. The determination of solvation energies requires computationally demanding thermal integration schemes [46]. These efforts can be avoided using the concept of the computational hydrogen electrode. It is based on the fact that at standard conditions (pH = 0, p = 1 bar, T = 298 K) U = 0 is defined as the electrode potential at which there is an equilibrium between a proton and an electron in aqueous solution $H^+(aq)+e^-$ and hydrogen in the gas phase, $\frac{1}{2}H_2(g)$. Furthermore, it is well known how the electrochemical potential of the proton and the electron change if the proton concentration and the electrode potential are varied [47], namely according to

$$\tilde{\mu}\left(H^+(aq)\right)+\tilde{\mu}(e^-)=\frac{1}{2}\mu(H_2(g))-eU_{SHE}-k_BT\ln(10)\mathrm{pH}\ , \tag{5}$$

where U_{SHE} is the electrode potential with respect to the standard hydrogen electrode (SHE). The success of the computational hydrogen electrode is based on the fact that it allows to derive adsorption energies with respect to solvated species without the need to determine any solvation energies.

This concept does not only work for hydrogen, it works also for any redox couple $\frac{1}{2}A_2+e^-\leftrightarrows A^-$, as applied by Hansen et al. to describe the electrochemical chlorine evolution at rutile oxide (110) surfaces [38]. Here we follow the same approach (note that there are typos in Ref. [38] in the corresponding equations), i.e., we derive the electrochemical potential for a halide A, where A stands for Cl, Br or I, as

$$\tilde{\mu}(A^-(aq))-\tilde{\mu}(e^-)=\frac{1}{2}\mu(A_2(g))+e\left(U_{SHE}-U^0\right)+k_BT\ln a_{A^-}\ , \tag{6}$$

where U^0 is the reduction potential of the corresponding halide and a_{A^-} its activity. The reduction potentials for the halides considered in this study are collected in Table 2.

The change of zero-point energies upon adsorption of the halogen atoms can safely be neglected [48] mainly because of their relatively large mass. For example, in the adsorption of chlorine on rutile oxide (110) surfaces they have been estimated to be in the order of 0.02 eV [38]. Furthermore, we also neglect the entropy change upon adsorption. In the following, we will also assume standard conditions, i.e., we assume that the activity of the halides a_{A^-} is unity. Thus we arrive at the following expression for the free energy of adsorption as a function of the electrode potential,

$$\Delta\gamma(U_{SHE})=\frac{N_{ads}}{A_s}\left(E_{ads}-e\left(U_{SHE}-U^0\right)\right)\ . \tag{7}$$

For other concentrations of the halides in the electrolyte, the electrode potential needs to be shifted by $k_BT\ln a_{A^-}$ which corresponds, e.g., to about 60 meV if the activity is changed by one order of magnitude at room temperature.

It should be emphasized that within our approach, the adsorption energy E_{ads} appearing in Eq. (7) is calculated without taking the electrochemical environment into account. Furthermore, the varying excess charge at the metal electrodes as a function of the electrode potential is also not considered. These are certainly severe approximations. Comparing our results with experimental findings is a first step to assess the validity of this approach.

3.2. Halides on Cu(111)

The first system we discuss is the adsorption of chlorine on Cu(111) which is a rather well-studied system in electrochemistry [1,49–52], among others motivated by the fact that chloride adlayers on copper electrodes are of major importance in corrosion and electroplating. Although there was some debate about the equilibrium structure of chloride on Cu(111), more recent studies indicate that a simple $\sqrt{3}\times\sqrt{3}$ structure with a coverage of 1/3 should result in an electrochemical environment [49,51]. In addition, a compressed chloride adlayer has been suggested [50,52]. It should be noted that on Cu(100) even nominal coverages of 1/2 have been observed [1,29].

Our prediction concerning the equilibrium structure of chlorine on Cu(111) as a function of the electrode potential at standard conditions is shown in Fig. 3. Note that these diagrams can be read as a kind of phase diagram. The structure with the lowest free energy of adsorption

Table 2
Reduction potentials of the halides considered in this work.

Redox couple	Reduction potential U^0 (V)
$\frac{1}{2}Cl_2+e^-\leftrightarrows Cl^-$	1.36
$\frac{1}{2}Br_2+e^-\leftrightarrows Br^-$	1.09
$\frac{1}{2}I_2+e^-\leftrightarrows I^-$	0.54

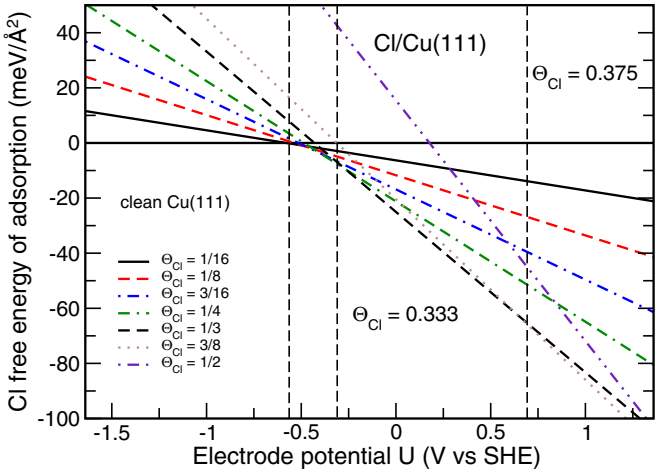

Fig. 3. Calculated electrochemical equilibrium coverage of chlorine on Cu(111) at standard condition as a function of the electrode potential vs. SHE.

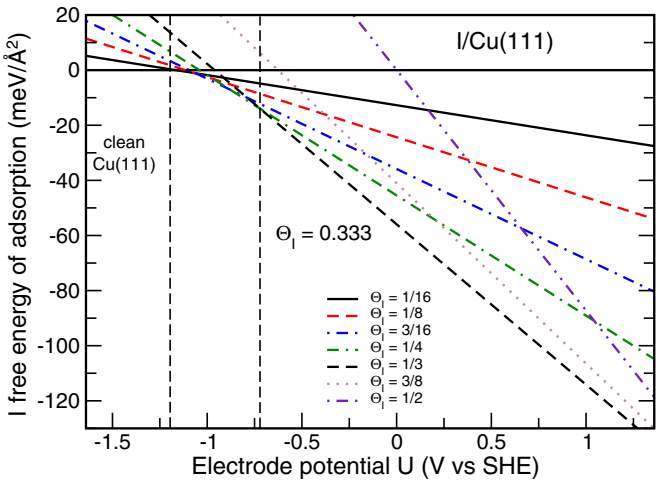

Fig. 4. Calculated electrochemical equilibrium coverage of iodine on Cu(111) at standard condition as a function of the electrode potential vs. SHE.

is supposed to be the thermodynamically stable structure. In Fig. 3 and the following figures we show the free energy curves in a potential range of about 3 eV. This is larger than the stability range of some of the considered systems. Still we have chosen such a broad range in order to make the diagrams clearly arranged.

We find that at potentials below −0.6 V, the clean Cu(111) electrode is stable. Between −0.6 V and −0.3 V, structures with increasing coverage become stable before at −0.3 V a large potential window opens in which the $\sqrt{3} \times \sqrt{3}$ structure is assumed to be realized in thermodynamical equilibrium. The onset of the formation of the chloride adlayer at about −0.3 V is consistent with the peaks assigned to the adsorption and desorption of Cl in cyclic voltammograms [49–51].

Hence our calculations confirm the prominent role the $\sqrt{3} \times \sqrt{3}$ structure plays for the adsorption of chlorine on Cu(111) under electrochemical conditions. The compressed chlorine adlayers which have been found on Cu(111) [50,52] cannot be addressed by our periodic setup as they have been identified to be an incommensurate adlayer with a rotated hexagonal structure [52]. Still, the fact that we find a chlorine adlayer structure corresponding to a coverage of $\Theta_{Cl} = 3/8$ which is almost as stable as the $\Theta_{Cl} = 1/3$ structure indicates that compressed chlorine adlayer structures with coverages slightly above 1/3 should indeed be possible.

Next, we address the equilibrium structures of iodine on Cu(111). Experimentally, basically only the $\sqrt{3} \times \sqrt{3}$ structure was observed [50]. Although initially no compression of the iodine adlayer as a function of the electrode potential was observed [50], later studies found uniaxially incommensurate iodide adlayers caused by a unidirectional compression of the $\sqrt{3} \times \sqrt{3}$−I at vacuum at higher iodine coverages [53] or in an electrochemical environment at more positive potentials close to the onset of the copper dissolution reaction [54].

The calculated free energy of adsorption of iodine on Cu(111) as a function of the electrode potential is plotted in Fig. 4. Iodine adsorption on Cu(111) occurs at lower potentials than chlorine adsorption which is in qualitative agreement with the experiment [51,54] although iodine adsorption on Cu(111) is weaker than chlorine adsorption, as Fig. 2 demonstrates. This lower onset potential is caused by the fact that the reduction potential of iodine is much lower than the one of chlorine (see Table 2).

We find a potential region between −1.2 V and −0.7 V in which a series of structures with increasing coverage becomes stable. At potentials above −0.7 V, only the $\left(\sqrt{3} \times \sqrt{3}\right)$ structure is found. Again, the uniaxially incommensurate compressed iodide adlayer could not be addressed by the periodic calculations since the corresponding superstructures are too large. For I/Cu(111), the $\Theta = 3/8$ is more unfavorable compared to the $\Theta = 1/3$ than in the case of Cl/Cu(111). This is consistent with the fact that Inukai et al. did not find any compression of the iodine adlayer in the potential window between −0.5 V and −0.7 V vs. SCE [50].

3.3. Halides on Pt(111)

Turning to the Pt(111) electrode, we start with the system Cl/Pt(111). Using in situ surface X-ray scattering, Lucas et al. were not able to detect any ordered chlorine adlayer over the entire potential range where chloride is present on the Pt(111) electrode [55]. They estimated the chloride coverage to be between 0.4 and 0.6. To the best of our knowledge, there is no study revealing an atomistic structure of chlorine on Pt(111) in an electrochemical environment. In a chronocoulometric study [56], the structure of Cl/Pt(111) was not addressed, however, it was found that the adsorbed species is basically a neutral chlorine atom which agrees nicely with our computational findings [12].

We find (see Fig. 5) that at standard conditions a chlorine adlayer on Pt(111) should start to form at potentials close to 0 V. This is a significantly higher onset-potential than on Cu(111) because of the weaker binding of chlorine to Pt(111) (see Fig. 2). Up to about 0.25 V, a chlorine layer with a coverage of 1/16 should be stable, followed by the $\sqrt{3} \times \sqrt{3}$ structure. This $\Theta = 1/3$ structure, however, is only stable up to 0.7 V where $\Theta = 3/8$ becomes more favorable. Furthermore, the layers

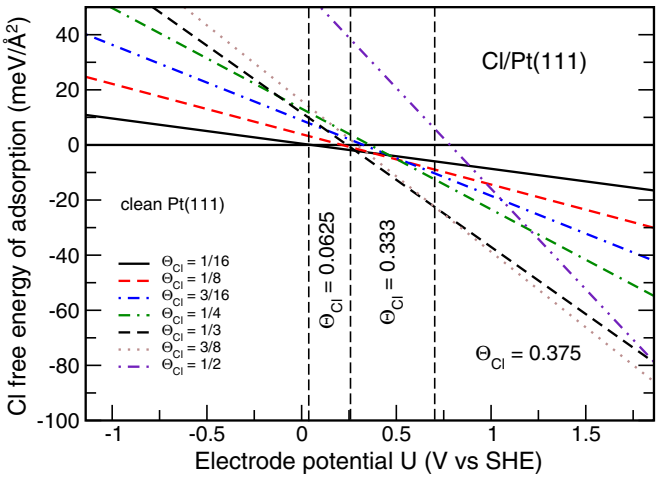

Fig. 5. Calculated electrochemical equilibrium coverage of chlorine on Pt(111) at standard condition as a function of the electrode potential vs. SHE.

corresponding to $\Theta = 1/3$ and $\Theta = 3/8$ are rather close in energy. This might yield an explanation why no specific ordered structure could be identified in the experiment [55].

For bromine on Pt(111), in situ STM experiments yielded asymmetric and hexagonal (3×3) structures at a coverage of $\Theta = 4/9$ [57]. Using X-ray scattering experiments, Lucas et al. [55] observed a series of high-order commensurate structures as a function of electrode potential which are poorly ordered unless the size of the unit cell is small. These unit cells corresponded to (3×3) and (7×7) structures with coverages of $\Theta = 4/9$ and $\Theta = 25/49$, respectively. Based on rotating disk experiments, Gasteiger et al. [58] found that in 0.1 M $HClO_4$ with 10^{-4} M Br^- bromide adsorption starts at about 0.1 V and reaches a coverage of about $\Theta = 0.42$ at 0.75 V.

As shown in Fig. 6, according to our calculations bromine starts to adsorb on Pt(111) at standard conditions at about −0.35 V with a $\Theta = 1/16$ structure. This onset occurs at lower potentials than chlorine adsorption on Pt(111) because both bromine bonding to Pt(111) is stronger than the chlorine bonding, and the reduction potential of bromine is lower than the one of chlorine. In a wide potential range from −0.1 V to 1.0 V, the $\left(\sqrt{3} \times \sqrt{3}\right)$ structure with $\Theta = 1/3$ is stable, followed above 1.0 V by the $\Theta = 3/8$ structure. Similar to Cl/Pt(111), the layers corresponding to $\Theta = 1/3$ and $\Theta = 3/8$ are rather close in energy.

In our calculations, we did not consider (3×3) and (7×7) structures, hence we cannot compare our results directly with experiment [55]. Still, our results are consistent with the fact that over a wide range of potentials, bromine coverages of $\Theta \geq 0.4$ have been found. Note that the $k_B T \ln a_{Br^-}$ term in Eq. (6) leads to a shift of the free energy curves by about 60 mV to higher potentials if the activity is decreased by one order of magnitude. Furthermore, increasing the pH-value of the electrolyte by one leads to the same shift. Considering such a shift, the observed potential range for bromide adsorption on Pt(111) [58] is compatible with our calculated order of stability.

In ultrahigh vacuum (UHV), iodine dosing of a Pt(111) leads to two ordered structures, $\left(\sqrt{3} \times \sqrt{3}\right)$ with a coverage of $\Theta = 1/3$ and $\left(\sqrt{7} \times \sqrt{7}\right)$ $R19.1°$ with $\Theta = 3/7$ [59].

In temperature-programmed desorption (TPD) experiments, Jo and White [15] observed a shift of the desorption peaks to lower temperatures with increasing coverage with is consistent with the lower iodine binding energies for higher coverages shown in Fig. 2. In addition, they found a non-monotonic decrease of the I/Pt(111) work function as a function of the iodine coverage which is well reproduced by our calculations [12].

Early in situ STM experiments confirmed the existence of the $\left(\sqrt{3} \times \sqrt{3}\right)$ structure also in an electrochemical environment [60]. Later X-ray scattering [55] and in situ STM experiments [61] found the coexistence of a hexagonal (3×3) structure with $\Theta = 4/9$ and the $\left(\sqrt{7} \times \sqrt{7}\right)$ $R19.1°$ structure under potential control.

Again, we have considered neither the (3×3) nor the $\left(\sqrt{7} \times \sqrt{7}\right)$ $R19.1°$ structure. As Fig. 7 shows, our calculations yield that iodine adsorption starts at −1.2 V, and above −0.75 V only the $\left(\sqrt{3} \times \sqrt{3}\right)$ is stable. As our calculations are done at the solid–vacuum interface, it is no surprise that the UHV structure of I/Pt(111) has been reproduced.

The onset potential of iodine adsorption on Pt(111) is very close to the one on Cu(111) because of the similar adsorption energies (see Fig. 2). As discussed above, whereas iodine adsorption on Pt(111) is stronger than chlorine adsorption on Pt(111), it is the other way around on Cu(111), which means that there is no general trend of the adsorption energies among the halides for metal electrodes.

3.4. Discussion

In the previous sections, we have compared experimental findings with respect to the stability of halide structures on Cu(111) and Pt(111) at electrochemical conditions with the predictions of a very simple thermodynamical model that does not explicitly take into account the electrochemical environment. The calculated stability range of the halide structures together with their corresponding coverage are in qualitative or even in semi-quantitative agreement with experiment. However, some characteristic quantitative differences between experiment and the simple thermodynamic model remain. This is partially due to the fact that we did not consider all structures observed in the experiment. Still, there are three main reasons that could be responsible for the discrepancies.

First of all, the change of the adsorption energy for varying surface excess charge or varying electric fields has not been taken into account. According to a DFT study, electric field effects should only play a minor role in the oxidation reaction on Pt(111) [62], however, it is not clear whether these findings can be transferred to halide adsorption.

Second, the aqueous environment was not explicitly considered. Now water is relatively weakly interacting with metal electrodes [7,63,64] so that chemisorption energies are only weakly influenced by the presence of water [65,66]. Therefore we do not expect that water layers change the adsorption energies of the halides significantly. However, reorientation of the water molecules due to the presence of

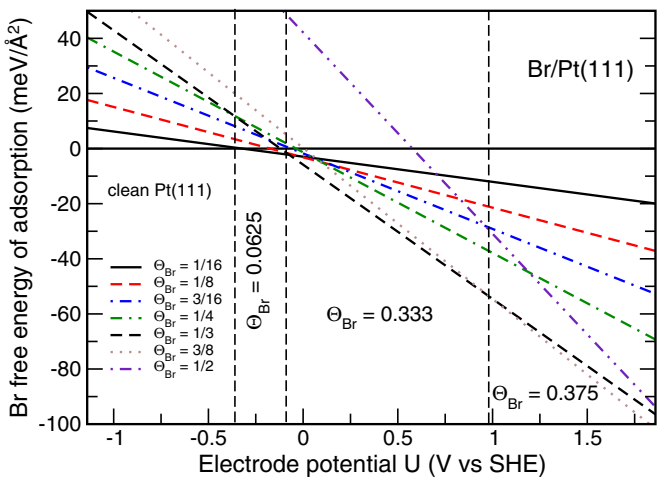

Fig. 6. Calculated electrochemical equilibrium coverage of bromine on Pt(111) at standard condition as a function of the electrode potential vs. SHE.

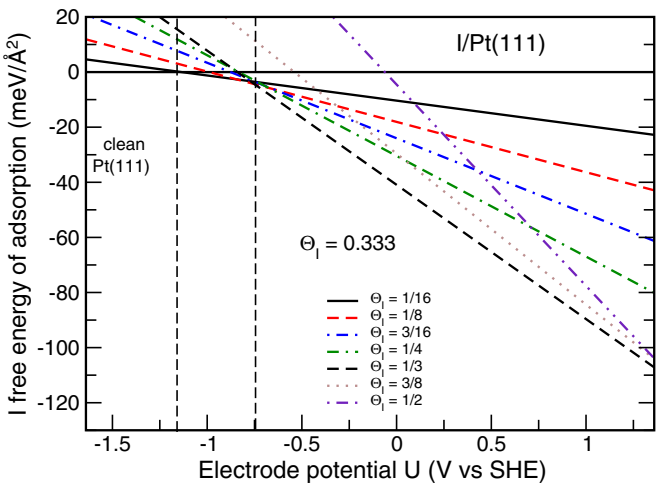

Fig. 7. Calculated electrochemical equilibrium coverage of iodine on Pt(111) at standard condition as a function of the electrode potential vs. SHE.

the halides might still affect the work function of the electrodes and thus the corresponding electrode potential.

Third, the presence of additional adsorbates is not taken into account. This is particularly important for Pt(111) where at low potentials hydrogen adsorption [67,68] and at higher potentials OH adsorption take place. There might be some competition for the adsorption sites. Furthermore, co-adsorbates influence the adsorption energy either through direct adsorbate–adsorbate interactions or indirectly through modifying the electronic properties of the substrate [69,70]. Both effects might affect the stability of the halide adsorption phases.

Last but not least, it should be mentioned that errors might of course also be introduced through the approximate nature of the exchange-correlation functional used in the DFT calculations. A quantitative assessment of the reliability of the functional, however, can only be achieved once the electrochemical interface is realistically modeled. Such a realistic modeling of the structure of electrochemical interfaces is not only interesting in its own right, it is also crucial for a reliable description of electrocatalytic processes as they occur, e.g., in fuel cells. Therefore we are in the process of studying the importance of all the effects discussed above in our ongoing work.

4. Conclusions

Using a very simple thermodynamical model corresponding to the computational hydrogen electrode [34,35], we have estimated the stability of halide structures on Cu(111) and Pt(111). According to our calculations, for all considered systems halide coverages between 1/3 and 3/8 should be stable in a wide potential range. Although in this model the electrochemical environment at the interface is not explicitly taken into account, the theoretical results are consistent with experimental observations. Thus this model offers a computationally convenient way to estimate anion coverages at electrochemical interfaces under potential control. Still further work is needed in order to assess the importance of the effects neglected in the simple thermodynamical model.

Acknowledgments

This research has been supported by the German Science Foundation (DFG) through the research unit FOR 1376 (DFG contract GR 1503/21-1) and by the Baden–Württemberg Foundation within the Network of Excellence *Functional Nanostructures*. Computer time has been provided by the BW-Grid of the federal state of Baden–Württemberg and by a computer cluster financed through the stimulus program "Electrochemistry for Electromobility" of the German Ministry of Education and Science (BMBF). Useful discussions with Jan Rossmeisl and Wolfgang Schmickler are gratefully acknowledged.

References

[1] O.M. Magnussen, Chem. Rev. 107 (2002) 679.
[2] D.V. Tripkovic, D. Strmcnik, D. van der Vliet, V. Stamenkovic, N.M. Markovic, Faraday Discuss. 140 (2009) 25.
[3] W. Schmickler, Chem. Rev. 96 (1996) 3177.
[4] R. Guidelli, W. Schmickler, Electrochim. Acta 45 (2000) 2317.
[5] A. Groß, Surf. Sci. 608 (2013) 249.
[6] S. Trasatti, Pure Appl. Chem. 58 (1986) 955.
[7] S. Schnur, A. Groß, New J. Phys. 11 (2009) 125003.
[8] S. Schnur, A. Groß, Catal. Today 165 (2011) 129.
[9] X. Lin, A. Groß, Surf. Sci. 606 (2012) 886.
[10] T. Roman, A. Groß, Catal. Today 202 (2013) 183.
[11] T. Roman, A. Groß, Phys. Rev. Lett. 110 (2013) 156804.
[12] F. Gossenberger, T. Roman, K. Forster-Tonigold, A. Groß, Beilstein J. Nanotechnol. 5 (2014) 152.
[13] W. Erley, Surf. Sci. 94 (1980) 281.
[14] E. Bertel, K. Schwaha, F.P. Netzer, Surf. Sci. 83 (1979) 439.
[15] S.K. Jo, J.M. White, Surf. Sci. 261 (1992) 111.
[16] P.S. Bagus, C. Wöll, A. Wieckowski, Surf. Sci. 603 (2009) 273.
[17] A. Migani, C. Sousa, F. Illas, Surf. Sci. 574 (2005) 297.
[18] I.A. Pašti, S.V. Mentus, Electrochim. Acta 55 (2010) 1995.
[19] A. Michaelides, V.A. Ranea, P.L. de Andres, D.A. King, Phys. Rev. Lett. 90 (2003) 216102.
[20] J.S. Filhol, M. Neurock, Angew. Chem. Int. Ed. 45 (2006) 402.
[21] C.D. Taylor, S.A. Wasileski, J.-S. Filhol, M. Neurock, Phys. Rev. B 73 (2006) 165402.
[22] E. Skúlason, G.S. Karlberg, J. Rossmeisl, T. Bligaard, J. Greeley, H. Jónsson, J.K. Nørskov, Phys. Chem. Chem. Phys. 9 (2007) 3241.
[23] S.A. Wasileski, M.J. Janik, Phys. Chem. Chem. Phys. 10 (2008) 3613.
[24] M. Otani, I. Hamada, O. Sugino, Y. Morikawa, Y. Okamoto, T. Ikeshoji, Phys. Chem. Chem. Phys. 10 (2008) 3609.
[25] J.A. Keith, T. Jacob, Angew. Chem. Int. Ed. 49 (2010) 9521.
[26] U. Benedikt, W.B. Schneider, A.A. Auer, Phys. Chem. Chem. Phys. 15 (2013) 2712.
[27] M.E. Björketun, Z. Zeng, R. Ahmed, V. Tripkovic, K.S. Thygesen, J. Rossmeisl, Chem. Phys. Lett. 555 (2013) 145.
[28] P. Quaino, N. Luque, G. Soldano, R. Nazmutdinov, E. Santos, T. Roman, A. Lundin, A. Groß, W. Schmickler, Electrochim. Acta 105 (2013) 248.
[29] M. Saracino, P. Broekmann, K. Gentz, M. Becker, H. Keller, F. Janetzko, T. Bredow, K. Wandelt, H. Dosch, Phys. Rev. B 79 (2009) 115448.
[30] A. Comas-Vives, J. Bandlow, T. Jacob, Phys. Chem. Chem. Phys. 15 (2013) 992.
[31] J. Carrasco, B. Santra, J. Klimec, A. Michaelides, Phys. Rev. Lett. 106 (2011) 026101.
[32] K. Tonigold, A. Groß, J. Comput. Chem. 33 (2012) 695.
[33] J. Carrasco, J. Klimes, A. Michaelides, J. Chem. Phys. 138 (2013) 024708.
[34] J.K. Nørskov, J. Rossmeisl, A. Logadottir, L. Lindqvist, J.R. Kitchin, T. Bligaard, H. Jónsson, J. Phys. Chem. B 108 (2004) 17886.
[35] J.K. Nørskov, T. Bligaard, A. Logadottir, J.R. Kitchin, J.G. Chen, S. Pandelov, U. Stimming, J. Electrochem. Soc. 152 (2005) J23.
[36] K. Reuter, M. Scheffler, Phys. Rev. B 65 (2001) 035406.
[37] I.C. Man, H.-Y. Su, F. Calle-Vallejo, H.A. Hansen, J.I. Martinez, N.G. Inoglu, J. Kitchin, T.F. Jaramillo, J.K. Nørskov, J. Rossmeisl, ChemCatChem 3 (2011) 1159.
[38] H.A. Hansen, I.C. Man, F. Studt, F. Abild-Pedersen, T. Bligaard, J. Rossmeisl, Phys. Chem. Chem. Phys. 12 (2010) 283.
[39] J.P. Perdew, K. Burke, M. Ernzerhof, Phys. Rev. Lett. 77 (1996) 3865.
[40] G. Kresse, J. Furthmüller, Phys. Rev. B 54 (1996) 11169.
[41] P.E. Blöchl, Phys. Rev. B 50 (1994) 17953.
[42] G. Kresse, D. Joubert, Phys. Rev. B 59 (1999) 1758.
[43] H.J. Monkhorst, J.D. Pack, Phys. Rev. B 13 (1976) 5188.
[44] M. Methfessel, A.T. Paxton, Phys. Rev. B 40 (1989) 3616.
[45] S. Peljhan, A. Kokalj, J. Phys. Chem. C 113 (2009) 14363.
[46] A.R. Leach, Molecular Modelling: Principles and Applications, 2nd edition Pearson, Harlow, 2001.
[47] W. Schmickler, E. Santos, Interfacial Electrochemistry, 2nd edition Springer, Berlin, 2010.
[48] A. Groß, M. Scheffler, J. Vac. Sci. Technol. A 15 (1997) 1624.
[49] M. Kruft, B. Wohlmann, C. Stuhlmann, K. Wandelt, Surf. Sci. 377–379 (1997) 601.
[50] J. Inukai, Y. Osawa, K. Itaya, J. Phys. Chem. B 102 (1998) 10034.
[51] P. Broekmann, M. Wilms, M. Kruft, C. Stuhlmann, K. Wandelt, J. Electroanal. Chem. 467 (1999) 307.
[52] Y. Gründer, A. Drünkler, F. Golks, G. Wijts, J. Stettner, J. Zegenhagen, O.M. Magnussen, Surf. Sci. 605 (2011) 1732.
[53] B. Andryushechkin, K. Eltsov, V. Shevlyuga, Surf. Sci. 472 (2001) 80.
[54] B. Obliers, P. Broekmann, K. Wandelt, J. Electroanal. Chem. 554–555 (2003) 183.
[55] C.A. Lucas, N.M. Markovic, P.N. Ross, Phys. Rev. B 55 (1997) 7964.
[56] N. Garcia-Araez, V. Climent, E. Herrero, J. Feliu, J. Lipkowski, J. Electroanal. Chem. 576 (2005) 33.
[57] S. Tanaka, S.-L. Yau, K. Itaya, J. Electroanal. Chem. 396 (1995) 125.
[58] H.A. Gasteiger, N.M. Markovi, P.N. Ross, Langmuir 12 (1996) 1414.
[59] T.E. Felter, A.T. Hubbard, J. Electroanal. Chem. 100 (1979) 473.
[60] S.L. Yau, C.M. Vitus, B.C. Schardt, J. Am. Chem. Soc. 112 (1990) 3677.
[61] J. Inukai, Y. Osawa, M. Wakisaka, K. Sashikata, Y.-G. Kim, K. Itaya, J. Phys. Chem. B 102 (1998) 3498.
[62] G.S. Karlberg, J. Rossmeisl, J.K. Nørskov, Phys. Chem. Chem. Phys. 9 (2007) 5158.
[63] A. Michaelides, Appl. Phys. A 85 (2006) 415.
[64] Y. Gohda, S. Schnur, A. Groß, Faraday Discuss. 140 (2008) 233.
[65] A. Roudgar, A. Groß, Chem. Phys. Lett. 409 (2005) 157.
[66] A. Roudgar, A. Groß, Surf. Sci. 597 (2005) 42.
[67] T.J. Schmidt, P.N. Ross Jr., N.M. Markovic, J. Electroanal. Chem. 524 (2002) 252.
[68] N.M. Marković, P.N. Ross Jr., Surf. Sci. Rep. 45 (2002) 117.
[69] B. Hammer, Phys. Rev. B 63 (2001) 205423.
[70] M. Lischka, C. Mosch, A. Groß, Surf. Sci. 570 (2004) 227.

E.4 Publication in chapter 4.4

The following article is used in chapter 4.4, it is reprinted and adapted from F. Gossenberger, T. Roman, and A. Gross, Electrochimica Acta 216 (2016), 152-159, with the permission from Elsevier.

Electrochimica Acta 216 (2016) 152–159

Contents lists available at ScienceDirect

Electrochimica Acta

journal homepage: www.elsevier.com/locate/electacta

Hydrogen and halide co-adsorption on Pt(111) in an electrochemical environment: a computational perspective

Florian Gossenberger, Tanglaw Roman, Axel Groß

Institute of Theoretical Chemistry, Ulm University, 89069 Ulm, Germany

ARTICLE INFO

Article history:
Received 7 April 2016
Received in revised form 29 July 2016
Accepted 23 August 2016
Available online 2 September 2016

ABSTRACT

The adsorbate structures on electrode surfaces in an electrochemical environment are controlled by thermodynamic parameters such as temperature, concentration, pH and electrode potential. Knowledge of these structures is important as specifically-adsorbed ions on an electrode impact catalytic reactions that take place at the electrode-electrolyte interface. From a theoretical point of view, the equilibrium structures of adsorbates can be conveniently estimated using the concept of the computational hydrogen electrode. Here we extend this concept to determine equilibrium co-adsorption structures of halides with hydrogen on Pt(111) as a function of the corresponding electrochemical potentials. We find that hydrogen-halide co-adsorption is of a competitive character, which means that mainly dense-packed structures of either halides or hydrogens are stable on the surface, in good agreement with experiment.

1. Introduction

The adsorption of anions on metal electrodes is of particular interest in electrochemistry which is concerned with structures and processes at the interface between an ion and an electron conductor [1]. An electric double layer is formed at the electrochemical interface between the electrode and the electrolyte consisting of an electronic charge on the electrode and a corresponding ionic counter charge in the electrolyte. Anions such as halides often adsorb specifically [2], i.e., they form chemical bonds with the metal surface. These adsorbed anions change the work function of the electrode [3,4], which is directly related to the electrode potential [5]. In addition, they affect the chemical properties of electrodes by either directly participating in reactions at the surface or by modifying the electronic properties of the electrodes or by simply blocking adsorption and reaction sites [6–11], or through cooperative effects, as in the underpotential deposition of metals [12].

In a previous paper we tackled the adsorption of halides on Pt(111) and Cu(111) [13] as a function of the electrode potential using the concept of the computational hydrogen electrode [14]. A similar work was also performed by McCrum *et al.* on halide adsorption at different Cu surfaces [15]. There is a rich literature on halide adsorption experiments on Pt(111) performed in ultra-high vacuum (UHV), air, or in electrochemical environments [2,16–36]. Our previous study confirmed the experimentally-observed high coverage [2] of halides on metal electrodes [13]. Note that it is not distinguishable whether a single adatom, which in general has a partial charge on the surface, was an ion or a neutral atom before adsorption. We therefore treat adsorbed halogen atoms and adsorbed halides as semantically identical; adsorbed hydrogen and adsorbed protons are likewise synonymous. However, any aqueous electrolyte also contains a certain concentration of protons, depending on the pH value. Especially platinum electrodes are covered by hydrogen at low electrode potentials [37,38] because of the favorable hydrogen adsorption energy on Pt [39]. Here we extend the concept of the computational hydrogen electrode to describe the co-adsorption of halides and protons from first principles, similar to what has been done in heterogeneous oxidation catalysis using the related concept of ab initio thermodynamics [40]. This is in particular interesting as there might be some attractive electrostatic interaction between cations such as protons and anions such as halides adsorbed on a metal electrode.

Yet, to the best of our knowledge, the co-adsorption of halides and hydrogen on platinum has not yet been systematically studied from a theoretical perspective. The particular mechanisms underlying adsorbate-adsorbate interactions are still the subject of considerable debate [41]. Here we will derive phase diagrams of the stable co-adsorption structure of hydrogen with chlorine, bromine and iodine. Furthermore, for given concentrations of the ions, we will determine the surface coverage of hydrogen and halides as a function of the electrode potential and compare the results with those of corresponding experiments.

2. Theoretical Background and Computational Details

The aim of this paper is to link total energies of density functional calculations of a co-adsorbate system to thermodynamic values such as pH or electrode potential in order to derive phase diagrams

http://dx.doi.org/10.1016/j.electacta.2016.08.117
0013-4686/

of adsorbate structures. As a concrete system, a Pt(111) electrode covered by hydrogen and halides will be addressed, based on the concept of the computational hydrogen electrode [14].

Stable adsorption on surfaces is associated with a gain in Gibbs free energy of adsorption which is typically given per adsorbing atom or molecule. However, in this paper we will normalize the Gibbs energy to surface area A_S as this is the relevant entity to address the stability of surface phases. The most stable adsorbate structure in thermal equilibrium is therefore the structure with the lowest Gibbs free energy of adsorption $\Delta\gamma$,

$$\Delta\gamma = \frac{1}{A_S}(G_{surf,ads} - G_{surf,0} - \sum_i n_i\mu_i). \quad (1)$$

In this equation $G_{surf,ads}$ and $G_{surf,0}$ are the Gibbs free energies of the adsorbate-covered and the clean surface, n_i is the number of adsorbed atoms of the type i per surface area A_S, and μ is the corresponding chemical potential of the ions in solution.

In the gas phase, the Gibbs free energy G and the chemical potential μ depend on temperature and partial pressure of the molecules. The latter corresponds to the thermodynamic activity in solution. As far as solids are concerned, the temperature and pressure-dependent change in the Gibbs energy is rather small compared with the change in the Gibbs energy of liquids or gases. Therefore it is feasible to neglect this dependence and to consider it only for the ions in solution $\mu_i(T, p_i)$.

Furthermore, the chemical potential of charged particles is influenced significantly by the presence of the electrode potential. This is reflected in the so-called electrochemical potential $\tilde{\mu} = \mu + zeU$, where z is an integer number for the charge of the particle, e the elementary electric charge and U the electrode potential. Note that we use the convention that the elementary electric charge is a negative number, in some publications a positive probe charge and an opposite sign are used. The adsorption energies of oxygen, hydrogen and hydroxyl on metal electrodes depend only very weakly on an applied electric field [14,42], which has been attributed to the small dipole moment associated with the adsorbed species [14]. Furthermore, it has been demonstrated that the energetics of the barriers in the formic acid degradation on Pt(111) is hardly influenced by varying an electric field [43]. This is obviously a consequence of the good screening properties of metals which is one of the reasons why the computational hydrogen electrode approach has been so successful in describing adsorption trends on metal electrodes as a function of the electrode potential.

Furthermore, a potential dependence of adsorption energies can also occur when the charge of an adsorbing ion is not fully transfered to the electrode but a fractional charge remains in the diffuse double layer, as discussed by Schmickler and Guidelli [44]. The exact amount of charge transfered to the electrode quantified through the so-called electrosorption valence cannot be measured, it can only be estimated, for example from the dipole moments associated with the adsorbed species [44]. Thus it could be shown that the electrosorption coefficients of halides adsorbed on Ag [45] and Au [46] are non-integer which is normally interpreted as an indication that double layer effects are important in adsorption.

However, the adsorption of Cl, Br and I on Pt(111) is associated with a strong polarization of the adsorbed atoms causing an anomalous work function change: it leads to a decrease of the work function instead of an increase as would be expected from the adsorption of negatively charged species [47,3,4]. In addition, a charge analysis yields a rather small net charge on the adsorbed halogen atoms [47]. This indicates that Pt acts differently compared to Ag and Au as far as the electrosorption valence in halide adsorption is concerned. This can be understood considering the fact that the d-band of Pt is not completely filled, in contrast to Ag and Au, resulting in a stronger interaction.

Table 1
Reduction potential of the halides considered in this work.

Redox couple	Reduction potential U^0 (V)
$\frac{1}{2}Cl_2 + e^- \rightleftharpoons Cl^-$	1.36
$\frac{1}{2}Br_2 + e^- \rightleftharpoons Br^-$	1.09
$\frac{1}{2}I_2 + e^- \rightleftharpoons I^-$	0.54

Jinnouchi et al. considered the influence of solvation and electric field effects by the electric double layer by combining explicit water layers and a implicit water model within a static solvation approximation [48]. They found that effects caused by the presence of the electric double layer on hydrogen adsorption energies are very small.

Hence we neglect the dependence of $G_{surf,ads}$ and $G_{surf,0}$ on temperature, partial pressure or activity, and electrode potential, so that Eq. (1) can be written as

$$\Delta\gamma = \frac{1}{A_S}\left(E_{surf,ads} - E_{surf,0} - \sum_i n_i\tilde{\mu}_i(T, p, U)\right). \quad (2)$$

The Gibbs energy G of both the adsorbate-covered and the clean surface can be evaluated using density functional theory (DFT) calculations. To be more precise, we can derive the internal energy U_{int} from the total energy E_{tot} in DFT. Furthermore, as the terms TS as well as pV are often quite small [49], we can approximate $G \approx U_{int}$.

To calculate the last term that corresponds to the electrochemical potential of the ions in solution, we use the concept of the computational hydrogen electrode [14]. It is based on the observation that under standard conditions (pH = 0, T = 298 K, p = 1 bar), defining the standard hydrogen electrode (SHE) there is an equilibrium between hydrogen molecules in the gas phase and solvated protons. Therefore the Gibbs free energy of the molecules in the gas phase μ_{H_2} is equal to the Gibbs free energy of the protons in aqueous solution plus the energy of an electron at the Fermi level in the metal $\tilde{\mu}_{H^+} + \tilde{\mu}_{e^-}$. Thus for this condition we do not need to compute the solvation energy of a proton in an aqueous solution but instead use the energy of the H_2 molecule in the gas phase as a reference which is much easier to derive from first principles. Note that within this approach it is the correct mode to consider the adsorption of a neutral hydrogen atom. This is equivalent to the assumption that upon adsorption the proton from solution recombines with the electron that has already be transfered to the Fermi energy.

Furthermore, it is also known how the electrochemical potential depends on concentration and electrode potential. For these other thermodynamic conditions we just have to correct the SHE expression by an additional term $-eU_{SHE}$ for the electrode potential and by $-k_BT\ln(10)$pH for the proton concentration.

$$\tilde{\mu}_{H^+} + \tilde{\mu}_{e^-} = \frac{1}{2}\mu_{H_2} - eU_{SHE} - k_BT\ln(10)\text{pH}. \quad (3)$$

Therefore it is possible to derive, starting from SHE conditions, the electrochemical potential at different electrode potentials and/or different concentrations. Hansen et al. pointed out that the same approach can be used for any redox couple $\frac{1}{2}A_2 + e^- \rightleftharpoons A^-$ [50]. In this way, this approach can be used to calculate the electrochemical potentials of any halides such as Cl^-, Br^-, and I^- by

$$\tilde{\mu}_{A^-} - \tilde{\mu}_{e^-} = \frac{1}{2}\mu_{A_2} + e(U_{SHE} - U^0) + k_BT\ln(a_{A^-}), \quad (4)$$

where U^0 is the reduction potential of the corresponding halide which are listed in Table 1, and a is the thermodynamic activity of the anion A^-. Since the reduction potential of hydrogen defines 0 V on the SHE scale, it does not appear in Eq. (3).

In the following, we will normalize the electrochemical potentials with respect to the total energy of the corresponding gas phase

species. The electrochemical potentials $\Delta\tilde{\mu}$ of the proton H^+ and the anions A^- are then given by

$$\begin{aligned}\Delta\tilde{\mu}_{H^+}(T,p,U) &= \tilde{\mu}_{H^+}(T,p,U) + \tilde{\mu}_{e^-} - \frac{1}{2}E_{H_2} \\ &= -eU_{SHE} - k_BT\ln(10)\text{pH}\end{aligned} \tag{5}$$

and

$$\begin{aligned}\Delta\tilde{\mu}_{A^-}(T,p,U) &= \tilde{\mu}_{A^-}(T,p,U) - \tilde{\mu}_{e^-} - \frac{1}{2}E_{A_2} \\ &= e(U_{SHE} - U^0) + k_BT\ln(a_{A^-})\end{aligned} \tag{6}$$

which means that the internal total energies $\frac{1}{2}E_{H_2}$ and $\frac{1}{2}E_{A_2}$, respectively, at standard conditions (that we will later derive from DFT calculations) have been taken out of the electrochemical potentials. When we then apply Eq. (2) to a co-adsorbed system of protons and halides, the Gibbs free energy of adsorption depends on the change of the chemical potentials of the protons $\Delta\tilde{\mu}_{H^+}(T,p,U)$ and the anions $\Delta\tilde{\mu}_{A^-}(T,p,U)$. Therefore the different co-adsorbed structures are planes in a three-dimensional diagram, where the *x*- and *y*-axes are the terms $\Delta\tilde{\mu}_{H^+}(T,p,U)$ and $\Delta\tilde{\mu}_{A^-}(T,p,U)$ and the *z*-axis corresponds to the Gibbs free energy of adsorption $\Delta\gamma$,

$$\Delta\gamma(T,p,U) = \frac{1}{A_S}(E_{ads}^{tot} - \sum_i n_i\Delta\tilde{\mu}_i(T,p,U)). \tag{7}$$

The adsorption energy E_{ads}^{tot} of n_H hydrogen atoms and n_A halide atoms per unit cell (with A=Cl, Br, or I) is evaluated according to

$$E_{ads}^{tot} = E_{ads/slab} - E_{slab} - \frac{n_H}{2}E_{H_2} - \frac{n_A}{2}E_{A_2} \tag{8}$$

where $E_{ads/slab}$, E_{slab}, E_{H_2} and E_{A_2} are the total energies of the adsorbate-covered metal slab, the isolated metal slab, the H_2 molecule and the A_2 halogen molecule, respectively. Note that in the following we will neglect any dependence of E_{ads}^{tot} on the thermodynamic conditions.

At given thermodynamic conditions, the stable adsorbate structure is given by the plane with the lowest Gibbs free energy of adsorption. It should be emphasized, that each area of stable equilibrium structures is derived from one DFT structure optimization. This makes the model computationally very attractive. However, the dependence of the adsorption energies on the presence of the electrolyte and of varying electrode potentials is entirely neglected. In principle, these dependencies can be included in the formalism of the computational hydrogen electrode. They are not taken into account here for the following reasons. First, adsorption energies of specifically adsorbed species such as hydrogen or CO are hardly modified by the presence of water, as shown by DFT calculations [51]. Furthermore, using an implicit water model is was also shown by first-principles calculations that H, O, and OH adsorption energies on Pt(111) are only modified by less than 0.1 eV due to the presence of water [52]. We also considered the interaction of an explicit water layer with a halide adsorbate layer at higher coverage above 0.3. We found that water molecules do not penetrate the halide layer but rather form a flat and dense water network above the adsorbed halide atoms indicative of a weak interaction. Second, on metals there is also little influence of any varying electric field on the adsorption energy [14], as already mentioned above.

Note also that the adsorption of hydroxide ions on the Pt(111) surface, which are always present in water, is not considered here as it is suppressed through the presence of halides because their adsorption energy of 1.2 to 1.7 eV is larger than the OH-adsorption energy [53].

All DFT calculations in this paper were performed in a periodic supercell approach, using the density functional program VASP [54]. The exchange and correlation energy was taken into account by the functional of Perdew, Burke and Ernzerhof (PBE) [55]. For the electron-core interaction the projector augmented wave method was used [56,57]. The electronic one-particle wave functions were expanded in a plane-wave basis set up to an energy cutoff of 500 eV.

The metal surface was represented by a slab of five atomic layers, the lower two layers were kept fixed at their bulk positions during the calculations and the upper three layers were completely relaxed. To model a variety of different surface structures and coverages, (3×3), $c(4\times2)$ and $(\sqrt{7}\times\sqrt{7}R19.1^\circ)$ surface unit cells were considered containing between 9 and 12 metal atoms per layer. The integration over the first Brillouin zone was done using a gamma-centered *k*-point mesh with $7\times7\times1$ special *k*-points and a Methfessel-Paxton smearing of 0.1 eV [58].

Table 2
Experimentally found surface structures of halides and co-adsorbed hydrogen on Pt(111).

Halide	Structure	Θ (ML)	Refs.
Cl	(3×3)	0.44	[16–21]
Cl	$c(4\times2)$	0.50	[20]
Br	(3×3)	0.44	[22–26]
Br	$(3\times3\sqrt{3}/2)$	0.44	[27]
Br	$(\sqrt{7}\times\sqrt{7}R19.1^\circ)$	0.57	[22]
I	$\sqrt{3}\times\sqrt{3}$	0.33	[28–31]
I	(3×3)	0.44	[22,30,32–35]
I	$(\sqrt{7}\times\sqrt{7}R19.1^\circ)$	0.43	[22,28–36]

3. Results and Discussion

3.1. Experimental data

Before discussing the results of our calculations, we first review the available experimental data on halide adsorption on Pt(111). Table 2 summarizes the results of some experimental studies of halide adsorption, which have been performed in UHV, air, or in electrochemical environments. Structures have been studied through both UHV and electrochemical in-situ techniques. Coverage/packing densities of adsorbed halides were deduced from Auger spectroscopic data in the vast majority of these studies. While several ordered structures of halides were found, a degree of uncertainty is always present in the assignment of adsorption sites.

As far as co-adsorbed systems are concerned, there are several studies that used HCl to introduce chlorine onto Pt(111) in UHV environments. High-resolution electron energy loss spectroscopy experiments [21] gave no hint of a Cl-H stretch for all HCl exposures used, indicating that HCl, upon adsorption, undergoes dissociation. Several studies [21,59] have suggested that the adsorption of HCl molecules does not simply lead to a Cl-covered platinum (111) surface, but to a metal surface that is covered by both adsorbed atomic H and Cl. Low exposures (up to 0.25 L) of HCl undergo complete dissociation on Pt(111) at 90 K to form a disordered mixture of adsorbed H and adsorbed Cl. The simple kinetics and lack of an ordered LEED pattern in this regime suggests high mobility of the adatoms and/or adsorption into a well-mixed, disordered phase containing both adsorbed H and adsorbed Cl [21].

Wagner et al. [21] also found that exposures of 0.5 to 2 L HCl produce an ordered (3×3) phase in UHV. The fact that the same LEED pattern is seen for dosed HCl as for dosed Cl_2 shows that the Pt-Cl interaction is sufficiently strong to establish the Cl adsorption structure. It has been suggested [21] that the co-adsorbed H is simply located in the areas unoccupied by Cl. The structure of the H atoms within the field of Cl atoms is unknown. One can question whether such structures even exist since H adatoms on pristine metal surfaces could be very mobile [60], but we also note that the presence of other adsorbed species can raise surface diffusion barriers [61], stabilizing co-adsorption. Hydrogen is

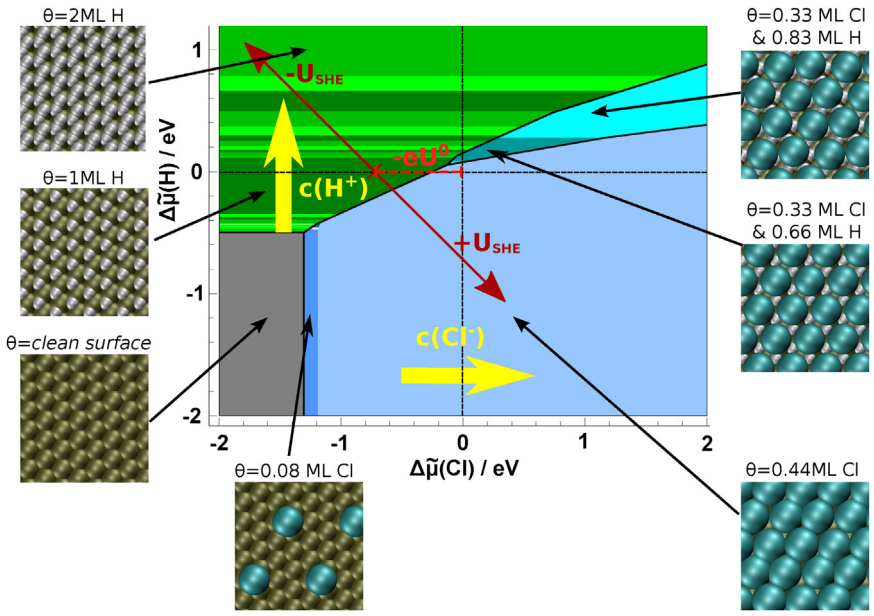

Fig. 1. Stable phases of co-adsorbed chlorine and hydrogen on Pt(111) as a function of the electrochemical potential of hydrogen and chlorine. The green areas correspond to hydrogen-containing adsorbate structures, the blue areas to chlorine-containing structures and the cyan areas to mixed structures of both hydrogen and chlorine. The yellow arrows illustrate the effect of increasing the concentration of the species individually. The red double-arrow represents the effect of varying the electrode potential for fixed concentrations.

believed to be co-adsorbed because the H_2 desorption following HCl dosing, though small, significantly exceeds the desorption area of background-derived hydrogen [21]. Adsorbed hydrogen leaves the surface through competing processes producing both H_2 and HCl. In contrast, in the study of Fukushima et al. [62] no hydrogen desorption was observed which led to the suggestion that atomic hydrogen and chloride exists in equal amounts on the (3×3) structures.

Chemisorbed iodide ions have been found to cause an overall decrease in the amount of adsorbed hydrogen on polycrystalline Pt surfaces [63]. There is practically no hydrogen adsorption on the surface covered by a monolayer of adsorbed iodide ions. This is consistent with the fact that on Pt(111), iodine forms a protective layer which prevents readsorption of contaminants while the clean sample cools to room temperature. Therefore it is possible to investigate iodine-covered Pt surfaces using STM in air [33,34]. On the other hand, a monolayer of hydrogen was claimed to be adsorbed even when the surface is covered by the maximum amount of chloride and bromide anions [63]. From the observed increase in the second peak in the I-V curves, which corresponds to more weakly-bound H, it has been concluded that adsorbed chloride and bromide on polycrystalline Pt affect the energy distribution of adsorbed hydrogen (decreasing the bond energy, rather than the total amount adsorbed), while the total amount of the adsorbed H does not change [63]. This is supported by the finding that different reaction rates on Pt(100) were obtained with and without hydrogen transfer, attributed to interdiffusion of adsorbed hydrogen atoms in mixed chloride domains [64].

In electrochemical environments, it has been reported earlier [65] that the co-adsorption of chloride and hydrogen atoms has a synergistic character: the presence of hydrogen adatoms enhances chloride adsorption. This conclusion was however later shown to be a result of a surface that contained step defects [66,59]. In these particular studies it was demonstrated that at positive potentials, where Cl and H adsorption overlap, the adsorption has a competitive character. There is also evidence that the adatoms are not necessarily ionic at electrode-electrolyte interfaces, as the surface dipole is close to zero [59]. This is confirmed by DFT calculations which show that chlorine adsorption has an covalent character and that even a pure chlorine coverage does not cause an significant change in the surface dipole moment [47,4].

3.2. Calculated phase diagrams for halide-hydrogen co-adsorption

In order to evaluate the phase diagram of stable halide-hydrogen co-adsorption phases, we first calculated the adsorption energies of 113 different structures within (3×3), $c(4 \times 2)$ and $(\sqrt{7} \times \sqrt{7}R19.1^\circ)$ geometries. The corresponding adsorption energies E_{ads} (Eq. (8)) that are listed in the supplementary material were then used in Eq. (7) to construct the planes giving the Gibbs free energy of adsorption $\Delta\gamma$ as a function of the electrochemical potentials $\Delta\tilde{\mu}_{A^-}$ and $\Delta\tilde{\mu}_{H^+}$.

In Fig. 1, the stable phases of co-adsorbed chlorine and hydrogen on Pt(111) as a function of the electrochemical potential of hydrogen and chlorine are plotted. The electrochemical potential depends on the concentration of the species and the electrode potential. The yellow arrows illustrate how the electrochemical potential varies when the concentrations of the chlorine anions and the protons are varied separately, the red arrows indicate the effect of varying the electrode potential for fixed concentrations. The structures of some of the stable phases are illustrated in the pictures surrounding the phase diagram.

It is interesting to note that only a very small portion of the phase diagram corresponds to a true co-adsorption structure of hydrogen and chlorine. The phase diagram is dominated by areas that correspond either to pure hydrogen-adsorption or pure chlorine-adsorption phases or to the clean surface. As mentioned above, one would naively expect that there is some electrostatic attraction between adsorbed cations (protons) and anions (chloride). However, the simple picture of anionic adsorption of halides on metal surfaces is obviously not correct. Experimentally, it is well-known that the adsorption of halogen atoms on metal surfaces leads to a reduction of the metal work function at low coverages [16,24]. In principle, one would expect an increase in the work function upon the adsorption of negatively charged species. We have recently shown in a periodic DFT study that these anomalous work function changes upon halogen adsorption can be explained by the

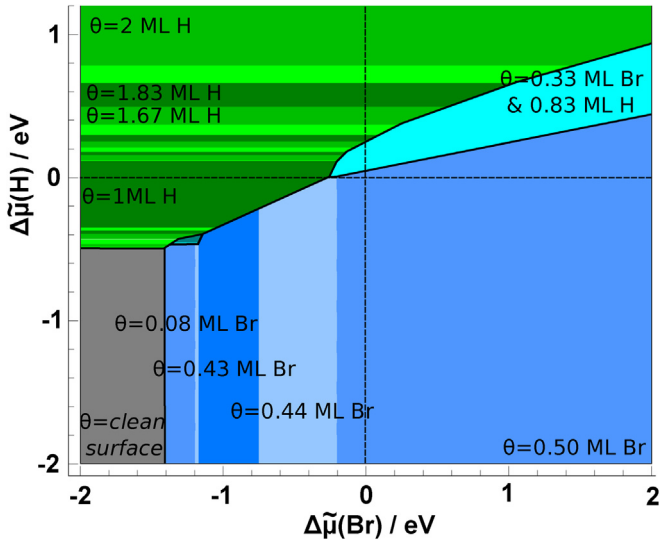

Fig. 2. Stable phases of co-adsorbed bromine and hydrogen on Pt(111) as a function of the electrochemical potentials of hydrogen and bromine.

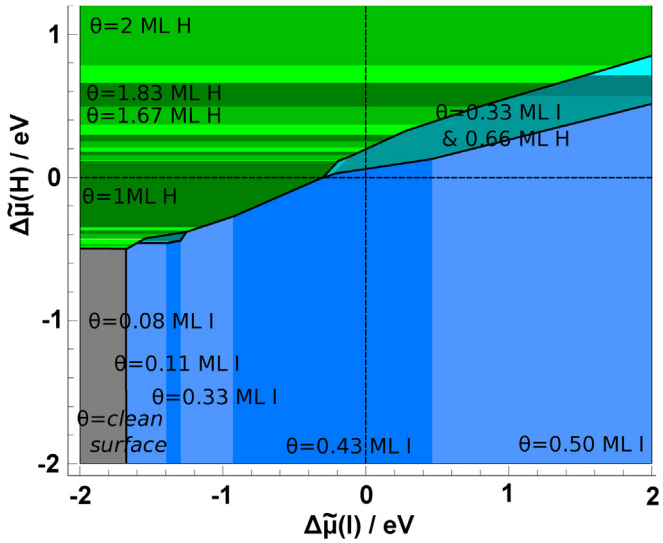

Fig. 3. Stable phases of co-adsorbed iodine and hydrogen on Pt(111) as a function of the electrochemical potentials of hydrogen and iodine.

significant polarization of the adsorbed halogen atoms [3] which is particularly strong for iodine, but also present for bromine and chlorine [47,4]. There is still a rather small net negative charge on the adsorbed halides, but the atomic polarization leads to a dipole moment at the surface that is opposite to what is expected for the adsorption of negatively charged species. Hydrogen adsorption on Pt(111) also leads to a small decrease in the work function [67], which means that there is a dipole-dipole repulsion between adsorbed hydrogen and halides. Furthermore, there might also be an indirect effect through the modification of the electronic and thus chemical properties of the Pt(111) electrode upon the adsorption of the species that leads to an effective repulsion [7,8]. According to the calculated phase diagram, mixed structures may only exist for unusually high concentrations of both anions and protons.

We have furthermore also evaluated the phase diagram of stable phases of hydrogen co-adsorbed with bromine (see Fig. 2) and iodine (Fig. 3). In principle, the phase diagrams of the three halides on Pt(111) look rather similar, indicating that the interactions of the adsorbed halides are comparable. For instance, our calculations yielded that the stabilities of the c(4 × 2) and the (3 × 3) halides structures are rather similar.

Still, there are characteristic differences. In the chloride adsorption regime, Pt(111) is covered with the dense (3 × 3) structure over a broad range of electrochemical potentials, whereas iodine shows five different stable patterns. Iodine is the only halide that exhibits a stable $\sqrt{3} \times \sqrt{3}$ adsorption structure at a coverage of 1/3 ML as has also been observed in experiments [28–31]. This $\sqrt{3} \times \sqrt{3}$ adsorption phase is particularly stable for iodine [13] compared to the higher coverage phases which might be caused by the fact that at higher coverages the significantly larger size of iodine compared to bromine and chlorine leads to a relatively larger repulsive interaction. Furthermore, iodine is the only halide for which the $(\sqrt{7} \times \sqrt{7}R19.1^\circ)$ structure is stable at a coverage of 3/7 ML at larger electrochemical potentials, again in agreement with the experiment [22,28–31,36,32–35].

We now focus on the regime in which hydrogen adsorption is stable. It is well known that under electrochemical conditions and low potentials, Pt(111) is covered by hydrogen [37,38]. There is still some controversy between experiment and theory regarding the exact hydrogen equilibrium coverage. Whereas experiments indicate that a full monolayer of adsorbed hydrogen on Pt(111) is only complete at -0.1 V and Pt(111) becomes only partially hydrogen-covered at higher potentials [68,38], DFT calculations rather yield a hydrogen coverage of 1 ML at positive potentials [69,39,52]. This is in fact also the case for our calculations here (for $\Delta\tilde{\mu}_{H^+} = 0\,eV$). Still, there is a qualitative agreement that there is a significant hydrogen coverage. Furthermore, note that a recent DFT study [70] using a charged electrode with the counter charge in a polarized electrolyte [71] closely supports the recent experimental findings [68] with respect to the hydrogen coverage as a function of potential.

In the electrochemical literature, this strongly-adsorbed hydrogen is typically referred to as underpotential deposited (upd) hydrogen [1]. The presence of this hydrogen upd layer also has a significant influence on the water structure on Pt(111) at low potential as it weakens the metal-water interaction [72].

There is another, weakly-adsorbed hydrogen species that has been observed which is called overpotential deposited (opd) hydrogen [1]. The role of this opd hydrogen in the hydrogen electrocatalysis has just been intensively discussed from a theoretical point of view [73]. In particular, on transition metal surfaces, this weakly-bound species might play an important role in the hydrogen evolution reaction which is for example a crucial step in the electrolysis of water [74]. Our calculations confirm that at more positive chemical potentials of hydrogen much higher coverages become stable, reflected the presence of opd hydrogen on Pt(111).

Note that the precise structure of ordered hydrogen phases on Pt(111) at different coverages is hard to identify by experimental techniques. This is due to two reasons: as hydrogen is a very weak scatterer, it cannot be easily detected by LEED, X-ray scattering, or STM. Furthermore, hydrogen can be very mobile – the hydrogen adatom's diffusion barrier on Pt(111) is in the order of only 0.06 eV, and can even be effectively lower when delocalized nuclear quantum states of the hydrogen atom are considered [60,75].

3.3. Adsorbate structures as a function of electrode potential

In electrochemical experiments, results are usually not reported as a function of electrochemical potentials, but rather as a function of the electrode potential for a given pH value and ion concentration. This information is all included in the phase diagrams Figs. 1–3. However, the explicit dependence of the stability of the considered adsorption phases on the electrode potential is not directly visible as the electrochemical potential scale has to be converted into an electrode potential scale. In fact, a variation of the electrode

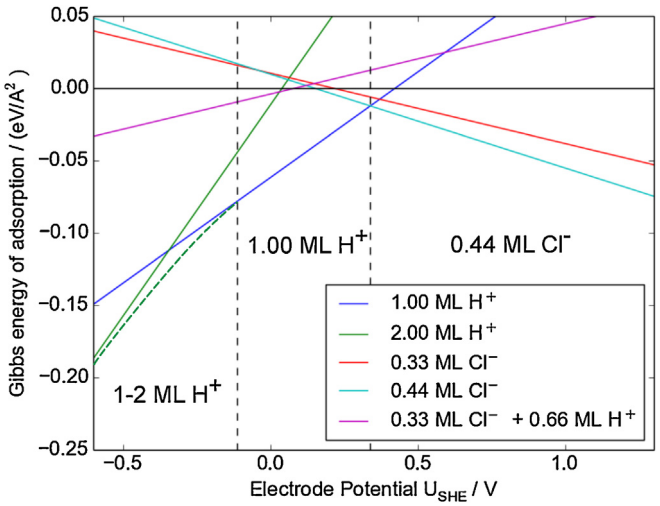

Fig. 4. Calculated electrochemical equilibrium coverage of chlorine and hydrogen, co-adsorbed on a Pt(111) surface under standard conditions. At low electrode potentials, a variety of different stable hydrogen coverages between one and two ML exists (compare Figs. 1–3). To keep the figure comprehensive and clear, the Gibbs energy of these coverages are represented by a green, dashed line and exemplified by the 1 and 2 ML structures.

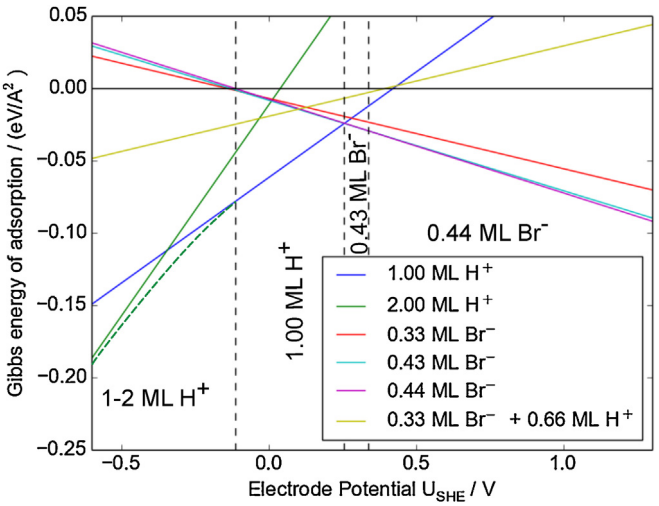

Fig. 5. Calculated electrochemical equilibrium coverage of bromine and hydrogen, co-adsorbed on a Pt(111) surface under standard conditions. The hydrogen coverage phases at low electrode potentials are represented in the same way as in Fig. 4.

potential with all other parameters kept unchanged corresponds to a diagonal cut through the two-dimensional phase diagrams, as illustrated in Fig. 1. The exact position of this diagonal depends on the concentrations.

In a previous paper, we addressed equilibrium adsorbate structures of halides on Cu(111) and Pt(111) as a function of the electrode potential, but without taking the effect of co-adsorbed hydrogen into account [13]. Here we present the stable structures of chlorine, bromine and iodine as a function of the electrode potential in Figs. 4–6, but this time with taking into account the presence of protons in the electrolyte. Furthermore, we have considered more possible structures than done in Ref. [13].

The diagrams in Figs. 4–6 still correspond to a given combination of pH value and anion activity. For all three figures, we have assumed "standard conditions", i.e., we have assumed pH = 0 and $a_{A^-} = 1$. This means that the cuts correspond to diagonals with slope −1 through the points $(\Delta\tilde{\mu}_{A^-}, \Delta\tilde{\mu}_{H^+}) = (-eU^0, 0)$ in the two-dimensional phase diagrams where U^0 is the corresponding reduction potential of the halides listed in Tab. 1. For these conditions, the free energy of adsorption can be expressed as

$$\Delta\gamma(U_{SHE}) = \frac{1}{A_S}(E^{tot}_{ads} - n_A e(U_{SHE} - U^0) + n_H e U_{SHE}). \quad (9)$$

For the pure halide and the pure hydrogen adsorption phases this equation simplifies to [13]

$$\Delta\gamma_{A^-}(U_{SHE}) = \frac{n_A}{A_S}(E^{A^-}_{ads} - e(U_{SHE} - U^0)) \quad (10)$$

$$\Delta\gamma_{H^+}(U_{SHE}) = \frac{n_H}{A_S}(E^{H^+}_{ads} + eU_{SHE}) \quad (11)$$

where E^i_{ads} is the adsorption energy per adatom, E^{tot}_{ads}/n_i. For other concentrations in the electrolyte, the reference point in the phase diagram needs to be shifted by $k_B T \ln a_{A^-}$ and/or by $k_B T \ln(10)$pH which at room temperature, e.g., corresponds to about 59 meV if the activity is changed by one order of magnitude or if the pH is changed by one, respectively.

Again, the one-dimensional cuts through the phase diagrams for chlorine, bromine and iodine co-adsorption with hydrogen plotted in Figs. 4–6 look rather similar which is not too surprising considering the fact that the phase diagrams are rather similar. For all considered systems, no ordered co-adsorption phase becomes stable as a function of electrode potential. The calculated dependence of the free energy of adsorption of the purely hydrogen-covered phases on the electrode potential agrees well with recent results obtained in DFT calculations with the aqueous electrolyte represented in a implicit solvent model [52]. There is a region at intermediate potentials in which both hydrogen adsorption and halide adsorption alone are thermodynamically stable, however, the adsorption has a competitive character, i.e., at lower potentials hydrogen adsorption is more stable, at higher potentials halide adsorption becomes more stable.

In the case of chloride and hydrogen adsorption on Pt(111) (see Fig. 4), chloride adsorption becomes thermodynamically stable at a potential of about 0.35 V. Experimentally, measurements of the chloride and the hydrogen Gibbs excesses [66,59] showed that in a narrow potential range $0.2 < U < 0.3$ V (SHE) hydrogen and chloride can adsorb simultaneously on Pt(111). Still, the analysis of the electrosorption valencies implies that the adsorption of hydrogen and chloride has a competitive character [66,59].

Note that the driving force for the adsorption of ions from solution is the gain in free energy per area upon adsorption. Hence an electrode surface might remain uncovered even when ions are present in solution as it rather corresponds to an open system in contact with a reservoir. This means that in contrast to, e.g., solid solutions the concentration of ions on the surface is no parameter that can be modified continuously. Consequently, two distinct adsorbate phases can in principle only exist simultaneously on the surface if they are associated with exactly the same free energy of adsorption per area, which is realized at the potentials in Figs. 4–6 where the curve of the most favorable hydrogen adsorption phase crosses the curve of the most favorable halide adsorption phase. These considerations imply that thermodynamically, the competitive co-adsorption of two distinct adsorption phases over a range of potentials should not be possible if the dependence of their free energies of adsorption on the electrode potential is different. However, the experimental results concerning the co-adsorption of hydrogen and chloride were derived from cyclic voltammetry so that kinetic effects influence the results. Hence we believe that the experimental findings of hydrogen and chloride co-adsorption in a competitive manner over a narrow potential range are not at variance with our conclusions based on the surface phase diagrams.

As far as bromine (Fig. 5) and iodine adsorption (Fig. 6) on Pt(111) is concerned, these systems should also not exhibit any synergistic character according to the phase diagrams, but rather be

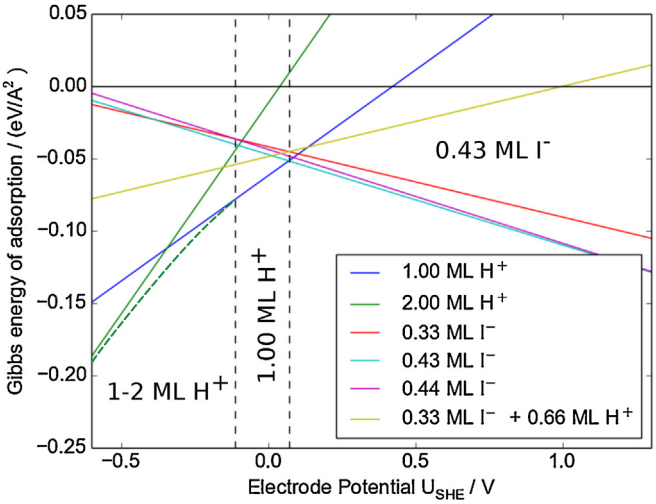

Fig. 6. Calculated electrochemical equilibrium coverage of iodine and hydrogen, co-adsorbed on a Pt(111) surface under standard conditions. The hydrogen coverage phases at low electrode potentials are represented in the same way as in Fig. 4.

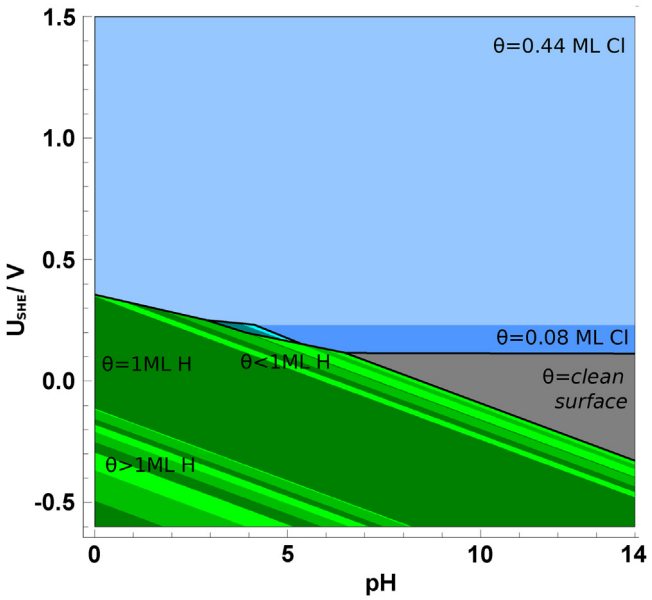

Fig. 7. Calculated Pourbaix diagram, i.e., a map of the stable phases of co-adsorbed chlorine and hydrogen on Pt(111) as a function of pH and electrode potential for a fixed chlorine concentration corresponding to an activity of 0.1.

competitive with respect to hydrogen co-adsorption. And indeed, for bromine adsorption, these results are consistent with the experimental observation that the substitution of hydrogen by bromine at Pt(111) [27,76] and Pt(100) [77,78] takes place in a very narrow potential range. Also for iodine adsorption on Pt(111), there is experimental evidence for the competitive character of the co-adsorption with hydrogen [30,79]. Note that according to our calculations the onset of halide adsorption for bromine and iodine is shifted to lower electrode potentials compared to chlorine. This is caused by their stronger binding to Pt(111) [13], but also by their lower reduction potentials, as an analysis of Eq. (10) indicates.

Note that we extended the electrode potential range in Figs. 4–6 to negative values below −0.5 V. In principle, at negative potentials hydrogen evolution would take place which is, however, kinetically hindered. For that reason, it is also experimentally possible to scan to negative electrode potentials. Our calculations show that at potentials below -0.1 V hydrogen coverages larger than unity should become stable. This reflects the experimentally well-established observation of the occurrence of opd hydrogen. Finally, we like to emphasize that the phase diagrams shown in Figs. 1, 2 and 3 can be directly transformed into Pourbaix diagrams, i.e., into maps of the stable phases as a function of pH and electrode potential. Taking the coadsorption of chlorine and hydrogen as an example, the phases along the red double arrow in Fig. 1 correspond to a cut through the Pourbaix diagram for pH=0 and a given Cl concentration that corresponds to an activity of one, i.e. this cut corresponds to the y-axis of a Pourbaix diagram. The whole Pourbaix diagram at room temperature can then be constructed by shifting the arrow by −59 meV along the y-axis of Fig. 1 for a change of the pH value by one and recording the phases along the arrow. Deriving the Pourbaix diagram from the phase diagram Fig. 1 thus corresponds to transforming a parallelogram into a rectangle.

As an example, we plot in Fig. 7 the Pourbaix diagram of co-adsorbed chlorine and hydrogen on Pt(111) for a fixed chlorine concentration with an activity of 0.1 which for an ideal solution would correspond to a chloride concentration of 0.1 M. The Pourbaix diagram contains regions of pure hydrogen adsorbate phases in greenish colors, pure chlorine phases in bluish colors and a region where the clean Pt(111) surface is stable in grey. There is also a very small region at about pH≈4 and $U \approx 0.2$ V where mixed hydrogen/chloride phases on Pt(111) are stable that are almost not visible in Fig. 1. The boundaries of the pure hydrogen phases exhibit a slope of −59 meV per change of the pH value of 1 which reflects the fact that hydrogen is involved in the formation of these phases. In contrast, the horizontal boundaries between the pure chlorine phases and the clean surface are indicative of the fact that hydrogen is not involved in the formation of these phases so that their absolute stability is independent of the pH value.

4. Conclusions

The co-adsorption of hydrogen with the halides chlorine, bromine and iodine on Pt(111) surface has been studied by density functional theory calculations. Using a thermodynamic model based on the concept of the computational hydrogen electrode, the stable adsorbate phases as a function of the electrochemical potentials of hydrogen and halides have been derived. Because of the repulsive interaction between adsorbed hydrogen and halogen atoms, their adsorption is mainly competitive, which means that either purely hydrogen-covered phases or purely halogen-covered phases are stable.

By performing cuts through the two-dimensional phase diagram we have determined the stable adsorbate structures on Pt(111) as a function of the electrode potential. In the presence of chloride anions, according to our calculations there is small potential window in which hydrogen and chloride could in principle both adsorb individually on Pt(111). Still, their adsorption occurs in a competitive way which means that there is an electrode potential at which adsorbed hydrogen is replaced by chlorine upon increasing the electrode potential. As adsorbate phases correspond to an open system in contact with a reservoir, in thermal equilibrium no phase-separated co-existence of two immiscible adsorbate structures can occur except when their free energy of adsorption per area is exactly the same. Nevertheless, due to kinetic hindering there might still be a potential range over which the simultaneous adsorption of two separate phases might be observed. These findings are in good agreement with corresponding experiments.

For bromine and iodine adsorption, the phase diagrams for the co-adsorption with hydrogen look very similar, only the replacement of hydrogen by these halides occurs at lower electrode potentials, caused by their stronger binding to Pt(111) and their lower reduction potentials. In general, our study confirms that the concept of the computational hydrogen electrode is rather useful

for determining the structure of metal electrode/electrolyte interfaces.

Acknowledgments

Useful discussion with Karsten Reuter, Technical University of Munich, Jacek Lipkowski, University of Guelph, and Sung Sakong, Universiy of Ulm, are gratefully acknowledged. This research has been supported by the German Science Foundation (DFG) through the research unit FOR 1376 (DFG contract GR 1503/21-2) and by the Baden-Württemberg Foundation within the Network of Competence "Functional Nanostructures" through project CT-04 ORR-Scale of the CleanTech program. The numerical work was performed on the computational resource bwUniCluster funded by the Ministry of Science, Research and Arts and the Universities of the State of Baden-Württemberg, Germany, within the framework program bwHPC5.

Appendix A. Supplementary Data

Supplementary data associated with this article can be found, in the online version, at http://dx.doi.org/10.1016/j.electacta.2016.08.117.

References

[1] W. Schmickler, E. Santos, Interfacial Electrochemistry, 2nd edition, Springer, Berlin, 2010.
[2] O.M. Magnussen, Chem. Rev. 107 (2002) 679.
[3] T. Roman, A. Groß, Phys. Rev. Lett. 110 (2013) 156804.
[4] T. Roman, F. Gossenberger, K. Forster-Tonigold, A. Groß, Phys. Chem. Chem. Phys. 16 (2014) 13630.
[5] S. Trasatti, Pure Appl. Chem. 58 (1986) 955.
[6] E. Spohr, G. Toth, K. Heinzinger, Electrochim. Acta 41 (1996) 2131.
[7] C.M. Wei, A. Groß, M. Scheffler, Phys. Rev. B 57 (1998) 15572.
[8] B. Hammer, Phys. Rev. B 63 (2001) 205423.
[9] M. Arenz, V. Stamenkovic, T. Schmidt, K. Wandelt, P. Ross, N. Markovic, Surf. Sci. 523 (2003) 199.
[10] D.V. Tripkovic, D. Strmcnik, D. van der Vliet, V. Stamenkovic, N.M. Markovic, Faraday Discuss. 140 (2009) 25.
[11] A. Groß, Surf. Sci. 608 (2013) 249.
[12] Z. Shi, S. Wu, J. Lipkowski, Electrochim. Acta 40 (1995) 9.
[13] F. Gossenberger, T. Roman, A. Groß, Surf. Sci. 631 (2015) 17.
[14] J.K. Nørskov, J. Rossmeisl, A. Logadottir, L. Lindqvist, J.R. Kitchin, T. Bligaard, H. Jónsson, J. Phys. Chem. B 108 (2004) 17886.
[15] I.T. McCrum, S.A. Akhade, M.J. Janik, Electrochim. Acta 173 (2015) 302.
[16] W. Erley, Surf. Sci. 94 (1980) 281.
[17] D.A. Stern, H. Baltruschat, M. Martinez, J.L. Stickney, D. Song, S.K. Lewis, D.G. Frank, A.T. Hubbard, J. Electroanal. Chem. 217 (1987) 101.
[18] I. Villegas, M.J. Weaver, J. Phys. Chem. 100 (1996) 19502.
[19] R. Schennach, E. Bechtold, Surf. Sci. 380 (1997) 9.
[20] M. Song, M. Ito, Bull. Korean Chem. Soc. 22 (2001) 267.
[21] F.T. Wagner, T.E. Moylan, Surf. Sci. 216 (1989) 361.
[22] C.A. Lucas, N.M. Marković, P.N. Ross, Phys. Rev. B 55 (1997) 7964.
[23] G.N. Salaita, D.A. Stern, F. Lu, H. Baltruschat, B.C. Schardt, J.L. Stickney, M.P. Soriaga, D.G. Frank, A.T. Hubbard, Langmuir 2 (1986) 828.
[24] E. Bertel, K. Schwaha, F. Netzer, Surf. Sci. 83 (1979) 439.
[25] S. Tanaka, S.-L. Yau, K. Itaya, J. Electroanal. Chem. 396 (1995) 125.
[26] B.C. Schardt, J.L. Stickney, D.A. Stern, A. Wieckowski, D.C. Zapien, A.T. Hubbard, Langmuir 3 (1987) 239.
[27] J.M. Orts, R. Gómez, J.M. Feliu, A. Aldaz, J. Clavilier, J. Phys. Chem. 100 (1996) 2334.
[28] T.E. Felter, A.T. Hubbard, J. Electroanal. Chem. 100 (1979) 473.
[29] H. Farrell, Surf. Sci. 100 (1980) 613.
[30] F. Lu, G.N. Salaita, H. Baltruschat, A.T. Hubbard, J. Electroanal. Chem. 222 (1987) 305.
[31] S.L. Yau, C.M. Vitus, B.C. Schardt, J. Am. Chem. Soc. 112 (1990) 3677.
[32] J.L. Stickney, S.D. Rosasco, G.N. Salaita, A.T. Hubbard, Langmuir 1 (1985) 66.
[33] B.C. Schardt, S.-L. Yau, F. Rinaldi, Science 243 (1989) 1050.
[34] S.C. Chang, S.L. Yau, B.C. Schardt, M.J. Weaver, J. Phys. Chem. 95 (1991) 4787.
[35] J. Inukai, Y. Osawa, M. Wakisaka, K. Sashikata, Y.-G. Kim, K. Itaya, J. Phys. Chem. B 102 (1998) 3498.
[36] J. Stickney, S. Rosasco, A. Hubbard, J. Electrochem. Soc. 131 (1984) 260.
[37] T. Schmidt, N. Markovic, J. Electroanal. Chem. 524 (2002) 252.
[38] N.M. Marković, P.N. Ross Jr., Surf. Sci. Rep. 45 (2002) 117.
[39] S. Schnur, A. Groß, Catal. Today 165 (2011) 129.
[40] J. Rogal, K. Reuter, M. Scheffler, Phys. Rev. B 75 (2007) 205433.
[41] S.T. Marshall, J.W. Medlin, Surf. Sci. Rep. 66 (2011) 173.
[42] J. Rossmeisl, J.K. Nørskov, C.D. Taylor, M.J. Janik, M. Neurock, J. Phys. Chem. B 110 (2006) 21833.
[43] H.-F. Wang, Z.-P. Liu, J. Phys. Chem. C 113 (2009) 17502.
[44] W. Schmickler, R. Guidelli, Electrochim. Acta 127 (2014) 489.
[45] M.L. Foresti, M. Innocenti, F. Forni, R. Guidelli, Langmuir 14 (1998) 7008.
[46] J. Lipkowski, Z. Shi, A. Chen, B. Pettinger, C. Bilger, Electrochim. Acta 43 (1998) 2875.
[47] F. Gossenberger, T. Roman, K. Forster-Tonigold, A. Groß, Beilstein J. Nanotechnol. 5 (2014) 152.
[48] R. Jinnouchi, K. Kodama, Y. Morimoto, J. Electroanal. Chem. 716 (2014) 31.
[49] K. Reuter, M. Scheffler, Phys. Rev. B 65 (2001) 035406.
[50] H.A. Hansen, I.C. Man, F. Studt, F. Abild-Pedersen, T. Bligaard, J. Rossmeisl, Phys. Chem. Chem. Phys. 12 (2010) 283.
[51] A. Roudgar, A. Groß, Chem. Phys. Lett. 409 (2005) 157.
[52] S. Sakong, M. Naderian, K. Mathew, R.G. Hennig, A. Groß, J. Chem. Phys. 142 (2015) 234107.
[53] N. Marković, H. Gasteiger, B. Grgur, P. Ross, J. Electroanal. Chem. 467 (1999) 157.
[54] G. Kresse, J. Furthmüller, Phys. Rev. B 54 (1996) 11169.
[55] J.P. Perdew, K. Burke, M. Ernzerhof, Phys. Rev. Lett. 77 (1996) 3865.
[56] P.E. Blöchl, Phys. Rev. B 50 (1994) 17953.
[57] G. Kresse, D. Joubert, Phys. Rev. B 59 (1999) 1758.
[58] M. Methfessel, A.T. Paxton, Phys. Rev. B 40 (1989) 3616.
[59] N. Garcia-Araez, V. Climent, E. Herrero, J.M. Feliu, J. Lipkowski, J. Electroanal. Chem. 582 (2005) 76.
[60] S.C. Badescu, P. Salo, T. Ala-Nissila, S.C. Ying, K. Jacobi, Y. Wang, K. Bedürftig, G. Ertl, Phys. Rev. Lett. 88 (2002) 136101.
[61] T. Roman, H. Nakanishi, H. Kasai, Phys. Chem. Chem. Phys. 10 (2008) 6052.
[62] T. Fukushima, M.-B. Song, M. Ito, Surf. Sci. 464 (2000) 193.
[63] V.S. Bagotzky, Y.B. Vassilyev, J. Weber, J.N. Pirtskhalava, J. Electroanal. Chem. 27 (1970) 31.
[64] B. Klötzer, E. Bechtold, Surf. Sci. 326 (1995) 218.
[65] N. Li, J. Lipkowski, J. Electroanal. Chem. 491 (2000) 95.
[66] N. Garcia-Araez, V. Climent, E. Herrero, J. Feliu, J. Lipkowski, J. Electroanal. Chem. 576 (2005) 33.
[67] P. Ferrin, S. Kandoi, A.U. Nilekar, M. Mavrikakis, Surf. Sci. 606 (2012) 679.
[68] D. Strmcnik, D. Tripkovic, D. van der Vliet, V. Stamenkovic, N. Markovic, Electrochem. Comm. 10 (2008) 1602.
[69] E. Skúlason, G.S. Karlberg, J. Rossmeisl, T. Bligaard, J. Greeley, H. Jónsson, J.K. Nørskov, Phys. Chem. Chem. Phys. 9 (2007) 3241.
[70] H.A. Asiri, A.B. Anderson, J. Phys. Chem. C 117 (2013) 17509.
[71] R. Jinnouchi, A.B. Anderson, J. Phys. Chem. C 112 (2008) 8747.
[72] T. Roman, A. Groß, Catal. Today 202 (2013) 183.
[73] E. Santos, P. Hindelang, P. Quaino, E.N. Schulz, G. Soldano, W. Schmickler, ChemPhysChem 12 (2011) 2274.
[74] R. de Levie, J. Electroanal. Chem. 476 (1999) 92.
[75] T. Roman, H. Nakanishi, W. Dino, H. Kasai, e-Journal of Surface Science and Nanotechnology 4 (2006) 619.
[76] N. Garcia-Araez, V. Climent, E. Herrero, J. Feliu, J. Lipkowski, J. Electroanal. Chem. 591 (2006) 149.
[77] N. Garcia-Araez, J.J. Lukkien, M.T. Koper, J.M. Feliu, J. Electroanal. Chem. 588 (2006) 1.
[78] N. Garcia-Araez, M.T.M. Koper, Phys. Chem. Chem. Phys. 12 (2010) 143.
[79] R. Oelgeklaus, J. Rose, H. Baltruschat, J. Electroanal. Chem. 376 (1994) 127.

E.5 Publication in chapter 4.5

The following article is used in chapter 4.5, it is reprinted and adapted from X. Lin, F. Gossenberger, and A. Gross, Ind. Eng. Chem. Res. 55 (2016), 42, 11107-11113, with the permission from Industrial & Engineering Chemistry Research.

I&EC research
Industrial & Engineering Chemistry Research

Article

pubs.acs.org/IECR

Ionic Adsorbate Structures on Metal Electrodes Calculated from First-Principles

Xiaohang Lin,[‡] Florian Gossenberger, and Axel Groß*

Institute of Theoretical Chemistry, Ulm University, 89069 Ulm, Germany

ABSTRACT: The equilibrium coverage of metal electrodes in contact with an electrolyte has been addressed by periodic quantum-chemical calculations based on density functional theory. The electrolyte has been treated in a grand-canonical approach using the concept of the computational hydrogen electrode. After briefly reviewing the theory and illustrating it using the coadsorption of bromide and hydrogen as an example, the interaction of nitrate with a Pb(111) electrode is addressed. A spontaneous reconstruction of the uppermost Pb layer is observed leading to the formation of a salt-like layer.

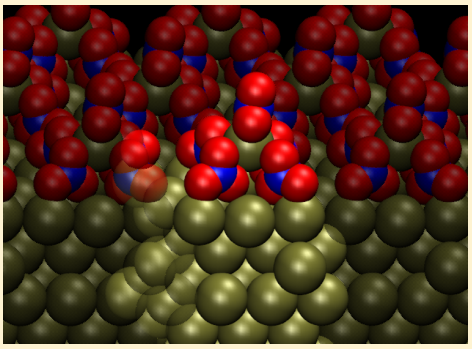

INTRODUCTION

Electrochemistry is concerned with structures and processes at the interface between an electron conductor, the electrode, and an ion conductor, the electrolyte.[1] The electrolyte is often in the liquid phase, in particular in electrocatalysis, containing ions to make it conductive. Typically, these ions, especially anions, are subject to an attractive interaction with electrodes leading to a concentration of the ions on or near the electrodes that is much higher than their equilibrium concentration in the bulk electrolyte.[2] These ions are part of the electrical double layer, but their interaction with the electrode can also modify the electronic and chemical and even structural properties of the electrodes significantly.[2−6] Because of this significant effect that the presence of ions in the electrolyte can have on electrode properties, it is important to understand and predict the thermodynamically stable structure of adsorbed ions as a function of environmental parameters such as ion concentration in the electrolyte and electrode potential.

The theoretical description of the interfaces of electrodes with liquid electrolytes represents a considerable conceptual and numerical challenge as both the liquid phase of the electrolyte and the presence of electrified surfaces need to be taken into account[7−9] which requires to perform computationally costly statistical averages and consider charged electrodes. Note that at electrochemical interfaces the reference for the adsorption energy has to be determined with respect to the corresponding species in solution. However, in a very elegant grand-canonical approach that is now coined computational hydrogen electrode (CHE)[10,11] the evaluation of solvation energies can be avoided. The CHE corresponds to the combination of atomistic calculations with a grand-canonical approach to describe the reference energy of the adsorbates.[12,13] It is particularly useful for electrochemical systems as it is based on the observation that at specific thermodynamic conditions species in solution are in equilibrium with corresponding gas-phase species which are much easier to describe theoretically.[10,11,14,15] In addition, the dependence of the reference energy on electrochemical parameters such as the electrode potential, pH, and ion concentration is known. Furthermore, at metal electrodes adsorption energies are often only weakly dependent on the presence of the electrochemical environment.[10,11,16−19] This concept has been rather successfully used to address electrocatalytic reactions on metal and oxide electrodes.[10,11,20−23] We have recently used this concept to derive the equilibrium coverage of halides on metal electrodes,[24] furthermore we extended this approach to address the coadsorption of halides and hydrogen on Pt(111).[25] We could successfully reproduce and explain the experimental observation[26−28] of the competitive adsorption of halides and hydrogen as a function of electrode potential.

In this paper, we will first briefly review the concept to derive the equilibrium coverage of ions on electrode surfaces from first-principles electronic structure calculations based on density functional theory (DFT) and illustrate the findings. We will then extend this approach to address the interaction of nitrate with Pb(111). This system was chosen because it corresponds to the electrochemical setup recently used in a single-atom transistor controlled by the electrode potential[29−32] as a model for a microscopic quantum device.[33] There we will demonstrate that the presence of anions in the electrolyte can lead to a severe restructuring of metal electrodes, for example leading to the formation of a salt layer.

Received: August 12, 2016
Revised: October 4, 2016
Accepted: October 4, 2016
Published: October 4, 2016

DOI: 10.1021/acs.iecr.6b03087
Ind. Eng. Chem. Res. 2016, 55, 11107−11113

COMPUTATIONAL DETAILS

The DFT calculations presented in this paper were done using the periodic electronic structure code VASP,[34] employing the Perdew, Burke and Ernzerhof (PBE) functional to account for the exchange and correlation effects.[35] For the electron−core interaction the projector augmented wave method was used.[36,37] The electronic one-particle wave functions were expanded in a plane-wave basis set up to an energy cutoff of 500 eV. Different surface unit cell sizes were employed in these studies. In each case it had been made sure that the special k-points sets used to replace the integration over the first Brillouin zone are chosen large enough to yield converged results.

Stable adsorbate phases are characterized by the minimum in the free energy of adsorption per surface area A_S:[24]

$$\Delta\gamma = \frac{1}{A_S}(G_{\mathrm{surf,ads}} - G_{\mathrm{surf,0}} - \sum_i n_i\mu_i) \tag{1}$$

Here $G_{\mathrm{surf,ads}}$ and $G_{\mathrm{surf,0}}$ are the Gibbs free energies of the adsorbate-covered and of the clean surface, n_i is the number of adsorbed atoms of the type i per surface area A_S, and μ is the chemical potential of the adsorbates in their corresponding reservoir. In electrochemical systems, the chemical potential has to be replaced by the electrochemical potential $\tilde{\mu}_i = \mu_i + z_i\, eU$, where z_i is the charge state of the particle, e is the elementary electric charge and U the electrode potential. As mentioned above, in electrochemical situations the electrochemical potential is given with respect to the solvated particle whose energy is hard to calculate as it involves a thermodynamic integration scheme. However, one can take advantage of the fact that there are specific thermodynamic conditions in which the solvated particle is in equilibrium with a corresponding particle in the gas phase. For example, the proton in solution is in equilibrium with the hydrogen molecule in the gas phase at standard conditions,

$$\mathrm{H^+ + e^- \rightleftharpoons \frac{1}{2}H_2} \tag{2}$$

In fact, this equilibrium defines the standard hydrogen electrode (SHE). This means that one can use the H_2 molecule in the gas phase as a reference which is much easier to evaluate than the proton in solution. Furthermore, it is known how the electrochemical potential of the proton in solution depends on electrode potential U and pH:

$$\tilde{\mu}_{\mathrm{H^+}} + \tilde{\mu}_{\mathrm{e^-}} = \frac{1}{2}\mu_{\mathrm{H_2}} - eU_{\mathrm{SHE}} - k_{\mathrm{B}}T\ln(10)\mathrm{pH} \tag{3}$$

This concept is not restricted to hydrogen, but can be used for any redox couple.[38] For example, for halides such as Cl^-, Br^-, and I^-, the corresponding relation for the electrochemical potential reads

$$\tilde{\mu}_{\mathrm{A^-}} - \tilde{\mu}_{\mathrm{e^-}} = \frac{1}{2}\mu_{\mathrm{A_2}} + e(U_{\mathrm{SHE}} - U^0) + k_{\mathrm{B}}T\ln(a_{\mathrm{A^-}}) \tag{4}$$

where U^0 is the reduction potential of the corresponding halide, and a is the thermodynamic activity of the anion A^-.

This is the essence of the concept of the computational hydrogen electrode. It still remains the problem that in eq 1, the free energies of adsorbate-covered electrode and the uncovered electrode need to be determined. It is common practice in applications of the computational hydrogen electrode to neglect entropic contributions and the influence of the electrochemical environment, namely the presence of the electrolyte and the variation of the electrode potential, in the determination of $G_{\mathrm{surf,ads}}$ and $G_{\mathrm{surf,0}}$. As far as metal electrodes are concerned, this approximation seems to be justified[10,11,16−19] because of the strong chemical interaction with electrodes and the good screening properties of metals. This allows the use of DFT total energies instead of free energies so that eq 1 can be replaced by

$$\Delta\gamma = \frac{1}{A_S}(E_{\mathrm{surf,ads}} - E_{\mathrm{surf,0}} - \sum_i n_i\tilde{\mu}_i(T, p, U)) \tag{5}$$

Finally we reformulate this expression by referring the electrochemical potentials of the solvated species to the corresponding stable gas-phase species and the electrochemical potential of the electrons[25] that corresponds to the Fermi energy of the metal electrode, similar to what is done in *ab initio* thermodynamics,[13] arriving at

$$\Delta\gamma(T, p, U) = \frac{1}{A_S}(E_{\mathrm{ads}}^{\mathrm{tot}} - \sum_i n_i\Delta\tilde{\mu}_i(T, p, U)) \tag{6}$$

where the adsorption energies $E_{\mathrm{ads}}^{\mathrm{tot}}$ are taken with respect to the gas-phase species. Note that in this particular formulation the dependence of the free energy of adsorption on entropic contributions entirely enters through the corresponding dependence of the electrochemical potentials of the species in the reservoir on temperature, pressure, and electrode potential.

RESULTS AND DISCUSSION

We will illustrate the approach to determine the thermodynamically stable adsorbate structure at electrochemical electrode/electrolyte interfaces using the coadsorption of hydrogen and bromine on Pt(111) as an example. Experimentally, it has been observed that the substitution of adsorbed hydrogen by bromine on Pt(111) as a function of electrode potential occurs in a very narrow potential range,[28,39] indicative of competitive adsorption. Cyclovoltammograms further show[40,41] that on the negative going scan the bromine desorption peaks appear at potentials negative to the hydrogen adsorption peaks on the clean surface, demonstrating that hydrogen is replaced by bromine. This is at first glance surprising because one would expect that there is an attractive electrostatic interaction between an adsorbed cation (proton) and an adsorbed anion (bromide).

As a first step, several adsorbate structures of hydrogen and bromine alone and both adsorbates together within (3×3), $c(4 \times 2)$ and $(\sqrt{7} \times \sqrt{7}R19.1°)$ surface unit cells were determined and the adsorption energy evaluated. The (3×3) and $(\sqrt{7} \times \sqrt{7}R19.1°)$ structure were observed in experiments[39,42,43] whereas the $c(4 \times 2)$ structure was seen for a chlorine adlayer on Pt(111).[44] In these calculations, no electrolyte was present. However, we have recently shown[45] that for halide coverages above $^1/_3$ closed water layers form above the halide adsorbate layer; that is, the water molecules do not penetrate into the halide adsorbate structure.

Note that according to eq 6, as a function of the electrochemical potentials of the proton and of bromide, each adsorbate structure is represented by a plane in a three-dimensional space spanned by $\Delta\tilde{\mu}_{\mathrm{H^+}}$, $\Delta\tilde{\mu}_{\mathrm{A^-}}$, and the Gibbs free energy of adsorption $\Delta\gamma$, and for a given set of electrochemical potentials the structure with the lowest $\Delta\gamma$ corresponds to the thermodynamically stable phase.

DOI: 10.1021/acs.iecr.6b03087
Ind. Eng. Chem. Res. 2016, 55, 11107−11113

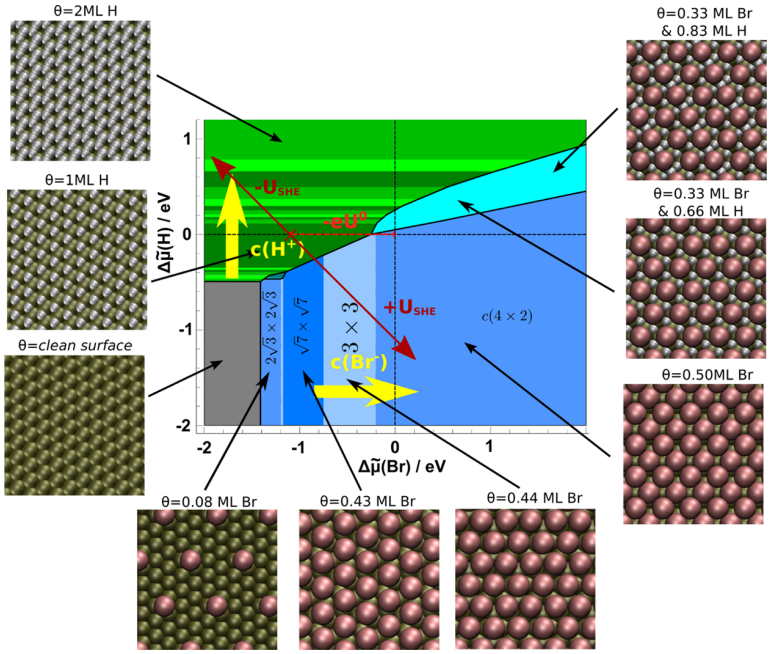

Figure 1. Stable phases of coadsorbed bromine and hydrogen on Pt(111) as a function of the electrochemical potentials of hydrogen and bromine. Bluish areas denote pure bromine coverages, greenish colors show pure hydrogen coverages, and the turquois area denotes a coadsorbed structure of both H and Br. Only the most stable structures are illustrated in the subfigures. Especially in the case of hydrogen adsorption there are regions where the stable coverage is a varying dynamic in between the subfigures. The red double arrow denoted by $-eU^0$ indicates a variation of the electrode potential with all other parameters kept fixed at standard conditions, whereas the yellow arrows illustrate the influence of the ion concentration.

The resulting phase diagram is plotted in Figure 1 together with an illustration of the structure of the stable phases. Most of the phase space is characterized by either a purely hydrogen-covered (greenish colors) or a purely bromine-covered (bluish colors) region. Typically there is an indirect repulsive interaction between adsorbates through adsorption-induced modifications of the metal substrate.[5] However, one could imagine that this might be compensated by an attractive dipole−dipole interaction between adsorbed anions and cations. However, there is apparently no attractive interaction between adsorbed hydrogen and bromide. This result can be understood considering the fact that the adsorption of bromine on Pt(111) leads to an anomalous work function decrease[46] caused by the strong polarization upon adsorption.[47−49] As a consequence, a dipole−dipole repulsion between adsorbed bromine and hydrogen results.

However, in electrochemistry, the electrochemical potential of solvated species is typically not specified, but rather the concentration and the electrode potential. The variation of the electrode potential at standard conditions is illustrated by the red arrows in Figure 1.

Hence it is rather helpful to transform the phase diagram into a Pourbaix diagram, that is, into a map of the stable phases as a function of pH and electrode potential. The Pourbaix diagram derived from the phase diagram plotted in Figure 1 is shown in Figure 2. For a given pH value, the stable surface structures as a function of the electrode potential can be immediately read off, information that is directly relevant for the interpretation of cyclic voltammograms. The diagram demonstrates that indeed upon increasing the electrode potential purely hydrogen-covered phases are replaced by purely bromine-covered phases. Because of the presence of bromine, the upper potential edge of the stable hydrogen phases is shifted to lower potentials,

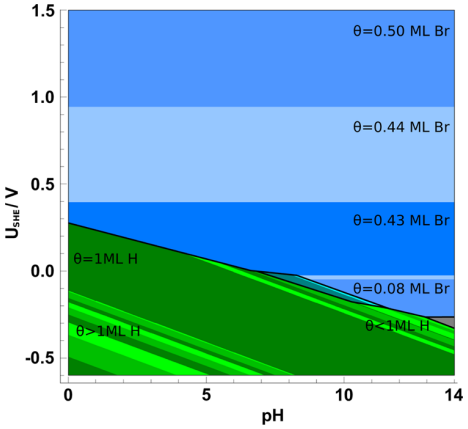

Figure 2. Calculated Pourbaix diagram, that is, a map of the stable phases of coadsorbed bromine and hydrogen on Pt(111) as a function of pH and electrode potential for a fixed bromine concentration corresponding to an activity of $a = 0.1$. The color code is the same as in Figure 1 where also the geometric structures of the corresponding phases are given. Greenish colors denote a pure hydrogen phase, bluish colors denote a pure bromine phase. In between the hydrogen and bromine phases, there is a thin region, where a coadsorbate structure with both species is stable. The gray area corresponds to a region where the clean, uncovered electrode is stable.

confirming the competitive nature of hydrogen and bromine inferred from the experiment.[28,39−41] Only at higher pH values there is a small pocket in which hydrogen and bromine coadsorption structures are stable, but only over a rather narrow potential range, thus confirming experimental findings.[39,50]

DOI: 10.1021/acs.iecr.6b03087
Ind. Eng. Chem. Res. 2016, 55, 11107−11113

The stable bromine phases correspond either to a $(\sqrt{7} \times \sqrt{7}R19.1°)$ structure with a coverage of $\Theta = {}^{3}/_{7}$ or a (3×3) structure with $\Theta = {}^{4}/_{9}$. Both structures have been observed in the experiment.[39,42,43] The calculated results for the coadsorption of hydrogen with chlorine and iodine are also all consistent with experimental observations[24] indicating the reliability of the approach outlined here based on the computational hydrogen electrode.

This same approach has also been used to evaluate the interaction of nitrate with Pb(111). Pb electrodes have recently been of interest as they are one of the materials used to realize a single-atom transistor in an electrochemical environment[29−32] which opens attractive perspectives to prepare microscopic quantum devices.[33] It is based on the fact that atomic-scale quantum point contacts can be reversibly switched as a function of the electrode potential. Still, the details of the operation of the single-atom transistor are not understood. Therefore, in a series of first-principles-based studies we have tried to elucidate possible mechanisms to form atomic contacts at Pb electrodes[51] and to determine the water structure at flat and stepped Pb electrodes.[45,52] We have now extended this project in order to assess the influence of nitrate (NO_3^-) on the structure of Pb electrodes as a nitrate-based electrolyte has been used in the experiments realizing the single-atom transistor.[31]

Again, the first step is to search for minimum energy adsorbate structures for various coverages. To the best of our knowledge, there is no experimental study identifying the structure of nitrate on Pb(111). Therefore, we have chosen a 3 × 3 surface unit cell that should be sufficiently large to allow the formation of different structures. Still it should be admitted that thus we might miss some stable structures. However, without prior knowledge of the periodicity of adsorbate structures a search for all possible arrangements is computationally extremely demanding.

The considered structures within the 3 × 3 surface unit cell are illustrated in Figure 3, the corresponding adsorption energies are shown in Figure 4. At low coverages, the molecules arrange on the unreconstructed Pb(111) surface, the adsorption energies become less negative with increasing coverage indicative of a repulsive interaction between the adsorbed nitrate molecules. Interestingly enough, at coverages starting from $\Theta = {}^{5}/_{9}$, Pb(111) spontaneously reconstructs upon exposure to nitrate. A lead atom is extracted from the Pb electrode and forms a Pb-NO_3 complex. This is associated with a significant energy gain. The ease to form such a complex involving the extraction of a Pb atom from the surface is obviously a consequence of the relatively low cohesive energy of lead of 2.03 eV/atom.[53] Note that in these calculations the presence of the electrolyte was ignored. However, water is relatively weakly interacting with lead. For example, the adsorption energy of water monomers on Pb(111) is only −0.07 eV.[52] Hence we do not expect that the chemically driven reconstruction of Pb(111) will be strongly modified by the presence of water.

The stable adsorption phases as a function of the electrode potential are plotted in Figure 5. To derive this phase diagram based on the concept of the computational hydrogen electrode, the following redox couple has been used to define a reference for nitrate,

$$2H^+(aq) + NO_3^-(aq) + e^- \rightleftharpoons NO_2(g) + H_2O(aq) \quad (7)$$

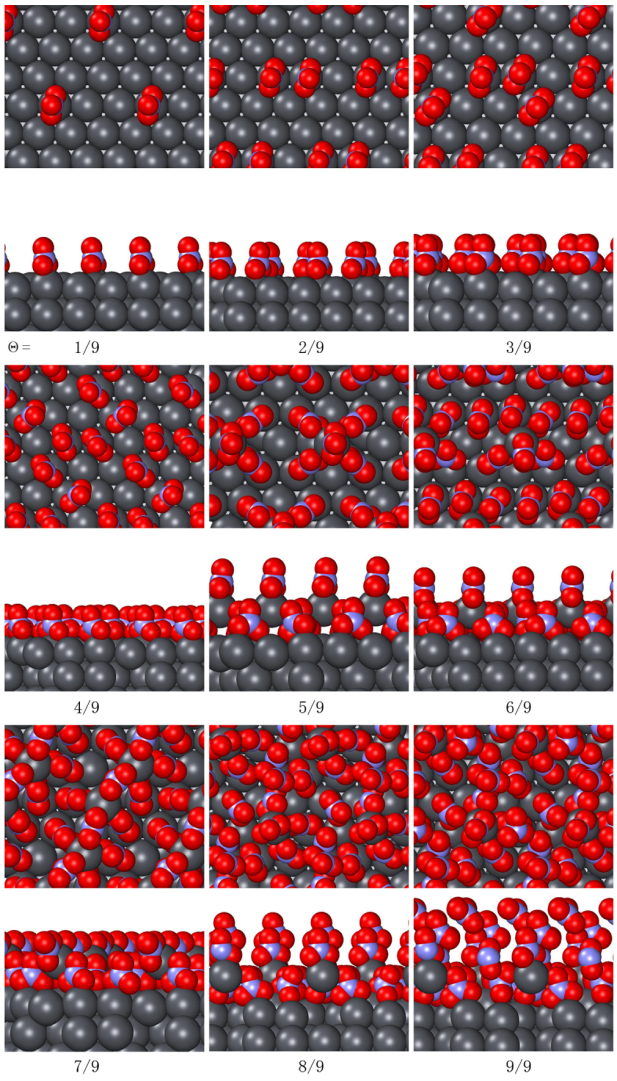

Figure 3. Illustration of the structures of nitrate adsorbed on Pb(111). Pb atoms are colored in dark gray, oxygen is red, and nitrogen is blue.

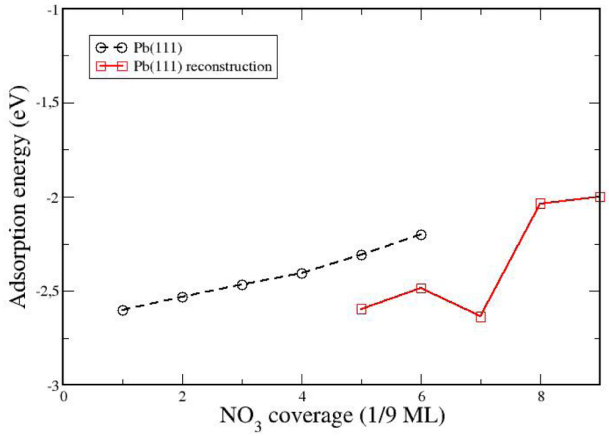

Figure 4. Adsorption energy of NO_3 on Pb(111) per molecule as a function of the coverage. Black circles denote adsorption on the unreconstructed electrode, red boxes correspond to adsorption involving a reconstruction of the Pb(111) electrode.

DOI: 10.1021/acs.iecr.6b03087
Ind. Eng. Chem. Res. 2016, 55, 11107−11113

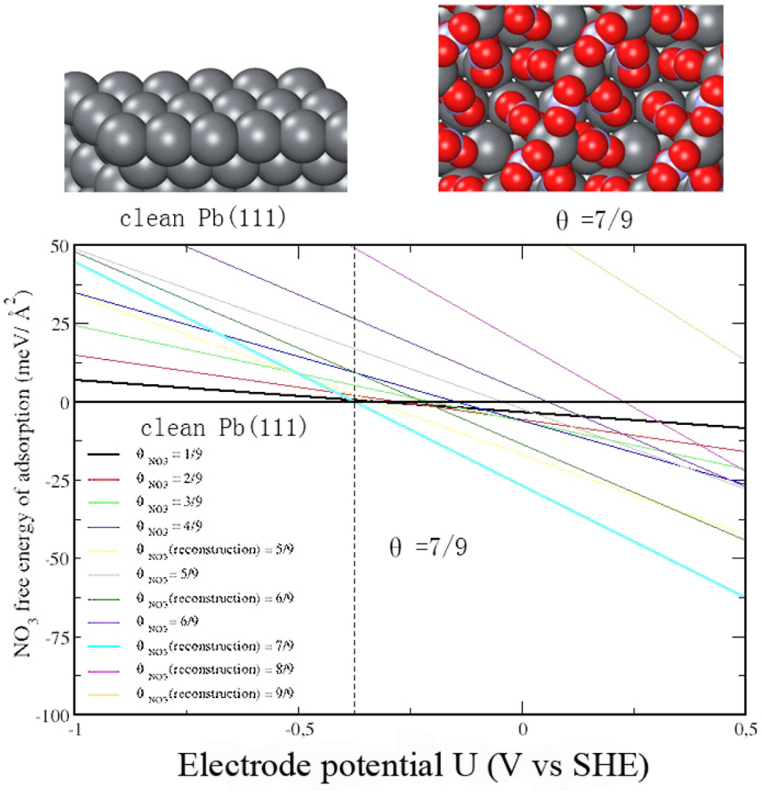

Figure 5. Phase diagram of the stable nitrate structures as a function of electrode potential.

Furthermore, a nitrate activity of $a_{NO_3^-} = 1$ has been assumed. Up to an electrode potential of about −0.4 V vs SHE, the clean Pb(111) electrode is thermodynamically favored. For higher electrode potentials, the reconstructed Pb(111) electrode at a nitrate coverage of $\Theta = {}^{7}/_{9}$ becomes stable over a wide potential window corresponding to the conditions typical for electrochemical experiments in aqueous electrolytes. Inspecting Figure 3 reveals that for this coverage a complete lead nitrate layer evolves. At lower coverages, this layer is not completed, at higher coverages a new layer starts to grow.

To understand the origin of the stability of the reconstructured Pb(111) electrodes at a nitrate coverage of $\Theta = 7/9$ involving the formation of a Pb−NO_3 complex even further, we compare in Figure 6 the structure of bulk lead nitrate with the corresponding complex on the Pb(111) surface. Panels a and c show the bulk unit cell of $Pb(NO_3)_2$ and the top view of reconstructed Pb(111) surface, respectively. The local nitrate arrangements around the lead atom in the bulk and in the surface complex are compared in panels b and d. Due to the lattice mismatch between bulk lead nitrate and Pb(111), no perfect agreement should be expected. Still the local arrangements are rather similar. We illustrate this by particularly considering the N−Pb−N angles with regard to the NO_3 groups nearest to the Pb atom. In the bulk, these angles have values of 83.6° and 116.9°, as indicated in Figure 6b. In the case of the reconstructed Pb(111) surface, these particular angles are only slightly modified to values of 93.9° and 112.4°, respectively, and the local coordination is also hardly changed, as Figure 6d shows. This indicates that the nitrate-induced surface reconstruction of Pb(111) can be viewed as the formation of a surface lead nitrate layer or as the initial step of lead nitrate salt formation,[54] despite lead nitrate readily dissolving in water.[55]

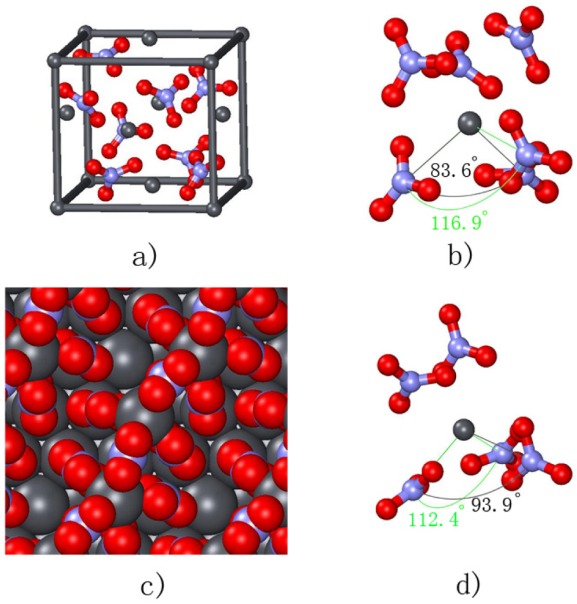

Figure 6. Comparison of the $Pb(NO_3)_2$ bulk structure and the structure of the lead nitrate complex formed spontaneously on Pb(111) at a nitrate coverage of $\Theta = {}^{7}/_{9}$. (a) Bulk unit cell of $Pb(NO_3)_2$, (b) arrangement of nitrate around a Pb atom in the bulk, (c) top view of reconstructed Pb(111) surface, (d) arrangement of nitrate around a Pb atom in the surface complex.

DOI: 10.1021/acs.iecr.6b03087
Ind. Eng. Chem. Res. 2016, 55, 11107−11113

Our results show that the exposure of a metal electrode to an aqeuous electrolyte can lead to a substantial surface restructuring. This is of course not the case for any anion-containing electrolyte. However, once such a surface reconstruction occurs, it significantly modifies the structural, electronic, and chemical properties of the electrode and should not be neglected.

The results presented in this study show that first-principles calculations using the concept of the computational hydrogen electrode are a powerful tool to determine equilibrium structures of metal electrode/aqueous electrolyte interfaces. In the determination of the adsorption energies entering the formalism, the explicit influence of the electrolyte and of varying electrode potentials has been neglected. This approximation is justified by the good screening properties of metals. However, there is certainly a need to assess the validity of this approximation by including the electrochemical environment explicitly. First steps along this route have already been taken.[17−19,23,56] For the results presented in this work, explicitly considering the electrochemical environment in the calculations will change the results quantitatively to a certain extent, but it is not expected that any qualitative trends will become modified.

CONCLUSIONS

The structure of metal electrode/aqueous electrolyte interfaces has been studied by first-principles calculations treating the electrochemical environment in a grand-canonical approach based on the concept of the computational hydrogen electrode. Phase diagrams of the thermodynamically stable adsorbate structures as a function of electrochemical potentials have been derived which allows, for example, a derivation of the Pourbaix diagrams which can be directly compared to experimental results. Regarding the coadsorption of hydrogen and bromine on Pt(111), the results were able to reproduce the experimentally observed competitive nature of the coadsorption. The presence of a nitrate-containing electrolyte over a lead electrode leads to a significant reconstruction of the lead electrode presenting the first steps of lead nitrate salt formation.

AUTHOR INFORMATION

Corresponding Author

*E-mail: Axel.Gross@uni-ulm.de.

Present Address

‡X.L.: School of Material Science and Engineering, Shandong University, 250061 Jinan, China; e-mail tonylxh12345@hotmail.com.

Notes

The authors declare no competing financial interest.

ACKNOWLEDGMENTS

This research has been supported by the German Research Foundation (DFG) through Contract GR 1503/21-2 within the DFG research unit FOR 1376 and by the Baden-Württemberg Foundation within the Network of Competence "Functional Nanostructures". Computer time has been provided by the bwHPC initiative and the bwHPC-C5 project funded by the Baden-Württemberg government (MWK) and the German Research Foundation (DFG). This contribution was identified by Session Chair Oleg Borodin (U.S. Army Research Laboratory, Adelphi, MD 20783, USA) as the Best Presentation in the session "Electrochemistry at Solid/liquid Interfaces" of the 2016 ACS Spring National Meeting in San Diego, CA.

REFERENCES

(1) Schmickler, W.; Santos, E. *Interfacial Electrochemistry*, 2nd ed.; Springer: Berlin, 2010.

(2) Tripkovic, D. V.; Strmcnik, D.; van der Vliet, D.; Stamenkovic, V.; Markovic, N. M. The role of anions in surface electrochemistry. *Faraday Discuss.* **2009**, *140*, 25−40.

(3) Tománek, D.; Wilke, S.; Scheffler, M. Hydrogen induced polymorphism of Pd(110). *Phys. Rev. Lett.* **1997**, *79*, 1329.

(4) Wei, C. M.; Groß, A.; Scheffler, M. Ab initio calculation of the potential energy surface for the dissociation of H_2 on the sulfur-covered Pd(100) surface. *Phys. Rev. B: Condens. Matter Mater. Phys.* **1998**, *57*, 15572.

(5) Hammer, B. Coverage dependence of N_2 dissociation at an N, O, or H precovered Ru(0001) surface investigated with density functional theory. *Phys. Rev. B: Condens. Matter Mater. Phys.* **2001**, *63*, 205423.

(6) Arenz, M.; Stamenkovic, V.; Schmidt, T.; Wandelt, K.; Ross, P.; Markovic, N. The effect of specific chloride adsorption on the electrochemical behavior of ultrathin Pd films deposited on Pt(111) in acid solution. *Surf. Sci.* **2003**, *523*, 199−209.

(7) Schnur, S.; Groß, A. Properties of metal-water interfaces studied from first principles. *New J. Phys.* **2009**, *11*, 125003.

(8) Schnur, S.; Groß, A. Challenges in the first-principles description of reactions in electrocatalysis. *Catal. Today* **2011**, *165*, 129−137.

(9) Sakong, S.; Forster-Tonigold, K.; Groß, A. The structure of water at a Pt(111) electrode and the potential of zero charge studied from first principles. *J. Chem. Phys.* **2016**, *144*, 194701.

(10) Nørskov, J. K.; Rossmeisl, J.; Logadottir, A.; Lindqvist, L.; Kitchin, J. R.; Bligaard, T.; Jónsson, H. Origin of the Overpotential for Oxygen Reduction at a Fuel-Cell Cathode. *J. Phys. Chem. B* **2004**, *108*, 17886−17892.

(11) Nørskov, J. K.; Bligaard, T.; Logadottir, A.; Kitchin, J. R.; Chen, J. G.; Pandelov, S.; Stimming, U. Trends in the Exchange Current for Hydrogen Evolution. *J. Electrochem. Soc.* **2005**, *152*, J23.

(12) Moll, N.; Kley, A.; Pehlke, E.; Scheffler, M. GaAs equilibrium crystal shape from first principles. *Phys. Rev. B: Condens. Matter Mater. Phys.* **1996**, *54*, 8844.

(13) Reuter, K.; Scheffler, M. Composition, structure, and stability of RuO_2(110) as a function of oxygen pressure. *Phys. Rev. B: Condens. Matter Mater. Phys.* **2001**, *65*, 035406.

(14) Roques, J.; Anderson, A. B. Theory for the Potential Shift for OH_{ads} Formation on the Pt Skin on Pt_3Cr(111) in Acid. *J. Electrochem. Soc.* **2004**, *151*, E85−E91.

(15) Roques, J.; Anderson, A. B. Pt_3Cr(111) Alloy Effect on the Reversible Potential of OOH(ads) Formation from O_2(ads) relative to Pt(111). *J. Fuel Cell Sci. Technol.* **2005**, *2*, 86−93.

(16) Roudgar, A.; Groß, A. Water bilayer on the Pd/Au(111) overlayer system: coadsorption and electric field effects. *Chem. Phys. Lett.* **2005**, *409*, 157.

(17) Rossmeisl, J.; Nørskov, J. K.; Taylor, C. D.; Janik, M. J.; Neurock, M. Calculated Phase Diagrams for the Electrochemical Oxidation and Reduction of Water over Pt(111). *J. Phys. Chem. B* **2006**, *110*, 21833−21839.

(18) Wang, H.-F.; Liu, Z.-P. Formic Acid Oxidation at Pt/H_2O Interface from Periodic DFT Calculations Integrated with a Continuum Solvation Model. *J. Phys. Chem. C* **2009**, *113*, 17502−17508.

(19) Jinnouchi, R.; Kodama, K.; Morimoto, Y. DFT calculations on H, OH and O adsorbate formations on Pt(111) and Pt(332) electrodes. *J. Electroanal. Chem.* **2014**, *716*, 31−44.

(20) Man, I. C.; Su, H.-Y.; Calle-Vallejo, F.; Hansen, H. A.; Martinez, J. I.; Inoglu, N. G.; Kitchin, J.; Jaramillo, T. F.; Nørskov, J. K.; Rossmeisl, J. Universality in Oxygen Evolution Electrocatalysis on Oxide Surfaces. *ChemCatChem* **2011**, *3*, 1159−1165.

(21) Halck, N. B.; Petrykin, V.; Krtil, P.; Rossmeisl, J. Beyond the volcano limitations in electrocatalysis - oxygen evolution reaction. *Phys. Chem. Chem. Phys.* **2014**, *16*, 13682−13688.

DOI: 10.1021/acs.iecr.6b03087
Ind. Eng. Chem. Res. 2016, 55, 11107−11113

(22) Nie, X.; Luo, W.; Janik, M. J.; Asthagiri, A. Reaction mechanisms of CO_2 electrochemical reduction on Cu(111) determined with density functional theory. *J. Catal.* **2014**, *312*, 108−122.
(23) Sakong, S.; Groß, A. The Importance of the Electrochemical Environment in the Electro-Oxidation of Methanol on Pt(111). *ACS Catal.* **2016**, *6*, 5575−5586.
(24) Gossenberger, F.; Roman, T.; Groß, A. Equilibrium coverage of halides on metal electrodes. *Surf. Sci.* **2015**, *631*, 17−22.
(25) Gossenberger, F.; Roman, T.; Groß, A. Hydrogen and halide co-adsorption on Pt(111) in an electrochemical environment: A computational perspective. *Electrochim. Acta* **2016**, *216*, 152 DOI: 10.1016/j.electacta.2016.08.117.
(26) Oelgeklaus, R.; Rose, J.; Baltruschat, H. On the rate of hydrogen and iodine adsorption on polycrystalline Pt and Pt(111). *J. Electroanal. Chem.* **1994**, *376*, 127−133.
(27) Garcia-Araez, N.; Climent, V.; Herrero, E.; Feliu, J.; Lipkowski, J. Thermodynamic studies of chloride adsorption at the Pt(111) electrode surface from 0.1 M $HClO_4$ solution. *J. Electroanal. Chem.* **2005**, *576*, 33−41.
(28) Garcia-Araez, N.; Climent, V.; Herrero, E.; Feliu, J.; Lipkowski, J. Thermodynamic studies of bromide adsorption at the Pt(111) electrode surface perchloric acid solutions: Comparison with other anions. *J. Electroanal. Chem.* **2006**, *591*, 149−158.
(29) Xie, F.-Q.; Nittler, L.; Obermair, C.; Schimmel, T. Gate-Controlled Atomic Quantum Switch. *Phys. Rev. Lett.* **2004**, *93*, 128303.
(30) Xie, F.-Q.; Maul, R.; Brendelberger, S.; Obermair, C.; Starikov, E. B.; Wenzel, W.; Schön, G.; Schimmel, T. Preselectable integer quantum conductance of electrochemically fabricated silver point contacts. *Appl. Phys. Lett.* **2008**, *93*, 043103.
(31) Xie, F.-Q.; Hüser, F.; Schön, G.; Obermair, C.; Schimmel, T.; Pauly, F. Conductance of atomic-scale Pb contacts in an electrochemical environment. *Phys. Rev. B: Condens. Matter Mater. Phys.* **2010**, *82*, 075417.
(32) Xie, F.-Q.; Maul, R.; Obermair, C.; Wenzel, W.; Schön, G.; Schimmel, T. Multilevel Atomic-Scale Transistors Based on Metallic Quantum Point Contacts. *Adv. Mater.* **2010**, *22*, 2033−2036.
(33) Hong, W.; Valkenier, H.; Meszaros, G.; Manrique, D. Z.; Mishchenko, A.; Putz, A.; Garcia, P. M.; Lambert, C. J.; Hummelen, J. C.; Wandlowski, T. An MCBJ case study: The influence of π-conjugation on the single-molecule conductance at a solid/liquid interface. *Beilstein J. Nanotechnol.* **2011**, *2*, 699−713.
(34) Kresse, G.; Furthmüller, J. Efficient iterative schemes for ab initio total-energy calculations using a plane-wave basis set. *Phys. Rev. B: Condens. Matter Mater. Phys.* **1996**, *54*, 11169.
(35) Perdew, J. P.; Burke, K.; Ernzerhof, M. Generalized gradient approximation made simple. *Phys. Rev. Lett.* **1996**, *77*, 3865.
(36) Blöchl, P. E. Projector augmented-wave method. *Phys. Rev. B: Condens. Matter Mater. Phys.* **1994**, *50*, 17953.
(37) Kresse, G.; Joubert, D. From ultrasoft pseudopotentials to the projector augmented-wave method. *Phys. Rev. B: Condens. Matter Mater. Phys.* **1999**, *59*, 1758.
(38) Hansen, H. A.; Man, I. C.; Studt, F.; Abild-Pedersen, F.; Bligaard, T.; Rossmeisl, J. Electrochemical chlorine evolution at rutile oxide (110) surfaces. *Phys. Chem. Chem. Phys.* **2010**, *12*, 283−290.
(39) Orts, J. M.; Gomez, R.; Feliu, J. M.; Aldaz, A.; Clavilier, J. Nature of Br Adlayers on Pt(111) Single-Crystal Surfaces. Voltammetric, Charge Displacement, and ex Situ STM Experiments. *J. Phys. Chem.* **1996**, *100*, 2334−2344.
(40) Salaita, G. N.; Stern, D. A.; Lu, F.; Baltruschat, H.; Schardt, B. C.; Stickney, J. L.; Soriaga, M. P.; Frank, D. G.; Hubbard, A. T. Structure and composition of a platinum(111) surface as a function of pH and electrode potential in aqueous bromide solutions. *Langmuir* **1986**, *2*, 828−835.
(41) Bittner, A.; Wintterlin, J.; Beran, B.; Ertl, G. Bromine adsorption on Pt(111), (100), and (110) - an STM study in air and in electrolyte. *Surf. Sci.* **1995**, *335*, 291−299.
(42) Lucas, C. A.; Markovic, N. M.; Ross, P. N. Adsorption of halide anions at the Pt(111)-solution interface studied by in situ surface x-ray scattering. *Phys. Rev. B: Condens. Matter Mater. Phys.* **1997**, *55*, 7964−7971.
(43) Magnussen, O. M. Ordered anion adlayers on metal electrode surfaces. *Chem. Rev.* **2002**, *107*, 679−725.
(44) Song, M.; Ito, M. STM observation of Pt111(3 × 3)-Cl and c(4 × 2)-Cl structures. *Bull. Korean Chem. Soc.* **2001**, *22*, 267.
(45) Groß, A.; Gossenberger, F.; Lin, X.; Naderian, M.; Sakong, S.; Roman, T. Water Structures at Metal Electrodes Studied by Ab Initio Molecular Dynamics Simulations. *J. Electrochem. Soc.* **2014**, *161*, E3015−E3020.
(46) Bertel, E.; Schwaha, K.; Netzer, F. P. Adsorption of bromine on Pt(111) - Observation of an irreversible order-disorder transition. *Surf. Sci.* **1979**, *83*, 439.
(47) Roman, T.; Groß, A. Periodic density-functional calculations on work function change induced by adsorption of halogens on Cu(111). *Phys. Rev. Lett.* **2013**, *110*, 156804.
(48) Gossenberger, F.; Roman, T.; Forster-Tonigold, K.; Groß, A. Work function change of platinum electrodes induced by halide adsorption. *Beilstein J. Nanotechnol.* **2014**, *5*, 152−161.
(49) Roman, T.; Gossenberger, F.; Forster-Tonigold, K.; Groß, A. Halide adsorption on close-packed metal electrodes. *Phys. Chem. Chem. Phys.* **2014**, *16*, 13630−13634.
(50) Garcia-Araez, N.; Lukkien, J. J.; Koper, M. T.; Feliu, J. M. Competitive adsorption of hydrogen and bromide on Pt(1 0 0): Mean-field approximation vs. Monte Carlo simulations. *J. Electroanal. Chem.* **2006**, *588*, 1−14.
(51) Lin, X.; Dasgupta, A.; Xie, F.; Schimmel, T.; Evers, F.; Groß, A. Exchange processes in the contact formation of Pb electrodes. *Electrochim. Acta* **2014**, *140*, 505−510.
(52) Lin, X.; Evers, F.; Groß, A. First-principles study of the structure of water layers on flat and stepped Pb electrodes. *Beilstein J. Nanotechnol.* **2016**, *7*, 533−543.
(53) Kittel, C. *Introduction to Solid State Physic*, 8th ed.; John Wiley & Sons: New York, 2004.
(54) Pauley, J. L.; Testerman, M. K. Basic Salts of Lead Nitrate Formed in Aqueous Media1. *J. Am. Chem. Soc.* **1954**, *76*, 4220−4222.
(55) Ferris, L. M. Lead Nitrate-Nitric Acid-Water System. *J. Chem. Eng. Data* **1960**, *5*, 242−242.
(56) Bonnet, N.; Morishita, T.; Sugino, O.; Otani, M. First-Principles Molecular Dynamics at a Constant Electrode Potential. *Phys. Rev. Lett.* **2012**, *109*, 266101.

DOI: 10.1021/acs.iecr.6b03087
Ind. Eng. Chem. Res. 2016, 55, 11107−11113

Name: Florian Gossenberger

Erklärung

Ich erkläre, dass ich die Arbeit selbständig verfasst und keine anderen als die angegebenen Quellen und Hilfsmittel verwendet habe.

Ulm, den .....

Florian Gossenberger